Università degli Studi di Padova

DIPARTIMENTO DI FISICA E ASTRONOMIA "GALILEO GALILEI"
Scuola di Dottorato di Ricerca in Fisica
Ciclo XVIII

Mean field and fluctuations for fermionic systems: from ultracold Fermi gases to cuprates

Direttore della Scuola:
Chiar.mo Prof. Andrea Vitturi

Dottorando:
Giacomo Bighin

Supervisore:
Chiar.mo Prof. Luca Salasnich

Co-supervisore:
Chiar.mo Prof. Pieralberto Marchetti

Anno Accademico 2015-16

Sommario

Questa tesi analizza il ruolo della teoria di campo medio e delle fluttuazioni in due differenti sistemi fermionici: il crossover BCS-BEC e i cuprati superconduttori ad alta temperatura critica.

Nella prima parte della tesi si introduce la teoria di campo medio e le fluttuazioni a livello Gaussiano per il crossover BCS-BEC, i.e. l'evoluzione continua osservata in sistemi ultrafreddi di fermioni neutri, da un regime di accoppiamento debole dove i fermioni formano coppie di Cooper, ad un regime di accoppiamento forte dove i fermioni formano dapprima dimeri molecolari bosonici, i quali poi condensano a temperature sufficientemente basse. Si analizzano alcuni problemi correlati al crossover: la frazione condensata nel caso di un gas di Fermi con sbilanciamento di spin, il decadimento di Beliaev per le eccitazioni collettive e il caso di un gas di Fermi bidimensionale, per il quale in particolare si calcolano la velocità del primo suono e le temperatura critica di Berezinskii-Kosterlitz-Thouless, in accordo molto buono con recenti dati sperimentali. Infine si analizza una procedura di regolarizzazione per l'equazione di stato nel limite deep-BEC che permette di derivare analiticamente il corretto rapporto tra la lunghezza di scattering fermionica e bosonica.

Nella seconda parte della tesi si introduce un approccio di gauge alla superconduttività nei cuprati nel quale la buca è decomposta nel prodotto di una particella che porta solo spin, lo spinone, e una particella che porta solo carica, l'holone. La statistica di ciascuna particella è modificata accoppiandola ad un campo di gauge che fornisce un flusso statistico, in un approccio analogo alla bosonizzazione di Chern-Simons. Si ottiene quindi un modello che prevede tre temperature caratteristiche che corrispondono, rispettivamente, alla comparsa di una densità finita di coppie di holoni incoerenti, di una densità finita di coppie di spinoni incoerenti e infine alla coerenza di fase che dà luogo alla superconduttività.

In particolare in questa tesi all'interno di tale modello si studia la densità di superfluido, dimostrando che il contributo spinonico e quello holonico si sommano secondo una regola del tutto analoga a quella di Ioffe-Larkin per la resistività, mostrando un ottimo accordo con i dati sperimentali nella regione di doping moderato fino all'optimal doping. Si dimostra anche il formalismo riproduce la quasi-universalità in doping osservata nei dati sperimentali e permette la derivazione analitica di una relazione che approssima la relazione di Uemura per doping moderati.

Abstract

This Thesis analyzes the role of a mean-field theory and of the fluctuations in two different fermionic systems: the BCS-BEC crossover and high-T_c superconducting cuprates.

In the first part of the Thesis we introduce the mean-field theory and the Gaussian-level fluctuations for the BCS-BEC crossover, i.e. the continuous evolution observed in ultracold neutral fermionic systems, from a weakly-coupled regime where fermions form Cooper pairs, to a strongly-coupled regime where the fermions at first form bosonic molecular dimers, subsequently undergoing Bose-Einstein condensation for low enough temperatures. We then analyze some problems related to the crossover: the condensate fraction for a spin-unbalanced Fermi gas, the Beliaev decay for collective excitations and the case of a two-dimensional Fermi gas, for which we calculate the first sound velocity and the Berezinskii-Kosterlitz-Thouless critical temperature, in very good agreement with recent experimental data. Finally we analyze a regularization procedure for the equation of state in the deep-BEC limit, allowing one to analytically derive the correct ratio between the fermionic and bosonic scattering lengths.

In the second part of the Thesis we introduce a gauge approach to superconductivity in cuprates in which the hole is decomposed as the product of a spinful neutral particle, the spinon, and a spinless charged particle, the holon. The statistics of each particle is modified by binding it to a gauge field providing a statistical flux, this approach being analogous to Chern-Simons bosonization. We thus obtain a model characterized by three characteristic temperatures corresponding, respectively, to the appearance of a finite density of incoherent holon pairs, of a finite density of incoherent spinon pairs and, finally, to the phase coherence leading to superconductivity.

Specifically in the present Thesis within this model we study the superfluid density, demonstrating that the spinon and holon contributions sum according to a Ioffe-Larking-like rule, analogous to that they found for resistivity, showing excellent agreement with experimental data in the moderate underdoping up to optimal doping region. We also demonstrated that the formalism reproduces the quasi-universality observed in experimental data at different dopings and allows for an analytical derivation of a relation that approximates the Uemura relation for moderate dopings.

Contents

List of Figures

List of Publications

This Thesis is based on the following research articles published in peer-reviewed journals:

1. G. Bighin and L. Salasnich, *"Finite-temperature quantum fluctuations in two-dimensional Fermi superfluids"*, Phys. Rev. B. **93**, 014519 (2016).

2. G. Bighin, L. Salasnich, P.A. Marchetti and F. Toigo, *"Beliaev damping of the Goldstone mode in atomic Fermi superfluids"*, Phys. Rev. A **92**, 023638 (2015).

3. P.A. Marchetti and G. Bighin, *"Gauge approach to superfluid density in underdoped cuprates"*, Europhys. Lett. **110**, 37001 (2015) (Selected as Editor's Choice).

4. L. Salasnich and G. Bighin, *"Scattering length of composite bosons in the three-dimensional BCS-BEC crossover"*, Phys. Rev. A **91**, 033610 (2015).

5. G. Bighin, G. Mazzarella, L. Dell'Anna and L. Salasnich, *"Pair condensation of polarized fermions in the BCS-BEC crossover"*, J. Phys. B **47**, 195302 (2014).

1 Introduction

Under the calm mask of matter
The divine fire burns

Vladimir Solovyev

This Thesis analyzes the role of a mean field treatment and of fluctuations in two different fermionic systems: the BCS-BEC crossover and high-T_c superconducting cuprates.

In Chapter 2 the Bardeen-Cooper-Schrieffer (BCS) theory of superconductivity and the Bose-Einstein condensation (BEC) are briefly reviewed. This serves as an introduction to the BCS-BEC crossover, i.e. the continuous evolution in a neutral fermionic system, as the fermion-fermion attractive interaction is tuned, from a weakly-coupled regime to a strongly coupled one. In the weakly-coupled BCS regime fermions form broad Cooper pairs, while in the strongly-coupled BEC regime they form tightly-bound molecules, i.e. composite bosons. The Cooper pairs in the BCS regime are, by definition, formed at zero-momentum and immediately condense defining the critical temperature T_c; the composite bosons in the BEC regime, on the other hand, are formed at a temperature T^* and eventually, as the temperature is lowered, undergo Bose-Einstein condensation at a different temperature $T_c < T^*$. The ultimate mechanism for condensation throughout the whole crossover is Bose-Einstein condensation, happening, however, in two profoundly different conditions, making the study of the crossover from one limit to the other a very interesting research topic.

The BCS-BEC crossover is at first considered from a historical perspective, starting from pioneering works in the 1960s up to recent analyses motivated

by the realization of the crossover in ultracold Fermi gases. Subsequently I analyze the experimental techniques allowing for such a realization: I briefly introduce optical and magnetic trapping for an ultracold gas, along with the concept of Feshbach resonance, which critically provides the possibility of tuning with continuity the attractive fermion-fermion interaction connecting the weakly-coupled and strongly-coupled regimes.

In Chapter 3 the mean-field formalism for the BCS-BEC crossover is introduced, deriving the gap and number equations which, jointly solved, completely determine the thermodynamics of the system at each point of the crossover. The equations are derived within a Hamiltonian approach and within a path integral approach. Afterwards we develop a mean-field description for a spin-unbalanced Fermi gas, focusing in particular on the condensate fraction in the uniform and trapped cases, comparing the latter with experimental data. This analysis is based on results published in Ref. [1].

In Chapter 4 the theory of order parameter fluctuations for the BCS-BEC crossover is introduced. While the mean-field theory can usually provide good results at zero temperature in the three-dimensional case, corrections beyond the mean-field picture are needed when investigating finite-temperature effects or when modeling lower-dimensionality systems. Moreover a mean-field theory only includes single-particle excitations, completely neglecting e.g. the sound mode. After a general derivation of the Gaussian fluctuation contribution to the thermodynamics of the system, three problems are analyzed:

- The Beliaev decay, i.e. the decay of a collective excitation in two lower frequency excitations in a superfluid. The original approximate treatment due to Landau decay is extended allowing for a non-collinear decay and is applied to the collective excitations of an ultracold Fermi gas, being the only allowed decay mode in the zero-temperature, low-energy limit. We show that, in this case, there can be substantial corrections with respect to the approximate theory. This analysis is based on results published in Ref. [2].

- The Berezinskii-Kosterlitz-Thouless transition in a two-dimensional Fermi gas: the role of fluctuations is enhanced in two dimensions, in fact fluctuations destroy the off-diagonal long-range order at any finite temperature and it has been demonstrated that the equation of state, even at T=0, requires the inclusion of fluctuations in order to correctly recover the composite boson limit in the deep-BEC regime. In this Thesis, based on the results published in Ref. [3], we investigate the Berezinskii-Kosterlitz-Thouless critical temperature, the first sound velocity and the second sound velocity. A comparison with experimental data for the critical temperature and the first sound shows very good agreement, confirming the enhanced role of fluctuations in lower

dimensionality and their fundamental relevance, particularly in the intermediate and BEC regimes.

- At last I derive a regularized equation of state in the deep-BEC limit, providing an analytical derivation of the relation

$$a_b = \frac{2}{3} a_s$$

between the scattering length of fermions a_s and that of the composite bosons a_b in the deep BEC limit. This result, based on Ref. [4], is in good agreement with other theoretical and Monte Carlo investigations and shows that the role of fluctuation is important in recovering a quantitatively correct composite boson limit even in three dimensions, the mean-field result being $a_b = 2a_s$.

As anticipated the subject of Chapter 5 is high-T_c superconducting cuprates. Materials in this class, the first of which was discovered in 1986, exhibit superconductivity up to very high temperatures, even exceeding 130 K in the case of $HgBa_2Ca_2Cu_3O_8$. Cuprates are still far from being completely understood from a theoretical point of view and there is no agreement on the microscopical pairing and superconductivity mechanisms, despite a great deal of experimental and theoretical efforts.

All cuprates are characterized by the presence of stacked CuO_2 planes, hence the name from Latin *cuprum*, copper, while the additional structures appearing between the planes change from material to material. The introduction of additional holes, or electrons in some materials, in the planes upon doping yields superconductivity. The critical temperature is maximum when the average concentration of additional holes is about 0.16 per lattice site.

It is commonly accepted that the physics of cuprates is essentially two-dimensional and that the main seat of superconductivity is to be found in the CuO_2 planes, the other structures and inter-layer couplings providing only higher order effects. Moreover many share the point of view that the $t - J$ model (large U limit of the Hubbard model) should be able to describe the relevant low-energy dynamics of cuprates.

In Chapter 5 I introduce and review a proposed solution consisting in a spin-charge gauge approach to high-T_c superconductivity and to the $t - J$ model, see Ref. [5] and references therein. This approach relies on a composite structure of the hole, which is decomposed as the product of a fermonic holon and a bosonic spinon. The particles are then bound to a gauge field providing a statistical flux, in a process analogous to Chern-Simons bosonization [6], allowing one to control the statistics for the holon and the spinon, subjected to the constraint that the hole must remain fermionic. However in two dimensions particles can have anyonic statistics, i.e. a particle exchange can introduce a phase shift in the many-body wavefunction, rather than just a ± 1 factor, resulting in a much wider range of choices.

The resulting scheme is very flexible, and can reproduce the slave-boson and the slave-fermion approaches as particular cases. Motivated by exact results obtained in one-dimensional systems, in the present work spinons and holons, dressed by their statistical flux, are semions, i.e. particles acquiring a $\pm$i factor upon exchange.

Within an an opportune approximated treatment superconductivity is achieved in three steps: at first a finite density of incoherent holon pairs is formed, and the correspondent crossover temperature is denoted by T_{ph}; at a lower crossover temperature a finite density of incoherent spinons pairs is formed, defining T_{ps}. Still the phase fluctuations destroy the coherence all the way down to a third, lower, critical temperature T_c, finally marking hole coherence and the full superconducting transition. With respect to the BCS-BEC crossover the composite nature of the hole leads to a composite approach to criticality, defining three different characteristic temperatures, the first two characterizing crossovers and the third a true phase transition. The pairing glue is provided by an emergent gauge field, as a result of an additional U(1) symmetry introduced by the spin-charge separation.

Within this framework I demonstrate the following properties, based on Ref. [7]:

- Holons and spinons give rise to two different contributions to the superfluid density ρ_s, respectively $\rho_{s,h}$ and $\rho_{s,s}$. They sum according to a Ioffe-Larkin-like composition rule:

$$\rho_s = \frac{\rho_{s,s}\rho_{s,h}}{\rho_{s,s} + \rho_{s,h}}.$$

- The superconducting transition is essentially of the 3D XY type; in particular the critical exponent for superfluid density is 2/3, in accordance with experimental data, but the three-dimensionality is not as a result of inter-layer coupling but of the intrinsic $2 + 1$-dimensional nature of the spinons. The whole temperature profile of superfluid density as derived within our formalism shows excellent agreement with experimental data in a broad doping range for moderate underdopings to the optimal doping region.

- The Uemura relation is essentially the empirical observation that, for underdoped cuprates, the zero-temperature superfluid density is proportional to the critical temperature. I provided an analytical derivation, showing that the spin-charge gauge approach is able to approximately reproduce the Uemura relation.

In particular it is worth noting that the spin-charge gauge approaches solves a dichotomy characterizing many experimental features of cuprates, i.e. the experimentally observed interplay between BCS-like and non-mean-field features. In the case of superfluid density the linear T-dependence of

superfluid density at low temperatures resembles BCS-like dynamics, however the non-mean-field critical exponent 2/3 observed in experiments is clearly not compatible with a BCS description and puts the transition in the 3D XY universality class. The Uemura relation is also at odds with a BCS-like description. In our approach holons and spinons contribute to the superfluid density according the Ioffe-Larkin-like composition rule, the holons being more relavant at low temperatures, modifying the low-temperature slope of ρ_s, the spinons being more relevant close to the critical temperature, determining the universality class of the transition. The experimental behavior is thus accurately reproduced.

Finally the superfluid density is used as a phenomenological tool to investigate the cuprate phase diagram. We identify, in opportunely normalized superfluid density data, three different universality classes which, we conjecture, can be interpreted and explained as three different coherence states of the spinon+holon system. An extension of the theoretical treatment for superfluid density away from the moderate to optimal doping region is the subject of currently ongoing work.

2

The BCS-BEC crossover

The main aim of this Chapter is the introduction of the BCS-BEC crossover, i.e. the continuous evolution observed in a fermionic system, when tuning the attractive fermion-fermion interaction, from a regime of weakly interacting Cooper pairs to a regime of strongly interacting tightly bound dimers. I shall cover the historical evolution that led to the development of the theory, starting from pioneering works in 1970s arriving at the current state-of-the-art theories motivated by the experimental realization of the crossover in ultracold Fermi atoms experiments, reviewing the most important experimental techniques employed in cooling and manipulating atoms, along with the major theoretical advances. In covering the history of the ideas of the BCS-BEC crossover I shall loosely follow the excellent account by some of the protagonists of this endeavor in Refs. [8–11].

2.1 The origins: superconductivity in Fermi systems and condensation in Bose systems

Before analyzing the BCS-BEC crossover it is worth introducing its parents, i.e. the Bardeen-Cooper-Schrieffer (BCS) theory of superconductivity and the Bose-Einstein condensation (BEC), which are the two main paradigms in the understanding of superconductivity and superfluidity [12].

The BCS theory, giving a fully microscopical explanation to the phenomenon of pairing leading to "conventional" superconductivity[1], as observed

[1]The term "classical" or "conventional" superconductor refers to a class of superconductive materials whose behavior exhibit a wide range of shared characteristics: the transition temperature T_c is much smaller than the Fermi temperature, the non-superconducting

e.g. in most elemental superconductors, is one of the greatest theoretical advances in Physics in the second half of the 20th century. First fully formulated in 1957 by J. Bardeen, L. Cooper and J. R. Schrieffer [14], the BCS theory explained a phenomenon observed more than half a century earlier, in 1911, by H. Kamerlingh Onnes[2].

We start from the Hamiltonian describing a number of atoms, considering the dynamics of each single electron and the dynamics of the nuclei as a whole, introducing the Coulomb attraction between electrons and nuclei, and the Coulomb repulsion between electrons and between nuclei:

$$\hat{H} = \sum_i \frac{\hat{p}_i^2}{2m} + \sum_\alpha \frac{\hat{P}_i^2}{2M_\alpha} + \frac{1}{2}\sum_{i\neq j} \frac{e^2}{|\hat{\mathbf{r}}_i - \hat{\mathbf{r}}_j|} + \frac{1}{2}\sum_{\alpha\neq\beta} \frac{Z_\alpha Z_\beta e^2}{|\hat{\mathbf{R}}_\alpha - \hat{\mathbf{R}}_\beta|} - \sum_{i\alpha} \frac{Z_\alpha e}{|\hat{\mathbf{r}}_i - \hat{\mathbf{R}}_\alpha|} \tag{2.1}$$

where latin indices run over the electrons, greek indices run over the nuclei, the $\hat{\mathbf{r}}$ and $\hat{\mathbf{p}}$ operators represent the position and momentum of each electron, while their uppercase counterpart refers to nuclei, m is the electron mass, M_α is the mass of the α-th nucleus and finally Z_α is the number of protons of the α-th nucleus. Virtually every problem in condensed matter[3] is encoded in the Hamiltonian in Eq. (2.1), which however is impossible to solve analytically, in fact even the most sophisticated numerical analyses can include at most tens or hundreds of atoms, while the typical number of particles in a condensed matter system is 10^{23}. The only way to proceed is clearly by approximation; in particular a simple but effective (to some extent) approximation can be derived by noting that as m and M_α are separated by at least three orders of magnitude, the dynamics of electrons and nuclei can be deemed as decoupled in first approximation, the so-called Born-Oppenheimer hypothesis [17].

Particularly in the case of metals one may consider a gas of conduction electrons moving over an average positive background: this is the jellium model [18]. The consequences of this approximation can be verified experimentally and the jellium model has been able to explain a number of experimentally-observed features [18], e.g. plasma frequency, response functions and the screening of the Coulomb interaction which modifies the usual Coulomb electron-electron potential adding an exponential tail:

$$V_{\mathrm{TF}} = \frac{1}{4\pi\epsilon_0}\frac{e^2}{|\mathbf{r}-\mathbf{r}'|} e^{-\frac{|\mathbf{r}-\mathbf{r}'|}{r_{\mathrm{TF}}}} \tag{2.2}$$

state above T_c is a normal electron gas, there are no other kinds of phase transitions, superconductivity is due to the formation of Cooper pairs, which in turn form by phonon exchange, see for instance [13]. "Conventional" materials are well described by usually the BCS theory, so that sometimes BCS and "conventional" are used interchangeably in the context of superconductivity.

[2] Kamerlingh Onnes' most significant original papers are collected in [15], a detailed historical account of the production of liquid helium which led to the discovery of superconductivity can be found in [16].

[3] Unless relativistic effects are relevant.

where r_{TF} is the Thomas-Fermi screening length. However the jellium model is not able to explain the superconductivity as observed for instance in elemental superconductors; one must somehow extend the approximation scheme in order to introduce the interaction of electrons with the crystal lattice. In fact a conduction electron traveling inside a metal can attract, due to the Coulomb interaction, the ions forming the crystal lattice, causing a small displacement in the crystal structure and creating a net positive charge. In turn another conduction electron may be at the same location at a later time, experiencing an indirect attraction due to the positive charge. This mechanism can be described as an effective phonon-mediated electron-electron attraction.

Critically the typical time scale of lattice vibrations is $\mathcal{O}\big(\omega_D^{-1}\big)$, ω_D being the Debye frequency. This time scale is way larger than the typical time scale associated to the motion of electrons $\mathcal{O}\big(\hbar\epsilon_F^{-1}\big)$, ϵ_F being the Fermi energy. As a consequence two electrons can interact through phonon exchange even when far away from each other, overcoming the Coulomb repulsion.

A very simplified model of this situation can be introduced with the following "toy" interaction potential

$$V_{\mathrm{eff}}(\mathbf{k},\mathbf{k}') = -|g_{\mathrm{eff}}|^2 \qquad \text{if } \epsilon_F - \hbar\omega_D \leq \frac{k^2}{2m}, \frac{k'^2}{2m} \leq \epsilon_F + \hbar\omega_D \tag{2.3}$$

describing the scattering between electron with momenta $\mathbf{k}$ and $\mathbf{k}'$, subjected to the conditions the electrons must be in the vicinity of the Fermi surface, otherwise they would not be available for scattering due to Pauli blocking, and that the energy transfer cannot be greater than the typical energy of lattice vibration, i.e. the Debye energy. The potential in Eq. (2.3) sketches only the basic feature, i.e. attraction, of more realistic treatments of electron-phonon interaction. The approximation turns out to be simple enough as to allow an analytical treatment, while being extremely accurate in describing the physics of superconductivity: in fact the complete BCS theory, building upon this approximation, predicts with quantitative accuracy many features of superconductivity in a wide range of materials [19].

The interaction term in the BCS Hamiltonian is then

$$\hat{H}_I = -|g_{\mathrm{eff}}|^2 \sum \hat{c}^\dagger_{\mathbf{k}_1+\mathbf{q},\sigma_1} \hat{c}^\dagger_{\mathbf{k}_2-\mathbf{q},\sigma_2} \hat{c}_{\mathbf{k}_1,\sigma_1} \hat{c}_{\mathbf{k_2}\sigma_2} \tag{2.4}$$

with obvious meaning of the momentum-space electron creation and annihilation operators, the sum being over the momenta $\mathbf{k}_1$, $\mathbf{k}_2$, $\mathbf{q}$ and the spin indices σ_1, σ_2 with the additional constraint

$$\epsilon_F - \hbar\omega_D \leq \epsilon \leq \epsilon_F + \hbar\omega_D \ , \tag{2.5}$$

i.e. the energy ϵ of each electron being confined in a $2\hbar\omega_D$ thick layer in the vicinity of the Fermi surface.

The next fundamental step in understanding the superconductivity phenomenon was done by Cooper [20], introducing the Cooper instability; he analyzed a simplified model consisting of two electrons interacting over a filled Fermi sea, demonstrating that an effective attractive electron-electron interaction, albeit small, can lead to the formation of a two-particle state, the Cooper pair. Moreover the Cooper pair is slightly energetically favorable, i.e. has slightly lower energy with respect to the Fermi level. Even if in most superconductors the attractive force is provided by the electron-phonon exchange, it is important noting that the Cooper instability mechanism works regardless of the origin of the attractive potential, in fact in ultracold atoms experiments Cooper pairs are realized as a result of an effective interaction tuned through a Feshbach resonance, see Section 2.3.

Cooper pairs are bosons, being composed of two fermions, and can condense at low enough temperature, the mechanism of Bose-Einstein condensation will be analyzed shortly. Electrons forming a Cooper pair are then radically different from "regular" conduction electrons in a metal, in particular they form a quantum state whose coherence extends up to a macroscopical level, this property being responsible for the features of a superconductor, in particular the peculiar resistance-less electric current flow.

The Bose-Einstein condensation, on the other hand, has a completely different history, the theoretical prediction of such a state given in 1924 by Bose and Einstein [21, 22] preceding its experimental observation by at least a decade: the superfluidity in ^{4}He firstly observed in 1938 [23, 24] can be explained in the framework of Bose-Einstein condensation at least qualitatively, even though the strong inter-particle interactions quantitatively modify the dynamics of the condensate. For a more direct observation of Bose-Einstein condensation one needs to go forward to 1995 when the Bose-Einstein condensation was observed in dilute vapors of rubidium and sodium [25, 26]. Recent advancements led to the observation of the Bose-Einstein condensation in a variety of bosonic systems, e.g. many different atomic species, molecules [27, 28], excitons [29, 30] and light [31].

It is worth noting [12] that particles that undergo Bose-Einstein condensation need to be bosons, i.e. carrying integer spin, and are most often[4] composite particles, introducing two different temperature scales, one associated with the formation of a composite bosonic object, T_p, where the subscript stands for "pairing", and one associated with the actual condensation, T_c, where the subscript stands for "critical" or "condensation"

Let us consider a system of non-interacting bosons of mass m at temperature T. The many-particle wave-function will be invariant upon the exchange of two coordinates

$$\Psi(\mathbf{r}_1, \mathbf{r}_2, \cdots, \mathbf{r}_N) = \Psi(\mathbf{r}_2, \mathbf{r}_1, \cdots, \mathbf{r}_N) \tag{2.6}$$

[4]This was always the case before the BEC of light [31].

Bose [21] first showed that the average occupation number of a system will be described by the Bose-Einstein distribution

$$n_{\mathbf{k}} = \frac{1}{e^{\beta(k^2/2m-\mu)} - 1} \,, \tag{2.7}$$

where $\beta \equiv (k_B T)^{-1}$ and k_B is the Boltzmann constant. The total number of particles for the system will then be

$$N = \sum_{\mathbf{k}} n_{\mathbf{k}} \approx \frac{V}{(2\pi)^3} \int \mathrm{d}^3 k \; n_{\mathbf{k}} \tag{2.8}$$

the second equality being valid in the limit of an infinitely extended system. Eq. (2.8) can be seen as a constraint to find μ given a certain N. In turn Einstein [22] showed that the statistical distribution in Eq. (2.7) implies that in a system of non-interacting bosons there will be critical temperature T_c defined by

$$T_c = \frac{2\pi\hbar^2}{k_B m} \left(\frac{n}{g_{3/2}(1)} \right)^{\frac{2}{3}} \,, \tag{2.9}$$

under which a macroscopical fraction of bosons will condense in the zero-momentum state; $g_{3/2}(1) = \zeta(3/2) \approx 2.612$. In the BCS case the Pauli exclusion principle forces all the low energy physics to happen at the Fermi level; of course this does not apply to a Bose system: the lowest energy, zero-momentum state will be occupied by a macroscopically large number of particles. In fact the condensate fraction, i.e. the ratio between the number of condensed particles and the total number of particles, is

$$\frac{N_0}{N} = 1 - \left(\frac{T}{T_c} \right)^{3/2} \tag{2.10}$$

It is worth stressing that the phase transition is purely quantum mechanical, and happens even in absence of particle-particle interactions, as opposed to most "conventional" phase transitions.

Leggett [13] advocates an alternative characterization of Bose-Einstein condensation, as originally proposed by Penrose and Onsager [32], by considering the eigenvalues of the one-particle density matrix

$$\rho_1(\mathbf{r}, \mathbf{r}') = \langle \psi^\dagger(\mathbf{r}) \psi^\dagger(\mathbf{r}') \rangle \tag{2.11}$$

where the $\psi^\dagger_\alpha(\mathbf{r})$ field operator creates a boson in position $\mathbf{r}$ and $\langle \# \rangle$ denotes the expectation value. The infinite-dimensional matrix $\rho_1(\mathbf{r}, \mathbf{r}')$ is by definition Hermitean and can thus be diagonalized having real eigenvalues, as

$$\rho_1(\mathbf{r}, \mathbf{r}') = \sum_i n_i \chi_i^*(\mathbf{r}) \chi_i(\mathbf{r}') \,. \tag{2.12}$$

and, intuitively, n_i can be regarded as the number of particle in the state described by $\chi_i^*(\mathbf{r})$. Following Penrose and Onsager [32] the system is said to be in a normal state if all the eigenvalues n_i are $\mathcal{O}(1)$, conversely the system is in a Bose-Einstein condensed state if one, or possibly more than one, of the eigenvalues is $\mathcal{O}(N)$, i.e. if one single state has macroscopical occupation. This has the advantage of naturally extending from the simple case of spinless bosons to more complicated cases. A spin index, or any other index referring to internal degrees of freedom of the particles, can be added to the position of the particle without loss of generality.

Moreover the definition in Eq. (2.13) naturally leads to the concept of off-diagonal long-range order (ODLRO) as a fundamental signal and characteristic of condensation [33]; in fact one may take the limit $\lim_{|\mathbf{r}-\mathbf{r}'|\to\infty} \rho_1(\mathbf{r},\mathbf{r}')$ in the single-particle density matrix in Eq. (2.12), observing that it factorizes as:

$$\lim_{|\mathbf{r}-\mathbf{r}'|\to\infty} \rho_1(\mathbf{r},\mathbf{r}') = \Psi^*(\mathbf{r}')\Psi(\mathbf{r}) \tag{2.13}$$

being non-zero only when the system is in a condensed state [33]: we related the macroscopical occupation of the ground state, a feature naturally defined in momentum space, to the non-decaying correlation at long distance, which is obviously observed in real space. In turn the ODLRO can be related to the gauge symmetry breaking, which is regarded by other as *the* fundamental signature of Bose-Einstein condensation [34–36].

2.2 The BCS-BEC crossover: an introduction

What does Bose-Einstein condensation have in common with the Bardeen-Cooper-Schrieffer theory of superconductivity? Let us go back for a moment to the BCS theory, one could think of it as essentially the condensation of Cooper pairs, which are bosonic objects, even if they are very extended in space, their typical dimensions being determined by the Pippard coherence length ξ_0 which typically is thousands of Å [37].

One could also imagine, in principle, of tuning the strength of the effective electron-electron interaction, making it stronger: clearly the Cooper pairs are going to shrink and end up, as the interaction is increased, forming tightly bound bosonic molecules. These molecules will follow the Bose-Einstein distribution and will condense below a certain critical temperature.

In both cases the condensation mechanism is due to Bose-Einstein condensation, however the Bose-Einstein condensation of Cooper pairs in the former case happens on top of a completely filled Fermi sea, at positive and finite chemical potential, while the BEC of bosonic molecules happens at the ground state and the bosonic chemical potential is zero. Even if the ultimate condensation mechanism is the same, and even if one can imagine continuously tuning the interaction "connecting" somehow one regime to

the other, clearly the two physical situations are profoundly different. The BCS-BEC crossover is essentially the continuous evolution in a fermionic system from a weakly-coupled BCS-like regime to a strongly-coupled regime which, eventually, undergoes Bose-Einstein condensation.

Let us try to shed more light on the phenomenon by extending the definition of condensation in Eq. (2.12) and in Eq. (2.13); Leggett's approach naturally generalizes to the whole BCS-BEC crossover [9], and the condensation can be defined as "the onset of a microscopical eigenvalue in the relevant reduced density matrix" [13], in particular in the case of fermions the relevant reduced density matrix is the two-particle density matrix

$$\rho_2(\mathbf{r}_1\sigma_1, \mathbf{r}_2\sigma_2, \mathbf{r}_3\sigma_3, \mathbf{r}_4\sigma_4) = \langle \psi^\dagger_{\sigma_1}(\mathbf{r}_1)\psi^\dagger_{\sigma_2}(\mathbf{r}_2)\psi_{\sigma_3}(\mathbf{r}_3)\psi_{\sigma_4}(\mathbf{r}_4)\rangle \tag{2.14}$$

where each $\psi^\dagger_\sigma(\mathbf{r})$ ($\psi^\dagger_\sigma(\mathbf{r})$) respectively creates (annihilates) a fermion with spin σ at position $\mathbf{r}$. Again, the reduced density matrix can be diagonalized with real eigenvalues, being Hermitean

$$\rho_2(\mathbf{r}_1\sigma_1, \mathbf{r}_2\sigma_2, \mathbf{r}_3\sigma_3, \mathbf{r}_4\sigma_4) = \sum_i n_i \chi_i(\mathbf{r}_1\sigma_1, \mathbf{r}_2\sigma_2)\chi^*_i(\mathbf{r}_3\sigma_3, \mathbf{r}_4\sigma_4) \tag{2.15}$$

and the highest eigenvalue n_i corresponds to the occupation of the lowest energy state, signaling the condensation if $\mathcal{O}(N)$ [38].

Following the approach in Ref. [33] one introduces the center of mass coordinates for each fermionic pair $\mathbf{R} \equiv (\mathbf{r}_1 + \mathbf{r}_2)/2$ and $\mathbf{R}' \equiv (\mathbf{r}_3 + \mathbf{r}_4)/2$ along with the relative distances $\mathbf{r} = \mathbf{r}_1 - \mathbf{r}_2$, $\mathbf{r}' = \mathbf{r}_3 - \mathbf{r}_4$. In presence of ODLRO the two-particle density matrix factorizes

$$\lim_{|\mathbf{R}-\mathbf{R}'|\to\infty} \rho_2(\mathbf{r}_1\uparrow, \mathbf{r}_2\downarrow, \mathbf{r}_3\uparrow, \mathbf{r}_4\downarrow) = F^*(\mathbf{r})F(\mathbf{r}') \,, \tag{2.16}$$

with $F(\mathbf{r}) = \langle \psi_\uparrow(\mathbf{r}/2)\psi_\downarrow(-\mathbf{r}/2)\rangle$, the limit being taken as the distance between the centers of the fermionic pairs $\mathbf{R}$ and $\mathbf{R}'$ goes to infinity, keeping however the fermionic pair sizes $\mathbf{r}$ and $\mathbf{r}'$ are finite. By analogy with the purely bosonic case in Eq. (2.13), it is easily seen that $F \neq 0$ implies Bose condensation, moreover by noting that F is the wave function of a Cooper pair one can conclude that condensation in a fermionic system essentially originates "from pairs of fermions forming Bose-Einstein degeneracy" [33]. In addition to that F can be related [13] to the condensate fraction of the system as follows

$$N_0 = 2\int \mathrm{d}\mathbf{r}\, |F(\mathbf{r})|^2 \tag{2.17}$$

and the condensate fraction will be object of extensive study in the context of an unbalanced Fermi gas in the present thesis in Chapter 3.

A natural and compelling question one would ask is the following: is it possible to experimentally realize this situation, in which the attractive fermion-fermion interaction can be tuned at one's will? It is extremely rare,

even in other subfields of Physics, to be able to tune the interaction of a system; for instance the vast majority of superconductors or superfluid systems lie either in the BCS or in BEC limit and it is not possible to modify the inter-particle interaction. The same happens in High Energy Physics, as the interaction vertexes of the Standard Model are fixed, and in Nuclear Physics.

The possibility of using ultracold Fermi atoms in order to realize a system whose interaction can be tuned is quite recent, dating back to 2004. Given these premises one may say that the issue of the BCS-BEC crossover would have been interesting only from a theoretical or conceptual point of view, nonetheless pioneering works in this field date back as far as the 1960s when independently Keldysh, Yang and Popov [33, 39, 40] studied the possibility of Bose condensation of paired fermions.

Subsequently Eagles [41] considered Zr-doped $SrTiO_3$, both in bulk and in thin films, observing that the usual assumption of the BCS theory $\epsilon_F \gg \hbar\omega_D$, where ϵ_F is the Fermi energy and ω_D is the Debye cutoff energy, does not apply to this system when the carrier concentration is sufficiently low. The carrier concentration can parametrize the crossover, and Eagles remarkably pointed out that the number equation and the gap equation need to be solved together self-consistently, after relaxing the constraint that the chemical potential should equal the Fermi energy, moreover he argued abandoning the BCS limit implies that pairing and condensation need not to happen at the same time, a consequence of the theory being that pairing without superconductivity is allowed. Another pioneering work is due to Leggett [42] who, motivated by the study of ^{3}He systems, noted that the weak-coupling BCS description of pairing can be extended to the strong coupling regime.

A fundamental characteristic of a BCS-like theory is that pairing and condensation are achieved at the same time, in other words, as the Cooper pairs by are by construction of the BCS trial wavefunction in a zero-momentum state, as soon as they are formed they collapse to the ground state. As soon as one increases the interaction away from the BCS limit it is clear that there is no reason for the pairing temperature and the condensation temperature to coincide; in fact the pairing temperature T^* grows unbounded as the BEC regime is approached, while the critical temperature T_c, determined by the condensation, approaches the constant value $k_B T_c \approx 0.218\epsilon_F$ [43].

The finite temperature properties of the BCS-BEC crossover, in particular the critical temperature, have been first studied in a pioneering work by Nozières and Schmitt-Rink [44] showing that, while the mean-field theory can describe the crossover at $T = 0$, finite-temperature effects are to be studied including order-parameter fluctuations[5]; they determined the critical

[5]The mean-field theory and the contribution of the fluctuations in different contexts are one of the main subjects of the present Thesis and will be thoroughly analyzed in Chapter 3 and in Chapter 4.

temperature as a function of the coupling showing that it evolves smoothly from the BCS limit to the BEC limit. Further investigations and refinements of the theory led to the complete determination of the phase diagram for the BCS-BEC crossover [43, 45], as reported in Fig. 2.1 and currently theoretical predictions quantitatively reproduce uniform and trapped Fermi gases across the crossover with great accuracy [46]. Referring to Fig. 2.1, as expected, the pairing temperature T^* coincides with the condensation temperature T_c only in the deep BCS limit. Below T_c the Fermi gas evolves from a BCS-like state of Cooper pairs, which are coherent in momentum space, to the BEC limit where fermions pair forming tightly bound bosonic molecules before condensing; above T_c we observe that T^* divides the normal Fermi liquid state, composed of unpaired fermions, from the Bose liquid state, where bosonic molecules are formed but not yet condensed. The whole crossover is parametrized as customary by the dimensionless quantity $y = (k_F a_s)^{-1}$, $k_F = (3\pi^2 n)^{1/3}$ being the Fermi momentum and a_s being the s-wave scattering length of the fermion-fermion potential. Strictly speaking usually the crossover region is determined by the condition $-1 \lesssim y \lesssim 1$, while the regions $y \gtrsim 1$ ($y \lesssim -1$) correspond, respectively, to the BEC (BCS) regimes.

It is worth noting that these theoretical investigations were pursued way before the advent of cool atoms experiments; however further motivation to investigate the intermediate pairing regime was given by the discovery [47] in 1986 of high-T_c superconductivity in cuprates and by the profusion of work that followed, both experimental investigations and theoretical attempts to explain the microscopical superconductivity mechanism. The observation that the correlation length for these materials is far smaller than the BCS one but still much greater than the coherence length of a Bose-Einstein condensate, puts them in the crossover regime and, even if the microscopical mechanism leading to superconductivity in cuprates is still not understood, hints to the fact that the physics of the BCS-BEC crossover may be relevant for cuprates.

However, in the very same years the road for the realization of cool atoms experiments was being paved, as the techniques for cooling and manipulating atoms were devised. A full analysis of these techniques would exceed the scope of the present thesis, however I shall briefly review the cooling techniques, the trapping techniques and the role of the Feshbach resonance.

2.3 A review of experimental techniques

When approaching the absolute zero, $T = -273.15°\mathrm{C}$ all the elements with the exception of Helium are in a solid state [48]. However it is possible to bring dilute atomic vapors to a metastable phase provided that the condition

$$\tau_3 \ll \tau_2 \tag{2.18}$$

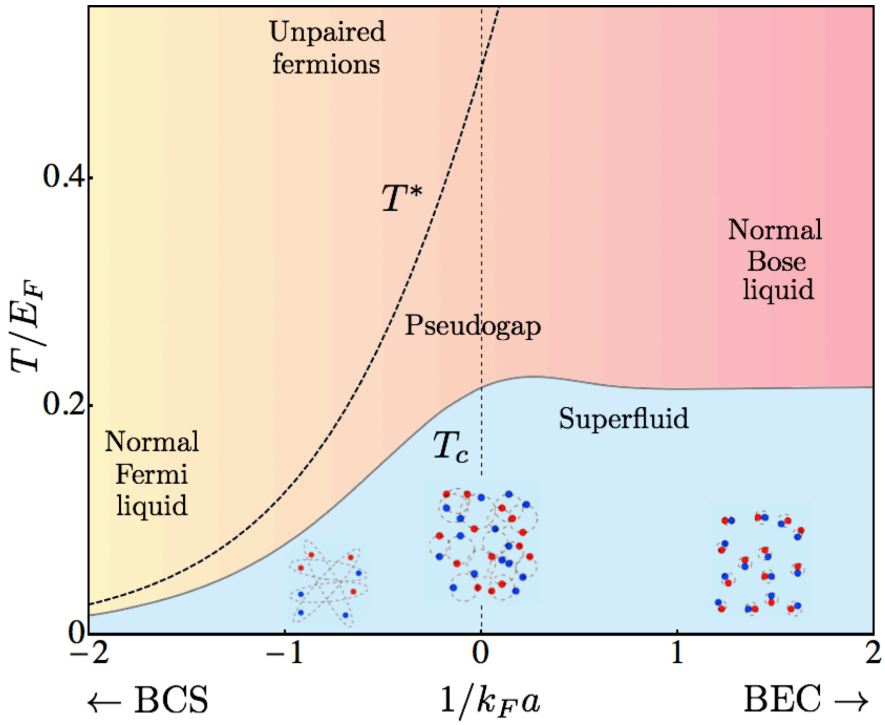

Figure 2.1: The phase diagram for the three-dimensional BCS-BEC crossover: the light blue area marks the superfluid phase, below the critical temperature T_c. The dashed line marks the pairing temperature T_p which coincides with T_c in the BCS limit. From [11].

holds, where $\tau_2 \sim n^2$ is the two-body scattering rate and $\tau_3 \sim n^3$ is the three-body recombination rate [49]. If the density is low enough the metastable phase lifetime allows for experiments to be carried out. Typical values for temperature and density of this metastable state are $T \sim 50\text{nK}$ and $n \sim 5 \cdot 10^{12}\text{cm}^{-3}$.

The majority of experiments regarding ultracold atoms is carried out using alkali atoms: these atomic species are chosen because of their simple electronic structure, which in turns yields a simple hyperfine structure: one single valence electron populates the outermost shell, on top of a completely filled shell, so that the electronic spin will be $S = 1/2$ and the only valence electron will be in the lowest angular momentum state, i.e. $\mathbf{L} = 0$. The total electronic angular momentum is $\mathbf{J} = \mathbf{S} + \mathbf{L}$, and summing it to the nuclear spin $\mathbf{I}$ one obtains the total angular momentum for the atom

$$\mathbf{F} = \mathbf{J} + \mathbf{I}\,. \tag{2.19}$$

Clearly either $F = I - 1/2$ or $F = I + 1/2$. It follows that in an alkali atom the total spin is determined by the nuclear spin: the atom will be a composite

boson if I is half-integer, i.e. for a odd number of nucleons, on the other hand it will be a composite fermion if I is integer, i.e. for an even number of nucleons. The atomic species ^{6}Li and ^{40}K are by far the most used in ultracold experiments: they have an even number of nucleons and consequently integer nuclear spin, so being composite fermions. Their hyperfine structure is shown in Fig. 2.2; at zero external magnetic field only the hyperfine $F = I \pm 1/2$ splitting is observed, in presence of a magnetic field the doublet splits into $(2S+1)(2I+1) = 4I+2$ different states [10].

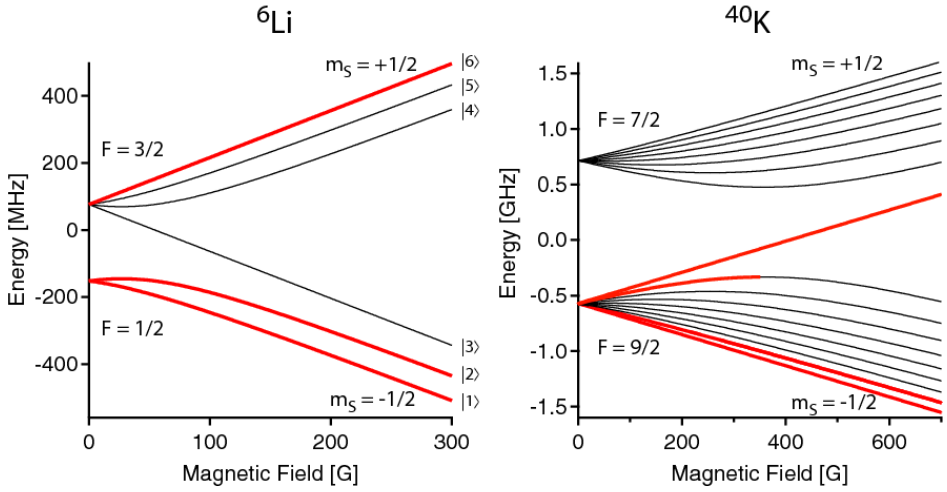

Figure 2.2: The hyperfine structure of ^{6}Li and ^{40}K as a function of the magnetic field, from Ref. [10].

The main experimental requirement in order to observe quantum degeneracy in atomic vapors is a low temperature; to be more quantitative we define the de Broglie thermal wavelength

$$\lambda_{\mathrm{dB}} = \frac{h}{\sqrt{2\pi m k_B T}} , \tag{2.20}$$

where h is Planck constant, k_B is Boltzmann constant, T is the temperature of the system and m is the mass of the particle for which the de Broglie wavelength is defined. One expects quantum effects to be relevant once the de Broglie thermal wavelength is of the same order of the interparticle separation $\ell = n^{-1/3}$. For instance, a gas of bosons the BEC condition in Eq. (2.9) can be rewritten as $n\lambda_{\mathrm{dB}}^3 \geq 2.612$. More generally and slightly less precisely the phase space density ρ defined as

$$\rho = n\lambda_{\mathrm{dB}}^3 \tag{2.21}$$

is often used [50] to estimate when quantum effect are relevant, using the condition $\rho \sim 1$. For this reason one will search for a low-temperature

limit; one may also think of increasing the density, however the metastability constraint in Eq. (2.18) forbids one from doing so, otherwise three-body recombination processes would destroy the system.

Let us now briefly review how an ultracold gas is realized experimentally. Typically at first an atomic beam is generated from an oven, at temperature in the order of magnitude of 500 K. The temperature is then drastically lowered through laser cooling. Let us consider an atom interacting with a laser beam, whose wavelength corresponds exactly to an absorption line of the atom: the atom can absorb a photon, by stimulated absorption, which will be emitted shortly after in a random direction. The net effect of this process is not going to modify the average kinetic energy of the atoms as a whole, as some of them will be accelerated, while other will be slowed down. However if we tune the laser beam frequency just below an absorption line, atom coming towards the light source will see the light, by Doppler effect, closer to the absorption frequency and will interact with the beam at an increased rate with respect to atoms moving away from the light source. By using six different laser beams, one for each direction, every atom will be slowed, on average, regardless of its initial direction. The fundamental introduction of laser cooling opened the way to the realization of ultracold atoms experiments and led, along with other cooling and trapping methods, to the award of the 1997 Nobel Prize for Physics to S. Chu [51], to C. Cohen-Tannoudji [52] and to W. D. Phillips [53].

At last the temperature is finally lowered using evaporative cooling: the potential well keeping the condensate-to-be in place is lowered to the point that some particle can escape from it: on average a number of highly energetic particles will escape due a higher kinetic energy, while the lower energetic particles will mostly stay inside the well. The potential well is then raised again to confine the condensate so that the particles can rethermalize to a lower temperature; in the end only the least energetic atoms have remained inside: the temperature will be lower.

Evaporative cooling is very effective in lowering the temperature of an atomic gas and is the only method through which, at the time of writing, degeneracy has been achieved in ultracold Fermi gas. However problems may arise, as an atomic gas is a metastable state, whose lifetime needs to be much longer than the time required for the most energetic component to evaporate. For this reason evaporative cooling is used only as the last cooling stage, and is enhanced being used in combination either with laser cooling or with radio-frequency induced evaporation [54].

In order to keep the condensate in place it must be trapped, a widely used trapping technique being magnetic trapping; the potential energy of an atom whose magnetic moment is $\boldsymbol{\mu}_m$ within an external magnetic field $\mathbf{B}$ is

$$U = -\boldsymbol{\mu}_m \cdot \mathbf{B} \tag{2.22}$$

and if the magnetic field is not uniform will exert a force on the atom. Atoms

can be classified in high-field seekers and low-field seekers accordingly to their propensity of going towards areas with higher or lower magnetic field, this characteristic being determined by the z component of the angular momentum F. It turns out it is possible to create a magnetic field with a minimum, trapping low-field seekers atoms. Usually magnetic techniques are used to keep in place the bulk of the condensate, while finer manipulations are implemented using optical techniques. Let us consider an atom placed into a laser beam; the oscillating electric field $E(\mathbf{r})$ will induce a dipole moment in the atom, while coupling at the same time with the dipole itself [55, 56], resulting in the following trapping potential

$$U(\mathbf{r}) = -\frac{1}{2}\langle \mathbf{d} \cdot \mathbf{E}(\mathbf{r}) \rangle \approx -\frac{1}{2}\alpha(\omega)\langle E^2(\mathbf{r}) \rangle \tag{2.23}$$

where $\mathbf{d} = \alpha(\omega)\mathbf{E}$ is the induced dipole moment, $\alpha(\omega)$ is the atomic polarizability of each atom as a function of the angular frequency ω and the angular brackets denote the time average. It follows that the oscillating electric field will exert a force on each atom proportional to the square of the electric field, moreover two interfering laser beams will create a constant intensity configuration, resulting in a constant periodic potential. For high enough intensity values the totality of the atoms will stay near the minimum of the standing wave, for lower intensities hopping between different minima will be allowed, obtaining an optical lattice [56]. Usually magnetic and optical trapping techniques are used together in a single device, the so-called MOT (magneto-optical trap).

The last ingredient needed to realize the BCS-BEC crossover in ultracold Fermi atoms is the possibility of tuning the atomic scattering length with continuity, which is possible through a Feshbach resonance: let us start by considering two identical alkali atoms in two different hyperfine states, scattering in the s-wave (open) channel, interacting through a potential $V_{\mathrm{bg}}(\mathbf{r})$ which is a function of the relative distance. Due to the high magnetic field typically used in ultracold atoms experiments, for instance in the case of ^{6}Li analyzed in Fig. 2.2 one can consider the atoms to be essentially completely polarized in the direction of the external magnetic field[6].

However it is in principle possible to have a spin singlet bound state, formed by a spin-up and a spin-down fermion; in this case two fermions will interact through a different potential which needs to support at least a bound state. This scattering channel is often called the "closed channel", see Fig. 2.3. The hyperfine interaction can trade nuclear spin for electron spin, effectively connecting the open and closed channel, allowing resonant tunneling [8].

The closed and open channel will have different spin configurations, so that by tuning the external magnetic field it will be possible to tune the energy of the bound state E_c, making it arbitrarily close to the open channel

[6]Without this simplifying assumption the theoretical description of the Feshbach resonance is just slightly more complicated, see for instance Ref. [57].

energy and almost degenerate, as outlined in Fig. 2.3. We call the energy difference between the bound state and the open channel the detuning and denote it with ν. As ν approaches zero the mixing between the open and closed channel will be very strong, strongly enhancing the cross-section. As E_c is varied crossing the zero energy threshold, as measured from the open channel, it can be shown that the effective scattering length goes from $+\infty$, when $E_c = 0^-$ to $-\infty$ when $E_c = 0^+$.

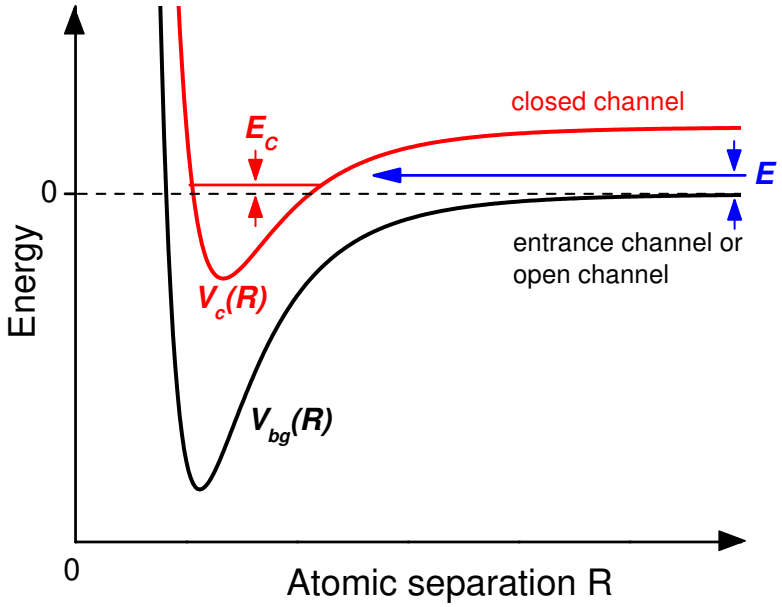

Figure 2.3: Feshbach resonance: the open and closed channel, the first (resonant) bound state in the closed channel is shown at energy E_c. The energy E_c can be varied w.r.t. the energy of the open channel by tuning the external magnetic field. From Ref. [58].

A precise description of this physical situation can be given by writing down the two-channel Hamiltonian for a system of interacting fermions across a Feshbach resonance [59]

$$\hat{H} = \sum_{\mathbf{k},\sigma} \epsilon_{\mathbf{k}} \hat{a}^\dagger_{\mathbf{k},\sigma} \hat{a}_{\mathbf{k},\sigma} + \sum_{\mathbf{q}} \left(\frac{\epsilon_{\mathbf{q}}}{2} + \nu \right) \hat{b}^\dagger_{\mathbf{q}} \hat{b}_{\mathbf{q}} + \sum_{\mathbf{q},\mathbf{k}} g_{\mathbf{k}} \left(\hat{b}^\dagger_{\mathbf{q}} \hat{a}_{\mathbf{q}/2-\mathbf{k},\downarrow} \hat{a}_{\mathbf{q}/2+\mathbf{k},\uparrow} + h.c. \right) \tag{2.24}$$

where the $\hat{a}$ ($\hat{a}^\dagger$) operators annihilate (create) a particle representing an atom in the open channel, respectively, whereas the $\hat{b}$ ($\hat{b}^\dagger$) operators annihilate (create) a molecule in the closed channel, respectively. The $g_{\mathbf{k}}$ matrix elements contains the details of the open channel-closed channel interaction and $\epsilon_{\mathbf{k}} = k^2/2m$. It can be shown this the Hamiltonian can be reduced to a single-

channel one [59]

$$\hat{H} = \sum_{\mathbf{k},\sigma} \epsilon_{\mathbf{k}} \hat{c}^{\dagger}_{\mathbf{k},\sigma} \hat{c}_{\mathbf{k},\sigma} + \sum_{\mathbf{q},\mathbf{k},\mathbf{k}'} U_{\mathbf{k},\mathbf{k}'} \hat{c}^{\dagger}_{\mathbf{q}/2+\mathbf{k},\uparrow} \hat{c}^{\dagger}_{\mathbf{q}/2-\mathbf{k},\downarrow} \hat{c}_{\mathbf{q}/2-\mathbf{k}',\downarrow} \hat{c}_{\mathbf{q}/2+\mathbf{k}',\uparrow} \,, \quad (2.25)$$

with an effective single-channel potential $U_{\mathbf{k},\mathbf{k}'}$ which will be a function of the original inter-channel potential and of the detuning ν [59]. This picture is valid if resonance is broad[7], for a narrow resonance the original two-channel treatment must be retained [60]. As the bound state in the closed channel is tuned the fermion-fermion scattering length changes as follows [58]:

$$a = a_{\mathrm{bg}} \left(1 - \frac{\Delta B}{B - B_0} \right) \quad (2.26)$$

where a_{bg} is the background scattering length, i.e. the scattering length without the Feshbach resonance, ΔB is the resonance width and B_0 is the position of the resonance. In the case of ^{6}Li the parameters of the most widely used resonance are [50]: $B_0 = 834G$, $B_0 + \Delta B = 534G$, $a_{\mathrm{bg}} = -1405 a_0$. The final result is that the scattering length of the interatomic potential can be changed just by tuning the magnetic field, in other words the magnetic field is exactly the turning knob needed in order to have a widely tunable interaction, allowing the BCS-BEC crossover.

We conclude this introductory Chapter with a final remark: it is hard to overstate the importance and unicity of this situation: in most physical systems the coupling constants are predetermined and can not be modified at one's will. The possibility of modifying the atomic scattering length using a Feshbach resonance is exceptional and makes ultracold Fermi gases the perfect workhorse for an enormous number of experiments. Throughout the years a plethora of experiments have been carried out manipulating ultracold atoms in many different ways, for instance:

- Additional confinements can be added, extending the idea of optical trapping, and in particular a gas can be trapped in quasi-2D configurations or in optical lattices [56]. A two-dimensional Fermi gas will be analyzed in this Thesis in Chapter 4.
- The polarization can be varied, by modifying the number of atoms in each spin state [61]. The condensate fraction for a spin-unbalanced Fermi gas will be analyzed in this Thesis in Chapter 3.
- Heteronuclear mixtures have been studied, observing the interaction of different atomic species with different mass [62].
- One could use atomic species with a strong dipolar momentum, observing novel features owing to the dipole-dipole long-range interactions [63].

[7] The notion of broad or narrow Feshbach resonance is defined comparing the resonance width ΔB, which will be introduced in Eq. (2.26), with the Fermi energy.

- Imaging techniques evolved as rapidly as manipulation techniques, leading, for instance, to the spectacular imaging of vortices in a superfluid [64].

This incomplete list outlines only the major and most important features; one should also remember that, besides equilibrium properties, recently many out-of-equilibrium properties of ultracold Fermi gases have also been investigated [62].

3

Mean-field treatment for the BCS-BEC crossover

In this Chapter we develop the mean-field treatment of an ultracold Fermi gas across the BCS-BEC crossover, as introduced in the previous Chapter. The introductory part follows the classic approach to the theory of the BCS-BEC crossover [13, 36, 65]; an equivalent path integral formulation is introduced mainly based on Refs. [66, 67]; this approach may not seem advantageous at mean-field level, however it allows for a clear and fast derivation of the contribution of Gaussian fluctuations of the order parameter, which will be introduced in Chapter 4.

The last Section, dealing with the condensate fraction [38, 68] of an unbalanced Fermi gas represents original research work carried out during my Ph.D. and published in Ref. [1].

3.1 Introduction: the extended BCS Hamiltonian

Let us consider a dilute, uniform, ultracold Fermi gas consisting of N fermions in two different hyperfine spin states. Each spin state is labeled by the pseudo-spin index $\sigma = \uparrow, \downarrow$, the gas is contained in a volume L^3 and is described within the grand-canonical ensemble at fixed chemical potential μ. We use the one-channel model as analyzed in Eq. (2.25). Within the second quantization formalism the Hamiltonian describing the system is the sum of a kinetic term

and an interaction term, namely $\hat{H} = \hat{T} + \hat{V}$ with $\hat{T}$ and $\hat{V}$ defined as follows:

$$\hat{T} = \sum_{\sigma=\uparrow,\downarrow} \int_{L^3} \mathrm{d}^3 r \; \hat{\psi}^\dagger_\sigma (\mathbf{r}) \left(-\frac{\hbar^2}{2m} \nabla^2 - \mu \right) \hat{\psi}_\sigma (\mathbf{r})$$
$$\hat{V} = \int \mathrm{d}^3 r \mathrm{d}^3 r' \; \hat{\psi}^\dagger{}_\uparrow (\mathbf{r}) \, \hat{\psi}^\dagger{}_\downarrow (\mathbf{r}') \, V (\mathbf{r} - \mathbf{r}') \, \hat{\psi}_\downarrow (\mathbf{r}') \, \hat{\psi}_\uparrow (\mathbf{r}) \; , \tag{3.1}$$

where the field operators $\hat{\psi}_\sigma (\mathbf{r})$ and $\hat{\psi}^\dagger_\sigma (\mathbf{r})$ respectively annihilate and create a fermion at position $\mathbf{r}$ with pseudo-spin[1] σ, m is the mass of each fermion and the integral is extended over a volume L^3. The first term $\hat{T}$ is simply the free Hamiltonian for a system of non-interacting fermions, while the second term $\hat{V}$ describes a generic interaction between opposite-spin fermions, scattering through a generic potential $V(\mathbf{r} - \mathbf{r}')$.

We introduce the particle number [69]

$$N = nL^3 = \sum_\sigma \int_{L^3} \mathrm{d}^3 r \; \langle \hat{\psi}^\dagger_\sigma (\mathbf{r}) \hat{\psi}_\sigma (\mathbf{r}) \rangle \tag{3.2}$$

which is most often fixed in experiments, and can be used as a constraint to fix the chemical potential μ. We also introduce the Fourier anti-transform for the fermionic field operators[2]:

$$\hat{\psi}_\sigma (\mathbf{r}) = \frac{1}{L^{3/2}} \sum_{\mathbf{k}} e^{\mathrm{i}\mathbf{k}\cdot\mathbf{r}} \hat{c}_{\mathbf{k},\sigma} \; , \tag{3.3}$$

relating them to their momentum space counterparts. Eq. (3.3) can be used to rewrite the interaction term as a momentum space sum:

$$\hat{V} = \frac{1}{L^3} \sum_{\mathbf{k},\mathbf{k}',\mathbf{q}} V_{\mathbf{k},\mathbf{k}'} \hat{c}^\dagger_{\mathbf{k}'+\mathbf{q}\uparrow} \hat{c}^\dagger_{-\mathbf{k}'\downarrow} \hat{c}_{-\mathbf{k}+\mathbf{q}\downarrow} \hat{c}_{\mathbf{k}\uparrow} \; . \tag{3.4}$$

having defined the matrix elements of the potential in momentum space, i.e.

$$V_{\mathbf{k},\mathbf{k}'} = \int_{L^3} \mathrm{d}^3 r \; e^{\mathrm{i}(\mathbf{k}-\mathbf{k}')\cdot\mathbf{r}} V(\mathbf{r}) \; . \tag{3.5}$$

We now replace the generic potential with a simple s-wave contact potential; by setting $V (\mathbf{r} - \mathbf{r}') = g_0 \; \delta^{(3)} (\mathbf{r} - \mathbf{r}')$ in the interaction term in Eq. (3.1), one obtains

$$\hat{V} = \int_{L^3} \mathrm{d}^3 r \; g_0 \hat{\psi}^\dagger{}_\uparrow (\mathbf{r}) \, \hat{\psi}^\dagger{}_\downarrow (\mathbf{r}) \, \hat{\psi}_\downarrow (\mathbf{r}) \, \hat{\psi}_\uparrow (\mathbf{r}) \tag{3.6}$$

[1] From now on for simplicity's sake the pseudo-spin will often be called spin, with a slight abuse of terminology.

[2] We write the equation for the annihilation operator, the equation for the creation operator being the Hermitean conjugate.

where $g_0 < 0$ is the strength attractive interaction; its physical significance will be analyzed later in Section 3.4, by relating g_0 to observable quantities. In momentum space one finds that for the contact potential $V_{\mathbf{k},\mathbf{k}} = g_0$, and the interaction term of the Hamiltonian reads

$$\hat{V} = \frac{g_0}{L^3} \sum_{\mathbf{k},\mathbf{k}',\mathbf{q}} \hat{c}^\dagger_{\mathbf{k}'+\mathbf{q}\uparrow} \hat{c}^\dagger_{-\mathbf{k}'\downarrow} \hat{c}_{-\mathbf{k}+\mathbf{q}\downarrow} \hat{c}_{\mathbf{k}\uparrow} \tag{3.7}$$

Obviously the interatomic potential is generally different from this approximation, which is only valid as long as gas is dilute; more quantitatively such an approximation holds if the diluteness condition is satisfied, i.e. if $k_F R \ll 1$ where k_F is the Fermi momentum and R is the typical potential range [70]. In a three-dimensional Fermi gas the Fermi energy is related to the Fermi wavevector k_F and to the density n as

$$\epsilon_F = \frac{\hbar^2 k_F^2}{2m} = \frac{\hbar^2 (3\pi^2 n)^{2/3}}{2m} \tag{3.8}$$

so that $k_F \propto n^{1/3}$. Introducing the average inter-particle spacing

$$\ell = n^{-1/3} \tag{3.9}$$

the diluteness condition can be rewritten as $R \ll \ell$, i.e. the requirement that the potential range is much smaller than the average atomic separation. The diluteness condition is tantamount to requiring that the physics of the system is dominated by two-body encounters and that the scattering length a_s, which regulates low-energy two-body scattering processes, is the only relevant quantity in the description of the interaction [48].

In principle the interaction term in Eq. (3.4) allows scattering processes with arbitrary momentum transfer, the Feynman diagram corresponding to the interaction term is shown if Fig. 3.1; however the so-called pairing Ansatz only takes into account the scattering between states with opposite momentum, with zero momentum transfer: how can this assumption be justified?

In the case of a weakly-interacting Fermi gas, having a well defined Fermi surface, one can consider that for $\mathbf{q} = 0$ the density of states is maximum, as any electron on the Fermi surface can scatter with a diametrically opposed electron. On the other hand, if some momentum is transferred in the scattering process the density of states is reduced, due Pauli blocking implying that states below the Fermi surface are unavailable [10].

However the scope of applicability of the pairing Ansatz is way greater, its validity extending to the whole zero-temperature BCS-BEC crossover, being able to give a comprehensive description [42, 69] of the evolution at $T = 0$ from the weak-coupling BCS limit to the strong-coupling BEC regime, through a continuous evolution [42, 71] without thermodynamics transitions. In fact, under the additional assumption of working at zero temperature,

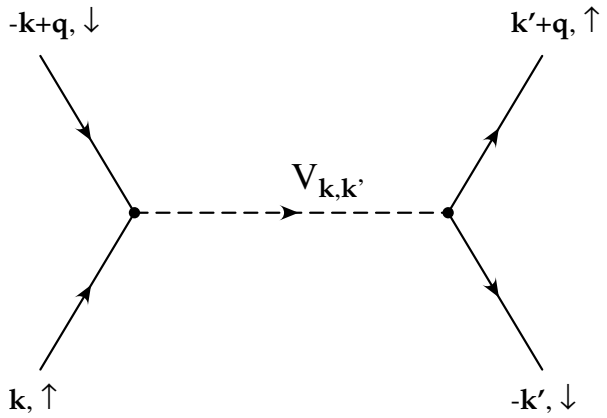

Figure 3.1: The scattering between two opposite-spin atoms, interacting through a generic potential with matrix elements in momentum space $V_{\mathbf{k},\mathbf{k}'}$. The pairing Ansatz considers only scattering between opposite-momentum states, with $\mathbf{q} = 0$, i.e. zero transferred momentum.

the condition that pairing must happen in the zero-momentum state is not restrictive [10].

We also anticipate that the many-particle ground state[3] constructed from zero-momentum pairs, as a consequence of the pairing Ansatz, besides correctly describing a filled Fermi sea typical of the BCS limit at $T = 0$, will also be able to describe tightly bound dimers characterizing the BEC limit at $T = 0$, justifying *a posteriori* the extension of the pairing Ansatz and of the BCS-like treatment to the whole crossover.

We can then take the interaction term as derived above in the $\mathbf{q} \to 0$ limit:

$$\sum_{\mathbf{k}\mathbf{k}'\mathbf{q}} c^{\dagger}_{\mathbf{k}+\mathbf{q},\uparrow} c^{\dagger}_{-\mathbf{k}\downarrow} c_{-\mathbf{k}'+\mathbf{q}\downarrow} c_{\mathbf{k}'\uparrow} \longrightarrow \sum_{\mathbf{k}\mathbf{k}'} c^{\dagger}_{\mathbf{k},\uparrow} c^{\dagger}_{-\mathbf{k}\downarrow} c_{-\mathbf{k}'\downarrow} c_{\mathbf{k}'\uparrow} \,. \tag{3.10}$$

In order to be able to treat the quartic interaction we introduce[4] the order parameter as follows [65]:

$$\Delta_0 = -\frac{g_0}{L^3} \sum_{\mathbf{k}} \langle c_{-\mathbf{k}\downarrow} c_{\mathbf{k}\uparrow} \rangle \,. \tag{3.11}$$

Clearly the expectation value of the $c_{-\mathbf{k}\downarrow} c_{\mathbf{k}\uparrow}$ operator should be zero over a state with a definite number of particles, in particular it will be zero when acting on the normal state; as we will see shortly the operator has, on the other hand, a finite value when its expectation value is calculated over the BCS ground state, signaling the appearance of a finite density of

[3] To be introduced in Section 3.2.

[4] An alternative and equivalent formulation will be introduced with the path integral formalism, by performing a Hubbard-Stratonovich transformation in the Cooper channel, neglecting then the fluctuations of the auxiliary Cooper field.

Cooper pairs. In the weak-coupling limit, when paring and condensation are achieved at the same temperature, Δ_0 can also serve at the order parameter of the superconducting transition; with a slight abuse of language Δ_0 is often referred to as the order parameter even across the whole BCS-BEC crossover.

We now use the newly-defined order parameter to write down a mean field-approximation of the Hamiltonian, i.e. an approximation in which the product of two operators is replaced as follows:

$$AB \approx \langle A\rangle B + A\langle B\rangle - \langle A\rangle\langle B\rangle \tag{3.12}$$

In the present context the mean field approximation is implemented as [65]:

$$\begin{aligned}
&\frac{g_0}{L^3}\sum_{\mathbf{k}\mathbf{k}'} c^\dagger_{\mathbf{k},\uparrow}c^\dagger_{-\mathbf{k}\downarrow}c_{-\mathbf{k}'\downarrow}c_{\mathbf{k}'\uparrow} \approx \\
\approx \frac{g_0}{L^3}\sum_{\mathbf{k}\mathbf{k}'} &\langle c^\dagger_{\mathbf{k},\uparrow}c^\dagger_{-\mathbf{k}\downarrow}\rangle c_{-\mathbf{k}'\downarrow}c_{\mathbf{k}'\uparrow} + c^\dagger_{\mathbf{k},\uparrow}c^\dagger_{-\mathbf{k}\downarrow}\langle c_{-\mathbf{k}'\downarrow}c_{\mathbf{k}'\uparrow}\rangle - \langle c^\dagger_{\mathbf{k},\uparrow}c^\dagger_{-\mathbf{k}\downarrow}\rangle\langle c_{-\mathbf{k}'\downarrow}c_{\mathbf{k}'\uparrow}\rangle = \\
&= -\sum_{\mathbf{k}}\Delta_0^* c_{-\mathbf{k}\downarrow}c_{\mathbf{k}'\uparrow} - \sum_{\mathbf{k}}\Delta_0 c^\dagger_{\mathbf{k},\uparrow}c^\dagger_{-\mathbf{k}\downarrow} + \frac{L^3}{g_0}\left|\Delta_0\right|^2 ,
\end{aligned} \tag{3.13}$$

finally obtaining the Bogoliubov mean-field Hamiltonian [50]:

$$\hat{H} = \sum_{\mathbf{k},\sigma}\epsilon_k c^\dagger_{\mathbf{k},\sigma}c_{\mathbf{k},\sigma} + \sum_{\mathbf{k}}\left(\Delta_0^* c_{\mathbf{k},\downarrow}c_{-\mathbf{k},\uparrow} + c^\dagger_{\mathbf{k},\uparrow}c^\dagger_{-\mathbf{k},\downarrow}\Delta_0\right) + \frac{L^3}{g_0}\left|\Delta_0\right|^2 \tag{3.14}$$

One can then cast the electron creation/annihilation operators into a spinor, using the Nambu-Gor'kov spinor formalism [36, 72]:

$$\Psi_{\mathbf{k}} = \begin{pmatrix} c_{\mathbf{k}\uparrow} \\ c^\dagger_{-\mathbf{k}\downarrow}\end{pmatrix} \qquad \Psi^\dagger_{\mathbf{k}} = \begin{pmatrix} c^\dagger_{\mathbf{k}\uparrow} \\ c_{-\mathbf{k}\downarrow}\end{pmatrix}^T \tag{3.15}$$

as:

$$\hat{H} - \mu\hat{N} = \sum_{\mathbf{k}}\Psi^\dagger_{\mathbf{k}}\underbrace{\begin{pmatrix}\xi_{\mathbf{k}} & -\Delta_0 \\ -\Delta_0^* & -\xi_{\mathbf{k}}\end{pmatrix}}_{=\mathbb{M}}\Psi_{\mathbf{k}} + \sum_{\mathbf{k}}\xi_{\mathbf{k}} + \frac{L^3}{g_0}\left|\Delta_0\right|^2 \tag{3.16}$$

where $\xi_{\mathbf{k}} = \hbar^2k^2/2m - \mu$. The second sum arises from the anticommutation of the fermionic fields; it is an additive constant to the energy of the system and will be neglected from now on.

We now simplify the Hamiltonian by searching for a different basis in which the matrix $\mathbb{M}$ is diagonal. At this stage, the non-diagonality of the Hamiltonian means that the fundamental excitations of the system are not just electrons or holes: switching to a different basis is the mathematical counterpart of finding a suitable combination of electrons and holes which is, indeed, a fundamental excitation for the system.

A Hermitean matrix $\mathbb{M} \in M_{2\times 2}(\mathbb{C})$ can be diagonalized by an unitary matrix, i.e. a matrix U such that $UU^\dagger = \mathbb{1} = U^\dagger U$. All 2×2 Hermitean matrices can be parameterized by two complex parameters u and v as

$$U = \begin{pmatrix} u^* & -v \\ v^* & u \end{pmatrix} \tag{3.17}$$

subject to the condition $|u|^2 + |v|^2 = 1$. By an adequate choice of the parameters the Hamiltonian in Eq. (3.16) is diagonalized in terms of the new fields

$$\begin{pmatrix} b_{\mathbf{k}\uparrow} \\ b^\dagger_{-\mathbf{k}\downarrow} \end{pmatrix} \equiv U_{\mathbf{k}} \Psi_{\mathbf{k}} = \begin{pmatrix} u^*_{\mathbf{k}} & -v_{\mathbf{k}} \\ v^*_{\mathbf{k}} & u_{\mathbf{k}} \end{pmatrix} \begin{pmatrix} c_{\mathbf{k}\uparrow} \\ c^\dagger_{-\mathbf{k}\downarrow} \end{pmatrix} = \begin{pmatrix} u^*_{\mathbf{k}} c_{\mathbf{k}\uparrow} - v_{\mathbf{k}} c^\dagger_{-\mathbf{k}\downarrow} \\ v^*_{\mathbf{k}} c_{\mathbf{k}\uparrow} + u_{\mathbf{k}} c^\dagger_{-\mathbf{k}\downarrow} \end{pmatrix} \tag{3.18}$$

as follows:

$$\hat{H} - \mu \hat{N} = \sum_{\mathbf{k}\sigma} b^\dagger_{\mathbf{k}\sigma} b_{\mathbf{k}\sigma} E_{\mathbf{k}} + \frac{L^3}{g_0} |\Delta_0|^2 \tag{3.19}$$

up to an irrelevant additive energy constant, the complex parameters $u_{\mathbf{k}}$ and $v_{\mathbf{k}}$ defining the transformation being subjected to the condition

$$|u_{\mathbf{k}}|^2 + |v_{\mathbf{k}}|^2 = 1 \, . \tag{3.20}$$

The newly-defined field operators satisfy the usual anticommutation relations, hence they represent fermionic (quasi-)particles; however they have a peculiar spectrum given by the energy eigenvalues of the new Hamiltonian

$$E_{\mathbf{k}} = \sqrt{\xi^2_{\mathbf{k}} + |\Delta_0|^2} \, . \tag{3.21}$$

3.2 The BCS ground state

To find the a suitable many-particle ground state we search for the vacuum state of the algebra $\left\{ b_{\mathbf{k}\sigma}, b^\dagger_{\mathbf{k}\sigma} \right\}$, i.e. a state which is annihilated by every $b_{\mathbf{k}\sigma}$. It is easily seen that this requirement is met by a state

$$|\mathrm{BCS}\rangle = \prod_{\mathbf{k}} b_{\mathbf{k}\uparrow} b_{-\mathbf{k}\downarrow} \mid 0\rangle \, , \tag{3.22}$$

which can be rewritten by means of the transformations in Eq. (3.18) in terms of the electron/hole operators as:

$$|\mathrm{BCS}\rangle = \prod_{\mathbf{k}} \left(u^*_{\mathbf{k}} + v_{\mathbf{k}} P^\dagger_{\mathbf{k}} \right) |0\rangle \tag{3.23}$$

where $|0\rangle$ is the vacuum state and the $P^\dagger_{\mathbf{k}} \equiv c^\dagger_{\mathbf{k}\uparrow} c^\dagger_{-\mathbf{k}\downarrow}$ operator creates a Cooper pair, in which the fermion have (as by definition) opposite momenta $\mathbf{k}$ and $-\mathbf{k}$ and opposite spins.

We already discussed the assumption that the pairing happens at zero momentum: the BCS ground state in Eq. (3.23) describes the coherent states of Cooper pairs, and it may seem tailored to the BCS regime; on the contrary it has been shown that its scope of application is way broader, and that it can be used *at zero temperature* across the full BCS-BEC crossover [69, 73], at the end of the present Section will we will verify that, in fact, the BCS wavefunction can describe the molecular dimers of the BEC limit of the crossover.

In order to find an expression for the parameters $u_{\mathbf{k}}$ and $v_{\mathbf{k}}$, we note that:

- The complex parameters $u_{\mathbf{k}}$ and $v_{\mathbf{k}}$ can be taken as real without loss of generality. As we have seen using a contact potential the order parameter does not depend on $\mathbf{k}$; moreover it can be made real through a global gauge transformation: suppose that $\Delta_0 = |\Delta_0| \, e^{\mathrm{i}\phi}$, then one can put into action the following transformation:

$$c_{\mathbf{k}\sigma} \longrightarrow e^{-\mathrm{i}\frac{\phi}{2}} c_{\mathbf{k}\sigma} \qquad c^\dagger_{\mathbf{k}\sigma} \longrightarrow e^{\mathrm{i}\frac{\phi}{2}} c^\dagger_{\mathbf{k}\sigma} \; ; \tag{3.24}$$

  of course the physics of the system is left unchanged and now $\Delta_0 \in \mathbb{R}$. As a consequence the matrix $\mathbb{M}$ is now real and can be diagonalized by an ortogonal transformation, i.e. the matrix $U_{\mathbf{k}}$ can be written as:

$$R_{\theta_{\mathbf{k}}} = \begin{pmatrix} \cos(\theta_{\mathbf{k}}) & -\sin(\theta_{\mathbf{k}}) \\ \sin(\theta_{\mathbf{k}}) & \cos(\theta_{\mathbf{k}}) \end{pmatrix} \tag{3.25}$$

  The corrispondence $u_{\mathbf{k}} = \cos(\theta_{\mathbf{k}})$ and $v_{\mathbf{k}} = \cos(\theta_{\mathbf{k}})$ shows that the parameters can be taken as real without loss of generality.

- It is also reasonable to assume that $u_{\mathbf{k}} = u_{|\mathbf{k}|}$, given the rotational invariance of the system.

Deriving an expression for $u_{\mathbf{k}}$ and $v_{\mathbf{k}}$ is now just a matter of finding the change of base matrix for the transformation $\Psi_{\mathbf{k}} \to U\Psi_{\mathbf{k}}$ and equating it to the entries of the matrix in Eq. (3.25); we then find:

$$\begin{cases} u^2_{\mathbf{k}} = \frac{1}{2}\left(1 + \frac{\xi_{\mathbf{k}}}{E_{\mathbf{k}}}\right) \\ v^2_{\mathbf{k}} = \frac{1}{2}\left(1 - \frac{\xi_{\mathbf{k}}}{E_{\mathbf{k}}}\right) \end{cases} \tag{3.26}$$

with $\xi_{\mathbf{k}} = \hbar^2 k^2/2m - \mu$ and $E_{\mathbf{k}} = \sqrt{\xi^2_{\mathbf{k}} + \Delta^2_0}$.

We impose that the Bogoliubov quasiparticles should follow a Fermi-Dirac distribution, being fermions

$$\begin{cases} \langle b^\dagger_{\mathbf{k}\sigma} b_{\mathbf{k}\sigma} \rangle = n_F(\mathbf{k}) \\ \langle b_{\mathbf{k}\sigma} b^\dagger_{\mathbf{k}\sigma} \rangle = 1 - n_F(\mathbf{k}) \\ \langle b_{\mathbf{k}\sigma} b_{\mathbf{k}\sigma} \rangle = 0 = \langle b^\dagger_{\mathbf{k}\sigma} b^\dagger_{\mathbf{k}\sigma} \rangle \end{cases} \tag{3.27}$$

with

$$n_F(\mathbf{k}) = \frac{1}{e^{\beta E_\mathbf{k}} + 1} \,. \tag{3.28}$$

By using Eqs. (3.27) and Eq. (3.11) one obtains the gap equation:

$$\Delta_0 = -\frac{g_0}{L^3} \sum_\mathbf{k} u_\mathbf{k} v_\mathbf{k} (1 - 2n_F(\mathbf{k})) = -\frac{g_0}{L^3} \sum_\mathbf{k} \frac{\Delta_0}{2E_\mathbf{k}} \tanh(\beta E_\mathbf{k}/2) \tag{3.29}$$

having used the identity $1 - 2n_F(\mathbf{k}) = \tanh(\beta E_\mathbf{k}/2)$. Finally the number equation can be found calculating the expectation value of the number density operator $n_{\mathbf{k}\sigma} = c^\dagger_{\mathbf{k}\sigma} c_{\mathbf{k}\sigma}$ summed over all spins and momenta:

$$\begin{aligned} n = \frac{N}{L^3} &= \frac{1}{L^3} \sum_{\mathbf{k}\sigma} \langle c^\dagger_{\mathbf{k}\sigma} c_{\mathbf{k}\sigma} \rangle = \frac{2}{L^3} \sum_\mathbf{k} \langle c^\dagger_{\mathbf{k}\uparrow} c_{\mathbf{k}\uparrow} \rangle = \\ &= \frac{2}{L^3} \sum_\mathbf{k} \left[u^2_\mathbf{k} \langle b^\dagger_{\mathbf{k}\uparrow} b_{\mathbf{k}\uparrow} \rangle + v^2_\mathbf{k} \langle b_{-\mathbf{k}\downarrow} b^\dagger_{-\mathbf{k}\downarrow} \rangle + u_\mathbf{k} v_\mathbf{k} \left(\langle b^\dagger_{\mathbf{k}\uparrow} b^\dagger_{-\mathbf{k}\downarrow} \rangle + \langle b_{-\mathbf{k}\downarrow} b_{\mathbf{k}\uparrow} \rangle \right) \right] = \\ &= \frac{2}{L^3} \sum_\mathbf{k} \left[u^2_\mathbf{k} n_F(\mathbf{k}) + v^2_\mathbf{k} (1 - n_F(\mathbf{k})) \right] = \frac{1}{L^3} \sum_\mathbf{k} \left(1 - \frac{\xi_\mathbf{k}}{E_\mathbf{k}} \tanh(\beta E_\mathbf{k}/2) \right) \end{aligned} \tag{3.30}$$

As opposed to the standard BCS problem the chemical potential μ is not fixed to ϵ_F, but it is calculated self-consistently by fixing the total number of particles. In fact the gap equation in Eq. (3.29) and the number equation in Eq. (3.30) are called the (extended) BCS equations and must be solved jointly in order to obtain the mean-field dynamics of a uniform Fermi gas.

One should also note that at zero-temperature $\lim_{T\to 0} \tanh(\beta E_\mathbf{k}/2) = 1$, so that the gap and number equations simplify to

$$\frac{1}{g_0} = -\frac{1}{L^3} \sum_\mathbf{k} \frac{1}{2E_\mathbf{k}} \tag{3.31}$$

and

$$n = \frac{1}{L^3} \sum_\mathbf{k} \left(1 - \frac{\xi_\mathbf{k}}{E_\mathbf{k}} \right) \,. \tag{3.32}$$

In fact the mean-field theory can provide qualitatively correct predictions at $T = 0$, whereas it fails in describing most finite temperature effects. We note that the integral appearing in Eq. (3.31) is divergent, a regularization procedure for the gap equation will be analyzed in Section 3.4.

The condensate number is defined as the number of fermionic pairs occupying the ground state: clearly a finite condensate number signals the onset of condensation, as also analyzed in Eq. (2.17). It is easily shown [38, 74] that in the present context the condensate number can be calculated as

$$N_0 = \sum_\mathbf{k} u^2_\mathbf{k} v^2_\mathbf{k} \tanh^2(\beta E_\mathbf{k}/2) \tag{3.33}$$

reducing in the zero-temperature limit to

$$N_0 = \sum_{\mathbf{k}} u_{\mathbf{k}}^2 v_{\mathbf{k}}^2 \,. \tag{3.34}$$

The integration can be carried out analytically and leading to the following expression [38] for N_0:

$$N_0 = V \frac{m^{3/2}}{8\pi\hbar^3} \Delta_0^{3/2} \sqrt{\frac{\mu}{\Delta_0} + \sqrt{1 + \frac{\mu^2}{\Delta_0^2}}} \,. \tag{3.35}$$

The condensate fraction, defined as $\phi = \frac{N_0}{N}$ has been extensively studied across the whole crossover, going from extremely small values in the deep-BCS regime, where only electrons at the Fermi level pair and condensed, to $\phi \sim 0.5$ in the deep-BEC regime, where all fermions are paired in bosonic dimers. The mean-field theory for the condensate fraction [38] shows good agreement with experimental data at $T = 0$ from the deep BCS regime to slightly beyond unitarity on the BEC side; for stronger interactions the agreement with experimental data is lost, likely due to the unreliability of experimental data due to three-body losses [38]. The condensate fraction for a spin-unbalanced Fermi gas will be analyzed in this Thesis in Section 3.5.

In conclusion of the present Section we stress that, following this approach, the BCS wavefunction is not a variational Ansatz whose parameters are to be optimized to have a minimum of the ground state energy expectation value. Rather we have demonstrated that the Bogoliubov quasiparticles are the fundamental excitations of the system described by the Hamiltonian in Eq. (3.16), created the ground state for the algebra of the Bogoliubov operators and finally calculated all other relevant quantities by requiring the same operators to follow the Fermi-Dirac distribution.

At last, as anticipated in the previous Section, an analysis of the wavefunction can provide a *a posteriori* justification of the usage of the pairing Ansatz and of the whole BCS description across the crossover, showing that the validity of the ground state in Eq. (3.23) extends up to the BEC regime at zero temperature. Let us start from the BCS limit: here a simultaneous solution of Eq. (3.29) and of Eq. (3.30), together with the condition in Eq. (3.20) gives the following density of states[5]

$$n_{\mathbf{k}} = \Theta(1 - |\mathbf{k}|/k_F) \tag{3.36}$$

describing the Fermi surface and a constant density of state up to $|\mathbf{k}| = k_F$. As the interaction gets stronger the step function at the Fermi wave-vector

[5] Comparing Eq. (3.30) and Eq. (3.26) and imposing $N = (2/L^3)\sum_{\mathbf{k}} n_{\mathbf{k}}$ one immediately sees that $n_{\mathbf{k}} = v_{\mathbf{k}}^2$.

smoothens and the Fermi surface disrupts. It can be rigorously shown that in the BEC limit the density distribution is [69]

$$n_{\mathbf{k}} = \frac{4(k_F a_s)^3}{3\pi(1+|\mathbf{k}|^2 a_s^2)^2} \tag{3.37}$$

which is proportional to the square of the Fourier transform of the wavefunction of molecular dimers, signaling that the BCS wavefunction in Eq. (3.23) can also reproduce, at least at a quantitative level, the physics of the strong BEC limit [42].

Still this picture should be regarded as an approximation, for instance the density fluctuations and hence the sound mode are completely neglected in this scheme. The extension of the mean-field theory to include order-parameter fluctuations and the sound mode will be the main object of Chapter 4. Moreover the present description correctly reproduces the BEC limit as a gas of tightly bound but weakly interacting bosons, however the boson-boson scattering length turns out to be $a_b = 2.0 a_s$, while more sophisticated approaches shows that the exact value should be $a_b = 0.6 a_s$; an analytical derivation of this relation is analyzed in Ref. [4] and will be reported in Section 4.4.

3.3 Extended BCS equations from the field integral

In the present Section we give an alternative and complementary description of the mean-field theory for the BCS-BEC crossover, deriving the same extended BCS equations in Eq. (3.29) and in Eq. (3.30) by means of a path integral approach [36, 67, 71, 75, 76]. This approach is completely equivalent to the treatment in Section 3.1 and Section 3.2, however it allows for an easier and more natural introduction of the beyond-mean-field theory of order parameter fluctuations which will be analyzed in Chapter 4.

The grand canonical partition function $\mathcal{Z}$ of d-dimensional system of interacting fermions at temperature T contained in a volume L^d, described within the grand canonical ensemble at fixed chemical potential μ can be written using the path integral formalism as

$$\mathcal{Z} = \int \mathcal{D}\psi_\sigma \mathcal{D}\bar{\psi}_\sigma e^{-S[\psi_\sigma, \bar{\psi}_\sigma]} \,. \tag{3.38}$$

With respect to Eq. (3.1) the field operators describing the fermions have been replaced by the anti-commuting Grassman field variables $\psi_\sigma(\mathbf{x}, \tau)$ and $\bar{\psi}_\sigma(\mathbf{x}, \tau)$, where τ is the imaginary time. The fields ψ and $\bar{\psi}$ satisfy anti-periodic boundary conditions in the imaginary time, representing a fermionic object, i.e. they obey the condition $\psi(\mathbf{x}, 0) = -\psi(\mathbf{x}, \hbar\beta)$ at every position in space and similarly for $\bar{\psi}$. Here $\beta = 1/(k_B T)$ and k_B is the Boltzmann constant. The path integral in Eq. (3.38) can then be thought of as a sum

over every configuration of the field, where each configuration is weighted by a factor $\exp(-S)$.

The action $S[\psi_\sigma, \bar{\psi}_\sigma] = S_{free}[\psi_\sigma, \bar{\psi}_\sigma] + S_{int}[\psi_\sigma, \bar{\psi}_\sigma]$ is a functional of the Grassman fields $\psi_\sigma(\mathbf{x}, \tau)$ and $\bar{\psi}_\sigma(\mathbf{x}, \tau)$ and describes the same physics as in Eq. (3.1), however within this formalism, the free and interaction part of the Hamiltonian in Eq. (3.1) are replaced by the free and interaction part of the action, namely

$$S_{free}[\psi_\sigma, \bar{\psi}_\sigma] = \int_0^{\hbar\beta} \mathrm{d}\tau \int \mathrm{d}^d x \sum_\sigma \bar{\psi}(\mathbf{x}, \tau) \left[\hbar \frac{\partial}{\partial \tau} - \frac{\hbar^2}{2m} \nabla^2 - \mu \right] \psi(\mathbf{x}, \tau) \tag{3.39}$$

and

$$S_{int}[\psi_\sigma, \bar{\psi}_\sigma] = \int_0^{\hbar\beta} \mathrm{d}\tau \int \mathrm{d}^d x \mathrm{d}^d y \; \bar{\psi}_\uparrow(\mathbf{x}, \tau) \bar{\psi}_\downarrow(\mathbf{y}, \tau) V(\mathbf{x} - \mathbf{y}) \psi_\downarrow(\mathbf{y}, \tau) \psi_\uparrow(\mathbf{x}, \tau) \; , \tag{3.40}$$

all the spatial integrals are extended over the volume L^d. Exactly as done before and for the very same reasons, typically for ultracold Fermi gases the interaction can be modeled by a contact interaction. When $V(\mathbf{x} - \mathbf{y}) = g_0 \; \delta(\mathbf{x} - \mathbf{y})$ the interaction part of the action in Eq. (3.40) simplifies to:

$$S_{int}[\psi_\sigma, \bar{\psi}_\sigma] = g_0 \int_0^{\hbar\beta} \mathrm{d}\tau \int \mathrm{d}^d x \; \bar{\psi}_\uparrow(\mathbf{x}, \tau) \bar{\psi}_\downarrow(\mathbf{x}, \tau) \psi_\downarrow(\mathbf{x}, \tau) \psi_\uparrow(\mathbf{x}, \tau) \tag{3.41}$$

and the Hubbard-Stratonovich transformation is immediately performed introducing the identity[6]

$$e^{-S_{int}[\psi_\sigma, \bar{\psi}_\sigma]} \propto \int \mathcal{D}\Delta \mathcal{D}\bar{\Delta} \; e^{-S_{hs}[\psi_\sigma, \bar{\psi}_\sigma, \Delta, \bar{\Delta}]} \tag{3.42}$$

where

$$S_{hs}[\psi_\sigma, \bar{\psi}_\sigma, \Delta, \bar{\Delta}] = - \int_0^{\hbar\beta} \mathrm{d}\tau \int \mathrm{d}^d x \; \left[\frac{|\Delta(\mathbf{x}, \tau)|^2}{g_0} + \right.$$
$$\left. + \bar{\Delta}(\mathbf{x}, \tau) \psi_\downarrow(\mathbf{x}, \tau) \psi_\uparrow(\mathbf{x}, \tau) + \Delta(\mathbf{x}, \tau) \bar{\psi}_\uparrow(\mathbf{x}, \tau) \bar{\psi}_\downarrow(\mathbf{x}, \tau) \right] \tag{3.43}$$

which can be verified by completing the square in the r.h.s. and performing a straightforward Gaussian integration over Δ, $\bar{\Delta}$ [36].

The newly introduced auxiliary fields $\Delta(\mathbf{x}, \tau)$ and $\bar{\Delta}(\mathbf{x}, \tau)$ are pairing fields, representing a Cooper pair[7]; being bosonic objects they obey symmetric

[6] The identity holds modulo a global multiplicative factor, hence the $\propto$ sign; however a global multiplicative constant in the partition function is irrelevant, as it becomes an additive constant when the free energy is calculated.

[7] The statement can be made more precise by noting, with Ref. [77], that the pairing field Δ at a classic level is just a shorthand for $\psi\psi$ and obeys the same equations of motion.

boundary conditions in imaginary time, i.e. $\Delta(\mathbf{x}, \hbar\beta) = \Delta(\mathbf{x}, 0)$ holds at every point in space, and similarly for $\bar{\Delta}(\mathbf{x}, \tau)$. The quartic interaction appearing in the original action due to the four-fermion vertex is now decoupled, however the simplification of eliminating the quartic interaction comes at the expense of introducing the new auxiliary fields Δ and $\bar{\Delta}$, whose dynamics will have to be treated in an approximate way.

The complete action can be written as

$$S[\psi_\sigma, \bar{\psi}_\sigma, \Delta, \bar{\Delta}] = \int_0^{\hbar\beta} \mathrm{d}\tau \int \mathrm{d}^d x \left[\bar{\Psi}(x) \left[-\mathbb{G}^{-1} \right]_x \Psi(x) - \frac{|\Delta(x)|^2}{g_0} \right] \quad (3.44)$$

having introduced the $(d+1)$-dimensional coordinate $x = (\mathbf{x}, \tau)$ for the sake of simplicity and having also introduced the Nambu-Gor'kov spinors in coordinate space

$$\Psi(x) = \begin{pmatrix} \psi_\uparrow(x) \\ \bar{\psi}_\downarrow(x) \end{pmatrix} \qquad \bar{\Psi}(x) = \begin{pmatrix} \bar{\psi}_\uparrow(x) & \psi_\downarrow(x) \end{pmatrix} , \quad (3.45)$$

and the physics of the system is encoded in the inverse Green's function, which in coordinate space representation reads:

$$\left[-\mathbb{G}^{-1} \right]_x = \begin{pmatrix} \hbar\partial_\tau - \frac{\hbar^2}{2m}\nabla^2 - \mu & -\Delta(\mathbf{x}, \tau) \\ -\bar{\Delta}(\mathbf{x}, \tau) & \hbar\partial_\tau + \frac{\hbar^2}{2m}\nabla^2 + \mu \end{pmatrix} \quad (3.46)$$

It is now convenient to introduce the frequency-momentum representation for the field operators. The Fourier transform for the fermionic field ψ_σ reads:

$$\psi_\sigma(\mathbf{k}, \mathrm{i}\omega_n) = \frac{1}{\sqrt{\beta L^d}} \int_{L^d} \mathrm{d}^d x \int_0^{\hbar\beta} \mathrm{d}\tau \exp(-\mathrm{i}\mathbf{k}\cdot\mathbf{x} + \mathrm{i}\omega_n\tau)\psi_\sigma(\mathbf{x}, \tau) \quad (3.47)$$

while, on the other hand, the bosonic field Δ has the following Fourier transform

$$\Delta(\mathbf{q}, \mathrm{i}\Omega_n) = \frac{1}{\sqrt{\beta L^d}} \int_{L^d} \mathrm{d}^d x \int_0^{\hbar\beta} \mathrm{d}\tau \exp(-\mathrm{i}\mathbf{q}\cdot\mathbf{x} + \mathrm{i}\Omega_n\tau)\Delta(\mathbf{x}, \tau) \quad (3.48)$$

having introduced the fermionic Matsubara frequencies $\omega_n = 2\pi n/\beta$ and the bosonic Matsubara frequencies $\Omega_m = (2m+1)\,\pi/\beta$.

It is now possible rewriting [67] the action in Eq. (3.44) in momentum space as:

$$S[\psi_\sigma, \bar{\psi}_\sigma, \Delta, \bar{\Delta}] = \sum_{k,k'} \bar{\Psi}(k) \left[-\mathbb{G}^{-1} \right]_{k,k'} \Psi(k') - \sum_q \frac{|\Delta(q)|^2}{g_0} \quad (3.49)$$

having introduced the $(d+1)$-dimensional momentum-space fermionic coordinates $k = (\mathbf{k}, \mathrm{i}\omega_n)$, the bosonic coordinates $q = (\mathbf{q}, \mathrm{i}\Omega_m)$ and the Nambu-Gor'kov spinors in complete analogy with Eq. (3.15):

$$\Psi(k) = \begin{pmatrix} \psi_\uparrow(\mathbf{k}, \mathrm{i}\omega_n) \\ \bar{\psi}_\downarrow(-\mathbf{k}, \mathrm{i}\omega_{-n}) \end{pmatrix} \qquad \bar{\Psi}(k) = \begin{pmatrix} \bar{\psi}_\uparrow(\mathbf{k}, \mathrm{i}\omega_n) \\ \psi_\downarrow(-\mathbf{k}, \mathrm{i}\omega_{-n}) \end{pmatrix}^T \quad (3.50)$$

The integration over the Ψ, $\bar{\Psi}$ fields is Gaussian and can be carried out exactly using the relation

$$\int \mathcal{D}\psi_\sigma \mathcal{D}\bar{\psi}_\sigma e^{-\sum_{k,k'} \bar{\Psi}(k)\mathbb{M}_{k,k'}\Psi(k')} = \mathrm{Det}\,\mathbb{M}(\mathbf{k}, \mathrm{i}\Omega_n) \tag{3.51}$$

so that the partition function is now written in an exact form as an path integral over the Δ, $\bar{\Delta}$ fields:

$$\mathcal{Z} = \int \mathcal{D}\Delta\mathcal{D}\bar{\Delta} \exp\left[\mathrm{Tr}\ln\left(-\mathbb{G}^{-1}\right) + \sum_{\mathbf{q},m} \frac{|\Delta(\mathbf{q}, \mathrm{i}\Omega_m)|^2}{g_0}\right] \tag{3.52}$$

and the trace $\mathrm{Tr}(\#)$ has to be taken in the Nambu-Gor'kov space and in the frequency-momentum space.

Up to this point the treatment has been kept exact and Eq. (3.52), albeit impossible to treat analytically, is an exact description of the system. In order to continue the analytical treatment it is necessary to decompose the pairing field Δ as the sum of a uniform and constant mean-field value[8], which will be self-consistently determined later as the saddle point of the action, and a fluctuation field:

$$\Delta(\mathbf{q}, \mathrm{i}\Omega_m) = \Delta_0\ \delta(\mathbf{q})\delta_{m,0} + \eta(\mathbf{q}, \mathrm{i}\Omega_m) \tag{3.53}$$

Referring to Eq. (3.49) the inverse Green function $\left[-\mathbb{G}^{-1}\right]_{k,k'}$ in frequency momentum representation is readily found starting from Eq. (3.44), introducing the frequency-momentum representations for the fields and letting the differential operators act on them. One can then decompose the inverse Green's function as the sum of a saddle-point contribution $-\mathbb{G}_{\mathrm{sp}}^{-1}$ and a fluctuation contribution $\mathbb{F}$

$$\left[-\mathbb{G}^{-1}\right]_{k,k'} = \left[-\mathbb{G}_{\mathrm{sp}}^{-1}\right]_{k,k'} + \left[\mathbb{F}\right]_{k,k'}, \tag{3.54}$$

with the the saddle point part, which is diagonal in momentum space

$$\left[-\mathbb{G}_{\mathrm{sp}}^{-1}\right]_{k,k'} = \begin{pmatrix} -\mathrm{i}\omega_n + \frac{\hbar^2k^2}{2m} - \mu & -\Delta_0 \\ -\Delta_0 & -\mathrm{i}\omega_n - \frac{\hbar^2k^2}{2m} + \mu \end{pmatrix} \delta(\mathbf{k}-\mathbf{k}')\delta_{n,n'} \tag{3.55}$$

and the fluctuation part

$$\left[\mathbb{F}\right]_{k,k'} = \begin{pmatrix} 0 & -\eta(\mathbf{k}+\mathbf{k}', \mathrm{i}\Omega_{n+n'}) \\ -\eta(\mathbf{k}+\mathbf{k}', \mathrm{i}\Omega_{n+n'}) & 0 \end{pmatrix}. \tag{3.56}$$

This notation is particularly convenient because the inverse Green function encodes the full physics of the system, and different approximation schemes will correspond to different choices for $-\mathbb{G}^{-1}$. In particular the simplest

[8] It is uniform in coordinate space and constant with respect to the imaginary time τ.

approximation scheme consists in completely ignoring the fluctuations, using the following replacement for the coordinate-space pairing field:

$$\Delta(\mathbf{x},\tau) \to \Delta_0 \ . \tag{3.57}$$

In momentum space this approximation is tantamount to requiring that the pairing must happen in a zero-momentum state, which is exactly the pairing Ansatz we analyzed in the previous Section:

$$\Delta(\mathbf{q},\mathrm{i}\Omega_m) \to \Delta_0 \ \delta(\mathbf{q})\delta_{m,0} \ . \tag{3.58}$$

Finally in terms of the inverse Green's function the approximation reads:

$$-\mathbb{G}^{-1} \to -\mathbb{G}_{\mathrm{sp}}^{-1} \ , \tag{3.59}$$

completely neglecting the fluctuation contribution coming from $\mathbb{F}$. Of course the action is greatly simplified, as the Δ field loses the dynamics and it is replaced by its saddle-point value Δ_0: it is no longer necessary integrating over the Δ, $\bar{\Delta}$ fields. The mean-field partition function obtained through this treatment reads

$$\mathcal{Z}_{\mathrm{mf}} = e^{-\beta\Omega_{\mathrm{eff}}} \tag{3.60}$$

with the effective grand potential

$$\Omega_{\mathrm{eff}} = -L^d\frac{\Delta_0^2}{g_0} - \frac{1}{\beta}\sum_{\mathbf{k}}\sum_{n}\ln\left[-\det\begin{pmatrix}-\mathrm{i}\omega_n+\xi_{\mathbf{k}} & -\Delta_0\\ -\Delta_0 & -\mathrm{i}\omega_n-\xi_{\mathbf{k}}\end{pmatrix}\right] \ . \tag{3.61}$$

with $\xi_{\mathbf{k}} = \hbar^2k^2/2m - \mu$. The gap equation is then found imposing the saddle point condition to the grand potential, i.e.:

$$\frac{\partial\Omega}{\partial\Delta_0} = 0 \tag{3.62}$$

yielding

$$\frac{1}{g_0} = \frac{1}{\beta}\sum_{\mathbf{k},n}\frac{1}{(\mathrm{i}\omega_n)^2 - E_{\mathbf{k}}^2} \tag{3.63}$$

with $E_{\mathbf{k}} = \sqrt{\xi_{\mathbf{k}}^2+\Delta_0^2}$. The sum over n is readily carried out using the identity

$$-\frac{1}{\beta}\sum_{n}\frac{1}{(\mathrm{i}\omega_n)^2 - x^2} = \frac{\tanh(\beta x/2)}{2x} \tag{3.64}$$

holding for fermionic Matsubara frequencies, which is derived by transforming an infinite series to a contour integration in the complex plane and deforming it; this technique is analyzed in Appendix A. Eq. (3.64) directly leads to the gap equation

$$\frac{1}{g_0} = -\frac{1}{L^d}\sum_{\mathbf{k}}\frac{\tanh(\beta E_{\mathbf{k}}/2)}{2E_{\mathbf{k}}} \ . \tag{3.65}$$

The number equation, on the other hand, is obtained again from the grand potential in Eq. (3.61), whose (formally divergent) Matsubara sum needs to be evaluated introducing complex convergence factors, owing to anti-commuting nature of the original ψ, $\bar{\psi}$ field, as thoroughly analyzed in Ref. [71]. Here we just report the final result, which is

$$\Omega_{\text{eff}} = -L^d \frac{\Delta_0^2}{g_0} + \sum_{\mathbf{k}} (\xi_{\mathbf{k}} - E_{\mathbf{k}}) - \frac{2}{\beta} \sum_{\mathbf{k}} \ln\left(1 + e^{-\beta E_{\mathbf{k}}}\right) \tag{3.66}$$

modulo an infinite constant which does not depend on the parameters of the theory and is then irrelevant; finally using the thermodynamic relation $N = -\partial\Omega/\partial\mu$, one gets

$$n = \frac{N}{L^d} = \frac{1}{L^d} \sum_{\mathbf{k}} \left(1 - \frac{\xi_{\mathbf{k}}}{E_{\mathbf{k}}} \tanh(\beta E_{\mathbf{k}}/2)\right) . \tag{3.67}$$

In conclusion we note that Eqs (3.67) and (3.65) in complete agreement with Eq. (3.29) and Eq.(3.30), showing the equivalence of the path integral formulation.

3.4 Regularized potential

A contact potential $V(\mathbf{r} - \mathbf{r}') = g_0 \delta^{(3)}(\mathbf{r} - \mathbf{r}')$ can be used to sketch a more realistic potential, but it has got two main problems:

- The approximation works only in the dilute limit, i.e. only as long as the interatomic distance is bigger than the scale length of the potential. One may expect that the approximation should break for small distances, i.e. for large momenta: the gap equation, indeed, has an ultraviolet divergence.

- It is not clear how the coupling constant g_0 relates to the physics of the system. Intuitively it is an interaction strength, related to the intensity of the attractive coupling, however one does not know how it relates to observable quantities. In order to solve the problem one has to find a relation between the coupling constant g_0 and some physically observable quantity, the most natural being the scattering length a_s. In turn the scattering length is easily tuned in ultracold Fermi gases, being related to the external magnetic field by Eq. (2.26).

In the present Section we derive a relation linking the potential strength g_0 to the scattering length a_s; as a result it will be possible to eliminate g_0 from the treatment, regularizing the gap equation, removing the ultraviolet divergence.

The derivation of such a relation involves some scattering theory. We will follow the approach in Refs. [36, 78]. Let us consider a scattering problem in which two particles are interacting through a δ-potential. We can separate the center of mass motion and the relative motion of the particles (the latter being the interesting one!), so that the relative motion is described by the Hamiltonian $\hat{H} = \hat{H}_0 + \hat{V}$, with $\hat{H}_0 = \hat{p}^2/2\mu$, with the reduced mass $\mu = {}^1\!/_2\, m$, as the two particles have the same mass. Let $|\phi\rangle$ be the eigenstate of the free Hamiltonian $\hat{H}_0$, i.e. a plane wave with energy E, and be $|\psi\rangle$ the eigenstate of the complete problem, with energy E as well. Then the time-dependent Schrödinger equation is equivalent[9] to the Lippman-Schwinger equation [79]:

$$|\psi\rangle = |\phi\rangle + \frac{1}{E - \hat{H}_0}\hat{V}\,|\psi\rangle \tag{3.68}$$

The equivalency can be verified by left multiplying for $E - \hat{H}_0$, obtaining, indeed, the Schrödinger equation for $|\psi\rangle$. A formal solution to can be obtained iterating Eq. (3.68):

$$\begin{aligned} |\psi\rangle = \Big(\mathbb{1} \;&+\; \frac{1}{E-\hat{H}_0}\hat{V} + \frac{1}{E-\hat{H}_0}\hat{V}\frac{1}{E-\hat{H}_0}\hat{V} + \\ &+\; \frac{1}{E-\hat{H}_0}\hat{V}\frac{1}{E-\hat{H}_0}\hat{V}\frac{1}{E-\hat{H}_0}\hat{V} + \dots\Big)\,|\phi\rangle \ . \end{aligned} \tag{3.69}$$

Moreover we introduce the $\hat{T}$ matrix

$$\hat{T} \equiv \hat{V} + \hat{V}\hat{G}_0\hat{T} \tag{3.70}$$

with $\hat{G}_0 = (E - \hat{H}_0)^{-1}$ and Eq. (3.69) can be rewritten as:

$$|\psi\rangle = |\phi\rangle + \frac{1}{E - \hat{H}_0}\hat{T}\,|\phi\rangle \ . \tag{3.71}$$

It is convenient to think of the $\hat{T}$ matrix as an operator taking the energy $E = \frac{q^2}{2m}$ as a parameter; its matrix elements in momentum space are:

$$\begin{aligned} T_{\mathbf{k}\mathbf{k}'}(E) = \big\langle \mathbf{k}'\big|\hat{T}\,(E)\big|\mathbf{k}\big\rangle &= \big\langle \mathbf{k}'\big|\hat{V}\big|\mathbf{k}\big\rangle + \big\langle \mathbf{k}'\big|\hat{V}\hat{G}_0\hat{T}\big|\mathbf{k}\big\rangle = \\ &= V_{\mathbf{k}\mathbf{k}'} + \sum_{\mathbf{p}\mathbf{p}'} V_{\mathbf{k}\mathbf{p}} G_{0,\mathbf{p}\mathbf{p}'}\,(q)\, T_{\mathbf{p}'\mathbf{k}'}(E) \end{aligned} \tag{3.72}$$

When the Green's function $G_{0,\mathbf{p}\mathbf{p}'}$ is expressed in momentum space representation it is diagonal and it has the following form [80]:

$$G_{0,\mathbf{p}\mathbf{p}'}(E) = \frac{\delta_{\mathbf{p}\mathbf{p}'}}{E - \frac{p^2}{2\mu}} = \delta_{\mathbf{p}\mathbf{p}'} G_{0,\mathbf{p}}(E) \tag{3.73}$$

[9] Strictly speaking the equation is ill-defined for every E in the spectrum of $\hat{H}_0$, by adding $\pm i\delta$ to the denominator and taking the $\delta \to 0$ limit one is able to solve this problem and to select, respectively, outgoing and incoming waves. In other words $\hat{G}_0 = (\hat{H}_0 - E)^{-1}$ is the Green function for the free case, and one has to choose how to go around the poles on the real axis.

defining $G_{0,\mathbf{p}}(E)$. We can further simplify the equation for the $\hat{T}$ matrix elements by inserting a contact potential which in momentum space reads $V_{\mathbf{kk}'} = g_0$ with no dependence upon the momenta, so that:

$$T_{\mathbf{kk}'}(E) = g_0 + g_0 \sum_{\mathbf{p}} G_{0,\mathbf{p}}(E)\, T_{\mathbf{pk}'}(E) = g_0 \left(1 + \sum_{\mathbf{p}} G_{0,\mathbf{p}}(E)\, T_{\mathbf{pk}'}(E)\right) . \tag{3.74}$$

It is easily verified that the expression between parentheses is akin to a geometric series, in fact iterating shows that the T matrix with a δ potential is

$$T_{\mathbf{kk}'}(E) = \lim_{n\to\infty} g_0 \left[1 + g_0\Theta(E) + (g_0\Theta(E))^2 + \cdots + (g_0\Theta(E))^n\right] \tag{3.75}$$

with

$$\Theta(E) = \sum_{\mathbf{p}} G_{0,\mathbf{p}}(E) = \sum_{\mathbf{p}} \frac{1}{E - \frac{p^2}{2\mu}} \tag{3.76}$$

so that our final result is, by summing the geometric series in Eq. (3.75), is

$$T_{\mathbf{kk}'}(E) = \frac{g_0}{1 - g_0\Theta(E)} . \tag{3.77}$$

Also it can be demonstrated [80] that in the low-energy, low-momentum limit one has $T_{\mathbf{kk}'}(E) = \frac{4\pi\hbar^2}{m} a_s$, so that we finally have a relation between g_0 and a_s:

$$\frac{4\pi\hbar^2}{m} a_s = \frac{g_0}{1 - g_0\Theta(0)} \tag{3.78}$$

which can be rearranged, reinstating the particle mass $m = 2\mu$ in the r.h.s., as:

$$\frac{m}{4\pi\hbar^2 a_s} = \frac{1}{g_0} + \sum_{\mathbf{p}} \frac{1}{\frac{p^2}{m}} . \tag{3.79}$$

The integral in the r.h.s. is ultraviolet-divergent, and cannot be used to relate the strength of the attractive potential g_0 to the scattering length a_s. A possible solution would consist in introducing a momentum cutoff Λ on the integral, carefully choosing Λ to be large enough not to interfere with the physical features of the system. In the present case a simpler solution can be used: the zero-temperature gap equation, in Eq. (3.31)

$$\frac{1}{g_0} = -\frac{1}{L^d} \sum_{\mathbf{k}} \frac{1}{2E_{\mathbf{k}}} \tag{3.80}$$

can be combined[10] with Eq. (3.79), eliminating g_0, finally obtaining the regularized gap equation [81]:

$$\frac{m}{4\pi\hbar^2 a_s} = \frac{1}{L^d} \sum_{\mathbf{k}} \left(\frac{m}{k^2} - \frac{1}{2E_{\mathbf{k}}}\right) \tag{3.81}$$

which can be finally used to determine Δ_0 as a function of a_s.

[10] Having converted the momentum sums to integrals $\sum_{\mathbf{k}} \approx (2\pi)^{-3} \int \mathrm{d}^3 k$ and vice-versa.

3.5 The unbalanced Fermi gas

In this Section we discuss the mean field treatment for an unbalanced Fermi gas, i.e. a Fermi gas in which the number of atoms in one (pseudo)-spin state is different from the number of atoms in the other state. This topic has been extensively studied, both from a theoretical [82–101] and experimental [61, 102, 103] point of view, its experimental realization exploits Rabi oscillations and evaporative cooling techniques to vary the number of fermions in each (pseudo)-spin species [67].

An unbalanced Fermi gas shows novel features and a far richer phase diagram with respect to the balanced counterpart. At $T = 0$ a quantum phase transition is observed between the superfluid and normal state; exotic phases characterized by non-zero momentum pairing have been predicted [104], moreover in a trapped unbalanced Fermi gas one expects to find a phase separated regime [61, 82, 83, 87, 91, 93, 95, 97, 100–102] in which an inner superfluid core is surrounded by an unbalanced normal state. The fundamental signature of such phase-separated regime is a jump in the density between the two phases, which has been analyzed theoretically [105] and observed experimentally [106].

We derive a zero-temperature mean-field treatment for an unbalanced Fermi gas, investigating the condensate fraction as a function of the fermion-fermion attractive strength and of the polarization, in the uniform and in the trapped case. We also report condensate density profiles, showing that, like the normal density, the condensate density undergoes a jump between the superfluid and normal phase. The results we report in this Section are published in Ref. [1].

3.5.1 The extended BCS equations

We consider a two-spin-component ($\sigma = \uparrow, \downarrow$) uniform Fermi gas contained in a volume L^3, with unequal spin populations, each fermion having mass m. The fermions interact via an attractive s-wave contact potential. Without an external confinement, the uniform system can be described by the following (Euclidean) Lagrangian density:

$$\mathscr{L} = \sum_{\sigma=\uparrow,\downarrow} \bar{\psi}_\sigma(\mathbf{r},\tau)\left(\hbar\frac{\partial}{\partial\tau} - \hbar^2\frac{\nabla^2}{2m} - \mu_\sigma\right)\psi_\sigma(\mathbf{r},\tau) + \\ + g_0\,\bar{\psi}_\uparrow(\mathbf{r},\tau)\,\bar{\psi}_\downarrow(\mathbf{r},\tau)\,\psi_\downarrow(\mathbf{r},\tau)\,\psi_\uparrow(\mathbf{r},\tau) \quad (3.82)$$

where ψ_σ, $\bar{\psi}_\sigma$ are the Grassmann field variables, $g_0 < 0$ is the strength coupling of the fermion-fermion attractive interaction and μ_σ is the chemical potential of the component σ.

The only difference with respect to the treatment in Section 3.3, whose Lagrangian can be read from Eq. (3.39) and Eq. (3.40), is the introduction

of a spin-dependent chemical potential μ_σ; we will see, however, that this seemingly innocuous change has many consequences and makes the treatment of the unbalanced Fermi gas rather more complicated than its balanced counterpart. We define the average chemical potential μ and the unbalance chemical potential ζ as the half-sum and the half-difference between the the two chemical potentials, respectively:

$$\mu = \frac{\mu_\uparrow + \mu_\downarrow}{2} \qquad \zeta = \frac{\mu_\uparrow - \mu_\downarrow}{2} \tag{3.83}$$

Without loss of generality, one can assume that the $\uparrow$ species is the majority component. The partition function function for the system can be written as

$$\begin{aligned} \mathcal{Z} &= \int \mathcal{D}\psi_\sigma \mathcal{D}\bar{\psi}_\sigma \; e^{-S\left[\psi_\sigma, \bar{\psi}_\sigma\right]} \\ S\left[\psi_\sigma, \bar{\psi}_\sigma\right] &= \int_0^{\hbar\beta} \mathrm{d}\tau \int_{L^3} \mathrm{d}^3 r \mathscr{L} \; , \end{aligned} \tag{3.84}$$

where $\beta = (k_B T)^{-1}$, T being the temperature.

The same mean-field treatment as in Section 3.3 is performed, in particular the quartic interaction is decoupled by means of a Hubbard-Stratonovich transformation, and the resulting pairing field is approximated by its uniform and constant saddle point value Δ_0, neglecting the fluctuations. After rewriting the field operators in momentum space representation, the physics of the system is then encoded in the 2×2 momentum-space Nambu-Gor'kov inverse Green function:

$$-\mathbb{G}^{-1} = \begin{pmatrix} -\mathrm{i}\omega_n - \frac{\hbar^2 k^2}{2m} + \mu + \zeta & -\Delta_0 \\ -\Delta_0 & -\mathrm{i}\omega_n + \frac{k^2}{2m} - \mu + \zeta \end{pmatrix} \tag{3.85}$$

from which, setting $\det\left(-\mathbb{G}^{-1}\right) = 0$ and solving for $\mathrm{i}\omega_n$ one gets the spectrum of single-particle excitations:

$$E_{\mathbf{k}}^{\pm} = \sqrt{\xi_{\mathbf{k}}^2 + \Delta_0^2} \pm \zeta \; , \tag{3.86}$$

where $\xi_{\mathbf{k}} = \frac{\hbar^2 k^2}{2m} - \mu$ as also found, for example, in Ref. [107], the $+$ $(-)$ sign holding for the $\uparrow$ $(\downarrow)$ component, respectively. Upon integration of the fermionic fields $\bar{\psi}(\mathbf{r}, \tau)$ and $\psi(\mathbf{r}, \tau)$ the summation over Matsubara frequencies yields the following effective grand potential [67]:

$$\Omega_{\text{eff}} = -L^3 \frac{\Delta_0^2}{g_0} + \sum_{\mathbf{k}} (\xi_{\mathbf{k}} - E_{\mathbf{k}}) - \frac{1}{\beta} \sum_{\mathbf{k}} \left[\ln\left(1 + e^{-\beta(E_{\mathbf{k}} - \zeta)}\right) + \ln\left(1 + e^{-\beta(E_{\mathbf{k}} + \zeta)}\right) \right] \tag{3.87}$$

with $E_{\mathbf{k}} = \sqrt{\xi_{\mathbf{k}}^2 + |\Delta_0|^2}$. From the effective grand potential (3.87) we obtain the extended BCS equations at finite temperature, in particular by imposing

the saddle point condition $\partial\Omega_{\text{eff}}/\partial\Delta_0 = 0$ one gets the gap equation

$$\frac{1}{g_0} = -\frac{1}{L^3}\sum_{\mathbf{k}} \frac{1}{E_{\mathbf{k}}} \frac{\sinh(\beta E_{\mathbf{k}})}{2\cosh(\beta\zeta) + 2\cosh(\beta E_{\mathbf{k}})} , \tag{3.88}$$

and using the thermodynamic relation for the number of fermions in the σ spin species $N_\sigma = -\frac{\partial}{\partial\mu_\sigma}\Omega_{\text{eff}}$ one gets the number equation for the average number of particles

$$N = \frac{N_\uparrow + N_\downarrow}{2} = \sum_{\mathbf{k}} \left(1 - \frac{\xi_{\mathbf{k}}}{E_{\mathbf{k}}} \frac{\sinh(\beta E_{\mathbf{k}})}{\cosh(\beta\zeta) + \cosh(\beta E_{\mathbf{k}})}\right) \tag{3.89}$$

and for the particle unbalance

$$\delta N = \frac{N_\uparrow - N_\downarrow}{2} = \sum_{\mathbf{k}} \frac{\sinh(\beta\zeta)}{\cosh(\beta\zeta) + \cosh(\beta E_{\mathbf{k}})} \tag{3.90}$$

and finally $N_{\uparrow,\downarrow} = N \pm \delta N$. The gap equation can be regularized as done in the balanced case by using Eq. (3.79) to eliminate g_0, yielding

$$\frac{m}{4\pi\hbar^2 a_s} = \frac{1}{2L^3}\sum_{\mathbf{k}} \left(\frac{1}{\epsilon_{\mathbf{k}}} - \frac{1}{E_{\mathbf{k}}} \frac{\sinh(\beta E_{\mathbf{k}})}{\cosh(\beta\zeta) + \cosh(\beta E_{\mathbf{k}})}\right) \tag{3.91}$$

A numerical simultaneous solution of Eq. (3.89), Eq. (3.90) and Eq. (3.91) in the $T \to 0$ limit provides a determination of μ and Δ as a function of $N_\uparrow$, $N_\downarrow$ and $y = (k_F a_s)^{-1}$. Moreover, in the zero temperature limit the grand potential from Eq. (3.87) reads

$$\Omega(T=0) = \sum_{\mathbf{k}} (\xi_{\mathbf{k}} - E_{\mathbf{k}}) - L^3\frac{\Delta_0^2}{g_0} + \sum_{|\mathbf{k}|\notin[k_-,k_+]} (E_{\mathbf{k}} - \zeta) \ .$$

with $k_- = \sqrt{\frac{2m}{\hbar^2}}\sqrt{\max\left(\mu - \sqrt{\zeta^2 - \Delta_0^2}, 0\right)}$ and $k_+ = \sqrt{\frac{2m}{\hbar^2}}\sqrt{\mu + \sqrt{\zeta^2 - \Delta_0^2}}$. The first two terms in Eq. (3.92) are identical to their balanced counterpart we already analyzed, the third term, however, contributes to thermodynamics of the system provided that the condition

$$\zeta \geq \zeta_c \equiv \sqrt{\Delta_0^2 + \min^2(\mu, 0)} \tag{3.92}$$

is met, corresponding to the magnetized superfluid (MS) regime. On the other hand, if $\zeta < \zeta_c$ the thermodynamics of the system is identical to that of an unbalanced system, because $k_- = k_+$ and the last summation in Eq. (3.92) extends over all momenta.

3.5.2 Condensate fraction

The condensate fraction is the ratio $\phi = \frac{N_0}{2N}$ with N_0 the condensate number of Fermi pairs [13, 38, 74] and N the total number of particles. The condensate fraction plays a crucial role in the description of a superfluid system: in two experiments [108, 109], the condensate fraction of Cooper pairs [33], which is directly related to the off-diagonal-long-range-order of the two-body density matrix of fermions as already analyzed in Eq. (2.17), has been investigated in dilute vapors of ultracold ^{6}Li atoms in the BCS-BEC crossover exhibiting a quite good agreement with mean-field theoretical predictions [38, 110] and Monte-Carlo simulations at zero temperature [111]. In the present Subsection we study the condensate fraction for the an unbalanced uniform Fermi gas.

Following the approach in Refs. [71, 112], using the Nambu-Gor'kov Green function, the condensate number N_0 is given by

$$N_0 = \frac{1}{\beta^2} \sum_{\mathbf{p}} \sum_{n} \sum_{m} \mathbb{G}_{21}\left(\mathbf{p}, \mathrm{i}\omega_n\right) \mathbb{G}_{12}\left(\mathbf{p}, \mathrm{i}\omega_m\right) \ , \tag{3.93}$$

and $\mathbb{G}_{21}$ and $\mathbb{G}_{12}$ are calculated by inverting the matrix in Eq. (3.85), namely

$$\mathbb{G}_{12}\left(\mathbf{k}, \mathrm{i}\omega_n\right) = -\frac{\Delta_0}{\left(\mathrm{i}\omega_n - \zeta\right)^2 - \xi_{\mathbf{k}}^2 - \left|\Delta_0\right|^2} = \mathbb{G}_{21}\left(\mathbf{k}, \mathrm{i}\omega_n\right) \ . \tag{3.94}$$

After performing the summation over the Matsubara fermionic frequencies, one obtains the condensate number in Eq. (3.93) as a function of the chemical potential μ and of the order parameter Δ_0:

$$N_0 = \sum_{\mathbf{k}} \frac{\Delta_0^2}{4E_{\mathbf{k}}^2} \left(\frac{1}{2} \tanh\left(\frac{\beta}{2} \left(E_{\mathbf{k}} + \zeta \right) \right) + \frac{1}{2} \tanh\left(\frac{\beta}{2} \left(E_{\mathbf{k}} - \zeta \right) \right) \right)^2 \tag{3.95}$$

Again we take the $T \to 0$ limit, finding

$$N_0 = \sum_{|\mathbf{k}| \notin [k_-, k_+]} \frac{\Delta_0^2}{4E_{\mathbf{k}}^2} \ , \tag{3.96}$$

similar to the condensate number in the balanced case $N_0 = \sum_{|\mathbf{k}|} \Delta_0^2 / 4E_{\mathbf{k}}^2$, except for the constraint on the momenta, excluding from the summation wave vectors whose modulus is between k_- and k_+. In fact, as discussed for the two-dimensional case in Ref. [113], even in the three-dimensional case in the zero-temperature limit the system can be thought of as a superfluid in which the particles with momenta $|\mathbf{k}| \in [k_-, k_+]$ contribute as normal state particles.

We use the formula for N_0 in Eq. (3.95) along with those obtained from Eqs. (3.89), (3.90) and (3.91) in the $T \to 0$ limit to numerically calculate the condensate fraction ϕ as a function both of the dimensionless interaction

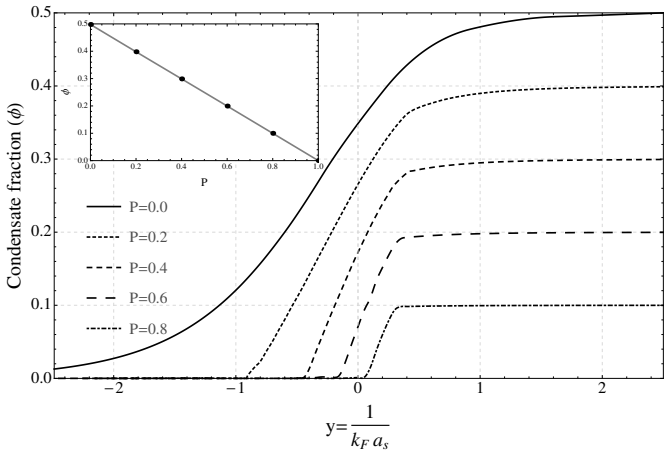

Figure 3.2: The condensate fraction $\phi = N_0/2N$, in the uniform case, as a function of the inverse dimensionless interaction parameter $y = (k_F a_s)^{-1}$ for different values of the polarization. In the inset ϕ as a function of the polarization $P = (N_\uparrow - N_\downarrow)/(N_\uparrow + N_\downarrow)$ for $y = 2$.

parameter $y = (k_F a_s)^{-1}$ and of the polarization $P = (N_\uparrow + N_\downarrow)/(N_\uparrow - N_\downarrow)$. The results are reported in Fig. 3.2.

In particular we observe that in the BCS regime a weak superfluidity is destroyed even for small values of the polarization P. On the other hand the behavior in the BEC limit is easily understood by observing than $N_\uparrow$ spin-up particle and $N_\downarrow$ particle will form $N_{\text{pairs}} = 2\min(N_\uparrow, N_\downarrow)$ boson-like bound pairs, while the remaining

$$N_{\text{normal}} = N - N_{\text{pairs}} = N_\uparrow - N_\downarrow = NP \tag{3.97}$$

fermions will form a normal-state Fermi gas. The former contribute to the condensate fraction, while the latter do not. Hence, by noting that N_{normal} is proportional to the polarization, and by also noting that $N_{\text{pairs}} = 2N - 2N_{\text{normal}}$, we expect to observe that in the deep BEC regime $N_{\text{pairs}} \propto (1 - P) \propto \phi$, as verified in the inset of Fig. 3.2 for $y = 2$.

3.5.3 Condensate fraction for a trapped system

A polarized Fermi gas is investigated experimentally by confining it in a trapping potential; as opposed to the balanced case, in presence of polarization a phase-separated regime shows up, rendering a realistic modeling of the trapping compelling when dealing with unbalanced spin populations.

We assume that the unbalanced Fermi gas is confined by a potential $V(\mathbf{r})$ given by the superposition of an isotropic harmonic trap part in the radial xy plane and a different harmonic confinement in the axial z direction:

$$V(\mathbf{r}) = \frac{m}{2}\left(\omega_\perp^2 \rho^2 + \omega_z^2 z^2\right) \tag{3.98}$$

with $\rho^2 = x^2 + y^2$, as in the experimental configuration in Ref. [61], here $\omega_\perp$ and ω_z are the transverse and axial trapping frequencies, respectively.

The external confinement is accounted for by defining a position-dependent chemical potential for each spin species

$$\mu_\sigma(\mathbf{r}) = \mu_\sigma - V(\mathbf{r}) \tag{3.99}$$

and treating the system as locally uniform,in local density approximation (LDA). As a consequence the average chemical potential is also non uniform, $\mu(\mathbf{r}) = \mu - V(\mathbf{r})$, while the unbalance chemical potential ζ remains uniform.

Consequently, the extended BCS equations have to be solved at each point of the space for a spatially-dependent gap $\Delta(\mathbf{r})$ for a given scattering length a_s. The zero-temperature free energy

$$F = \Omega(T=0) + \sum_\sigma \mu_\sigma N_\sigma \tag{3.100}$$

exhibits two minima, that is one for a nonvanishing order parameter, say $\Delta_{0,\mathrm{BCS}}(\mathbf{r})$ (superfluid phase), and one for $\Delta_0 = 0$ (normal phase). In the balanced case the minimum corresponding to the superfluid phase is always a global minimum, in the present case, on the other hand, that is not the case and the interplay between the two minima is the reason for the phase separation.

By requiring that the superfluid and the normal states have the same free energy, one determines the boundary between the superfluid and the normal phase. It turns out that the superfluid phase always occupies the inner part of the system, being eventually surrounded by a normal-state outer cloud. We define R_{BCS} as the radius, measured along the z axis, of the inner superfluid component. In the present treatment the normal fermions are dealt with approximately as two non interacting Fermi gases with local densities

$$n_\sigma(\mathbf{r}) = \frac{\left(\frac{2m}{\hbar^2}\left(\mu(\mathbf{r}) \pm \zeta\right)\right)^{\frac{3}{2}}}{6\pi^2} \,. \tag{3.101}$$

In describing the normal state mixture that surrounds the SF inner core, we define the Thomas-Fermi radii for the two components[11]:

$$R^{\mathrm{TF}}_{\uparrow,\downarrow} = \sqrt{\frac{2\left(\mu \pm \zeta\right)}{m\omega_z^2}} \,, \tag{3.102}$$

where the sign + (−) holds for the ↑ (↓) component, respectively, with the majority spin-up species occupying the larger volume. Moving along the

[11] Here we measure the radii along the z-axis. In principle, one could rescale the system lengths along the radial direction by a factor of $\omega_z/\omega_\perp$ so that the system can be regarded as spherically symmetric.

z axis starting from the center of the trap, when $z < R_{\rm BCS}$ the system is in a superfluid state, while for $R_{\rm BCS} < z < R_{\uparrow}^{\rm TF}$ the system consists of a normal-state mixture. Provided that the polarization is smaller than a critical value above which the superfluid is destroyed [114] and $R_{\rm BCS} = 0$, we always have a phase-separated regime.

In Fig. 3.3, we report the condensate and the total density profiles as functions of the axial coordinate z for three different scattering lengths. In accordance with other theoretical works [96, 97] and with experimental data [106] the superfluid phase ends abruptly at $R_{\rm BCS}$: the condensate fraction thus jumps from a finite value to zero, as a manifestation of the phase separation.

Our results for the condensate fraction as a function of the polarization are plotted in Fig. 3.4, showing the comparison with the experimental findings reported in Ref. [61]. We use the same trap parameters and the same total number of fermions as reported in the Supplemental Material of Ref. [61], i.e. $\omega_\perp = 2\pi \cdot 192\,\mathrm{Hz}$, $\omega_z = 2\pi \cdot 23\,\mathrm{Hz}$, and $N = 2.3 \cdot 10^7$. Fig. 3.4 .

In our mean-field theory the condensate fraction is essentially linear as a function of the polarization. Our results reasonably fit the experimental data at low polarizations, up to $P \sim 0.25$. For higher polarizations the closer P to the critical polarization the greater the discrepancy between our predictions and the from-laboratory results, even taking into account that the experimental data are affected by a 20% error on the number of particles.

For instance we observe that for $y = -0.44$, $y = 0$ and $y = 0.11$, the critical polarization is at least 0.98. Experimental observations, on the other hand, report that the critical polarization, while approaching 1 in the strong coupling regime, should decrease for weaker interaction strengths. In particular, a critical polarization $P_c = 0.77$ is observed at unitarity, see, for example, [106]. This overestimation of the critical polarization by the mean-field theory has been also reported by [115] and [84]. The reason of this disagreement lies on the treatment of the non-superfluid phases as non-interacting Fermi gases, neglecting the binding energy of the mixed state [115]. We mention that the corrections to the normal phase, introduced, only for $y = 0$, in Ref. [115] allows to predict with great precision the critical polarization.

In conclusion, in this Section we calculated the condensate fraction a a uniform Fermi gas and by using a local-density approximation approach we extended the result to model a trapped system. Our approach can reproduce the phase separation, however the condensate fraction as a function of the polarization agrees with experimental data only for low polarization. An improved treatment would require a more realistic model of the normal-state mixture surrounding the superfluid inner core.

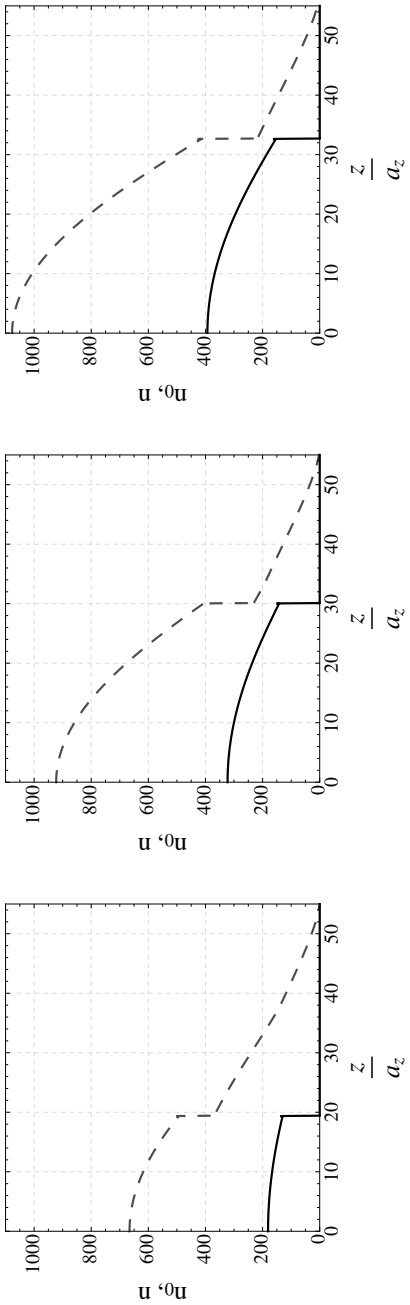

Figure 3.3: The condensate density profile n_0, solid line, and total density profile n, dashed line, for three different scattering lengths (from left to right: $y = -0.44$, $y = 0.0$, $y = 0.11$), as a function of the axial coordinate z. The chemical potentials have been adjusted to have $N = 2.3 \cdot 10^7$ and $P \sim 0.2$. The axial coordinate and the density are in units of the trap characteristic length $a_z = \frac{\hbar}{\sqrt{m\omega_z}}$ and of $n_z = \left(\frac{2m}{\hbar^2}\omega_z\right)^{3/2}$, respectively.

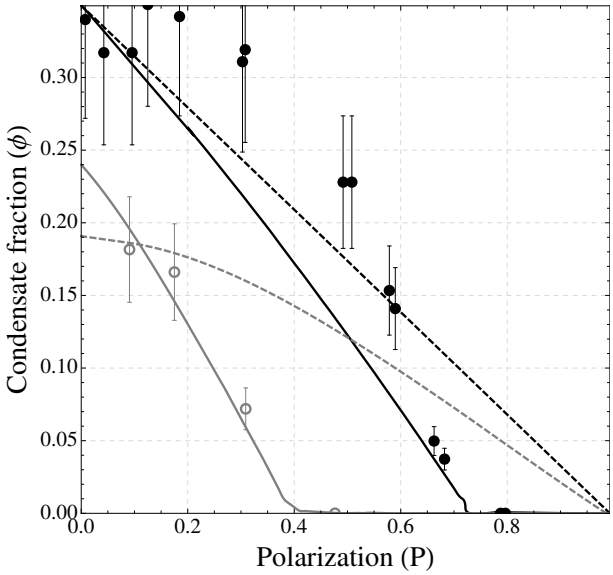

Figure 3.4: The condensate fraction ϕ as a function of the polarization P for different values of the dimensionless interaction parameter $y = 1/(k_F a_s)$ (Black lines and points: $y = 0.0$, Grey lines and points: $y = -0.44$). The points represent experimental data, as reported by [61]. We observe that when modeling the harmonic trapping potential (dashed lines), our theoretical predictions match experimental data only at low polarizations, due to an incorrect estimate of the phase boundary. The error bars are calculated by assuming that the error on the condensate fractions comes only from the 20% reported error on the number of atoms [61].

4

Beyond mean field: collective excitations in the BCS-BEC crossover

The mean-field description of the BCS-BEC crossover introduced in the previous Chapter can provide a good agreement with experiments at zero temperature. However, it completely neglects order parameter fluctuations and excitations other than the single-particle modes, e.g. the sound mode is completely neglected. In the present Chapter the Gaussian fluctuations for the order parameter are taken into account, on top of the mean-field approximation derived in the previous Chapter.

The field-theoretical approach in Ref. [67] is followed for the introduction of the fluctuation formalism, and I am grateful to Prof. Jacques Tempere for hosting me in his research group at University of Antwerp from March 2014 to June 2014. During this very fruitful period of collaboration I learned many techniques, many of which related to the order parameter fluctuations, which greatly helped me in the second part of my Ph.D.; moreover during my stay in Belgium I met an original and friendly research group, whom I thank for hosting me.

The main formalism is introduced in Section 4.1 and the fluctuation partition function is derived, describing the contributions of bosonic collective excitations to the thermodynamics of the system. Subsequently the following topic are considered:

- The damping of collective modes at zero temperature in the BCS-BEC crossover. In Section 4.2, at first a hydrodynamical theory is developed for an improved treatment of the Beliaev decay and is subsequently applied to the collective modes of Fermi gas across a broad Feshbach

resonance. The analysis is based on results published in Ref. [2].

- The two-dimensional BCS-BEC crossover. The role of the fluctuations is more relevant in lower dimensionality systems [116], for $d \leq 2$, d being the number of spatial dimensions, they completely destroy the off-diagonal long-range order at finite temperature: in Section 4.3 we investigate the role of fluctuations in a 2D Fermi gas, deriving a Gaussian-level equation of state and calculating the superfluid density, the speed of the first and second sound and the Berezinskii-Kosterlitz-Thouless critical temperature. The analysis is based on results published in Ref. [3].

- Finally in the last Section, based on Ref. [4], an analytical result for the scattering length of composite bosons in the deep-BEC limit is derived. The fluctuations here modify the mean-field result $a_b = 2a_s$ to $a_b = 0.6a_s$, in very good agreement with Monte Carlo and experimental data.

4.1 Collective excitations in the BCS-BEC crossover: general theory

In the previous Chapter, before introducing the saddle-point approximation, we derived an exact expression for the partition function for an attractive Fermi gas at temperature T, within the grand canonical ensemble at chemical potential μ. In particular by introducing the pairing field Δ, $\bar{\Delta}$ through the Hubbard-Stratonovich transformation and integrating out the fermions we obtained Eq. (3.52), which reads

$$\mathcal{Z} = \int \mathcal{D}\Delta\mathcal{D}\bar{\Delta} \exp\left[\mathrm{Tr}\ln\left(-\mathbb{G}^{-1}\right) + \sum_{\mathbf{q},m} \frac{|\Delta(\mathbf{q}, \mathrm{i}\Omega_m)|^2}{g_0}\right] \tag{4.1}$$

using the same notation as in Section 3.3, in particular $g_0 < 0$ is the strength of the attractive potential, $\Delta(\mathbf{q}, \mathrm{i}\Omega_m)$ is the Fourier transform of the pairing field, Ω_m are bosonic Matsubara frequencies and finally $-\mathbb{G}^{-1}$ is the inverse Green function. The pairing field can be expressed as the sum of a uniform (in coordinate space) and constant (with respect to the imaginary time τ) saddle point value Δ_0 and the fluctuations around that value. In frequency-momentum representation one gets

$$\Delta(\mathbf{q}, \mathrm{i}\Omega_m) = \Delta_0 \ \delta(\mathbf{q})\delta_{m,0} + \eta(\mathbf{q}, \mathrm{i}\Omega_m) \tag{4.2}$$

and consequently the Green function $-\mathbb{G}^{-1}$ can be decomposed as

$$-\mathbb{G}^{-1} = -\mathbb{G}_{\mathrm{sp}}^{-1} + \mathbb{F} \ , \tag{4.3}$$

with

$$\left[-\mathbb{G}_{\rm sp}^{-1}\right]_{k,k'} = \begin{pmatrix} -\mathrm{i}\omega_n + \frac{k^2}{2m} - \mu & -\Delta_0 \\ -\Delta_0 & -\mathrm{i}\omega_n - \frac{k^2}{2m} + \mu \end{pmatrix} \delta(\mathbf{k}-\mathbf{k}')\delta_{n,n'} \tag{4.4}$$

and

$$\left[\mathbb{F}\right]_{k,k'} = \begin{pmatrix} 0 & -\eta(\mathbf{k}+\mathbf{k}', \mathrm{i}\Omega_{n+n'}) \\ -\eta(\mathbf{k}+\mathbf{k}', \mathrm{i}\Omega_{n+n'}) & 0 \end{pmatrix} . \tag{4.5}$$

We stress that Eq. (4.1) is exact but cannot be treated analytically and must be dealt with in an approximate way: in the mean field approximation the full inverse Green function $-\mathbb{G}^{-1}$ is replaced by its mean-field approximation $-\mathbb{G}_{\rm sp}^{-1}$, the pairing field Δ, $\bar{\Delta}$ loses its dynamics and the functional integration in Eq. (4.1) is no longer necessary.

The aim of the present Section is the derivation of a more accurate approach, taking into account the fluctuations contained in $\mathbb{F}$ in an approximate way, rather than completely ignoring them as done when deriving the mean-field theory. In particular the object $\ln\left(-\mathbb{G}^{-1}\right)$ appearing in Eq. (4.1) can be rewritten as follows

$$\ln\left(-\mathbb{G}^{-1}\right) = \ln\left(-\mathbb{G}_{\rm sp}^{-1}\left(\mathbb{1} - \mathbb{G}_{\rm sp}\mathbb{F}\right)\right) = \ln\left(-\mathbb{G}_{\rm sp}^{-1}\right) + \ln\left(\mathbb{1} - \mathbb{G}_{\rm sp}\mathbb{F}\right) , \tag{4.6}$$

the first term $\ln\left(-\mathbb{G}_{\rm sp}^{-1}\right)$ giving exactly the mean-field contribution. As the saddle-point value Δ_0 for the pairing field is calculated self-consistently by minimizing the action, one expects the fluctuations η, $\bar{\eta}$ around the saddle point to be small, justifying an expansion of the second logarithm in the r.h.s. of Eq. (4.6) in powers of $\mathbb{F}$, as each non-zero entry of $\mathbb{F}$ is proportional to η or $\bar{\eta}$. Going on with the expansion one finds:

$$\ln\left(\mathbb{1} - \mathbb{G}_{\rm sp}\mathbb{F}\right) = -\sum_{n=1}^{\infty} \frac{\left(\mathbb{G}_{\rm sp}\mathbb{F}\right)^n}{n} \approx -\mathbb{G}_{\rm sp}\mathbb{F} - \frac{1}{2}\mathbb{G}_{\rm sp}\mathbb{F}\mathbb{G}_{\rm sp}\mathbb{F} + \mathcal{O}\left(\eta^3\right) , \tag{4.7}$$

having neglected terms above Gaussian order in the fluctuations. The Gaussian approximation scheme can then be written in terms of the inverse Green function as

$$-\mathbb{G}^{-1} \to -\mathbb{G}_{\rm sp}^{-1} - \mathbb{G}_{\rm sp}\mathbb{F} - \frac{1}{2}\mathbb{G}_{\rm sp}\mathbb{F}\mathbb{G}_{\rm sp}\mathbb{F} . \tag{4.8}$$

As a consequence the partition function for the system in Eq. (4.1) can be written as $\mathcal{Z} = \mathcal{Z}_{\rm mf}\mathcal{Z}_{\rm fl}$, i.e the product of the "old" mean-field contribution $\mathcal{Z}_{\rm mf}$ we previously found, see e.g. Eq. (3.60), times a new fluctuation contribution [67]:

$$\begin{aligned} \mathcal{Z}_{\rm fl} &= \int \mathcal{D}\eta\mathcal{D}\bar{\eta}\; e^{-S_{\rm fl}[\eta,\bar{\eta}]} \\ S_{\rm fl}[\eta,\bar{\eta}] &= \frac{1}{2}\,\mathrm{Tr}(\mathbb{G}_{\rm sp}\mathbb{F}\mathbb{G}_{\rm sp}\mathbb{F}) - \sum_{\mathbf{q},m} \frac{\left|\eta(\mathbf{q}, \mathrm{i}\Omega_m)\right|^2}{g_0} \end{aligned} \tag{4.9}$$

with the same notation as in Section 3.3, in particular Ω_m are bosonic Matsubara frequencies; the linear terms in η, $\bar{\eta}$ vanished due to the saddle point condition imposed for Δ_0.

After a lengthy but straightforward calculation, involving the frequency-momentum space representations of the $\mathbb{G}_{\mathrm{sp}}^{-1}$ and $\mathbb{F}$ matrices as introduced in Eq. (3.55) and Eq. (3.56), the effective fluctuation action can be recast in the following Gaussian form

$$S_{\mathrm{fl}} = \frac{1}{2}\sum_{\mathbf{q},m} \begin{pmatrix} \bar{\eta}(\mathbf{q}, \mathrm{i}\Omega_m) & \eta(-\mathbf{q}, -\mathrm{i}\Omega_m) \end{pmatrix} \mathbb{M}(\mathbf{q}, \mathrm{i}\Omega_m) \begin{pmatrix} \eta(\mathbf{q}, \mathrm{i}\Omega_m) \\ \bar{\eta}(-\mathbf{q}, -\mathrm{i}\Omega_m) \end{pmatrix} \quad (4.10)$$

and the $\mathbb{M}$ matrix [67, 117, 118] is the inverse pair fluctuation propagator and describes the dynamics of the bosonic collective excitations of the theory. Its matrix elements are given, after carrying out a Matsubara summation, by [67, 118]

$$\begin{aligned} M_{11}(\mathbf{q}, \mathrm{i}\Omega_m) = &-\frac{1}{g_0} + \sum_{\mathbf{k}} \frac{\tanh(\beta E_{\mathbf{k}}/2)}{2E_{\mathbf{k}}} \times \\ &\times \left[\frac{(\mathrm{i}\Omega_m - E_{\mathbf{k}} + \xi_{\mathbf{k}+\mathbf{q}})(E_{\mathbf{k}} + \xi_{\mathbf{k}})}{(\mathrm{i}\Omega_m - E_{\mathbf{k}} + E_{\mathbf{k}+\mathbf{q}})(\mathrm{i}\Omega_m - E_{\mathbf{k}} - E_{\mathbf{k}+\mathbf{q}})} + \right. \\ &\left. - \frac{(\mathrm{i}\Omega_m + E_{\mathbf{k}} + \xi_{\mathbf{k}+\mathbf{q}})(E_{\mathbf{k}} - \xi_{\mathbf{k}})}{(\mathrm{i}\Omega_m + E_{\mathbf{k}} - E_{\mathbf{k}+\mathbf{q}})(\mathrm{i}\Omega_m + E_{\mathbf{k}} + E_{\mathbf{k}+\mathbf{q}})} \right] , \end{aligned} \quad (4.11)$$

and

$$\begin{aligned} M_{12}(\mathbf{q}, \mathrm{i}\Omega_m) = &-\Delta_0^2 \sum_{\mathbf{k}} \frac{\tanh(\beta E_{\mathbf{k}}/2)}{2E_{\mathbf{k}}} \times \\ &\times \left[\frac{1}{(\mathrm{i}\Omega_m - E_{\mathbf{k}} + E_{\mathbf{k}+\mathbf{q}})(\mathrm{i}\Omega_m - E_{\mathbf{k}} - E_{\mathbf{k}+\mathbf{q}})} + \right. \\ &\left. + \frac{1}{(\mathrm{i}\Omega_m + E_{\mathbf{k}} - E_{\mathbf{k}+\mathbf{q}})(\mathrm{i}\Omega_m + E_{\mathbf{k}} + E_{\mathbf{k}+\mathbf{q}})} \right] , \end{aligned} \quad (4.12)$$

with the same notation as in the previous Chapter, in particular $\xi_{\mathbf{k}} = \hbar^2 k^2/2m - \mu$ and $E_{\mathbf{k}} = \sqrt{\xi_{\mathbf{k}}^2 + \Delta_0^2}$. The remaining matrix elements are defined by the relations

$$M_{11}(\mathbf{q}, -i\Omega_m) = M_{22}(\mathbf{q}, i\Omega_m) \ , \quad (4.13)$$

$$M_{12}(\mathbf{q}, -i\Omega_m) = M_{21}(\mathbf{q}, i\Omega_m) \, . \quad (4.14)$$

and when doing numerical calculations the unphysical parameter g_0 can be eliminated with the aid of Eq. (3.79) exactly as done in regularizing the gap equation. By integrating out the $\eta(\mathbf{r}, \tau)$, $\bar{\eta}(\mathbf{r}, \tau)$ fields we get the Gaussian contribution to the finite-temperature grand potential [117, 118]

$$\Omega_{\mathrm{fl}} = \frac{1}{2\beta}\sum_{\mathbf{q},m} \ln(\det \mathbb{M}(\mathbf{q}, \mathrm{i}\Omega_m)) \quad (4.15)$$

and the full Gaussian-level grand potential for the system is given by the sum of the saddle-point (mean field) and fluctuations contribution, i.e.

$$\Omega = \Omega_{\rm mf} + \Omega_{\rm fl} \ . \tag{4.16}$$

The gap equation remains unchanged as the saddle point is found at mean-field level, the number equation, on the other hand, gets a new contribution from $\Omega_{\rm fl}$, namely

$$N = -\frac{\partial \Omega}{\partial \mu} = -\frac{\partial \Omega_{\rm mf}}{\partial \mu} - \frac{\partial \Omega_{\rm fl}}{\partial \mu} - \frac{\partial \Omega_{\rm fl}}{\partial \Delta_0}\frac{\partial \Delta_0}{\partial \mu} \ . \tag{4.17}$$

The role of last term in the r.h.s. of Eq. (4.17) has been widely debated [118]. If neglected the theory would reproduce the Nozières-Schmitt-Rink (NSR) approach [44], while its inclusion, considering Δ_0 as an independent variable, leads to the present approach, known as Gaussian pair fluctuation (GPF). It has been demonstrated [118] that in the two-dimensional case the GPF approach makes the number equation convergent, on the other hand it would be otherwise affected by divergencies if the NSR approach was chosen. Moreover it has been argued [119] that even in the three-dimensional case the last term in Eq. (4.17) is less relevant numerically but should not be neglected.

4.2 Landau hydrodynamics and the Beliaev decay

In the present Section we introduce a hydrodynamic description of a superfluid, subsequently applying it to the description of the collective excitations in a Fermi gas.

Excitations in a superfluid can be described using the quantum hydrodynamics approach developed by Landau [120]; a clear advantage of this formalism is the possibility of describing superfluids with non-contact interactions and with a varying number of particles by introducing higher order terms by means of a perturbative expansion around the mean field solution.

Collective excitations in a superfluid are destroyed either by Landau damping, due to their interaction with the thermal cloud, or by Beliaev damping, due to their decay into two, or more, lower energy excitations. There is competition between these two damping modes: whereas Landau damping is relevant at finite temperatures, with a vanishing cross section as the temperature goes to zero, Beliaev damping remains the only allowed decay mode at $T = 0$.

Therefore the Beliaev decay represents a test of Landau's hydrodynamic theory. First evidences of a phonon decay have been observed in superfluid liquid ^{4}He [121, 122]; more recently the Beliaev decay has been observed in a trapped Bose-Einstein condensate (BEC) of rubidium atoms [123, 124]; an analogous process has been proposed in order to explain the absence

of equilibrium in one dimensional interacting bosons, see Ref. [125] and references therein.

In the first part of the present Section we focus on Beliaev decay and derive an improved version of the classical result [120, 126, 127] based on the observation that while the original derivation requires a nonlinear term in the spectrum, nonetheless it treats the kinematics in a low-momentum approximation as if the spectrum was effectively linear. We show that this treatment can be extended and that, in particular, the inclusion of a gradient term in the Hamiltonian yields a Bogoliubov-like spectrum for the bosonic excitations [128]. We calculate the decay rate for the Beliaev damping and show that even for low momenta and small nonlinearities a realistic spectrum can give appreciable differences with respect to the linear approximation of the standard result.

The motivation for this work is the application to an attractive Fermi gas in the second part of this Section: as the attractive interaction between atoms is tuned, the gas at $T = 0$ goes with continuity from a Bardeen-Cooper-Schrieffer (BCS) weakly-interacting regime, to a strongly interacting gas of bosonic dimers. This scenario can be described [36, 71, 76] by introducing the complex Cooper pairing field, which will acquire a non-zero expectation value below the critical temperature. As the phase of the order parameter is macroscopically locked below the critical temperature [72, 129], spontaneously breaking the $U(1)$ symmetry, its fluctuations correspond to the gapless mode predicted by the Goldstone theorem. These collective modes turn out to be fundamental in quantitatively describing the dynamics of an ultracold Fermi gas [130]; after briefly analyzing the Goldstone mode, we show that its linewidth gets substantially enhanced due to the Beliaev decay process. We also show that our improved description of the decay yields substantial deviations from the standard approximation.

4.2.1 Beliaev damping: an improved treatment

We briefly introduce Landau's quantum hydrodynamics [120, 127], a semi-phenomenological description of a superfluid which can be, however, rigorously justified and derived from the microscopical theory as discussed in Ref. [131]. An exact expression for the internal energy of a classical liquid in a sound wave is $E = \int \mathrm{d}^3x(\frac{1}{2}\rho v^2 + \rho e)$, where v is the local velocity of the fluid, and ρ the local density. Here e represents the internal energy of the fluid for unit mass; Landau's original treatment [120, 126] assumes it to be dependent only on the density ρ, and as a consequence the dispersion relation for the sound waves is linear. On the other hand by adding a gradient term as

$$e(\rho) \to e(\rho, \nabla\rho) = e(\rho) + \lambda \frac{\hbar^2}{8m^2} \frac{(\nabla\rho)^2}{\rho^2} \tag{4.18}$$

higher order terms appear in the dispersion relation as shown in [128], m being the mass of a fluid particle, λ being a dimensionless coefficient which can be fixed *a posteriori*. Within the quantum hydrodynamics framework the velocity and density fields of a fluid are promoted to quantum operators, so that the Hamiltonian for a quantum fluid is:

$$\hat{H} = \int \mathrm{d}^3x \left[\frac{1}{2} \hat{\mathbf{v}} \cdot \hat{\rho}\hat{\mathbf{v}} + \hat{\rho} e(\hat{\rho}, \nabla\hat{\rho}) \right] \tag{4.19}$$

where the term involving the velocity operator has been opportunely symmetrized to be Hermitean. We rewrite the velocity in terms of a velocity potential $\hat{\mathbf{v}} = \nabla\hat{\phi}$ and the density by separating the equilibrium value ρ from its fluctuations as $\hat{\rho} = \rho + \hat{\rho}'$. The new operators can be written expanding in plane waves:

$$\hat{\rho}' = \frac{1}{\sqrt{2L^3}} \sum_{|\mathbf{k}|\neq 0} A_{\mathbf{k}} \left(\hat{b}_{\mathbf{k}} e^{\mathbf{i}\mathbf{k}\cdot\mathbf{r}} + \hat{b}^\dagger_{\mathbf{k}} e^{-\mathbf{i}\mathbf{k}\cdot\mathbf{r}} \right) \tag{4.20}$$

$$\hat{\phi} = \frac{1}{\sqrt{2L^3}} \sum_{|\mathbf{k}|\neq 0} \mathrm{i}\hbar B_{\mathbf{k}} \left(b_{\mathbf{k}} e^{\mathbf{i}\mathbf{k}\cdot\mathbf{r}} - b^\dagger_{\mathbf{k}} e^{-\mathbf{i}\mathbf{k}\cdot\mathbf{r}} \right) \tag{4.21}$$

with L^3 the volume of the system; the $b_{\mathbf{q}}$ ($b^\dagger_{\mathbf{q}}$) operators annihilate (create) a bosonic excitation over the fundamental state of the liquid $|\Omega\rangle$, and obey the canonical commutation relationships.

We impose that $\hat{\rho}'$ and $\hat{\phi}$ should be canonically conjugate variables

$$[\hat{\phi}(\mathbf{r}), \hat{\rho}'(\mathbf{r}')] = -\mathrm{i}\hbar\delta(\mathbf{r} - \mathbf{r}') \tag{4.22}$$

this constraint being fulfilled by $B_{\mathbf{k}} = A^{-1}_{\mathbf{k}}$. The exact treatment of a quantum liquid in Eq. (4.19) can be expanded in powers of the field operators: the first to give a contribution is the second order, here the theory can be diagonalized to a theory of non-interacting bosons, i.e. $\hat{H}^{(2)} = \sum_{\mathbf{k}} \hbar\omega_{\mathbf{k}} \hat{b}^\dagger_{\mathbf{k}} \hat{b}_{\mathbf{k}}$, and the requirement for $\hat{H}^{(2)}$ to be diagonal fully fixes $A_{\mathbf{k}}$ as:

$$A_{\mathbf{k}} = \sqrt{\frac{\hbar k \rho}{u}} \left(1 + \lambda \frac{\hbar^2}{8m^2} \frac{k^2}{c^2} \right)^{-\frac{1}{4}} \tag{4.23}$$

and the dispersion for the bosons has the usual Bogoliubov structure

$$\omega_{\mathbf{k}} = u\hbar k \sqrt{1 + \lambda \frac{\hbar^2}{4m^2} \frac{k^2}{u^2}} \tag{4.24}$$

u being the sound velocity of the sound waves in the quantum liquid. Clearly the original linear theory can be recovered by setting $\lambda = 0$ and removing the gradient terms. The present formalism, as opposed to the Gross-Pitaevskii equation [132, 133], allows for the decay of a collective excitation in a

superfluid, in particular extending the treatment to the third order one immediately sees that the decay of one excitation into two is allowed: this process is the Beliaev decay [126] described above. The third order term of the Hamiltonian is:

$$\hat{H}^{(3)} = \int \mathrm{d}^3 r \Big[(\nabla\hat{\phi}) \frac{\hat{\rho}'}{2} (\nabla\hat{\phi}) + \frac{1}{6} \left(\frac{\mathrm{d}}{\mathrm{d}\rho} \frac{u^2}{\rho} \right) \hat{\rho}'^3 - \lambda \frac{\hbar^2}{8m^2} (\nabla\hat{\rho}')^2 \frac{\hat{\rho}'}{\rho^2} \Big] \,. \quad (4.25)$$

Before going on with the treatment of the Beliaev decay we briefly comment on the scope of application of the present theory; as already mentioned it can be shown [131] that the hydrodynamic Hamiltonian in Eq. (4.19) can be rigorously derived from a description of the Bose gas; this procedure involves integrating out the "fast fields", effectively defining a momentum scale k_c below which the perturbative expansion should be valid. Following Ref. [131] one can estimate this quantity for a weakly interacting Bose gas; here k_c is the momentum marking the separation between a linear spectrum and the free-particle quadratic spectrum, and from Eq. (4.24) one gets

$$\hbar k_c \simeq \frac{2mu}{\sqrt{\lambda}} \quad (4.26)$$

this condition marking, as argued in Ref. [131], the upper limit for the validity of the perturbation theory.

In order to study the Beliaev decay we calculate the matrix element:

$$H^{(3)}_{if} = \langle i | H^{(3)} | f \rangle \quad (4.27)$$

between the following initial and final states:

$$|i\rangle = \hat{b}^\dagger_{\mathbf{p}} |\Omega\rangle \quad (4.28)$$

$$|f\rangle = \hat{b}^\dagger_{\mathbf{q}_1} \hat{b}^\dagger_{\mathbf{q}_2} |\Omega\rangle \quad (4.29)$$

The matrix element in Eq. (4.27), when Eqs. (4.20) and (4.21) are plugged in, is essentially the expectation value over $|\Omega\rangle$ of a number of terms composed of six creation/annihilation operators; after a lengthy but straightforward calculation reported in Appendix B, one obtains

$$H^{(3)}_{if} = \frac{(2\pi\hbar)^3}{(2V)^{\frac{3}{2}}} \cdot \delta^{(3)}(\mathbf{p} - \mathbf{q}_1 - \mathbf{q}_2) \cdot 3 \sqrt{\frac{u}{\rho} p q_1 |\mathbf{p} - \mathbf{q}_1|} \left(1 + \chi_\theta \frac{\rho^2}{u^2} \frac{\mathrm{d}}{\mathrm{d}\rho} \frac{u^2}{\rho} \right) \quad (4.30)$$

where θ is the angle between $\mathbf{p}$ and $\mathbf{q}_1$, the other angles being fixed by the condition $\mathbf{q}_2 = \mathbf{p} - \mathbf{q}_1$ enforced by the δ function. We also defined:

$$\chi_\theta^{-1} = \frac{p - q_1}{|\mathbf{p} - \mathbf{q}_1|} (1 + \cos(\theta)) + \cos(\theta) \,. \quad (4.31)$$

In deriving Eq. (4.30) we neglected all the terms containing λ; it can be checked that they give $\propto p^7$ and $\propto p^9$ contributions to the decay width,

whereas the leading contribution will turn out to be $\propto p^5$. However the nonlinear dispersion relation is relevant when discussing the kinematics: the differential decay rate is calculated using Fermi's golden rule[1]:

$$\mathrm{d}w = \frac{2\pi}{\hbar}|H_{if}^{(3)}|^2\delta(E_f - E_i)\frac{V^2}{(2\pi\hbar)^6}\mathrm{d}^3q_1\mathrm{d}^3q_2 \tag{4.32}$$

and $E_f - E_i = \hbar\omega_{\mathbf{p}} - \hbar\omega_{\mathbf{q}_1} - \omega_{\mathbf{q}_2}$, $\omega_{\mathbf{k}}$ is the spectrum as derived in Eq. (4.24). The integration over d^3q_2 is performed using the momentum conservation constraint appearing in $|H_{if}^{(3)}|$, the integration over the angular part of d^3q_1 removes the δ function related to energy conservation, fixing at the same time the decay angle θ_0, and finally the radial integration remains explicit. The final result for the decay rate is:

$$w = \frac{9}{32\pi\rho\hbar^4}\int_0^p q^2|\mathbf{p}-\mathbf{q}|_0^2\frac{\left(1+\chi_{\theta_0}\frac{\rho}{u^2}\frac{\mathrm{d}}{\mathrm{d}\rho}\frac{u^2}{\rho}\right)^2}{|f'(\cos\theta_0,p,q)|}\mathrm{d}q \tag{4.33}$$

where $|\mathbf{p}-\mathbf{q}|_0^2 = |p^2+q^2-2pq\cos\theta_0|$ for the sake of shortness,

$$f(\cos\theta,p,q) = \frac{1}{u}\frac{|\mathbf{p}-\mathbf{q}|}{pq}\left(\hbar\omega_p - \hbar\omega_q - \hbar\omega_{|\mathbf{p}-\mathbf{q}|}\right) \tag{4.34}$$

is essentially the energy conservation constraint, f' is its derivative with respect to the first argument and $\theta_0 = \theta_0(p,q)$ is the only zero of f in the interval $[-\pi,\pi]$, and represents the allowed decay angle given the incoming and outgoing momenta.

Equation (4.33) is the main result of the present Subsection, and will be employed in the next Subsection in studying the Beliaev decay of collective excitation in an attractive Fermi gas. We stress that w in Eq. (4.33) is a function of just ρ, u and of the incoming momentum p; moreover the exact form of the spectrum, including the λ coefficient, contributes indirectly to the final result, by modifying f and, consequently, θ_0. We also note the kinematics constraints can be satisfied and the decay is allowed only if the aforementioned zero of f exists, an equivalent condition being that the spectrum should grow faster than linearly.

Let us make the physical meaning of the last remark clearer, expanding the spectrum in Eq. (4.24) in powers of k:

$$\hbar\omega_{\mathbf{k}} = uk + \alpha k^3 + \mathcal{O}\left(k^4\right) \tag{4.35}$$

where α has the same sign as λ. The energy conservation constraint in the low momentum limit reads $1-\cos\theta = 3\alpha(p-q)^2$ and can be fulfilled only

[1]The square of the δ function imposing momentum conservation is to be interpreted as in [120]: $\left[\delta^{(3)}\left(\mathbf{p}-\mathbf{q}_1-\mathbf{q}_2\right)\right]^2 = \frac{V}{(2\pi\hbar)^3}\delta^{(3)}\left(\mathbf{p}-\mathbf{q}_1-\mathbf{q}_2\right)$

if $\alpha \geq 0$, i.e. only if the spectrum grows linearly or more than linearly; for $\alpha < 0$ no decay is allowed.

We now focus on the strictly linear case $\alpha = 0$. Energy and momentum can be conserved only if $\theta_0 = 0$, i.e. the momenta of the decaying excitation and those of the decay products are parallel. Even for very small values of α the decay kinematics deviates significantly from the aforementioned linear situation as θ_0 increases.

We stress that, even if the standard treatment of Beliaev decay [120, 126] correctly identifies $\alpha \geq 0$ as a necessary condition for the decay to happen, then $\alpha = 0$ in the kinematics is a critical assumption; on the other hand the present treatment by including the gradient term in Eq. (4.19) allows for a realistic, Bogoliubov-like spectrum.

Let us derive the standard result from the more general Eq. (4.33): having set $\lambda = 0$ for a linear spectrum $\hbar\omega_{\mathbf{k}} = u|\mathbf{k}|$ one has that $\theta_0 = 0$, $f' = 1$ and also $\chi = \frac{1}{3}$. Moreover noting that $\int_0^p q^2|p-q|^2 \mathrm{d}q = p^5/30$, we recover Beliaev's original approximation [120, 126], which we report here for the sake of completeness:

$$w = p^5 \frac{3}{320\pi\rho\hbar^4} \left(1 + \frac{\rho^2}{3u^2}\frac{\mathrm{d}}{\mathrm{d}\rho}\frac{u^2}{\rho}\right)^2 \tag{4.36}$$

To conclude we note that for a weakly-interacting Bose gas Eq. (4.36) further simplifies, because in this case

$$\frac{\rho^2}{u^2}\frac{\mathrm{d}}{\mathrm{d}\rho}\frac{u^2}{\rho} = 0 \,. \tag{4.37}$$

Alternatively the weakly-interacting Bose gas regime can also be investigated, as done in Ref. [124], starting from the atomic Hamiltonian, introducing the Bogoliubov approximation and isolating the relevant decay vertices. The present hydrodynamic approach is different because it can be derived, as already mentioned, by separating the fast and slow components of the fields, introducing a momentum scale k_c, whereas the Bogoliubov approximation merely separates the zero-momentum contribution. We expect the two approaches to yield the same results for $k \lesssim k_c$, as we verified. The hydrodynamic approach, however, is better suited for analyzing the collective excitations of an attractive Fermi gas.

4.2.2 Beliaev damping for an attractive Fermi gas

We now consider a three-dimensional, uniform dilute gas of interacting Fermi atoms; the atoms are neutral and have two spin species. The analysis of this system across the BCS-BEC crossover has been the subject of Chapter 3. In particular using the path integral formalism [36, 71, 76] the fermions are represented by the complex Grassman fields $\psi_\sigma(\mathbf{r}, \tau), \bar{\psi}_\sigma(\mathbf{r}, \tau)$, with the spin

index $\sigma =\uparrow,\downarrow$ and the partition function for the system at temperature T, with chemical potential μ is:

$$\mathcal{Z} = \int \mathcal{D}\psi_\sigma \mathcal{D}\bar{\psi}_\sigma \ \exp\left(-\frac{1}{\hbar}\, S\right) , \tag{4.38}$$

with the following action and (Euclidean) Lagrangian density:

$$S = \int_0^{\hbar\beta} \mathrm{d}\tau \int_{L^3} \mathrm{d}^3 r \ \mathscr{L} \tag{4.39}$$

$$\mathscr{L} = \sum_\sigma \bar{\psi}_\sigma \left[\hbar\partial_\tau - \frac{\hbar^2}{2m}\nabla^2 - \mu\right] \psi_\sigma + g_0\, \bar{\psi}_\uparrow \bar{\psi}_\downarrow \psi_\downarrow \psi_\uparrow \tag{4.40}$$

as usual $\beta = 1/(k_B T)$, k_B is the Boltzmann constant, L^3 is the volume of the system and $g_0 < 0$ is the strength of the contact interaction between atoms.

We follow the usual treatment, decoupling the quartic interaction by means of a Hubbard-Stratonovich transformation and introducing the pairing field Δ. As analyzed in detail in Chapter 3 the pairing field can be decomposed as the sum of a saddle-point contribution Δ_0 and a fluctuation field η. Neglecting the fluctuations and integrating out the fermionic field ψ, $\bar{\psi}$ one gets the following mean-field zero-temperature thermodynamic grand-potential

$$\Omega_{\mathrm{mf}} = -\sum_{\mathbf{k}} (E_{\mathbf{k}} - \xi_{\mathbf{k}}) - L^3 \frac{\Delta_0^2}{g_0} \ . \tag{4.41}$$

where $\xi_{\mathbf{k}} = \hbar^2 k^2/(2m) - \mu$ and $E_{\mathbf{k}} = \sqrt{\xi_{\mathbf{k}}^2 + \Delta_0^2}$ is the spectrum of elementary single-particle fermionic excitations. The number and the gap equations for the system can be readily obtained from the mean-field grand potential Ω_{mf}, allowing one to determine the pairing gap Δ_0 and the mean-field value of the chemical potential μ as a function of the crossover, namely as a function of $y = (k_F a_s)^{-1}$, the reader may refer to Chapter 3 for a detailed analysis of the mean-field treatment.

Let us now analyze the fluctuations contribution to the present theory, as derived in Section 4.1: reinstating the fluctuations fields $\eta(\mathbf{r},\tau)$, $\bar{\eta}(\mathbf{r},\tau)$ up to the quadratic (Gaussian) order [117, 134] the partition function reads:

$$\mathcal{Z} = \mathcal{Z}_{\mathrm{mf}} \int \mathcal{D}\eta \mathcal{D}\bar{\eta} \ \exp\left(-\frac{S_{\mathrm{fl}}[\eta,\bar{\eta}]}{\hbar}\right) , \tag{4.42}$$

having defined the Gaussian action:

$$S_{\mathrm{fl}}[\eta,\bar{\eta}] = \frac{1}{2}\sum_q (\bar{\eta}(q), \eta(-q)) \ \mathbb{M}(q) \begin{pmatrix} \eta(q) \\ \bar{\eta}(-q) \end{pmatrix} \tag{4.43}$$

with $q = (\mathbf{q}, \mathrm{i}\Omega_m)$, and $\Omega_m = 2\pi n/\beta$ are the Bose Matsubara frequencies. At $T = 0$ the inverse propagator for the pair fluctuations $\mathbb{M}$ has the following matrix elements [117, 118]:

$$\mathbb{M}_{11}(q) = \frac{1}{g_0} + \sum_{\mathbf{k}} \left(\frac{u^2 u'^2}{\mathrm{i}\Omega_n - E - E'} - \frac{v^2 v'^2}{\mathrm{i}\Omega_n + E + E'} \right) \tag{4.44}$$

$$\mathbb{M}_{12}(q) = \sum_{\mathbf{k}} uvu'v' \left(\frac{1}{\mathrm{i}\Omega_n + E + E'} - \frac{1}{\mathrm{i}\Omega_n - E - E'} \right) \tag{4.45}$$

where $u = u_{\mathbf{k}} = \sqrt{\frac{1}{2}(1 + \frac{\xi_{\mathbf{k}}}{E_{\mathbf{k}}})}$, $v = v_{\mathbf{k}} = \sqrt{1 - u_{\mathbf{k}}^2}$, $u' = u_{\mathbf{k}+\mathbf{q}}$, $v' = v_{\mathbf{k}+\mathbf{q}}$, $E = E_{\mathbf{k}}$, $E' = E_{\mathbf{k}+\mathbf{q}}$. As in the finite-temperature case the remaining matrix elements are defined by the relations: $\mathbb{M}_{22}(q) = \mathbb{M}_{11}(-q)$, $\mathbb{M}_{21}(q) = \mathbb{M}_{12}(q)$.

A completely equivalent description can be given, after a unitary transformation, in terms of the (linearized) phase and amplitude of the fluctuation field, which can be decomposed as $\eta(\mathbf{q}, \mathrm{i}\Omega_m) = (\lambda(\mathbf{q}, \mathrm{i}\Omega_m) + \mathrm{i}\theta(\mathbf{q}, \mathrm{i}\Omega_m))/\sqrt{2}$. The Gaussian level action now reads:

$$S_{\mathrm{fl}} = \frac{1}{2} \sum_{\mathbf{q}} \begin{pmatrix} \lambda^* & \theta^* \end{pmatrix} \begin{pmatrix} \mathbb{M}_{11}^E + \mathbb{M}_{12} & \mathrm{i}\mathbb{M}_{11}^O \\ -\mathrm{i}\mathbb{M}_{11}^O & \mathbb{M}_{11}^E - \mathbb{M}_{12} \end{pmatrix} \begin{pmatrix} \lambda \\ \theta \end{pmatrix} \tag{4.46}$$

in terms of the even/odd components in $\mathrm{i}\omega_n$ of the $\mathbb{M}$ matrix elements [135, 136], i.e. $\mathbb{M}_{ab}^{E/O}(\mathbf{q}, \mathrm{i}\Omega_m) = \frac{1}{2}(\mathbb{M}_{ab}(\mathbf{q}, \mathrm{i}\Omega_m) \pm \mathbb{M}_{ab}(\mathbf{q}, -\mathrm{i}\Omega_m))$. As soon as the Cooper pairing field $\Delta(\mathbf{r}, \tau)$ acquires a non-zero expectation value, i.e. under T_c, as a consequence of the $U(1)$ symmetry breaking one expects to observe the gapless Goldstone mode [76]. The phase-amplitude representation introduced in Eq. (4.46) allows for an easy verification of this statement, in fact it can be shown that in the low momentum, $T = 0$ limit the phase and amplitude fluctuations are decoupled [136]: the off-diagonal entries in Eq. (4.46) go to zero, and the phase (Goldstone) mode is gapless, while the amplitude (Higgs) mode exhibits a mass gap. From now on up to the end of the present Section we will study the system at $T = 0$. Focusing on the former mode, we observe that, indeed, by solving for ω the equation

$$\det \mathbb{M}(\mathbf{q}, \mathrm{i}\Omega_m \to \omega) = 0 \tag{4.47}$$

we obtain the spectrum of the bosonic collective mode, showing a gapless branch. Notably in the BEC regime $y \gtrsim 1$, and across the whole crossover for low enough momenta, this mode takes (within very good approximation) the familiar Bogoliubov-like form

$$\hbar\omega_{\mathbf{q}} = \sqrt{\epsilon_{\mathbf{q}} \left(\lambda \epsilon_{\mathbf{q}} + 2mc_s^2 \right)}\,, \tag{4.48}$$

with $\epsilon_{\mathbf{k}} = \hbar^2 k^2/(2m)$; the sound speed c_s, along with the parameter λ, depends on $y = 1/(k_F a_s)$. We use this spectrum in the deep BEC limit, while

in the intermediate regime near unitarity we solve numerically Eq. (4.47) to get the "exact" spectrum within the present Gaussian approximation scheme. When comparing the "exact" spectrum so obtained with the Bogoliubov approximate form, one also has to remember that a natural momentum scale can be defined by studying whether and when the dispersion enters the two-particle continuum reaching the threshold energy [137]:

$$E_{\rm th}(\mathbf{q}) = \min_{\mathbf{k}}(E_{\mathbf{k}} + E_{\mathbf{k}+\mathbf{q}}) \tag{4.49}$$

above which a Cooper pair breaks down in two fermions. As far as the present work is concerned it is important noting that $\omega_{\mathbf{q}}$ grows more (less) than linearly if $\lambda > 0$ ($\lambda < 0$), moreover the parameter λ can be calculated easily either from a numerical solution of Eq. (4.47) or using the techniques in Ref. [138]. It turns out that λ is a monotonically increasing function of $y = 1/(k_F a_s)$. In particular λ takes negative values in the deep BCS regime and changes its sign for $y = y_c \approx -0.14$; referring to the previous Subsection we can then conclude that no Beliaev decay will happen for $y < y_c$.

We now want to adapt Eq. (4.33) to the present theory. We start by noticing that if the spectrum has the form in Eq. (4.48), then the decay angle θ_0 defined in the previous Subsection has an analytic expression:

$$\cos\theta_0(p,q) = \frac{m^2c_s^2}{\lambda pq\hbar^2} + \frac{q}{2p} + \frac{p}{2q} + \\ - \frac{\sqrt{m^2c_s^4 + 2mc_s^2\lambda\left(\epsilon_p + \epsilon_q\right) - 2\lambda\hbar\omega_{\mathbf{p}}\hbar\omega_{\mathbf{q}} + \lambda^2\left(\epsilon_p^2 + \epsilon_q^2\right)}}{2\lambda pq\frac{\hbar^2}{2m}} . \tag{4.50}$$

We note that for the special case $\lambda = 1$, $2mc_s^2 = 2$ Eq. (4.50) coincides with the result in Ref. [124].

Finally the more complicated expression inside the parenthesis in Eq. (4.33) can be expressed using the techniques devised in Ref. [139] as:

$$\frac{\rho^2}{u^2}\frac{\mathrm{d}}{\mathrm{d}\rho}\frac{u^2}{\rho} = -\frac{30\epsilon(y) - 8y\epsilon'(y) - 3y^2\epsilon''(y) + y^3\epsilon'''(y)}{30\epsilon(y) - 18y\epsilon'(y) + 3y^2\epsilon''(y)} \tag{4.51}$$

as a function of $\epsilon(y) = \frac{5}{3}\epsilon_F^{-1}\mathcal{E}$, where $\mathcal{E}$ is the bulk energy per particle of an interacting Fermi gas; when calculating our final results we compared $\epsilon(y)$ as fitted in [139] from experimental data with its mean field counterpart, observing no appreciable differences as far as the quantity in Eq. (4.51) is concerned. Consistently with the result found in Eq. (4.37) for the weakly-interacting Bose gas, the quantity in Eq. (4.51) tends to zero in the deep BEC limit.

We calculate the Beliaev decay width for the Goldstone collective mode of an attractive Fermi gas; as previously noted there is no decay in the BCS regime up to $y = y_c \approx -0.14$, as the spectrum as a function of $|\mathbf{q}|$ grows less

than linearly. For higher values of y we can associate an imaginary part to the Goldstone mode spectrum, as

$$\mathrm{Im}\,\hbar\omega_{\mathbf{p}} = -\frac{\hbar w}{2} \tag{4.52}$$

using w from Eq. (4.33). In Fig. 4.1 we report the real spectra $\omega_{\mathbf{p}}$, obtained from Eq. (4.47), for three values of $y = 1/(k_F a_s)$, from unitarity to the BEC regime ($y = 0$, $y = 0.5$, $y = 1$), along with their imaginary part due to the Beliaev decay.

A collective excitation in a superfluid Fermi gas cannot have arbitrarily high energy, as it will be damped either by the dissociation mechanism at the threshold energy E_{th}, decaying into two fermions, or by the Beliaev mechanism, decaying into two lower frequency collective excitations. Either way a natural energy cutoff can be associated to a bosonic excitation.

Referring to the left pane of Fig. (4.1) we start at unitarity ($y = 0$) where the Beliaev decay width is quite narrow: here a collective excitation will mainly decay by hitting the threshold energy E_{th} and breaking down into two fermions [137]. On the other hand, approaching the BEC regime ($y = 0.5$, $y = 1.0$) the Beliaev decay width gets larger before the collective spectrum touches E_{th}: here the preferred decay mode for a collective excitation will be decaying into two lower frequency collective excitations. This trend, i.e. the progressively bigger importance of the Beliaev mechanism approaching the BEC regime, can be observed by comparing the three panes in Fig. (4.1).

In order to define an energy cutoff due to the Beliaev mechanism, we can match the real and the imaginary part of $\omega_{\mathbf{p}}$ similarly identifying a scale beyond which a collective excitation is no longer well-defined due to the Beliaev decay. This remark is made clear by looking at the pair fluctuation spectral function

$$A_{\eta\eta}(\mathbf{k}, \omega) = -2\,\mathrm{Im}\,G_{\eta\eta}(\mathbf{k}, \omega + \gamma_{\mathbf{k}}) \tag{4.53}$$

plotted in Fig. (4.2). As noted in [118], it can be interpreted as the contribution to the density from the fluctuations at a given wave number $\mathbf{q}$ and given energy ω. In the previous equation ω is assumed to be real and $\gamma_{\mathbf{k}} = -\frac{\hbar w}{2}$ is the imaginary component of the spectrum due to the Beliaev decay, $G_{\eta\eta}$ is the Green's function obtained by inverting the matrix in Eq. (4.43) and taking the $(1, 1)$ entry. We observe that for low momenta most of the spectral weight is peaked around the dispersion relation, which is marked by a dashed line, assuming the usual Lorentzian structure. However, as the spectrum continues after $p \simeq k_F$, for high momenta the line broadening effect due to the Beliaev decay effectively destroys the collective excitation, and the spectral weight is distributed over a large region. The border between these two regimes can also be approximately found by imposing the aforementioned condition $\mathrm{Re}\,\omega_{\mathbf{k}} = \mathrm{Im}\,\omega_{\mathbf{k}}$, which can be easily read from Fig. (4.2): when the

real part of the dispersion is bigger than the imaginary part, the expression in Eq. (4.53) has a narrow peak; as the imaginary part of the spectrum gets bigger the Lorentzian structure of the peak is lost and the excitation is no longer well defined.

We can conclude that, as we go from the BCS to the BEC regime, the dissociation mechanism at $E_{\rm th}$ gets less and less relevant, as the collective mode spectrum gets further away from $E_{\rm th}$; at the same time, the Beliaev decay channel opens at $y = y_c$ and gets progressively more relevant. Finally in Fig. (4.3) we compare the decay width, as predicted by the present theory, with the original linear approximation [120, 126]: even for relatively small momenta our treatment shows relevant differences with respect to the standard treatment. The differences get larger in the BEC regime, consistently with the fact that the nonlinearity term λ in the spectrum is bigger; however we stress that even for nearly linear spectra, see the cases $y = 0$ and $y = 0.5$ in Fig. (4.1), the correction due to the present treatment can amount up to 25% for $\frac{p}{k_F} \simeq 1$.

In conclusion we briefly comment on the scope of applicability of the present theory to the fermionic case; adapting Eq. (4.26) one finds

$$k_c \simeq \frac{2mc_s}{\sqrt{\lambda}} \tag{4.54}$$

and we do not expect the theory to be applicable above this momentum threshold; a direct calculation shows that starting at unitarity, up to the moderate BEC regime we considered in Fig. (4.1) and Fig. (4.2), k_c assumes respectively the following values: $k_c = 3.06 k_F$, $k_c = 1.72 k_F$, $k_c = 1.31 k_F$. The evolution of k_c/k_F in the unitary to moderate BEC regime we analyze in the present work is plotted in the inset of Fig. 4.3, in the deep BEC limit we get [140]

$$k_c \simeq \frac{1}{2}\frac{\Delta_0^2}{|\mu|} \, . \tag{4.55}$$

We notice that for the cases we considered, the momentum scale k_c marking the breakdown of the perturbation theory is higher or equal to the scale at which a collective excitation is no longer well defined due to a high decay rate; we conclude then that the present treatment is consistent.

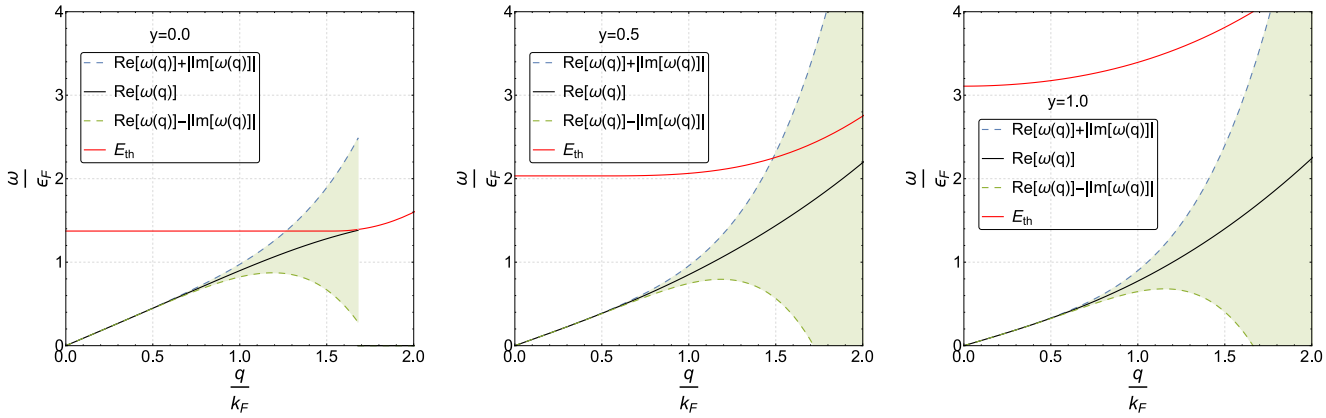

Figure 4.1: The collective mode spectrum for $y = (k_F a_s)^{-1} = 0.0$, $y = 0.5$, $y = 1.0$, from left to right. The black line represent the real part of the spectrum, while the dashed lines represent $\pm$ the imaginary part, the bold red line represents the threshold energy E_{th}. In this figure $\hbar = 1$.

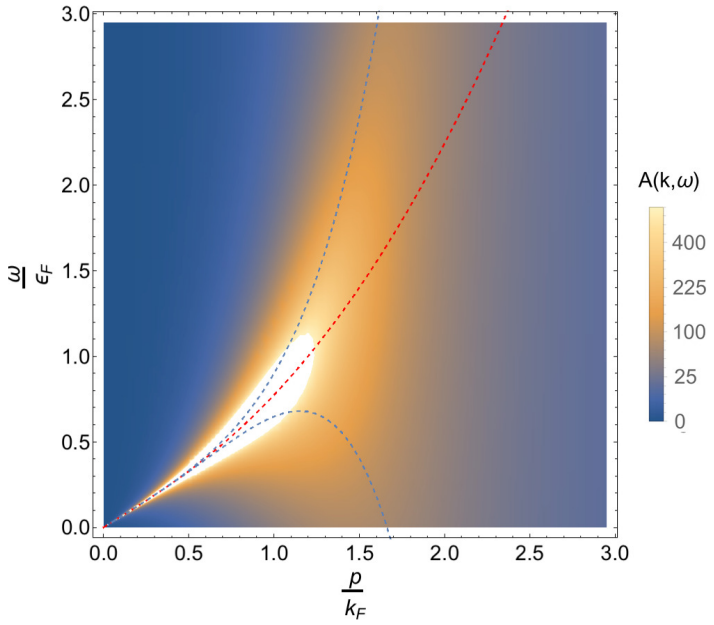

Figure 4.2: The pair fluctuation spectral function $A_{\eta\eta}(\mathbf{k},\omega)$ for $y = (k_F a_s)^{-1} = 1$, the dashed red line shows the corresponding spectrum, the dashed blue lines correspond to the imaginary part of the spectrum, like in Fig. 4.1. For $\frac{p}{k_f} \gtrsim 1$ the line broadening due to the Beliaev decay effectively destroys a collective excitation, this is also approximately the scale marking the end of the validity of the perturbative approach. For comparison here $E_{\text{th}} > 3\epsilon_F$. In this figure $\hbar = 1$.

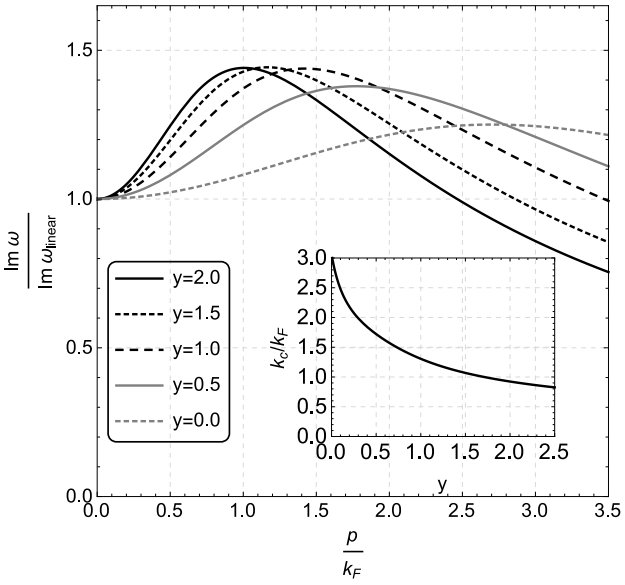

Figure 4.3: The Beliaev decay width calculated from Eq. (4.33) divided by the original Beliaev result (linear approximation), for different values of $y = 1/(k_F a_s)$. The inset shows the evolution of k_c/k_F as defined in Eq. (4.54) in the unitary to moderate BEC regime we investigate.

4.3 The two-dimensional Fermi gas: first sound, second sound and BKT critical temperature

Quantum fluctuations play a crucial role in low-dimensional systems [116]: the finite temperature properties of a two-dimensional Fermi gas across the BCS-BEC crossover are substantially different from its three-dimensional counterpart. In particular, in accordance with the Mermin-Wagner-Hohenberg theorem [141–143] for $d \leq 2$ there can not be a finite condensate density at finite temperature, as the fluctuations destroy the off-diagonal long-range order; nonetheless two-dimensional systems can exhibit algebraic off-diagonal long-range order, allowing for the existance of a quasi-condensante up to a certain critical temperature, due to the Berezinskii-Kosterlitz-Thouless (BKT) mechanism [144, 145].

Along with the appearance of algebraic long-range order, as observed for the first time in superfluid ^{4}He, then in an ultracold Bose gas [146], in an exciton-polariton gas [147] and very recently in an ultracold Fermi gas [148], the other fundamental signature of the BKT mechanism at work is the universal jump in the superfluid density [149], going discontinuously from a finite value to zero at the critical temperature, as observed in thin ^{4}He films [150]. This scenario suggests that in a two-dimensional system the role of quantum fluctuations should be crucial in describing several aspects of the system [151], as opposed to the 3D case for which one could expect from a mean-field theory at least qualitative agreement. In fact it has been observed that Gaussian fluctuations strongly modify both the chemical potential and the pairing parameter, particularly in the intermediate and strong coupling regions [152]; it has also been shown that the correct composite-boson limit is recovered by introducing Gaussian fluctuations [153].

The determination of a full Gaussian-level equation of state needs, however, a proper regularization scheme to remove divergences. In the present work we use convergence factors in the pair-fluctuation propagator [117, 152] to numerically calculate the $T = 0$ state equation for a system of interacting fermions across the BCS-BEC crossover.

We investigate beyond-mean-field effects for a two-dimensional Fermi gas at finite temperature: we calculate the first and second sound velocities, as a function of the temperature and of the binding energy, and then calculate the BKT critical temperature from the Kosterlitz-Nelson condition [149]. In particular this last theoretical prediction is compared with recently obtained experimental results [148], showing excellent agreement with experimental data in the intermediate and BEC regimes.

4.3.1 Theoretical framework

The treatment of a two-dimensional (2D) Fermi gas presents some differences with respect to the three-dimensional (3D) treatment previously analyzed.

For this reason we briefly retrace the derivation of the mean-field and of the fluctuations theory, emphasizing the differences and the new features. The partition function of a system of ultracold, dilute, interacting spin 1/2 fermions contained in a two-dimensional volume L^2, at temperature T, with chemical potential μ can be described within the path-integral formalism [71, 76] analogously as the three-dimensional case analyzed in Chapter 3:

$$\mathcal{Z} = \int \mathcal{D}\psi_\sigma \mathcal{D}\bar{\psi}_\sigma e^{-\frac{1}{\hbar}\int_0^{\hbar\beta} \mathrm{d}\tau \int_{L^2} \mathrm{d}^2 r \mathscr{L}} \tag{4.56}$$

with the following (Euclidean) Lagrangian density

$$\mathscr{L} = \bar{\psi}_\sigma \left[\hbar\partial_\tau - \frac{\hbar^2}{2m}\nabla^2 - \mu\right] \psi_\sigma + g_0\, \bar{\psi}_\uparrow\, \bar{\psi}_\downarrow\, \psi_\downarrow\, \psi_\uparrow \,, \tag{4.57}$$

where $\psi_\sigma(\mathbf{r},\tau)$ and $\bar{\psi}_\sigma(\mathbf{r},\tau)$ are complex Grassmann fields, $\sigma = \uparrow, \downarrow$ is the spin index, m is the mass of a fermion, having defined $\beta = (k_B T)^{-1}$, k_B being the Boltzmann constant. The strength of the attractive s-wave potential is $g_0 < 0$. In two-dimensions, as opposed to three dimensional case, g_0 be implicitely related to the bound state energy ϵ_b [81, 154] by the following bound state equation:

$$-\frac{1}{g_0} = \frac{1}{2L^2} \sum_{\mathbf{k}} \frac{1}{\epsilon_{\mathbf{k}} + \frac{1}{2}\epsilon_b} \,. \tag{4.58}$$

with $\epsilon_{\mathbf{k}} = \hbar^2 k^2/(2m)$. It should also be stressed that in 2D, as opposed to the three-dimensional case, a bound state exists even for arbitrarily weak interactions, making ϵ_b a good variable to describe the whole BCS-BEC crossover. The quartic interaction can be decoupled by using a Hubbard-Stratonovich transformation, introducing in the process the new auxiliary pairing fields Δ, $\bar{\Delta}$ [71, 76], in completely analogy with the three-dimensional case already discussed. The newly introduced pairing field can be split into a uniform, constant saddle-point value Δ_0 and the fluctuations around this value as follows:

$$\Delta(\mathbf{r},\tau) = \Delta_0 + \eta(\mathbf{r},\tau) \,, \tag{4.59}$$

and neglecting the fluctuation fields η, $\bar{\eta}$ gives us a simple mean-field theory, which is generally unreliable in the present case, due to the fundamental role of fluctuations in two dimensions, but still constitutes the starting point for more refined approaches. The functional integral defining the mean-field partition function can be carried out exactly, yielding

$$\mathcal{Z}_{\mathrm{mf}} = \exp\left(-\beta\, \Omega_{\mathrm{mf}}\right) = \exp\left(\mathrm{Tr}\left[\ln\left(-\mathbb{G}_{\mathrm{sp}}^{-1}\right)\right] + \beta L^2 \frac{\Delta_0^2}{g_0}\right) \,, \tag{4.60}$$

the trace being taken in coordinate space and in the Nambu-Gor'kov space, with the inverse Green function:

$$-\mathbb{G}_{\mathrm{sp}}^{-1} = \begin{pmatrix} \hbar\partial_\tau - \frac{\hbar^2}{2m}\nabla^2 - \mu & \Delta_0 \\ \Delta_0 & \hbar\partial_\tau + \frac{\hbar^2}{2m}\nabla^2 + \mu \end{pmatrix} \tag{4.61}$$

and the single-particle excitation spectrum is found solving for the poles of the Nambu-Gor'kov Green's function $\mathbb{G}_{\rm sp}$ in momentum space [71]:

$$E_{\mathbf{k}} = \sqrt{(\epsilon_{\mathbf{k}} - \mu)^2 + \Delta_0^2}\,. \tag{4.62}$$

As opposed to the three-dimensional case, in two dimensions for $T = 0$ the $\mathbf{k}$-integration for $\Omega_{\rm mf}$ can be carried out analytically in the 2D case, one gets:

$$\Omega_{\rm mf}(\mu, \Delta_0) = -\frac{mL^2}{4\pi\hbar^2}\Big[\mu^2 + \mu\sqrt{\mu^2+\Delta_0^2} + \frac{1}{2}\Delta_0^2 - \Delta_0^2 \ln\Big(\frac{-\mu+\sqrt{\mu^2+\Delta_0^2}}{\epsilon_b}\Big)\Big]\,. \tag{4.63}$$

From the grand potential we impose the saddle-point condition for Δ_0, i.e. $(\partial\Omega_{\rm mf}/\partial\Delta_0)_{\mu,V} = 0$, obtaining the gap equation:

$$\Delta_0 = \sqrt{2\epsilon_b(\mu + \frac{1}{2}\epsilon_b)}\,, \tag{4.64}$$

plugging this result back into the mean-field grand potential we get the mean-field equation of state:

$$\Omega_{\rm mf}(\mu) = -\frac{mL^2}{2\pi\hbar^2}(\mu + \frac{1}{2}\epsilon_b)^2\,. \tag{4.65}$$

Restoring the fluctuation fields η, $\bar\eta$ at a Gaussian level, the partition function reads [117]:

$$\mathcal{Z} = \mathcal{Z}_{\rm mf} \int \mathcal{D}\eta\mathcal{D}\bar\eta\ \exp\Big\{-\frac{S_{\rm fl}[\eta,\bar\eta]}{\hbar}\Big\}\,, \tag{4.66}$$

where

$$S_{\rm fl}[\eta,\bar\eta] = \frac{1}{2}\sum_Q (\bar\eta(Q), \eta(-Q))\ \mathbb{M}(Q) \begin{pmatrix} \eta(Q) \\ \bar\eta(-Q) \end{pmatrix} \tag{4.67}$$

having introduced the Fourier-transformed version of the fluctuation fields, with $Q = (\mathbf{q}, \mathrm{i}\Omega_m)$, $\Omega_m = 2\pi m/\beta$ being the Bose Matsubara frequencies. The fluctuation fields η, $\bar\eta$ can be formally integrated, allowing us to write down the Gaussian-level contribution to the grand potential:

$$\Omega_{\rm fl}(\mu, \Delta_0) = \frac{1}{2\beta}\sum_Q \ln\det(\mathbb{M}(Q))\,. \tag{4.68}$$

We do not report here the full expression for the inverse pair fluctuation propagator matrix $\mathbb{M}$, it can be found for instance in [117, 118]; by imposing the condition $\det(\mathbb{M}) = 0$ at $T = 0$ one can find the collective excitation spectrum, which will have, in the low-momentum limit, the following expression

$$\hbar\omega_{\mathbf{q}} = \sqrt{\epsilon_q\,(\lambda\epsilon_q + 2mc_s^2)} \tag{4.69}$$

λ and c_s being a function of the crossover. Like in the mean-field case we can insert Eq. (4.64) into Eq. (4.68) getting $\Omega_{\text{fl}}(\mu)$.

The grand-potential in Eq. (4.68) cannot be evaluated as is, being affected by divergencies related to the modeling of the interaction using a contact pseudo-potential rather than a realistic one. Many different regularization approaches can be used, like the dimensional regularization in 2D in the BEC limit [153], the counterterms regularization in 3D in the BEC limit[2] or regularization with convergence factors [117, 152]. The first two are more suited to obtain analytical results, particularly in the BEC limit, while the last method has been shown to be suited to obtain numerical results across the whole crossover [152]. Wanting to investigate numerically the whole crossover, our grand potential is regularized by introducing convergence factors [117, 152]:

$$\Omega_{\text{fl}}(\mu, \Delta_0) = \frac{1}{2\beta} \sum_Q \ln \left[\frac{\mathbb{M}_{11}(Q)}{\mathbb{M}_{22}(Q)} \det(\mathbb{M}(Q)) \right] e^{i\Omega_m 0^+} . \tag{4.70}$$

Inserting the gap equation as before we get the Gaussian contribution $\Omega_{\text{fl}}(\mu)$ to the equation of state. From the equation of state then one gets μ as a function of the crossover. The pairing gap Δ_0 is found by inserting μ into Eq. (4.64).

The chemical potential μ and the pairing gap Δ_0 at $T = 0$ are plotted in Fig. 4.5 as a function of the scaled binding energy ϵ_b/ϵ_F and are compared with their mean-field counterparts. Clearly in the strongly-interacting regime the validity of the mean-field approximation is limited and the contribution from the fluctuations provides a substantial modification.

4.3.2 First and second sound

The first sound velocity c_s is calculated from the regularized grand potential in Eq. (4.70), by using the zero-temperature thermodynamic relation [155]:

$$c_s = \sqrt{\frac{n}{m}\frac{\partial \mu}{\partial n}} = \sqrt{-\frac{n}{m}\left(\frac{1}{L^2}\frac{\partial^2 \Omega(\mu)}{\partial \mu^2}\right)^{-1}} . \tag{4.71}$$

Using the mean-field equation of state to calculate the chemical potential, one would find $c_s(\mu_{\text{mf}}) = v_F/\sqrt{2}$ across the whole BCS-BEC crossover, v_F being the Fermi velocity [81, 138]. Our equation of state with Gaussian fluctuations yields, as expected, a critically different c_s: it slowly tends to the aforementioned value in the BCS limit, showing, on the other hand, a remarkable difference in the intermediate and BEC regimes, tending to the composite boson limit derived in Ref. [153]. We plot this result in Fig. 4.4. By adapting the thermodynamic approach of Ref. [156] we verified that the T-dependence of c_s in the superfluid phase is very weak, see the inset of Fig. 4.4.

[2] See Ref. [4] or Section 4.4.

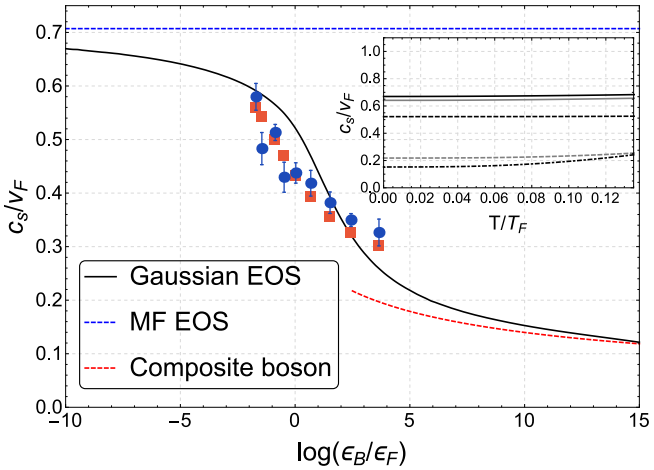

Figure 4.4: The first sound velocity at $T = 0$, calculated using μ and Δ_0 from the Gaussian-level equation of state (black solid line), and using their mean-field counterparts (blue dashed line), which give a constant value $c_s/v_F = 1/\sqrt{2}$. In the strong coupling regime a full Gaussian-level equation of state is needed to correctly describe thermodynamic quantities, there our prediction correctly tends to the composite boson limit (red dotted line). Inset: temperature dependence for $\log(\epsilon_b/\epsilon_F) = -10, -5, 0, 5, 10$ (from top to bottom).

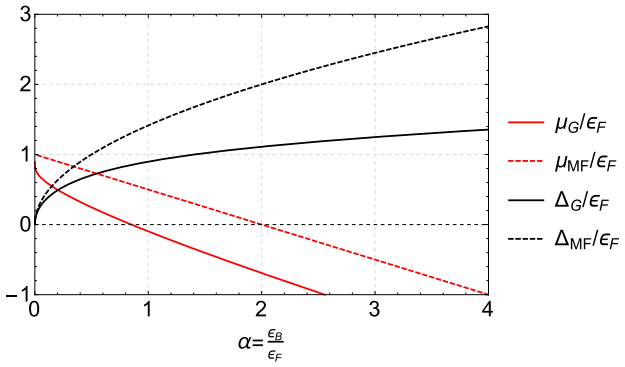

Figure 4.5: The chemical potential μ (red lines) and the pairing gap Δ_0 (black lines) in units of the Fermi energy, as calculated from the mean-field equation of state (dashed lines) and from the Gaussian-level equation of state (solid lines), as a function of the scaled binding energy ϵ_b/ϵ_F.

Beside the first sound, propagating through density waves, a superfluid can also sustain the second sound, a purely quantum-mechanical phenomenon propagating through a temperature wave [157]. In order to calculate the second sound velocity we follow the treatment in [156] starting from the free energy of the system, substantially treating it as a gas of independent single

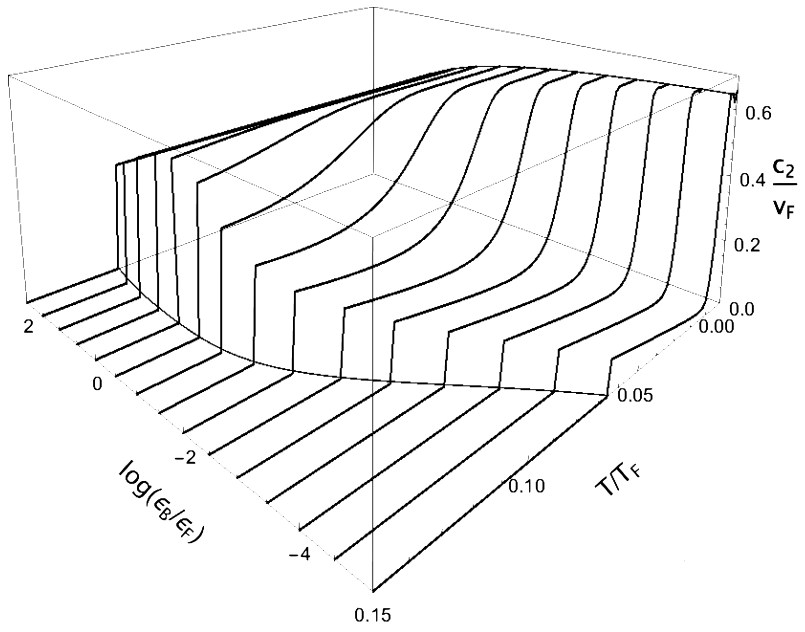

Figure 4.6: The second sound velocity, as a function of the temperature T/T_F, for varying values of ϵ_b/ϵ_F. The characteristic structure with a minimum followed by a linear increase evolves into a constant second sound velocity approaching the BEC regime.

particle and collective excitations, neglecting hybridization through Landau damping; this approach will be justified shortly when discussing the BKT critical temperature. We find the fermion single particle contribution to the free energy:

$$F_{\rm sp} = -\frac{2}{\beta}\sum_{\mathbf{k}} \ln\left[1 + e^{-\beta E_{\mathbf{k}}}\right] \tag{4.72}$$

and the bosonic one, from collective excitations:

$$F_{col} = \frac{1}{\beta}\sum_{\mathbf{q}} \ln\left[1 - e^{-\beta\omega_{\mathbf{q}}}\right] . \tag{4.73}$$

The total free energy is then $F = F_0 + F_{col} + F_{\rm sp}$ where the zero-temperature energy F_0 is a T-independent constant, unimportant as far as the present work is concerned. The entropy is readily calculated as $S = -(\partial F/\partial T)_{N,L^2}$ and introducing the entropy per particle $\bar{S} = S/N$ the second sound velocity is [120, 157, 158]:

$$c_2 = \sqrt{\frac{1}{m}\frac{\bar{S}^2}{\left(\frac{\partial \bar{S}}{\partial T}\right)_{N,L^2}}\frac{n_s}{n_n}} . \tag{4.74}$$

In contrast with the 3D case [156] here the second sound has a discontinuity at the critical temperature, as a consequence of the universal jump in the superfluid density, as also noted in [159, 160]; the critical temperature will be calculated in the next Subsection. Our results are reported in Fig. 4.6, we note that the second sound velocity shows a characteristic minimum in the BCS and intermediate regimes, as also noted in the 3D unitary case [156], evolving into an approximately constant second sound velocity approaching the BEC regime.

4.3.3 Critical temperature: the Berezinskii-Kosterlitz-Thouless transition

The low-temperature physics of a 2D attractive Fermi gas is essentially different from that of a 3D gas: the Mermin-Wagner-Hohenberg theorem [141–143] prohibits the symmetry breaking at finite temperatures, so that one can find off-diagonal long-range order and a finite condensate density only at $T = T_c = 0$. However quasi-condensation, i.e. the the algebraic decay of the phase correlator

$$\langle \exp(\mathrm{i}\theta(\mathbf{r}))\exp(\mathrm{i}\theta(0))\rangle \sim |\mathbf{r}|^{-\eta} \tag{4.75}$$

where η is a T-dependent exponent and θ is the phase of the order parameter, is observed up to a finite temperature $T_{\rm BKT}$, known as the Berezinskii-Kosterlitz-Thouless (BKT) critical temperature [144, 145]. The other fundamental signature of the BKT mechanism is the universal jump in superfluid density

at the critical temperature, i.e. $n_s(T^-_{\rm BKT}) \neq (T^+_{\rm BKT}) = 0$. The transition temperature is determined through the Kosterlitz-Nelson [149] condition

$$k_B T_{\rm BKT} = \frac{\hbar^2 \pi}{8m} n_s(T_{\rm BKT}) \tag{4.76}$$

which allows one to calculate $T_{\rm BKT}$, known the superfluid density. Within the present framework we write the superfluid density as

$$n_s = n - n_{n,f} - n_{n,b} \tag{4.77}$$

where n is the density of the system and $n_{n,f}$ and $n_{n,b}$ are normal density contributions arising, respectively, from the single particle excitations and from the bosonic collective excitations. Using Landau's quasiparticle excitations formula [161] for fermionic:

$$n_{n,f} = \frac{\beta}{2} \int \frac{{\rm d}^2 k}{(2\pi)^2} k^2 \frac{e^{\beta E_{\mathbf{k}}}}{(e^{\beta E_{\mathbf{k}}} + 1)^2} \tag{4.78}$$

and for bosonic excitations:

$$n_{n,b} = \frac{\beta}{2} \int \frac{{\rm d}^2 q}{(2\pi)^2} q^2 \frac{e^{\beta \omega_{\mathbf{q}}}}{(e^{\beta \omega_{\mathbf{q}}} - 1)^2} \, . \tag{4.79}$$

The single particle excitation spectrum is $E_{\mathbf{k}} = \sqrt{(\hbar^2 k^2/(2m) - \mu)^2 + \Delta_0^2}$, as derived in Eq. (4.62), while the collective excitations spectrum can be read from Eq. (4.69). Three profiles of superfluid density as a function of temperature, for different values of the attractive potential strength, are reported in Fig. 4.7.

As noted in Ref. [134] Eq. (4.78) and Eq. (4.79) hold as long as there is no Landau damping hybridizing the collective modes with fermionic single-particle excitations, otherwise the bosonic normal density would need to be modified. In our case one can easily verify that for $\epsilon_b/\epsilon_F \gtrsim 1$ the condition $\epsilon_b \gg k_B T$ holds in the whole temperature region of interest, strongly suppressing the pair breakup and the Landau damping [134]. On the other hand, for $\epsilon_b/\epsilon_F \lesssim 1$ we verify that the critical temperature is determined by the fermionic contribution to the normal density, as one would expect, making eventual corrections to $n_{n,b}$ neglectable. We then conclude that Eq. (4.78) and Eq. (4.79) correctly describe the normal density for the entire superfluid phase.

By numerically solving Eq. (4.76) we find the transition temperature $T_{\rm BKT}$ at different points of the BCS-BEC crossover. Our results, shown in Fig. 4.8, are compared with very recently obtained experimental data in Ref. [148], showing a excellent agreement with experimental data at least for $\epsilon_b/\epsilon_F \gtrsim 1$.

We stress that with respect to other derivations of $T_{\rm BKT}$ in the 2D BCS-BEC crossover [118, 162] the present theoretical prediction of $T_{\rm BKT}$ includes

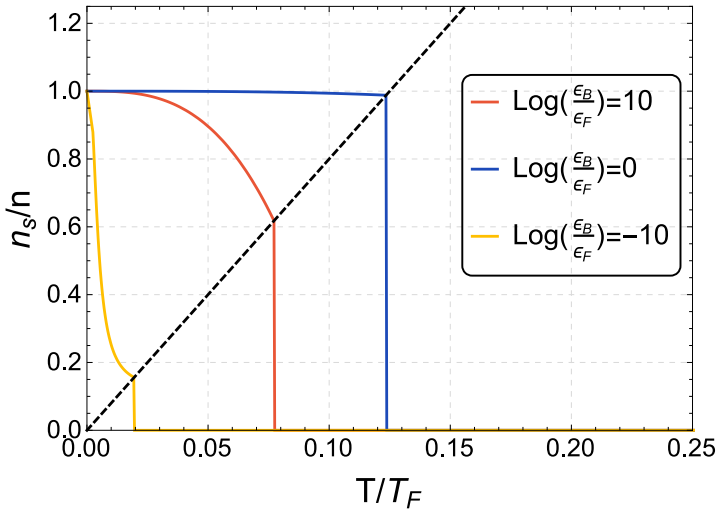

Figure 4.7: Superfluid density for three different values of the scaled binding energy, from the weakly-coupled regime to the strong interacting one. The black dashed line marks the Nelson-Kosterlitz condition, setting the Berezinskii-Kosterlitz-Thouless critical temperature T_{BKT}.

the contribution from a Gaussian-level equation of state along with the contribution from the bosonic collective excitations. These contributions are critical in correctly fitting experimental data, as clear from in Fig. 4.8. We find that a theory of fermionic only excitations, like those developed in [118, 162] or in a slightly different context in [163], overestimates the critical temperature in the intermediate and strong-coupling regimes. Conversely, not using a Gaussian equation of state underestimates the critical temperature in the BCS regime, see Fig. 4.8.

Moving towards the BCS side of the crossover, however, the agreement is slightly worse, the experimental T_{BKT} being bigger than $0.125\epsilon_F$; by inserting into Eq. (4.76) the relation $n = m/(\hbar^2\pi)\epsilon_F$ it is easily seen that the critical temperature is not allowed to exceed the value $T_{\mathrm{BKT}} = 0.125\epsilon_F$, under the very general assumption that the superfluid density is a decreasing function of the temperature with $n_s(T = 0) = n$. Thus we conclude that the slightly worse compatibility observed cannot be reproduced within the framework of the Kosterlitz-Nelson criterion, as defined by Eq. (4.76), and should be attributed to different physics, like the mesoscopic effects mentioned in [164] in the same regime. Nonetheless we stress that our results are still within 1.2σ from experimental data, when statistical and systematic errors are taken into account.

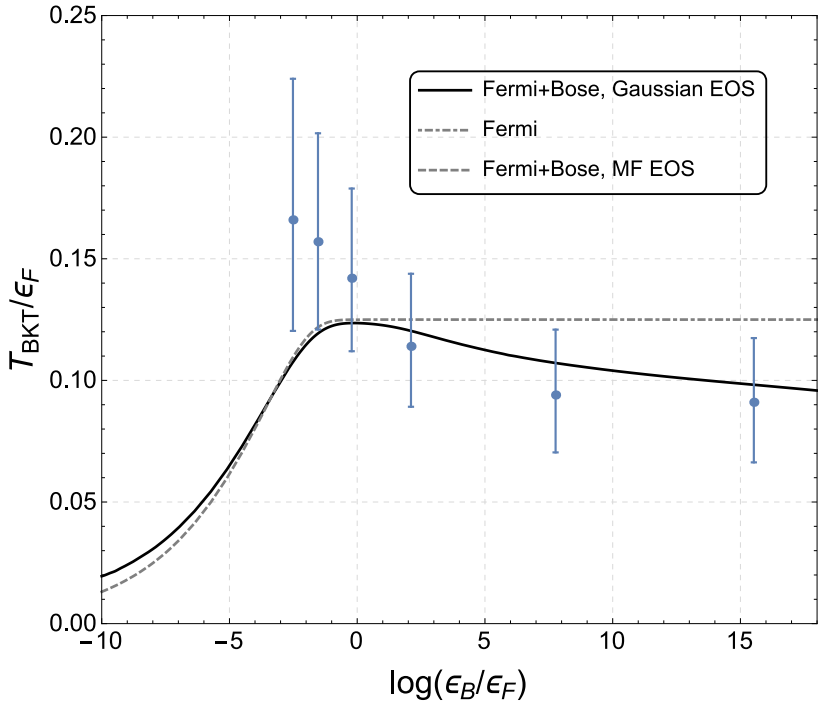

Figure 4.8: Our theoretical prediction for T_{BKT} (black solid line) as compared to the recent experimental observation reported in [148], temperature estimated through algebraic decay, the error bars account for statistical and systematic errors. Our prediction uses a Gaussian equation of state, including the contribution from single particle modes and collective excitations. A theory with fermionic only excitations (gray dot-dashed line) fails to provide an agreement with experimental data in the BEC regime, whereas a theory using a mean-field equation of state would underestimate T_{BKT} in the weak coupling regime (gray dashed line).

4.4 Regularization in the deep-BEC limit

In this Section we investigate the relation between the fermionic scattering length a_s and the boson-boson scattering length in the deep-BEC regime a_b, as analyzed in Ref. [4].

Performing a cutoff regularization of the zero-point energy the bosonic and fermionic scattering lengths are found to be related by $a_b = (2/3)\ a_s$, in good agreement with other theoretical investigations [117, 165, 166] and Monte Carlo simulations [111]. We stress however that the present result is fully analytical, contrary to all other beyond-mean-field predictions [111, 117, 165–167], and it is based on a transparent cutoff regularization and subsequent renormalization[3].

4.4.1 Mean field and fluctuations in the deep BEC limit

We consider a three-dimensional Fermi gas of ultracold and dilute two-spin-component neutral atoms. As usual the atomic fermions are described in the path integral formalism by the complex Grassmann fields $\psi_\sigma(\mathbf{r},\tau)$, $\bar{\psi}_\sigma(\mathbf{r},\tau)$ with spin $\sigma = (\uparrow,\downarrow)$ [36, 76]. The partition function $\mathcal{Z}$ of the uniform system at temperature T, in a three-dimensional box of volume L^3, and with chemical potential μ can be written as

$$\mathcal{Z} = \int \mathcal{D}\psi_\sigma \mathcal{D}\bar{\psi}_\sigma\ \exp\left(-\frac{1}{\hbar}\ S[\psi_\sigma,\bar{\psi}_\sigma]\right), \tag{4.80}$$

where

$$S[\psi_\sigma,\bar{\psi}_\sigma] = \int_0^{\hbar\beta} d\tau \int_{L^3} d^3r\ \mathscr{L} \tag{4.81}$$

is the Euclidean action functional and $\mathscr{L}$ is the Euclidean Lagrangian density, given by

$$\mathscr{L} = \bar{\psi}_\sigma \left[\hbar\partial_\tau - \frac{\hbar^2}{2m}\nabla^2 - \mu\right]\psi_\sigma + g_0\,\bar{\psi}_\uparrow\,\bar{\psi}_\downarrow\,\psi_\downarrow\,\psi_\uparrow \tag{4.82}$$

where g_0 is the strength of the s-wave inter-atomic coupling [36, 76]. Summation over the repeated spin index σ in the Lagrangian is intended and $\beta \equiv 1/(k_B T)$ and k_B is the Boltzmann constant.

Through the usual Hubbard-Stratonovich transformation [36, 76] the Lagrangian density $\mathscr{L}$, quartic in the fermionic fields, can be rewritten as a quadratic form by introducing the auxiliary complex scalar field $\Delta(\mathbf{r},\tau)$. As already seen in Chapter 3 and in this Chapter the auxiliary field Δ is to be decomposed as the sum of a constant and uniform contribution Δ_0, to be determined self-consistently, and the fluctuations around this value

$$\Delta(\mathbf{r},\tau) = \Delta_0 + \eta(\mathbf{r},\tau)\ , \tag{4.83}$$

[3] An similar approach using dimensional regularization has been used in the two-dimensional case [153].

where $\eta(\mathbf{r},\tau)$ is the complex paring field of bosonic fuctuations [36, 71, 76].

By neglecting bosonic fluctuations, i.e. by setting $\eta(\mathbf{r},t)=0$, and integrating over the fermionic fields $\psi_\sigma(\mathbf{r},t)$ and $\bar{\psi}_\sigma(\mathbf{r},t)$ as analyzed in detail in Chapter 3 one gets immediately the mean-field (saddle-point and fermionic single-particle) partition function [36, 71, 76]

$$\mathcal{Z}_{\rm mf}=\exp\left(-\frac{S_{\rm mf}}{\hbar}\right)\,, \tag{4.84}$$

where

$$\frac{S_{\rm mf}}{\hbar}=-\sum_{\mathbf{k}}\left[2\ln\left(2\cosh\left(\beta E_{\mathbf{k}}/2\right)\right)-\beta(\epsilon_{\mathbf{k}}-\mu)\right]-\beta L^3\frac{\Delta_0^2}{g_0}\,, \tag{4.85}$$

with $\epsilon_{\mathbf{k}}=\hbar^2k^2/(2m)$ and

$$E_{\mathbf{k}}=\sqrt{(\epsilon_{\mathbf{k}}-\mu)^2+\Delta_0^2} \tag{4.86}$$

is the energy of the fermionic single-particle elementary excitations. At zero temperature ($\beta\to+\infty$) the mean-field grand potential $\Omega_{\rm mf}=-k_BT\ln\mathcal{Z}_{\rm mf}$ becomes

$$\Omega_{\rm mf}=-\sum_{\mathbf{k}}\left(E_{\mathbf{k}}-\epsilon_{\mathbf{k}}+\mu\right)-L^3\frac{\Delta_0^2}{g_0}\,. \tag{4.87}$$

The constant, uniform and real gap parameter Δ_0 is obtained by minimizing $\Omega_{\rm mf}$ with respect to Δ_0, namely

$$\left(\frac{\partial\Omega_{\rm mf}}{\partial\Delta_0}\right)_\mu=0\,. \tag{4.88}$$

As opposed to the treatment in Chapter 3 here we impose a cutoff on the gap equation

$$-\frac{1}{g_0}=\frac{1}{L^3}\sum_{|\mathbf{k}|<\Lambda}\frac{1}{2E_{\mathbf{k}}}\,, \tag{4.89}$$

where the ultraviolet cutoff Λ is introduced to avoid the divergence of the right side of Eq. (4.89) in the continuum limit $\sum_{\mathbf{k}}\to L^3\int d^3\mathbf{k}/(2\pi)^3$.

Equation (3.79), relating the bare interaction strength g_0 to the physical s-wave scattering length a_s of fermions is also rewritten introducing a cutoff [168]

$$-\frac{m}{4\pi\hbar^2a_s}=-\frac{1}{g_0}-\frac{1}{L^3}\sum_{|\mathbf{k}|<\Lambda}\frac{1}{2\epsilon_{\mathbf{k}}}\,, \tag{4.90}$$

so that, after integrating over the momenta, it reads

$$-\frac{m}{4\pi\hbar^2a_s}=-\frac{1}{g_0}-\frac{m}{2\pi^2\hbar^2}\Lambda\,. \tag{4.91}$$

We stress that in the strong-coupling BEC limit, where $g_0 \to -\infty$, the second term on the right of Eq. (4.91) dominates and $a_s = \pi/(2\Lambda) \to 0^+$ when Λ is sent to infinity [168].

Inserting Eq. (4.90) into Eq. (4.89) we obtain the regularized gap equation

$$-\frac{m}{4\pi\hbar^2 a_s} = \frac{1}{L^3}\sum_{|\mathbf{k}|<\Lambda}\left(\frac{1}{2E_{\mathbf{k}}} - \frac{1}{2\epsilon_k}\right) , \tag{4.92}$$

where one can safely take the limit $\Lambda \to +\infty$, recovering the usual treatment analyzed in Chapter 3, in particular finding the energy gap Δ_0 as a function of the chemical potential μ and the scattering length a_s. We stress that in the BCS limit, where $a_s \to 0^-$, the chemical potential μ is positive and $\mu/\Delta_0 \to +\infty$. At unitarity, where $a_s \to \pm\infty$, one finds $\mu/\Delta_0 = 0.8604$ showing that the chemical potential μ is still positive. In the BEC regime, where $a_s \to 0^+$, the chemical potential becomes negative and it is given by

$$\mu = -\frac{\hbar^2}{2ma_s^2} + \frac{1}{4}\frac{ma_s^2}{\hbar^2}\Delta_0^2 , \tag{4.93}$$

while $\mu/\Delta_0 \to -\infty$. Notice that $\epsilon_b = \hbar^2/(ma_s^2)$ is the binding energy of the atomic dimers (composite bosons) which are formed at unitarity [45, 81, 168] and clearly $\mu = -\epsilon_b/2$ in the deep BEC limit.

Let us go back to the zero-temperature grand potential in Eq. (4.87). In the BCS limit, where $a_s \to 0^-$, the energy gap Δ_0 goes to zero and the mean-field grand potential becomes that of a non-interacting Fermi gas, namely

$$\Omega_{\rm mf} = -L^3\,\frac{2}{15\pi^2}\left(\frac{2m}{\hbar^2}\right)^{3/2}\mu^{5/2} . \tag{4.94}$$

In the BEC limit, where $a_s \to 0^+$, the mean-field grand potential reads [45]

$$\Omega_{\rm mf} = -L^3\,\frac{1}{256\pi}\left(\frac{2m}{\hbar^2}\right)^{3/2}\frac{\Delta_0^4}{|\mu|^{3/2}} . \tag{4.95}$$

We point out that in this limit both Δ_0 and $|\mu|$ diverge but $|\mu|$ diverges faster and the grand potential $\Omega_{\rm mf}$ goes to zero.

Fluctuations are accounted for as reviewed in Section 4.1, in particular the action is expanded around Δ_0 up to the quadratic (Gaussian) order in $\eta(\mathbf{r},t)$ and $\bar\eta(\mathbf{r},t)$, yielding

$$\mathcal{Z} = \mathcal{Z}_{\rm mf}\int \mathcal{D}\eta\mathcal{D}\bar\eta\,\left(-\frac{S_{\rm fl}[\eta,\bar\eta]}{\hbar}\right) , \tag{4.96}$$

where

$$S_{\rm fl}(\eta,\bar\eta) = \frac{1}{2}\sum_q (\bar\eta(q),\eta(-q))\;\mathbb{M}(q)\begin{pmatrix}\eta(q)\\ \bar\eta(-q)\end{pmatrix} \tag{4.97}$$

is the Gaussian action of fluctuations in the reciprocal space with $q = (\mathbf{q}, i\Omega_m)$ the 4-vector denoting the momenta $\mathbf{q}$ and Bose Matsubara frequencies $\Omega_m = 2\pi m/\beta$. The 2×2 matrix $\mathbb{M}(q)$ is the inverse fluctuation propagator, as analyzed in Section 4.1. The energy $\hbar\omega_{\mathbf{q}}$ of the bosonic collective excitations can be extracted from $\mathbb{M}(q)$ [117, 118, 134, 138, 168] and it is given by

$$\hbar\omega_{\mathbf{q}} = \sqrt{\epsilon_{\mathbf{q}}\left(\lambda\epsilon_{\mathbf{q}} + 2mc_s^2\right)} \tag{4.98}$$

where $\epsilon_{\mathbf{q}} = \hbar^2 q^2/(2m)$ is the free-particle energy, λ takes into account the first correction to the familiar low-momentum phonon dispersion $\hbar\omega_{\mathbf{q}} \simeq c_s\hbar q$ and c_s is the sound velocity. Both λ and c_s depend on the chemical potential μ and the energy gap Δ_0. In particular, one finds [81, 138]

$$\lambda = \begin{cases} -\frac{128}{135}\frac{\mu^2}{\Delta_0^2} & \text{BCS limit} \\ \frac{1}{8} & \text{unitarity} \\ \frac{1}{4} & \text{BEC limit} \end{cases} \tag{4.99}$$

and

$$mc_s^2 = \begin{cases} \frac{2}{3}\mu & \text{BCS limit} \\ \frac{2}{3}\mu & \text{unitarity} \\ \frac{1}{8}\frac{\Delta_0^2}{|\mu|} & \text{BEC limit} \end{cases} \tag{4.100}$$

Integrating over the bosonic fields $\eta(q)$ and $\bar{\eta}(q)$ in Eq. (4.96), at zero temperature we find the grand potential

$$\Omega = -\lim_{\beta\to+\infty}\frac{1}{\beta}\ln\left(\mathcal{Z}\right) = \Omega_{\text{mf}} + \Omega_{\text{fl}} \tag{4.101}$$

where Ω_{mf} is given by Eq. (4.87), while Ω_{fl} reads

$$\Omega_{\text{fl}} = \frac{1}{2}\sum_{|\mathbf{q}|<\Lambda}\hbar\omega_{\mathbf{q}}\,. \tag{4.102}$$

This is the zero-point energy of bosonic collective excitations [45, 134, 168], and again an ultraviolet cutoff Λ is introduced to avoid the divergence in the continuum limit $\sum_{\mathbf{q}} \to V\int d^3\mathbf{q}/(2\pi)^3$.

4.4.2 Scattering length of composite bosons in the BEC limit

Expanding Eq. (4.102) in powers of Λ [168] we find:

$$\frac{\Omega_{\text{fl}}}{L^3} = \frac{\hbar^2}{40\pi^2 m\lambda^{1/4}}\Lambda^5 + \frac{mc_s^2}{12\pi^2\lambda^{1/2}}\Lambda^3 - \frac{m^3c_s^4}{4\pi^2\lambda^{3/2}}\Lambda + \frac{8m^4c_s^5}{15\pi^2\hbar^2\lambda^2} + \mathcal{O}\left(\frac{1}{\Lambda}\right) \tag{4.103}$$

We note that the first two terms are truly divergent; the third term, despite being $\propto \Lambda$ is indeed convergent, as we are going to show shortly and the fourth term is subleading in the BEC limit.

We then want to regularize the Λ^5 and Λ^3 terms and this can be done by redefining the bare parameters [169] in the mean-field grand potential in Eq. (4.95), introducing their renormalized counterparts. One then finds that the following regularization pattern removes the divergencies at the leading order:

$$\begin{cases} \Delta_0 \longrightarrow \Delta_0 + \frac{16\sqrt{2}}{5} \frac{|\mu|^{\frac{3}{2}}}{\Delta_0^3} \left(\frac{\hbar^2}{2m}\right)^{\frac{5}{2}} \Lambda^5 \\ |\mu| \longrightarrow |\mu| - \frac{128}{9\pi^3} \frac{|\mu|^{\frac{1}{2}}}{\Delta_0^2} \left(\frac{\hbar^2}{2m}\right)^{\frac{5}{2}} \Lambda^5 \end{cases} \tag{4.104}$$

having used the deep-BEC relations in Eqs. (4.99), (4.100) and, as previously discussed, the fact that in the strong-coupling BEC limit the cutoff Λ can be obtained from Eq. (4.91) and it reads

$$\Lambda = \frac{\pi}{2a_s} \, . \tag{4.105}$$

We now analyze the leading convergent contribution, i.e. the Λ term of Eq. (4.103); even though it seems divergent, being proportional to Λ, actually it is not because in the BEC limit c_s^4 goes to zero faster than $1/\Lambda$.

Using Eqs. (4.93), (4.99), (4.100) and (4.105) in the deep BEC regime we have $|\mu| = \hbar^2/(2ma_s^2)$, $\lambda = 1/4$, $mc_s^2 = \Delta_0^2/(8|\mu|)$, and the Λ term of Eq. (4.103) becomes

$$\Omega_{\rm fl} = -L^3 \, \frac{\alpha}{256\pi} \left(\frac{2m}{\hbar^2}\right)^{3/2} \frac{\Delta_0^4}{|\mu|^{3/2}} \, , \tag{4.106}$$

with $\alpha = 2$. It is important to stress that Eq. (4.106) is formally the same formula found by Diener, Sensarma, and Randeria [117] by using a different regularization procedure. The difference is that they have determined numerically the parameter α finding $\alpha = 2.61$ [117], while here we derive $\alpha = 2$ analytically.

In the BEC limit, taking into account Eqs. (4.95) and (4.106) the total grand potential is given by

$$\Omega = \Omega_{\rm mf} + \Omega_{\rm fl} = -L^3 \frac{(1+\alpha)}{256\pi} \left(\frac{2m}{\hbar^2}\right)^{3/2} \frac{\Delta_0^4}{|\mu|^{3/2}} \, , \tag{4.107}$$

with $(1+\alpha) = (1+2) = 3$. Here the grand potential Ω depends explicitly on both μ and Δ_0. Consequently, the total number N of fermions must be calculated as follows

$$N = -\left(\frac{\partial \Omega}{\partial \mu}\right)_{L^3,\Delta_0} - \left(\frac{\partial \Omega}{\partial \Delta_0}\right)_{L^3,\mu} \frac{\partial \Delta_0}{\partial \mu} \, , \tag{4.108}$$

and the number density $n = N/L^3$ reads

$$n = \frac{(1+\alpha)}{16\pi} \left(\frac{2m}{\hbar^2}\right)^{3/2} \frac{\Delta_0^2}{|\mu|^{1/2}} \, . \tag{4.109}$$

This expression shows that, at fixed number density n, in the BEC limit, where both $|\mu|$ and Δ_0 go to infinity, one has $|\mu| \sim \Delta_0^4$ and, from Eq. (4.107) it follows that Ω goes to zero. To obtain Eq. (4.109) we have used Eq. (4.108) but also Eq. (4.93), which immediately gives

$$\frac{\partial \Delta_0}{\partial \mu} = \frac{2\hbar^2}{m a_s^2 \Delta_0} \simeq 4 \frac{|\mu|}{\Delta_0} \tag{4.110}$$

Taking into account Eq. (4.109), the equation (4.93) for the chemical potential in the BEC limit can be rewritten as

$$\mu = -\frac{\hbar^2}{2m a_s^2} + \frac{\pi \hbar^2}{m} \frac{a_s}{(1+\alpha)} n \ , \tag{4.111}$$

where the second term in the r.h.s. is half of the chemical potential $\mu_b = 4\pi\hbar^2 a_b n_B / m_b$ of composite bosons of mass $m_b = 2m$, density $n_b = n/2$, and boson-boson scattering length

$$a_b = \frac{2}{(1+\alpha)} a_s = \frac{2}{3} a_s \ . \tag{4.112}$$

This result is in good agreement with other beyond-mean-field theoretical predictions: $a_b \simeq 0.75 a_s$ of Pieri and Strinati [167], $a_b \simeq 0.60 a_s$ of Petrov, Salomon and Shlyapnikov [165] (and also Astrakharchik, Boronat, Casulleras, and S. Giorgini [111]), and $a_b \simeq 0.55 a_s$ of Hu, Liu and Drummond [166] (and also Diener, Sensarma and Randeria [117]). On the other hand the mean-field result is quite different, namely $a_b = 2a_s$ [71]. Contrary to all other derivations [117, 165–167] our result is fully analytical.

5

A gauge approach to cuprates

In this Chapter I will present some original results derived within a theoretical model for high-T_c superconductivity in cuprates. After an introduction to the high-T_c superconductivity in cuprates and a review of the main experimental properties in Section 5.1, the model [5] for hole doped cuprates will be introduced and reviewed in Section 5.2: the hole is decomposed in the product of a charged spinless holon and a neutral spin $1/2$ spinon, each one bound to a Chern-Simons flux through which the statistical properties of each particle can be changed. The appearance of a finite density of incoherent holons, followed by a finite density of incoherent spinons and finally by the coherence for the recombined electron marks three critical temperatures the last of which we identify as the superconducting transition temperature.

Subsequently I will turn to the superfluid density which is the main subject of the present Chapter; a preliminary investigation of this experimental feature within the aforementioned model is the subject of Ref. [170], the complete account presented in detail here in Section 5.3 follows the thoroughly revised and improved version published in Ref. [7] and includes the discussion of the separate contributions arising from the holon and spinon section, a derivation of a Ioffe-Larkin-like rule for the composition of the two contributions, an analysis of the universality properties in the underdoped regime and a comparison with experimental data.

Finally I will present some novel developments, in particular I will analyze the behavior of the superfluid density in the overdoped region, showing that normalized superfluid density data hints at three different coherence states of the holon+spinon subsystem. I will also present and discuss an improved version of the phase diagram for the model.

Throughout this Chapter natural units $\hbar = k_B = 1$ are often intended.

5.1 Experimental review

The corpus of experimental papers regarding high-T_c cuprates is very large, in fact more than 100 000 scientific papers have been published[1] on the topic after the initial discovery of high-T_c superconductivity in cuprates by Bednorz and Müller in 1986 [47]: clearly a full review of experiments far exceeds the scope of the present Thesis. I shall discuss only the universal features present in all high-T_c cuprates, in addition to that I will analyze some main experimental features, with particular emphasis on those more relevant for the present work.

The term *cuprates* denotes a broad class of materials which, in particular conditions, exhibit superconductivity at very high critical temperatures, even exceeding 130 K at atmospheric pressure in the case of $HgBa_2Ca_2Cu_3O_8$ [172]. Cuprates have been posing and still pose a great challenge to the theorist as the microscopical mechanism behind superconductivity in these materials is still not completely understood, despite a huge theoretical and experimental effort, motivated also by technological implications.

Cuprates are characterized by a number of different features, their chemical compositions being very diverse; following the approach in Ref. [13] we focus on the common and universal features, which most likely are related to the microscopical mechanism of superconductivity in these materials, frequently neglecting the material-dependent features. All high-T_c cuprates share the following features:

- They are composed by a number of stacked CuO_2 layers, hence the name "cuprates", from Latin *cuprum*, copper. The planes can be described as a square lattice, with a copper atom at each lattice site, and an oxygen atom halfway between each couple of copper atoms. Between the planes lie a number of different structures, usually either mono-elemental "spacer" layers mirroring the structure of the CuO_2 planes or "charge reservoirs". Usually each unit cell has n CuO_2 layers and $n-1$ "spacer" layers in between. These structures characterize each different cuprate compound and can affect the superconductivity, i.e. by reducing or increasing the maximum critical temperature or by completely destroying any superconductivity. Among many combinations and stoichiometries it is clear that the only necessary and essential feature for the onset of superconductivity is the presence of the CuO_2 planes.

  Conventionally the a and b crystallographic axes are chosen along the CuO_2 planes, while the c axis is orthogonal to them. It is widely believed that the CuO_2 planes are the main seat of superconductivity [13, 173]: inter-layer coupling effects are present, but they should not

[1] This figure is from more than a decade ago [171], it could easily be doubled by now.

play a key role in the onset of superconductivity. This quasi-2D nature of cuprates is supported by experimental evidence regarding transport properties. There is also evidence that the Cooper pairing mechanism takes place independently layer by layer [13]. As a consequence most theoretical models developed throughout the years aim at modeling the essentially two-dimensional physics of the CuO_2 planes, neglecting the inter-layer effects.

The lattice parameter along the a and b axes is 3.8 Å, the lattice parameter along the c axis varies from material to material due to the many different structures between the layers, it is in the order of magnitude of tens of Å.

- The superconductivity is due to the formation of Cooper pairs, but the pairing mechanism cannot be simply explained in terms of the BCS theory. In fact the most spectacular manifestation of superconductivity in cuprates is the extraordinarily high critical temperature, which is not compatible with the standard scenario of phonon-mediated pairing [174].

- The order parameter has $d_{x^2-y^2}$ symmetry [175, 176].

- The stoichiometry in superconducting cuprates can be changed by adding some impurities or by replacing a fraction of an element with a different one. This process is referred to as doping. The critical temperature T_c strongly depends upon the doping.

  For instance one could start with the undoped (so-called "parent compound") $La_2Cu_2O_4$, adding strontium impurities replacing lanthanum atoms, modifying the stoichiometry to $La_{2-x}Sr_xCu_2O_4$. A number of chemical formulas for the most common cuprate compounds are reported in the following table, besides the standard chemical formula we also report the notation $(CuO_2)_n\,A_{n-1}X$ proposed by Leggett [13] emphasizing the chemical structure of the unit cell with n CuO_2 planes separated by $n-1$ "spacer" layers with chemical formula A and a number of other structures, with chemical formula X.

Common name	Standard chemical formula	n	Notation as proposed by Leggett
BSCCO	$Bi_2Sr_2CaCu_2O_{8+\delta}$	2	$(CuO_2)_2CaBi_2Sr_2O_{4+\delta}$
YBCO	$YBa_2Cu_3O_{6+\delta}$	2	$(CuO_2)_2YBa_2CuO_{2+\delta}$
LSCO	$La_{2-x}Sr_xCuO_4$	1	$(CuO_2)La_{2-x}Sr_xO_2$
HgBCO	$HgBa_2Ca_2Cu_3O_8$	3	$(CuO_2)_3Ca_2HgBa_2O_2$
NCCO	$Nd_{2-x}Ce_xCuO_4$	1	$(CuO_2)Nd_{2-x}Ce_xO_2$
∞-layer	$Sr_xCa_{1-x}CuO_2$	1	$(CuO_2)Sr_xCa_{1-x}$

For the aforementioned reasons we focus on the universal planar copper-oxygen structures: in every compound the net effect of the impurity is to inject holes (i.e. remove electrons) into the CuO_2 planes[2]. In fact the vast majority of experimental features observed in cuprates are a function of the doping δ, i.e. the concentration of injected holes and of the temperature. As a consequence the conventional phase diagram for cuprates has the doping δ on the x axis and the temperature T on the y axis, see Fig. 5.1.

Of course this supports the point of view that the physics of superconductivity in cuprates is essentially determined by what happens in the CuO_2 planes: the details of which element is providing the additional holes are deemed of secondary importance, the most important feature being the how many holes effectively go to the CuO_2 planes. In other words the physics outside the planes seems to play a secondary role in most experimental features of cuprates.

- A closer look at the phase diagram in Fig. 5.1 shows that superconductivity begins at about $\delta \sim 0.05$ and ends at $\delta \sim 0.27$, with a maximum for $\delta \sim 0.16$, outlining the so-called superconducting dome. The shape of the dome is very well approximated by a parabola, which can be parameterized as [13, 177]:

$$T_c(\delta) \simeq T_{c,\max}\left(1 - 82.6(\delta - 0.16)^2\right) . \tag{5.1}$$

  The doping $\delta \sim 0.16$ is the so-called optimal doping for which the critical temperature reaches its maximum value; it is customary to refer to the regions with lower (higher) doping as, respectively, underdoped (overdoped) region.

- The phase diagram is very rich, with many different regions out of the superconductive transition, whose physics is far from being completely and thoroughly understood. Referring to Fig 5.1 we note that for high doping values a cuprate is in the Fermi liquid regime, whose behavior is well understood within the usual theoretical approaches to metals [13]. Lowering the doping the metallic characteristics become progressively more and more different from what one would expect for a standard metal, hence the name of the regime, strange metal. The transition from the Fermi liquid to the strange metal regime appears to be continuous, as a crossover: for instance the in-plane d.c. resistivity, one of the most studied features of cuprates, can be parameterized as $\rho(T) \sim T^\alpha$ with $\alpha = 2$ in the Fermi liquid regime as one would expect. However as

[2]We note that there is also a minority of cuprates in which electrons, rather than holes, are added upon doping to the CuO_2 planes. The behavior of these materials is similar but not identical to hole-doped cuprates. These materials are not considered in the present work.

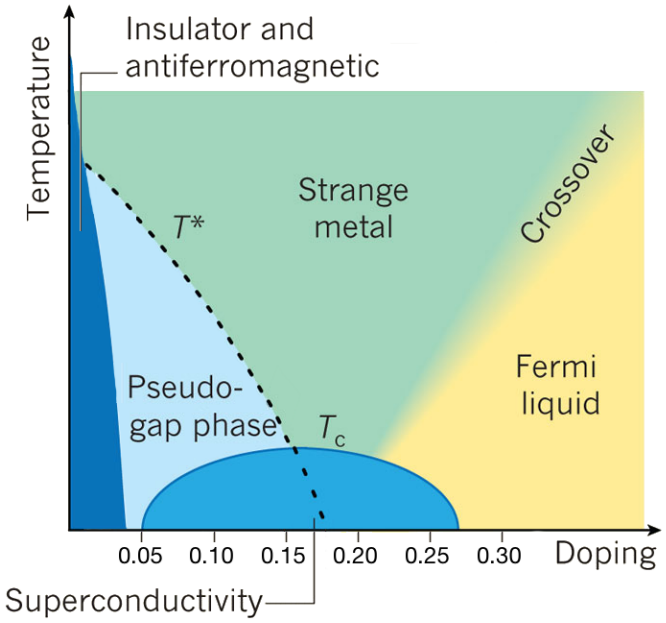

Figure 5.1: Cuprates phase diagram, adapted from [178].

the strange metal regime is approached α gets smaller so that at the optimal doping the resistivity is a linear function of temperature, i.e. $\alpha = 1$.

For even even lower doping, after what might still be a crossover, marked by the dashed line in Fig 5.1, lies the pseudogap phase. The crossover temperature is commonly referred to as T^*. The pseudogap phase is characterized by a strong reduction of the spectral weight hence its name, and exhibits many anomalous properties, the role of which is still debated. Here the resistivity as a function of the temperature exhibits an inflection point, which many consider as *the* experimental signature of the strange metal-pseudogap "transition" [179]; for lower temperatures the resistivity is a sublinear function of temperature until it reaches a minimum, then it either drops to zero as a result of entering the superconducting dome, or apparently diverges if there is no phase transition down to $T = 0$. Finally for even lower doping levels a cuprate enters an anti-ferromagnetic Mott insulator phase.

- The Fermi liquid and strange metal regimes are characterized by a large Fermi surface (enclosed volume $\sim 1 - \delta$). On the other hand the pseudogap regime has a small Fermi surface (enclosed volume $\sim \delta$), composed of Four fermi arcs, shrinking as the temperature is lowered becoming four nodal points as the superconducting phase is reached. Thus the Fermi surface in the pseudogap regime has the same symmetry

as the order parameter in the superconducting phase, and actually appears to be evolving into the nodal points of superconductivity, supporting the point of view that the pseudogap should be a precursor of superconductivity.

- The superfluid density will be the main subject of Section 5.3, so we postpone a review of this important experimental feature to that Section.

5.1.1 From the CuO_2 planes to the Zhang-Rice singlets

A closer look at the CuO_2 planes in the parent compound of cuprates shows that each Cu atom is in the $+2$ oxidation state with all its orbital completely filled, except for an unpaired electron in the outermost $2d_{x^2-y^2}$ orbital. On the other hand the O atoms are in the -2 oxidation state and the outermost $2p$ shell is completely filled. An equivalent description can be given in terms of holes, stating that for $\delta = 0$ in a cuprate there is a hole on each copper site. Due to the nearest-neighbor exchange interaction the holes on each copper site have a staggered anti-ferromagnetic spin configuration.

When additional holes are injected into the planes as a consequence of the doping of the parent compound, they primarily reside on a hybridized p oxygen orbital of the four oxygen atoms surrounding a copper, a pictorial representation of this situation is shown in Fig. 5.2. These structures formed by a hole on a hybridized oxygen orbital forming a spin singlet with an opposite-spin hole on a copper site are called Zhang-Rice singlets [180] and are generally believed to describe the low-energy dynamics of cuprates. It can be shown that this single-band description can be derived from the two Hubbard model [180] separately describing the copper and oxygen orbitals, furthermore there are also experimental observations supporting the description in terms of Zhang-Rice singlets [181].

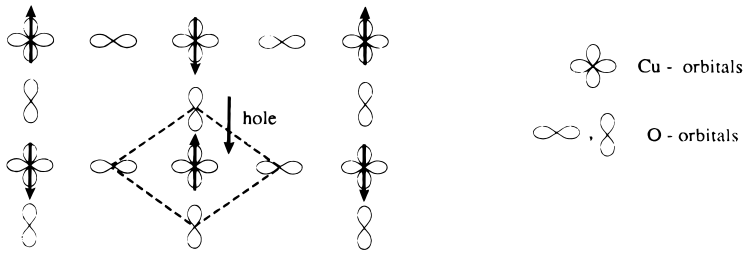

Figure 5.2: The low-temperature dynamics of the holes in the CuO_2 planes can be described in terms Zhang-Rice singlets, i.e. a hole residing on a hybridized p oxygen orbital shared between four oxygen atoms forming a spin singlet with a hole residing on a copper site. Image adapted from [6].

Let us try to derive a model describing the basic physics of Zhang-Rice singlets[3]. A singlet overlaps with an overlap centered on a neighboring site, so that a hole residing on the oxygen hybridized orbital has a finite hopping probability of jumping on a neighboring hybridized oxygen orbital. A description within the Hamiltonian formalism will contain the following term:

$$\hat{H}_{\text{kinetic}} = -t \sum_{\langle i,j \rangle} \left(\sum_{\alpha} \hat{c}^{\dagger}_{i\alpha} \hat{c}_{j\alpha} + h.c. \right) \ , \tag{5.2}$$

where $c_{i,\alpha}$ ($c^{\dagger}_{i,\alpha}$) respectively annihilates (creates) a hole in position i with spin α. The hopping happens over an anti-ferromagnetic background, so that one introduces an anti-ferromagnetic Heisenberg term:

$$\hat{H}_{\text{Heisenberg}} = J \sum_{\langle i,j \rangle} \mathbf{S}_i \cdot \mathbf{S}_j \tag{5.3}$$

and the spin operator is[4]

$$\mathbf{S}_i = \sum_{\alpha.\beta} \hat{c}^{\dagger}_{i\alpha} \frac{\boldsymbol{\sigma}_{\alpha\beta}}{2} \hat{c}_{i\beta} \ . \tag{5.4}$$

Finally one has to consider that the energy penalty for having two holes residing on the same hybrid orbital surrounding a copper site is much higher than the other energies scales at play: in first approximation one may impose a no-double-occupancy constraint, provided by the Gutzwiller projector:

$$\hat{P}_G = \prod_i \left(1 - \hat{n}_{i\uparrow} \hat{n}_{i\downarrow}\right) \ , \tag{5.5}$$

where the number operator is $\hat{n}_i = \sum_{\alpha} \hat{c}^{\dagger}_{i\alpha} \hat{c}_{i\alpha}$. A minimal model encompassing all these features is the $t - J$ model:

$$\hat{H} = \hat{P}_G \left[\sum_{\langle ij \rangle} -t \hat{c}^{\dagger}_{i\alpha} \hat{c}_{j\alpha} + J \mathbf{S}_i \cdot \mathbf{S}_j \right] \hat{P}_G \ . \tag{5.6}$$

Usually the introduction of the Gutzwiller projector is challenging due to its high non-linearity, in particular when using perturbative approaches. The present formalism allows for an exact treatment the Gutzwiller projector.

[3] A more detailed derivation of the $t - J$ model from Zhang-Rice singlets can be found in Ref. [173].

[4] The vector $\boldsymbol{\sigma} = (\sigma_x, \sigma_y, \sigma_z) = \left(\begin{pmatrix} 0 & 1 \\ 1 & 0 \end{pmatrix}, \begin{pmatrix} 0 & -\mathrm{i} \\ \mathrm{i} & 0 \end{pmatrix}, \begin{pmatrix} 1 & 0 \\ 0 & -1 \end{pmatrix} \right)$ is the Pauli matrices vector, we omit the hat symbol over the spin operator for simplicity's sake.

5.2 A gauge approach to high-T_c superconductivity in cuprates

5.2.1 The $t-J$ model: bosonization and spin-charge separation

As explained in the previous section the $t-J$ is thought to encode the fundamental features leading to superconductivity in cuprates, and constitutes the starting point for the model used in the present Chapter. Typical values of t and J for cuprates are $t \approx 0.4\,\mathrm{eV}$ and $J \approx 0.13\,\mathrm{eV}$ and can be inferred through the analysis of the spin-waves modes in the parent compound [182], these values being universal for all cuprates. In particular the fact that $J/t \sim 0.3$ puts cuprates in the strong correlation regime. On the other-hand the no-double-occupancy constraint and the Gutzwiller projection can be justified by considering a three-band model describing the copper and oxygen orbitals: the Mott gap $\Delta \sim 2\,\mathrm{eV}$ between Zhang-Rice singlets states and the upper Hubbard band [183] is much higher than t, J.

More realistic models would also include a next-nearest-neighbor hopping term t', which is particularly important in correctly reproducing the exact shape of the Fermi surface, leaving however the critical properties and the superconductive transition essentially unchanged; the t' term has been analyzed also in the present framework, e.g. in Refs. [184, 185]. As opposed to the t and J terms the magnitude of the t' term is strongly material-dependent[5].

Our starting point is the following Hamiltonian [188], describing the same system as in Eq. (5.6) where, in addition, the particle number is controlled by the chemical potential μ:

$$\hat{H} = \hat{P}_G \left[\sum_{\langle ij \rangle} -t \hat{c}^{\dagger}_{i\alpha} \hat{c}_{j\alpha} + \mu \sum_j \hat{n}_j + J \mathbf{S}_i \cdot \mathbf{S}_j \right] \hat{P}_G \tag{5.7}$$

the sum over the repeated index α being intended. The partition function for the system can be written within the path-integral formalism as

$$\mathcal{Z}(\beta, \mu) = \int \mathcal{D}\Psi \mathcal{D}\Psi^* e^{-S(\Psi, \Psi^*)} \tag{5.8}$$

with the following action:

$$S_{\text{t-J}} = \int_0^{\beta} \mathrm{d}\tau \left\{ \sum_{\langle i,j \rangle} \left(-\frac{J}{2} \left| \Psi^*_{i,\alpha} \Psi_{j,\alpha} \right|^2 + \left[-t \left(\Psi^*_{i,\alpha} \Psi_{j,\alpha} + h.c. \right) \right] \right) + \right.$$
$$\left. + \sum_i \Psi^*_{i,\alpha} \left(\partial_0 + \mu \right) \Psi_{i,\alpha} + \sum_{i,j} u_{i,j} \Psi^*_{i,\alpha} \Psi^*_{j,\beta} \Psi_{j,\beta} \Psi_{i,\alpha} \right\} \tag{5.9}$$

[5] For instance in the case of BSCCO $t'/t \simeq -0.3$, while for LSCO $t/t' \simeq -0.1$, see e.g. Ref. [186] or Ref. [187].

having introduced the Grassmann fields Ψ and Ψ^* representing the hole in stead of the annihilation and creation operators, τ being the imaginary time coordinate. The two-body potential $u_{i,j}$ is equivalent to the no-double-occupancy constraint of the Gutzwiller projector:

$$u_{i,j} = \begin{cases} +\infty & i = j \\ -\frac{J}{4} & i,j \text{ nearest neighbors} \\ 0 & \text{otherwise} \end{cases} \tag{5.10}$$

To proceed with an analytical treatment of the model the quartic interaction must be decoupled with the usual Hubbard-Stratonovich transformation [189, 190], yielding

$$S_{t-J}(\Psi,\Psi^*,X,X^*) = \int_0^\beta \mathrm{d}\tau \sum_{\langle ij\rangle} \frac{2}{J} X^*_{\langle ij\rangle} X_{\langle ij\rangle} + \left[(-t + X_{\langle ij\rangle})\Psi^*_{i\alpha}\Psi_{j\alpha} + h.c.\right] + \\ + \sum_i \Psi^*_{i\alpha}\left(\partial_0 + \mu\right)\Psi_{i\alpha} + \sum_{i,j} u_{i,j}\Psi^*_{i\alpha}\Psi^*_{j\beta}\Psi_{j\beta}\Psi_{i\alpha} \tag{5.11}$$

having introduced the pairing field $X_{\langle ij\rangle}$, and the functional integration in Eq. (5.8) now needs to be extended over the X and X^* fields.

The treatment we are about to introduce relies on the idea of spin charge-separation, i.e. the concept that the fundamental excitations in the $t-J$ model should be holons and spinons, i.e. particles carrying respectively only charge and only spin, rather than electron or holes [6, 191, 192]. This point of view is supported by the observation of spin-charge separation in 1D systems, even in one-dimensional cuprate-like structures [193], along with a great deal of theoretical work in 2D, supported by experimental hints of spin-charge separation in the two-dimensional $t-J$ model [194].

The spin-charge separation idea is implemented within the present formalism by decomposing the electron creation operator as the product of a holon and a spinon operator:

$$\Psi_{x\alpha} = h^*_x \Sigma_{x\alpha} \ , \tag{5.12}$$

more precisely h_x is a 1-component fermionic (Grassman) field, while Σ_x is a 2-component bosonic (complex) field. The no-double-occupancy constraint is automatically satisfied as h is a spinless fermion, while the condition

$$\Sigma^*_{x\alpha}\Sigma_{x\alpha} = 1 \tag{5.13}$$

at each lattice site ensures that $\sum_\alpha \Psi^*_{x\alpha}\Psi_{x\alpha} = h^*_x h_x$. We stress that the decomposition in Eq. (5.12) adds an additional U(1) invariance to theory, as the holonic and spinonic fields are defined up to a local phase factor

$$\begin{cases} h_j \longrightarrow h_j e^{\mathrm{i}\Lambda_j} \\ \Sigma_{j\alpha} \longrightarrow \Sigma_{j\alpha} e^{\mathrm{i}\Lambda_j} \end{cases} \qquad \Lambda_j \in [0, 2\pi[\ . \tag{5.14}$$

To distinguish this invariance from other invariances of the theory we name it the h/s symmetry and denote its group as $\mathrm{U}(1)_{h/s}$.

When decomposing the electron as the product of a holon and a spinon like in Eq. (5.12) one is free to choose the statistics for the holon and for the spinon, provided that the recombined hole is still fermionic. If the system were three dimensional the choice would be constrained by the fact that the fermionic electron can only be the product of a fermion and a boson. In two dimension there are many more possibilities as, beside the usual fermions and bosons acquiring a ∓ 1 factor upon exchange, there can also be particles acquiring a phase factor upon exchange [195]. These particle are called anyons and clearly the anyonic statistics generalize the fermionic and bosonic ones in two dimensions.

We follow the idea initially advocated by Laughlin that the holon and the spinon should be semions [196, 197], i.e. objects acquiring a $\pm\mathrm{i}$ phase factor upon exchange. The phase factor is halfway between the fermionic and bosonic cases on the unit circle in the complex plane, hence the name *semions*. This idea can be implemented in a very elegant way by extending the Chern-Simons bosonization approach to the present case. A statistical flux is bound to a particle, changing its statistical properties. The simplest example is the Jordan-Wigner transformation in 1D [198]:

$$\hat{c}_j^\dagger = \hat{a}_j^\dagger e^{-\mathrm{i}\pi \sum_{l<j} \hat{a}_l^\dagger \hat{a}_l} \tag{5.15}$$

where $\hat{c}^\dagger$ is a fermionic creation operator, $\hat{a}^\dagger$ is a bosonic creation operator, and the phase factors counts the number of exchanges reproducing the correct statistics for the field. The same idea can be extended to our two dimensional case, in the path integral formalism, binding a statistical flux to the holon and to the spinon

$$\Psi_{x\alpha}(B,V) = \left[e^{\mathrm{i}\int_{\gamma_x} B} h_x^*\right]\left[P\left(e^{\mathrm{i}\int_{\gamma_x} V}\right)_{\alpha\beta}\Sigma_{x\beta}\right] \tag{5.16}$$

where γ_x is an arbitrary path on the two-dimensional from the point x to infinity, P denotes the path ordering and B and V are respectively U(1) and SU(2) gauge fields whose dynamics will be explained shortly.

The choice of the gauge group $\mathrm{U}(1)\times\mathrm{SU}(2)$ is motivated by the physics of the system, in particular the U(1) gauge field is related to the charge degrees of freedom and will take care of the statistics of the charge-carrying holons, while the SU(2) gauge field is related to the spin degrees of freedom and will determine the statistics of the spin-carrying spinons. The $t-J$ Hamiltonian in Eq. (5.7) is invariant under the U(1) transformation

$$\hat{c}_{j\alpha} \to e^{\mathrm{i}\lambda_j}\hat{c}_{j\alpha} \qquad \lambda_j \in \mathbb{R} \tag{5.17}$$

and under the SU(2) transformation

$$\hat{c}_{j\alpha} \to U_{\alpha\beta}\hat{c}_{j\beta} \qquad U \in \mathrm{SU}(2)\ . \tag{5.18}$$

so that the newly-introduced Chern-Simons gauge fields B and V will gauge the original symmetries of the model. Further motivation for this choice comes from the analogous 1D theory obtained from dimensional reduction: in that context the $\mathrm{U}(1) \times \mathrm{SU}(2)$ gauge group has been shown to recover the correct critical exponents [188, 199].

Let us make this intuitive description more rigorous by introducing the following theorem[6] [6, 188], establishing a link between the partition function[7] expressed in terms of the electron field Ψ and the partition function of a system expressed in terms of a field Φ coupled to the gauge fields B and V, whose statistics are determined by B and V:

$$\int \mathcal{D}\Psi\mathcal{D}\Psi^* e^{-S(\Psi,\Psi^*|A)} = \\ = \frac{\int \mathcal{D}B\mathcal{D}V \int \mathcal{D}\Phi\mathcal{D}\Phi^* e^{-\left[S(\Phi,\Phi^*|A+B+V)+k_{\mathrm{U}(1)}S_{\mathrm{C.S.}}(B)+k_{\mathrm{SU}(2)}S_{\mathrm{C.S.}}(V)\right]}}{\int \mathcal{D}B\mathcal{D}V e^{-\left[k_{\mathrm{U}(1)}S_{\mathrm{C.S.}}(B)+k_{\mathrm{SU}(2)}S_{\mathrm{C.S.}}(V)\right]}} . \quad (5.19)$$

We denote the original action, minimally coupled the electromagnetic field A by $S(\Psi, \Psi^*|A)$ and we replace it by the same action coupled to the electromagnetic field A and to the statistical gauge fields B and V, a kinetic term giving dynamics to B and V is also added:

$$S(\Psi, \Psi^*|A) \longrightarrow S(\Phi, \Phi^*, A+B+V)+k_{\mathrm{U}(1)}S_{\mathrm{C.S.}}(B)+k_{\mathrm{SU}(2)}S_{\mathrm{C.S.}}(V) \quad (5.20)$$

and the dynamics of the gauge field are given by the Chern-Simons action:

$$S_{\mathrm{C.S.}}(B) = \frac{1}{4\pi\mathrm{i}} \int_0^\beta \mathrm{d}\tau \int \mathrm{d}^n x \; \epsilon^{\mu\nu\rho} B_\mu \partial_\nu B_\rho \quad (5.21)$$

$$S_{\mathrm{C.S.}}(V) = \frac{1}{4\pi\mathrm{i}} \int_0^\beta \mathrm{d}\tau \int \mathrm{d}^n x \; \epsilon^{\mu\nu\rho} \,\mathrm{tr}\left[V_\mu \partial_\nu V_\rho + \frac{2}{3} V_\mu V_\nu V_\rho\right] \quad (5.22)$$

and the fermionic field is replaced by

$$\Psi_\alpha(x) \longrightarrow \Phi_\alpha(\gamma_x|B,V) \equiv \left[e^{\mathrm{i}\int_{\gamma_x} B} h_x^*\right]\left[P\left(e^{\mathrm{i}\int_{\gamma_x} V}\right)_{\alpha\beta} \Sigma_{x\beta}\right] \quad (5.23)$$

When considering the products in square brackets, i.e. the holon coupled to the U(1) statistical flux and the spinon coupled to the SU(2) statistical flux the global statistics are determined by the coupling constants $k_{\mathrm{U}(1)}$ and $k_{\mathrm{SU}(2)} = +1$. It can be shown that the choice

$$k_{\mathrm{U}(1)} = -2 \qquad k_{\mathrm{SU}(2)} = +1 \quad (5.24)$$

[6] Refs. [6, 188] call the theorem "bosonization formula", as the Φ field is initially bosonic there, and is re-fermionized later. Here a more compact approach is used, more in the spirit of Ref. [5], the statistical fluxes are tuned so that Φ is fermionic to begin with and the bosonization formula actually connects two fermionic representations.

[7] We can consider X as an additional gauge field like A in Eq. 5.11. After applying Eq. 5.19 the integration over the auxiliary field X is carried out.

leaves the correct fermionic statistics for the recombined hole while making the holons and spinons, when bound to their statistical fluxes, semions.

We stress that the statistics of the holon and spinon when bound to the respective statical fluxes are determined by the gauge fields B and V, which in turn depend the coefficients in Eq. (5.24), changing them allows one to modify the statistic, in particular the slave boson and slave fermion approaches can be recovered as particular case [6] with an appropriate choice of $k_{\mathrm{U}(1)}$ and $k_{\mathrm{SU}(2)}$ [200]. It is known that the slave fermion and slave boson approaches, although formally completely equivalent, give different result when the mean-field approximation is taken: this means that the mean-field approximation is removing relevant information. As a solution one may include further information beyond the mean-field or, alternatively, choose a different starting point more suited to preserve the real physics of the system upon mean-field approximation. Arguably the present gauge approach, retaining the U(1) and SU(2) symmetries of the $t-J$ model is a good choice in 1D and should provide a better starting point also in 2D.

The partition function is now calculated by integrating over all the matter and gauge fields, and explicitly introducing the constraint in Eq. (5.13)

$$\mathcal{Z}(\beta,\mu)=\int \mathcal{D}h\mathcal{D}h^{*}\mathcal{D}\Sigma_{\alpha}\mathcal{D}\Sigma_{\alpha}^{*}\mathcal{D}B\mathcal{D}V e^{-S(h,h^{*},\Sigma_{\alpha},\Sigma_{\alpha}^{*},B,V)}\delta\left(\Sigma^{*}\Sigma-1\right) \quad (5.25)$$

We also note that, when the action is expressed in terms of holons and spinons, the no-double-occupancy constraint is automatically satisfied, as the holons are spinless fermions: as anticipated the Gutzwiller projector is treated in a non-perturbative way in the present formalism.

As a result of the above procedure we obtain an action for the $t-J$ model in terms of holons and spinons whose statistics is modified by the statistical fluxes provided by the gauge fields B and V:

$$\begin{aligned}S=\int_{0}^{\beta}\mathrm{d}\tau\Big\{&\Big[h_{j}^{*}(\partial_{0}-\mathrm{i}B_{0}(j)-(\mu+1/2J))h_{j}+\mathrm{i}B_{0}(j)+\\&+\left(1-h_{j}^{*}h_{j}\right)\Sigma_{j\alpha}^{*}\left(\partial_{0}+\mathrm{i}V_{0}(j)\right)_{\alpha\beta}\Sigma_{j\beta}\Big]+\\&-t\sum_{\langle ij\rangle}\Big[(h_{j}^{*}e^{\mathrm{i}\int_{\langle ij\rangle}B}h_{i}\Sigma_{i\alpha}^{*}(Pe^{\mathrm{i}\int_{\langle ij\rangle}V})_{\alpha\beta}\Sigma_{j\beta}+h.c.)+\\&+\frac{J}{2}(1-h_{i}^{*}h_{i})(1-h_{j}^{*}h_{j})(|\Sigma_{i\alpha}^{*}(Pe^{\mathrm{i}\int_{\langle ij\rangle}V})_{\alpha\beta}\Sigma_{j\beta}|^{2}-1/2)\Big]\Big\}\\&-2S_{\mathrm{C.S.}}(B)+S_{\mathrm{C.S.}}(V)\end{aligned} \quad (5.26)$$

The doping, i.e. the concentration of additional holes injected in the CuO_2 planes with respect to the parent compound, is $\delta=\mu+J/4$.

5.2.2 Gauge fixings

The action in Eq. (5.26) cannot be used in order to calculate the partition function for the system: unphysical degrees of freedom have been added in the spin-charge separation process and when introducing the statistical fluxes. Namely the system is invariant under the $\mathrm{U}(1)_{h/s} \times \mathrm{U}(1) \times \mathrm{SU}(2)$ group. The symmetry introduced by the spin-charge decomposition and analyzed in Eq. (5.27) is still a symmetry after the introduction of the statistical fluxes [200]:

$$\begin{cases} h_j \longrightarrow h_j e^{\mathrm{i}\Lambda(j)} \\ \Sigma_{j\alpha} \longrightarrow \Sigma_{j\alpha} e^{\mathrm{i}\Lambda(j)} \end{cases} \qquad \Lambda(x) \in [0, 2\pi[\ , \tag{5.27}$$

the second U(1) subgroup corresponds to the electric charge and to the field B_μ

$$\begin{cases} h_j \to h_j e^{\mathrm{i}\Lambda(j)} \\ h_j^* \to h_j^* e^{-\mathrm{i}\Lambda(j)} \\ B_\mu(x) \to B_\mu(x) + \partial_\mu \Lambda(x) \end{cases} \qquad \Lambda(x) \in \mathbb{R} \tag{5.28}$$

and finally the SU(2) subgroup corresponds to the spin degrees of freedom and to the field V_μ

$$\begin{cases} \Sigma_j \to g(j)^\dagger \Sigma_j \\ \Sigma_j^* \to \Sigma_j^* g \\ V_\mu(x) \to g(x) V_\mu(x) g^\dagger(x) - \mathrm{i} g(x) \partial_\mu g^\dagger(x) \end{cases} \qquad g(x) \in \mathrm{SU}(2) \ . \tag{5.29}$$

In this Subsection we introduce a gauge fixing for the U(1) and SU(2) invariances, postponing the fixing of the $\mathrm{U}(1)_{h/s}$ to a latter moment. The U(1) invariance is gauge-fixed by imposing the Coulomb gauge:

$$\partial_\mu B^\mu = 0 \ . \tag{5.30}$$

Noting that B_0 appears linearly in the action and can be integrated, one obtains:

$$B_\mu = \bar{B}_\mu + \delta B_\mu \ , \tag{5.31}$$

with

$$\bar{B} = \frac{1}{2} \sum_j \partial_\mu \arg(x - j) \tag{5.32}$$

and

$$\delta B_\mu(x) = \frac{1}{2} \sum_j h_j^* h_j \partial_\mu \arg(x - j) \tag{5.33}$$

where the static part $\bar{B}_\mu$ provides a π-flux phase, i.e. $\exp\big(\mathrm{i} \int_\Box \bar{B}\big) = -1$ for every plaquette, $\Box$ being the boundary of a plaquette [5].

The SU(2) invariance is gauge-fixed by imposing the Néel gauge, retaining the anti-ferromagnetic bipartite structure of the original lattice

$$\Sigma_j = \sigma_x^{|j|} \begin{pmatrix} 1 \\ 0 \end{pmatrix} \tag{5.34}$$

$$\Sigma_j^* = \begin{pmatrix} 1 & 0 \end{pmatrix} \sigma_x^{|j|} \tag{5.35}$$

with $|j| \equiv j_1 + j_2$. Having fixed the spinon configuration corresponds to the fact that the low-energy spinon dynamics are essentially fluctuations over a static anti-ferromagnetic background: the spin degrees of freedom have been transferred to the gauge field V and its SU(2) transformations g upon which one needs to extend the functional integration. The integration over the gauge field V is then split as an integration over a field $V^\mu_{(c)}$, obeying the Coulomb gauge condition

$$\partial_\mu V^\mu_{(c)} = 0 \tag{5.36}$$

and its gauge transformations g

$$V = g^\dagger V_{(c)} g + g^\dagger \partial g \tag{5.37}$$

g being a SU(2)-valued field. Similarly as before the 0 component of V appears linearly in the action and can be integrated providing the following constraint[8]:

$$V_\mu^{(c)} \simeq \sum_j \left(1 - h_j^* h_j\right) \left(\sigma_x^{|j|} g_j^\dagger \frac{\sigma_a}{2} g_j \sigma_x^{|j|}\right)_{11} \partial_\mu \arg(x-j)\sigma_a \tag{5.38}$$

At the end of the gauge-fixing procedure the action is $S = S_1 + S_2$ where

$$S_1(h, h^*, A, U) = \int_0^\beta \mathrm{d}\tau \Big\{ \sum_j \left[h_j^*(\partial_0 - \mu)h_j + \mathrm{i}(1 - h_j^* h_j)A_j\right] + \\ - t \sum_{\langle ij \rangle} (h_i U_{\langle ij \rangle} h_j^* + h.c.) \Big\} \tag{5.39}$$

and

$$S_2(h, h^*, U) = \int_0^\beta \mathrm{d}\tau \sum_{\langle ij \rangle} \frac{J}{2} (1 - h_i^* h_i)(1 - h_j^* h_j) \left(|U_{\langle ij \rangle}|^2 - 1/2\right) \tag{5.40}$$

having defined the auxiliary lattice gauge fields

$$\mathrm{i}A_j \sim \left(\sigma_x^{|j|} g_j^\dagger \partial_0 g_j \sigma_x^{|j|}\right)_{11} \tag{5.41}$$

$$U_{\langle ij \rangle} \sim e^{\mathrm{i}\int_{\langle ij \rangle}(\bar{B} + \delta B)} \left(\sigma_x^{|i|} g_i^\dagger (P e^{\mathrm{i}\int_{\langle ij \rangle} V^{(c)}}) g_j \sigma_x^{|j|}\right)_{11} \tag{5.42}$$

[8]The constraint is approximate, an exact treatment can be found in [5].

In conclusion of the present subsection we review the result obtained: starting from a path integral representation of the $t-J$ model we have split the hole into the product of a spinon and a holon. By binding them to a statistical flux we can modify the statistics, in particular we have chosen semionic statistics for both the holon and the spinon. The gauge fields B and V can be chosen as in Eq. (5.31) and in Eq. (5.38), while the effective action in terms of holon, spinons and statistical fluxes is given by Eq. (5.39) and Eq. (5.40). The h/s symmetry introduced by the spin-charge separation still needs to be fixed.

As a final consistency check we count the degrees of freedom of the theory we obtained: the Grassman fields h and h^* account for 2 d.o.f., while the 3 degrees of freedom are carried by $g \in \mathrm{SU}(2)$. The h/s symmetry, still to be fixed, would provide an additional constraint (-1 d.o.f.) giving a total of 4 d.o.f., in agreement with the original theory in terms of Ψ_α and Ψ^*_α.

5.2.3 Optimization of the spinon configuration

It is not possible to proceed with the usual BCS treatment of the pairing, choosing a saddle-point value for the holons and for the spinons, eventually reinstating the fluctuations in an approximate way, as done in the context of the BCS-BEC crossover in the previous Chapters: in the present case the fields A_j and $U_{\langle ij\rangle}$ depend on both the charge and spin degrees of freedom, hindering a simultaneous diagonalization of the action in terms of h and g [201].

A different approach consists in looking for a holon-dependent spinon configuration $g^m_j(h,h^*)$ maximizing the partition function, i.e. minimizing the action. Afterwards the fluctuations around the optimal configuration can be added, either in an exact or in an approximate way. We stress that finding a spinon configuration optimizing the partition function given a fixed holon configuration is akin to the Born-Oppenheimer approximation in which "fast" and "slow" variables are separated [17], and in fact a justification for the optimization procedure lies in the observation that the holon effective mass is much bigger than its spinon counterpart in the $t \gg J$ limit [200].

In this subsection we will summarize the main result for this optimization procedure, whose complete treatment can be found in Ref. [200]. We state the following theorem: the partition function defined as

$$\Xi(A,U) = \int \mathcal{D}h\mathcal{D}h^* e^{-S(h,h^*,A,U)} \tag{5.43}$$

has the following upper bound

$$|\Xi(A,U)| \leq \int \mathcal{D}h\mathcal{D}h^* e^{-\left[S_1\left(h,h^*,0,\hat{U}\right)+S_2(h,h^*,0)\right]} \tag{5.44}$$

where $\hat{U}$ is the time-independent configuration of the U field maximizing

$$\int \mathcal{D}h\mathcal{D}h^* \; e^{-[S_1(h,h^*,0,U)+S_2(h,h^*,0)]}\Big|_{\partial_0 U=0} \; . \tag{5.45}$$

While it is not possible to find a spinon configuration strictly saturating the bound, it is however possible to find a configuration saturating the bond on average. Once this configuration has been determined an exact treatment is still possible by introducing the fluctuations around this optimal configuration. In the small temperature and small doping limit we can parameterize the optimal configuration as follows [200]:

$$g_j = \bar{g}_j R_j \tilde{g}_j = e^{-\frac{\mathrm{i}}{2}\sum_{i\neq j}(-1)^i \sigma_z \arg(i-j)} R_j e^{\mathrm{i}\frac{\pi}{2}(-1)^{|j|}\sigma_y h_j^* h_j} \tag{5.46}$$

where $R_j \in \mathrm{SU}(2)$ can be conveniently expressed in CP^1 form:

$$R_j = \begin{pmatrix} b_{j1} & -b_{j2}^* \\ b_{j2} & b_{j1}^* \end{pmatrix} \qquad b_{j\alpha}^* b_{j\alpha} = 1 \tag{5.47}$$

b_α being a two-component complex field satisfying the constraint $b_\alpha^* b_\alpha = 1$ at every lattice site. The optimal spinon configuration, as defined above, is then given by $R_j = \mathbb{1}$ and the fluctuations can be taken into account by including the fluctuations around the optimal value. The $V^{(c)}$ SU(2) statistical gauge field can be written in a much simpler form when acting over an optimal spinon configuration

$$\bar{V}_\mu = -\sum_j h_j^* h_j \frac{(-1)^j}{2} \partial_\mu \arg(x-j)\sigma_z \tag{5.48}$$

and the remainder $\delta V = V^{(c)} - \bar{V}$ can be seen as the back-reaction of the spinon fluctuations away from their optimal configuration. On the other hand, the non-fluctuating part $\bar{V}_\mu$ describes spin vortices attached on each holon site.

Finally the effective action can be written as $S = S_h + S_s$ with

$$\begin{aligned} S_h = \int_0^\beta \mathrm{d}\tau \Bigg\{ & \sum_j h_j^* \left[\partial_0 - \left(\sigma_x^{|j|} R_j^\dagger \partial_0 R_j \sigma_x^{|j|}\right)_{11} - t\delta\right] h_j + \\ & + \sum_{\langle ij\rangle} \left[-t h_j^* e^{\mathrm{i}\int_{\langle ij\rangle} \bar{B}+\delta B} h_i \left(\sigma_x^{|i|} R_i^\dagger P \left(e^{\mathrm{i}\int_{\langle ij\rangle}(\bar{V}+\delta V)}\right) R_j \sigma_x^{|i|}\right)_{11} + h.c.\right] \Bigg\} \end{aligned} \tag{5.49}$$

and

$$S_s = \int_0^\beta \mathrm{d}\tau \left\{ \sum_j \left(\sigma_x^{|j|} R_j^\dagger \partial_0 R_j \sigma_x^{|j|} \right)_{11} + \right.$$
$$\left. + \sum_{\langle ij \rangle} \frac{J}{2} \left(1 - h_i^* h_i\right) \left(1 - h_j^* h_j\right) \left[\left| \left(\sigma_x^{|i|} R_i^\dagger P e^{\mathrm{i} \int_{\langle ij \rangle} \left(\bar{V} + \delta V \right)} R_j \sigma_x^{|i|} \right)_{11} \right|^2 - \frac{1}{2} \right] \right\} \tag{5.50}$$

the holonic and spinonic part being formally separated; however they are still "connected" by the statistical gauge fields and by the h/s gauge invariance.

5.2.4 Effective action for holons and spinons

The treatment has been kept exact up to this point. The derivation of the optimal spinon configuration g^m assumes the low temperature, low doping limit but if the fluctuations are added in a complete way, i.e. the SU(2)-valued field R spans all the group configurations, the theory is still exact.

The main approximation of the present approach consists in neglecting the back-reaction of the spinon fluctuations in the gauge field V, i.e. setting $\delta V = 0$, which is reasonable provided the spinon fluctuations are small enough [200]. After this approximation the field operator formed by the spinon and its statistical flux is

$$\left(P e^{\mathrm{i} \int_{\gamma_x} \bar{V}} \right) \Sigma_j = e^{\mathrm{i} \int_{\gamma_j} \bar{V}} \bar{g}_j R_j \sigma_x^{|j|} \begin{pmatrix} 1 \\ 0 \end{pmatrix} . \tag{5.51}$$

which is now describing a boson.

The statistical flux modifies the statistics of the matter field it is bound to: in fact neglecting δV changes the statistical properties of the combination in Eq. (5.51), and, as a consequence, the fermionic statistics of the hole are also modified. For consistency one may also neglect the holon fluctuations in the gauge field B, thus setting $\delta B = 0$. Doing so the correct fermionic statistic for the electron is recovered. The holon field, along with its statistical flux is now

$$e^{\mathrm{i} \int_{\gamma_x} \bar{B}} h_x^* . \tag{5.52}$$

and it is now describing a fermion. It should be noted that in 1D the semionic statistics are fundamental in deriving the correct physics and the correct critical exponents [188]; it is conjectured, however, that in 2D they should be less relevant at this level, as the holon and spinon form a bound state [200].

In order to proceed let us calculate the link variable appearing in Eq.

(5.49) and in Eq. (5.50):

$$R_i^\dagger e^{\mathrm{i}\int_{\langle ij\rangle}\bar{V}} R_j = \begin{pmatrix} \alpha_{\langle ij\rangle} b_{i1}^* b_{j1} + \alpha_{\langle ij\rangle}^* b_{i2}^* b_{j2} & -\alpha_{\langle ij\rangle} b_{i1}^* b_{j2}^* + \alpha_{\langle ij\rangle}^* b_{i2}^* b_{j1}^* \\ -\alpha_{\langle ij\rangle} b_{i2} b_{j1} + \alpha_{\langle ij\rangle}^* b_{i1} b_{j2} & \alpha_{\langle ij\rangle} b_{i2} b_{j2}^* + \alpha_{\langle ij\rangle}^* b_{i1} b_{j1}^* \end{pmatrix} \equiv \equiv \begin{pmatrix} AM_{ij} & -RVB_{ij} \\ RVB_{ij}^* & AM_{ij}^* \end{pmatrix} \tag{5.53}$$

having introduced

$$\alpha_{\langle ij\rangle} = e^{\frac{\mathrm{i}}{2}\int_{\langle ij\rangle}\bar{V}_z} \ . \tag{5.54}$$

The appearance of a RVB-like term [191] along with an Affleck-Marson-like [202] term at the same time is a peculiarity of the semionic approach of the present theory [5], not appearing in the slave boson or in the slave fermion approaches.

Skipping the time-derivatives introduced by the path integral formalism for the sake of clarity, the physics of holons and spinons is encoded in the holon hopping term:

$$t\sum_{\langle ij\rangle} h_j^* e^{\mathrm{i}\int_{\langle ij\rangle}\bar{B}} h_i AM_{ij} \tag{5.55}$$

and in the spinon Heisenberg term:

$$\frac{J}{2}\sum_{\langle ij\rangle}\left(1-h_i^*h_i\right)\left(1-h_j^*h_j\right)\left(|RVB_{ij}|^2 - 1/2\right) \ . \tag{5.56}$$

We stress, though, that the dynamics of holons and spinons are however still linked by the V field appearing in the AM and RVB factors and by h/s gauge invariance which still needs to be gauge fixed. At first we analyze the free holon dynamics, considering the holon hopping term in Eq. (5.55); the modulus of the Affleck-Marston factor AM_{ij} can be deemed as constant due to the slow nature of the $\bar{V}$ field for low doping concentrations, its phase $\exp(\mathrm{i}\theta_{ij})$, however, cannot be neglected and needs to be accounted for; we rewrite the holon hopping term as

$$t\sum_{\langle ij\rangle} h_j^* e^{\mathrm{i}\int_{\langle ij\rangle}\bar{B}} e^{\mathrm{i}\theta_{ij}} h_i \ . \tag{5.57}$$

The static gauge field $\bar{B}$ derived in Eq. (5.32) induces a π-flux phase on each plaquette, so having a 2×2 periodicity in terms of the lattice spacing, as shown in Fig. 5.3. It is thus natural, using a standard procedure [203], to divide the lattice in four sublattices. Denoting each lattice site through the coordinates (j_1, j_2), it will belong to the (1) sublattice if both j_1 and j_2 are even; to the (2) sublattice for j_1 odd, j_2 even; to the (3) sublattice for j_1 even, j_2 odd and finally to the (4) sublattice is j_1 and j_2 are both odd. We then group them creating the Néel sublattices, $A = \{(1),(3)\}$ and $B = \{(2),(4)\}$,

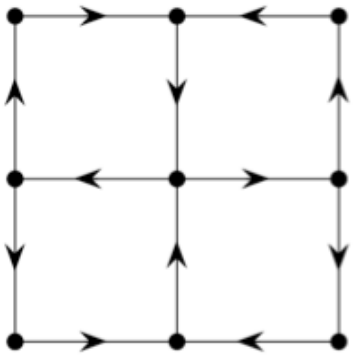

Figure 5.3: The π-flux per plaquette, in Eq. (5.33), has a 2×2 periodicity.

in a checkerboard fashion. A similar treatment can be applied to the field operators, denoting with $h^{(a)}$ the restriction of the holon field to the a-th sublattice it is convenient to define the following spinors

$$\Psi_1 = \begin{pmatrix} \Psi_1^{(A)} \\ \Psi_1^{(B)} \end{pmatrix} = \begin{pmatrix} e^{-\mathrm{i}\frac{\pi}{4}} h^{(1)} + e^{\mathrm{i}\frac{\pi}{4}} h^{(4)} \\ e^{-\mathrm{i}\frac{\pi}{4}} h^{(3)} + e^{\mathrm{i}\frac{\pi}{4}} h^{(2)} \end{pmatrix} \tag{5.58}$$

$$\Psi_2 = \begin{pmatrix} \Psi_2^{(A)} \\ \Psi_2^{(B)} \end{pmatrix} = \begin{pmatrix} e^{-\mathrm{i}\frac{\pi}{4}} h^{(2)} + e^{\mathrm{i}\frac{\pi}{4}} h^{(3)} \\ e^{-\mathrm{i}\frac{\pi}{4}} h^{(4)} + e^{\mathrm{i}\frac{\pi}{4}} h^{(1)} \end{pmatrix} \tag{5.59}$$

through which the low-energy effective holon action in the continuum limit can be recast [200] as the action of gapless Dirac fermions

$$S_h = \int \mathrm{d}^3x \sum_{r=1}^{2} \bar{\Psi}_r [\gamma_0(\partial^0 - \delta - e_r z_\alpha^* \partial_0 z_\alpha) + t(\gamma_\mu \partial^\mu - e_r z_\alpha^* \gamma_\mu \partial^\mu z_\alpha)] \Psi_r \tag{5.60}$$

with sublattice-depending charge $e_1 = +1$, $e_2 = -1$ and as usual the gamma matrices in 2D are $\gamma_\mu = (\sigma_z, \sigma_y, \sigma_x)$, moreover $\bar{\Psi}_i = \gamma_0 \Psi_i^\dagger$. The emergent self-generated U(1) gauge field $A_\mu \sim z_\alpha \partial_\mu z_\alpha$ accounts for the h/s gauge symmetry.

Now we turn to the spinons, referring to the action in Eq. (5.50) it is particularly useful to rewrite $b_{j\alpha}^* \boldsymbol{\sigma}_{\alpha\beta} b_{j\beta}$ separating the ferromagnetic and anti-ferromagnetic degrees of freedom

$$b_{j\alpha}^* \boldsymbol{\sigma}_{\alpha\beta} b_{j\beta} \sim \boldsymbol{\Omega}_j + (-1)^{|j|} \epsilon \mathbf{L}_j \tag{5.61}$$

where ϵ is the lattice constant, with the constraints $\boldsymbol{\Omega}_j^2 = f \lesssim 1$ and $\boldsymbol{\Omega} \cdot \mathbf{L} = 0$. It is also convenient to Taylor expand the phase factor appearing in the link variable in Eq. (5.53), owing to the slow-varying nature of the $\bar{V}$ field for low doping concentrations:

$$e^{-\mathrm{i}\int_{\langle ij \rangle} \bar{V}_z} \approx 1 + \epsilon(-\mathrm{i}\bar{V}_z(j)) + \frac{\epsilon^2}{2}\epsilon(-\mathrm{i}\bar{V}_z(j))^2 + O(\epsilon^3)\,. \tag{5.62}$$

We use this approximation in the effective spinon action in Eq. (5.50), rewriting it in terms of $\mathbf{\Omega}$ and $\mathbf{L}$; after the integration of the ferromagnetic part $\mathbf{L}$ the low-energy effective action in the continuum limit reads:

$$S_s \simeq \int \mathrm{d}^3x \frac{1}{g}[(\partial_0 \mathbf{\Omega})^2 + v_s^2(\partial_\mu \mathbf{\Omega})^2 + \mathbf{\Omega}^2(\bar{V}_z)^2] \tag{5.63}$$

with $g = 8\epsilon^2/\tilde{J}$ and $v_s = \tilde{J}\epsilon$. Rewriting $\mathbf{\Omega}$ in the CP^1 form as

$$\mathbf{\Omega} = z^*_{j\alpha} \boldsymbol{\sigma}_{\alpha\beta} z_{j\beta} \tag{5.64}$$

we introduce the complex boson field z, z^*, with the constraint $z^*_{j\alpha} z_{j\alpha} = f$. Comparing Eq. (5.61) and Eq. (5.61) it is clear that this new field corresponds to the spinon field b, b^* after the ferromagnetic degrees of freedom have been integrated out; for this reason from now on when speaking of spinons we will always refer to the new fields z_α, z^*_α. Averaging the field V one can obtain through a Sine-Gordon transformation [200, 204] the effective spinon mass

$$m_s^2 = \langle \bar{V}_z^2 \rangle \sim \frac{1}{2}|\delta \ln \delta| \tag{5.65}$$

which, finally, enters the effective action for spinons:

$$S_s = \frac{1}{g} \int_{\mathbb{R}^2 \times [0,\beta]} \mathrm{d}^3x \left[v_s^{-2} \left| (\partial_0 - z^*_\beta \partial_0 z_\beta) z_\alpha \right|^2 + \left| (\partial_\mu - z^*_\beta \partial_\mu z_\beta) z_\alpha \right|^2 + m_s^2 z^*_\alpha z_\alpha \right] , \tag{5.66}$$

which is essentially a non-linear σ model with doping-dependent mass m_s. As in the holon case the emergent U(1) gauge field $A_\mu \sim z_\alpha \partial_\mu z_\alpha$ is minimally coupled as a consequence of the h/s gauge symmetry.

The effective actions in Eq. (5.60) and Eq. (5.66) describe the dynamics of holons and spinons; in the next Subsections we shall analyze the pairing processes for holon, spinons and finally the superconductive transition.

5.2.5 Holon pairing

The pairing between holons is indirect, being mediated by the spin-vortices surrounding each holon site. To understand the mechanism one may start from the J term as in Eq. (5.56) in the continuum limit, expanding the RVB factors to the second order and introducing the z_α, z^*_α field as before, obtaining

$$\tilde{J} \int \mathrm{d}^2x (\bar{V}_z(x))^2 z^*_\alpha(x) z_\alpha(x) \tag{5.67}$$

with $\tilde{J} = (1 - 2\delta)J$. Averaging over the spinons and introducing the effective interaction $J_{\text{eff}} \equiv \tilde{J}\langle z^* z \rangle$ and plugging in the expression for $\bar{V}$ in Eq. (5.48) we get

$$J_{\text{eff}} \sum_{i,j} (-1)^{|i|+|j|} \Delta^{-1}(i-j) h^*_i h_i h^*_j h_j \tag{5.68}$$

Δ being the 2D lattice Laplacian. It is important noting that the sum is *not* constrained over nearest neighbors, so that the term above describes a long-range interaction between holons, which turns out to be attractive if they are on different Nèel sublattices, repulsive otherwise.

As the interaction is mediated by the field V, one may visualize the mechanism by considering spin vortices, described by the V field, centered on each holon site, with chirality depending upon the Nèel sublattice they are in. Eq. (5.68) shows that these spin vortices attract each other if they are on different sublattices, otherwise they repel each other. The effective coupling J_{eff} is obtained through a statistical average over the spinons:

$$J_{\text{eff}} = \tilde{J}\langle z^* z\rangle = \tilde{J}\int d^2q (q^2+m_s^2)^{-1/2} = J(1-2\delta)(\sqrt{\Lambda^2+m_s^2}-m_s) \quad (5.69)$$

$\Lambda \sim 1$ being an ultra-violet cutoff. Instead of exactly treating the interaction provided by the term in Eq. (5.68) one may give a simplified, effective description by introducing a Coulomb potential with a screening length ℓ_s equal to the average holon distance $\ell_s \sim 1/\sqrt{\delta}$

$$V_{\text{eff}}(\mathbf{p}) \approx \frac{J_{\text{eff}}}{p^2+\ell_s^{-2}}\ , \quad (5.70)$$

considering only the attractive part. Within this approximation the pairing temperature for holon T_{ph} can be estimated as

$$T_{ph} \approx \frac{J_{\text{eff}}}{2\pi} \quad (5.71)$$

under which a finite density of incoherent holon pairs appears, i.e. $\langle |h_i^* h_j^*|\rangle \neq 0$, due to a Kosterlitz-Thouless-like transition.

Again the lattice periodicity complicates the holon treatment, which is to be split in different regions of the Brillouin zone, and the coupling between different regions is subleading and can be neglected [205]. The correct treatment of holon pairing allows one to recover the correct d-wave symmetry of the order parameter as observed experimentally and to correctly reproduce the Fermi arcs as observed in ARPES data [5, 183, 184].

For brevity's sake here we just report the gap equation, which can be obtained through the standard BCS treatment of the theory

$$\Delta^h_{\alpha,\mathbf{k}} = \sum_{\mathbf{q}} V_{\text{eff}}(\mathbf{k}-\mathbf{q})\,\frac{\Delta^h_{\alpha,\mathbf{q}}}{2\epsilon_{\alpha,\mathbf{q}}}\tanh\left(\frac{\epsilon_{\alpha,\mathbf{q}}}{2T}\right) \quad (5.72)$$

where $\alpha = R, L$ is a "flavor" index, corresponding to the two branches of the Fermi surface where R (L) stands, respectively for the right (left) region of the magnetic Brillouin zone, i.e. for the right region $-\pi \leq k_x \leq \pi$, $0 \leq k_y \leq \pi$;

for more details see for instance Ref. [206]. In first approximation the R and L "flavors" are considered as fully decoupled. The dispersion relation is

$$\epsilon_{\alpha,\mathbf{k}} = \sqrt{(v_F k \pm \mu)^2 + |\Delta^h_{\alpha,\mathbf{k}}|^2} \tag{5.73}$$

μ being the chemical potential for holons, $v_F = 2t$ being the Fermi energy for holons. The solution of the gap equation shows a pronounced peak at $k = k_F$, defining $\Delta^h_0 = \left|\Delta^h(k = k_F)\right|$ it can be approximated within very good agreement by the following fit:

$$\Delta^h_0 = \ell Z(\delta)\sqrt{\delta}\exp\left(-\frac{5J}{4\tilde{\ell}Z(\delta)}\right) \tag{5.74}$$

with $v_\Delta = \sqrt{2}\Delta^h_0/k_F$, ℓ being the holon screening length and

$$Z(\delta) = v_s\langle z^* z\rangle = v_s\sqrt{\Lambda^2 + m_s^2} - m_s\ . \tag{5.75}$$

The phase of the holon order parameter ϕ_h has been neglected due to the BCS treatment. It can be reintroduced in approximation for the full holon Hamiltonian, valid at low energies in the vicinity of the four nodal points. The h/s symmetry is restored by Peierls substitution, leading to the following nodal Hamiltonian for the R holons

$$\mathcal{H}^h = \begin{pmatrix} v_F\left(-\mathrm{i}\partial_+ - A_+\right) + A_0 & -v_\Delta e^{\mathrm{i}\phi^h}\partial_- \\ v_\Delta e^{-\mathrm{i}\phi^h}\partial_- & v_F\left(\mathrm{i}\partial_+ - A_+\right) - A_0 \end{pmatrix} \tag{5.76}$$

5.2.6 Spinon pairing

In order to understand the origin of the attractive interaction for spinons we consider the four-fermion interaction in the J term in Eq. (5.56):

$$\frac{J}{2}\sum_{\langle ij\rangle} h_i^* h_i h_j^* h_j \left|RVB_{ij}\right|^2\ . \tag{5.77}$$

This term can be neglected in the normal state, where $\langle h_i^* h_i h_j^* h_j\rangle \approx \delta^2$; moreover being $J > 0$ in our approach it provides a *repulsive* spinon-spinon interaction. In the present Subsection we show that, as opposed to the normal state, for a sufficiently high density of incoherent holons the energy of the system is actually lowered when two holon pair in an RVB state, due to the increasing h/s gauge attraction between holons and spinons, forcing the hole to recombine. This mechanism provides an indirect attractive force for the spinon-spinon pairing. We apply the usual Hubbard-Stratonovich [189, 190] transformation to the term in Eq. (5.77), obtaining

$$-\sum_{\langle ij\rangle}\frac{2|\Delta^s_{ij}|^2}{J\tau^2} + \Delta^{s*}_{ij}\epsilon^{\alpha\beta}z_{i\alpha}z_{j\beta} + h.c. \tag{5.78}$$

and the holons have been treated in mean-field approximation, defining $\tau = |\langle h_i h_j \rangle|$. On the other hand the spinon order parameter is defined as:

$$\Delta^s_{ij} = \frac{J\tau^2}{2} \langle \epsilon^{\alpha\beta} z_{i\alpha} z_{j\beta} \rangle \ . \tag{5.79}$$

Including the pairing term the full action for spinons can be written as $S_s = \int d^3x \mathscr{L}$ and the (Euclidean) Lagrangian density now reads[9]:

$$\mathscr{L}_s = \sum_{\mu=0,1,2} z^*_\alpha \left[(\partial_\mu - \mathrm{i}A_\mu) + m_s^2 \right] z_\alpha + \Delta^{s*}_i(\mathbf{x}) \epsilon^{\alpha\beta} z_\alpha \partial_i z_\beta + h.c. \tag{5.80}$$

The order parameter has been rewritten as $\Delta^{s*}_i(\mathbf{x})$ where the index i denotes the spatial direction; moreover it can be rewritten in an approximate way separating the phase and amplitude parts as

$$\Delta^s_i(\mathbf{x}) \simeq \Delta^s_{i,0} e^{\mathrm{i}\phi^s(\mathbf{x})} \tag{5.81}$$

where the spinon phase ϕ_s depends on the spatial position only and the amplitude $\Delta^s_{i,0}$ depends on the spatial direction only. We stress that the self-emergent gauge field $A_\mu \sim z_\beta \partial_\mu z_\beta$ as a result of the h/s symmetry has been introduced in Eq. (5.80). In fact the h/s gauge symmetry is still present, the action being invariant under the following set of transformations:

$$\begin{cases} z_\alpha \longrightarrow z_\alpha e^{\mathrm{i}\Lambda} \\ A_\mu \longrightarrow A_\mu + \partial_\mu \Lambda \quad \Lambda(\mathbf{x}) \in [0, 2\pi[\\ \phi^s \longrightarrow \phi^s + 2\Lambda \end{cases} \tag{5.82}$$

provided that also the holon sector is transformed as follows

$$\begin{cases} h \longrightarrow h e^{\mathrm{i}\Lambda} \\ \phi^h \longrightarrow \phi^h + 2\Lambda \end{cases} \quad \Lambda(\mathbf{x}) \in [0, 2\pi[\tag{5.83}$$

Wanting to work with fields neutral under the h/s gauge transformations, we redefine the spinon field as

$$\tilde{z}_1 \equiv z_1 e^{\mathrm{i}\phi^s} \qquad \tilde{z}_2 \equiv z^*_2 e^{-\mathrm{i}\phi^s} \ . \tag{5.84}$$

We can also introduce a gauge-neutral version of the h/s gauge field and, to complete our description in terms of h/s gauge invariant quantities, we introduce the electron phase ϕ:

$$a_\mu = A_\mu - \frac{1}{2}\partial_\mu \phi^h \qquad \phi = \phi^h - \phi^s \tag{5.85}$$

[9]Temporarily setting $g = 1$ and $v_s = 1$.

The effective action can be rewritten in terms of the new gauge-invariant quantities just introduced and has the following (Euclidean) Lagrangian density:

$$\mathscr{L}_s = Z^\dagger(\mathbf{x})\,\Gamma_s(\mathbf{x})\,Z(\mathbf{x}) \tag{5.86}$$

having defined the doublet $Z = (\tilde{z}_1, \tilde{z}_2)^T$ and the 2×2 kernel[10]:

$$\Gamma_s = \sum_{\mu=0,1,2} \left[\partial_\mu - \mathrm{i}\left(a_\mu - {}^1\!/_2\partial_\mu\phi\right)\sigma_z - \mathrm{i}\,\mathrm{Im}\left(\Delta^s_{\mu,0}\right)\sigma_x - \mathrm{i}\,\mathrm{Re}\left(\Delta^s_{\mu,0}\right)\sigma_y\right]^2 + m_s^2 - \left|\Delta^s_{\mu,0}\right|^2 \tag{5.87}$$

Our goal is to understand the physics leading to spinon pairing and to a finite density of incoherent spinon RVB pairs; in order to do so it convenient to rewrite the kernel Γ_s introducing a fictitious SU(2) gauge field Y_μ

$$\Gamma_s = \sum_{\mu=0,1,2} \left(\partial_\mu - \mathrm{i}Y_\mu\right)^2 + M^2 \tag{5.88}$$

with $M \equiv \sqrt{m_s^2 - 2\left|\Delta^s_0\right|^2}$, $Y_\mu = \sum_{a=x,y,z} Y^a_\mu \sigma_a/2$ and

$$Y^a_\mu = \begin{pmatrix} 0 & 0 & a_0 + \partial_0\phi \\ \mathrm{Im}\left(\Delta^s_{1,0}\right) & \mathrm{Re}\left(\Delta^s_{1,0}\right) & a_1 + \frac{1}{2}\partial_1\phi \\ \mathrm{Im}\left(\Delta^s_{2,0}\right) & \mathrm{Re}\left(\Delta^s_{2,0}\right) & a_2 + \frac{1}{2}\partial_2\phi \end{pmatrix} \tag{5.89}$$

Integrating out the spinons one gets the following effective action

$$S^s_{eff}\left[a_\mu, \Delta^s_0, \partial_\mu\phi\right] = \ln\det\left(\Gamma_s\right) - \frac{2\left|\Delta^s_0\right|^2}{J\tau^2} \tag{5.90}$$

which can be treated in an approximate way, in particular we Taylor-expand S_{eff} in powers of the gauge field, while treating Δ_s exactly:

$$S^s_{eff} \approx S^{s,0}_{eff}\left[0, 0, \Delta_s\right] + S^{s,2}_{eff}\left[\partial_\mu\phi, a_\mu, \Delta_s\right] + ... \tag{5.91}$$

Using an established approach [44, 207] we first determine the saddle point value for the modulus of order parameter, subsequently considering the role of the phase fluctuations. Neglecting the phase and the gauge field is tantamount to considering only the first term in the expansion in Eq. (5.91), it reads:

$$S^{s,0}_{\mathrm{eff}} = -\frac{2\left|\Delta^s_0\right|^2}{J\tau^2} + \sum_{\omega,\mathbf{k}} \ln\left[\left(\omega^2 + E^2_-(\mathbf{k})\right)\left(\omega^2 + E^2_+(\mathbf{k})\right)\right] \tag{5.92}$$

and describes the physics of a gas of spinons with the following peculiar dispersion relation

$$E_\pm(\mathbf{k}) = \sqrt{\mathbf{k}^2 + m_s^2 \pm 2\left|\Delta^s_0\right|\left|\mathbf{k}\right|}\,. \tag{5.93}$$

[10] The 0 component of the order parameter is $\Delta^s_{0,0} = 0$.

On the other hand the second term in the expansion, i.e. the phase-gauge part is essentially a three-dimensional anisotropic gauged XY (Stueckelberg) model, $S^{s,2}_{\text{eff}} = \int \mathrm{d}^3x \mathscr{L}^{s,2}_{\text{eff}}$ with

$$\mathscr{L}^{s,2}_{\text{eff}} = \frac{1}{6\pi M}\{[\partial_\mu a_\nu - \partial_\nu a_\mu]^2 + |\Delta^s_0|^2[2(a_0 + \partial_0\frac{\phi}{2})^2 + (\mathbf{a} + \nabla\frac{\phi}{2})^2]\} \quad (5.94)$$

Now a complete treatment for the gap equation would require finding the saddle point value for the complete action $S^s_{\text{eff}}[a, \Delta^s_0] = S^{s,0}_{\text{eff}}[\Delta^s_0] + S^{s,2}_{\text{eff}}[a, \Delta^s_0] + S^h_{\text{eff}}[a]$, the last term coming from the holon nodal description in Eq. (5.76). However, it turns out that the holon contribution to spinon pairing is subleading [5]. The partition function $\mathcal{Z}_g = \int \mathcal{D}a_\mu \ \exp\left(-S^{s,2}_{\text{eff}}\right)$ for the anisotropic gauged 3D XY model can be integrated, after finally fixing the h/s symmetry, to give:

$$\mathcal{Z}_g = \prod_{\omega,\mathbf{k}} \frac{(3\pi M)^{3/2}}{(\omega^2 + \frac{1}{2}|\Delta^s_0| + \frac{1}{2}|\mathbf{k}|^2)^{1/2}(\omega^2 + \frac{1}{2}|\Delta^s_0| + |\mathbf{k}|^2)^{1/2}} \quad (5.95)$$

The contribution from the partition function $\mathcal{Z}_g$ is accounted for only in an approximate way into the gap equation; in fact it turns out that the factor appearing at the denominator, corresponding to the vector bosons degrees of freedom, give subleading contributions. The $(3\pi M)^{3/2}$, on the other hand, enters the gap equation in a fundamentally important way, and is actually needed in order to achieve pairing, confirming the necessity of the gauge part of the theory contained in $S^{s,2}_{\text{eff}}$ in order to obtain spinon pairing. Motivated by this scenario we write the free energy as the sum of the free energy F from the $S^{s,0}_{\text{eff}}$ plus the contribution from the M term:

$$\frac{1}{V}F[\Delta^s_0] \approx \frac{1}{\beta V}\sum_{\omega,\mathbf{k},\sigma=\pm} \ln\left(\omega^2 + E^2_\sigma(\mathbf{k})\right) - \frac{3\Lambda^3}{4}\left[\ln m_s^2 - \frac{2|\Delta^s_0|^2}{m_s^2}\right] - \Lambda^2\frac{|\Delta^s_0|^2}{J\tau^2} \quad (5.96)$$

Λ being an ultraviolet cutoff. Deriving with respect to Δ^s_0 one gets the gap equation

$$0 = \frac{2\Lambda}{3m_s^2} - \frac{\Lambda^2}{J\tau^2} - \frac{1}{2|\Delta^s_0|V}\sum_{\mathbf{k}}\left[\frac{|\mathbf{k}|}{E_-(\mathbf{k})\tanh\left(\frac{E_-(\mathbf{k})}{2T}\right)} - \frac{|\mathbf{k}|}{E_+(\mathbf{k})\tanh\left(\frac{E_+(\mathbf{k})}{2T}\right)}\right]. \quad (5.97)$$

A numerical analysis of Eq. (5.97) shows that there is no solution for $\tau = 0$, i.e. when a finite density of incoherent holon is not present. Similarly, if we do not account for the gauge interaction, i.e. without the first term coming from the M gauge term, the gap equation does not have a solution for finite values of $|\Delta^s_0|$, in agreement with the fact that the interaction in the present

treatment is essentially repulsive and the actual pairing glue is provided by the gauge interaction overcoming the original repulsion.

In particular Eq. (5.97) determines a temperature $T_{ps} \lesssim T_{ph}$ below which a finite density of spinon RVB pairs, and hence a finite density of hole pairs, is to be found. It has been noted that such a state should support a Nernst signal and it has been shown, in fact, that T_{ps} calculated within the present formalism as a function the doping shows good agreement with experimental data [5] for the onset of the Nernst signal [208].

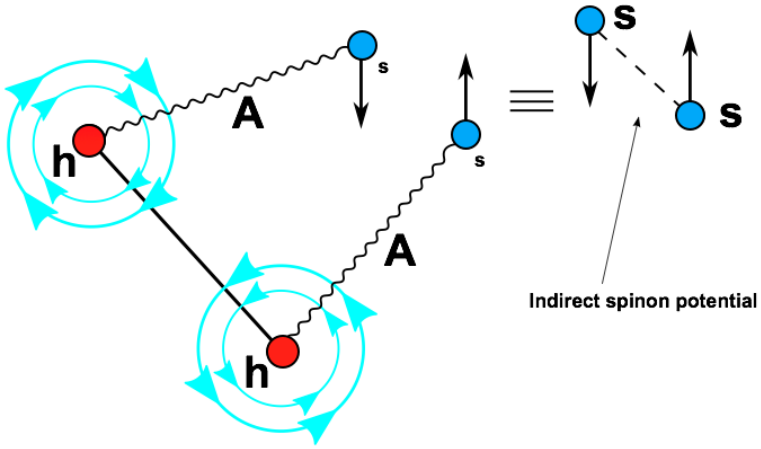

Figure 5.4: Indirect spinon pairing potential: holons on different Nèel sublattices experience an attractive force due to the attractive interaction (solid line) of opposite chirality spin vortices; subsequently the h/s gauge interaction (wavy line) binds spinons and holons together. This is the mechanism for superconductivity in the present approach; as far as spinons are concerned it can be seen as an effective indirect (holon-mediated) spinon-spinon potential.

5.2.7 Superconductivity and phase diagram

Let us "recombine the electron", introducing the order parameter for the electron

$$\Delta^c_{ij} = \langle \epsilon^{\alpha\beta} c_{i\alpha} c_{j\beta} \rangle = \langle \epsilon^{\alpha\beta} z_{i\alpha} z_{j\beta} \rangle \langle h^*_i h^*_j \rangle \tag{5.98}$$

In terms of the holon and spinon order parameters[11] it reads [5]:

$$\Delta_c \sim \frac{\Delta^s}{\Delta^h} = \frac{\Delta^s_0}{\Delta^h_0} e^{i(\phi^h - \phi^s)} \, . \tag{5.99}$$

From Eq. (5.99) one readily concludes that even when a finite density of holons and spinons and hence of hole pairs is present, the superconductivity may still be destroyed by a highly fluctuating phase, i.e. $\langle e^{\mathrm{i}\phi} \rangle = 0$, if

[11] Here $\Delta_s = \Delta^s_0 e^{\mathrm{i}\phi_s}$ and $\Delta_s = \Delta^h_0 e^{\mathrm{i}\phi_h}$.

the gauged XY model in equation (5.94) is in the high-temperature vortex proliferation phase. On the other hand when the gauged XY model enters the low-temperature phase the phase stabilizes and finally $\Delta_c \neq 0$. However the "temperature" governing the transition is not the physical temperature T; the effective temperature, as can be read e.g. from Eq. (5.94), is given by the coupling constant of the gauged XY model, approximately inversely proportional to the modulus of the spinon order parameter $|\Delta_0^s|$.

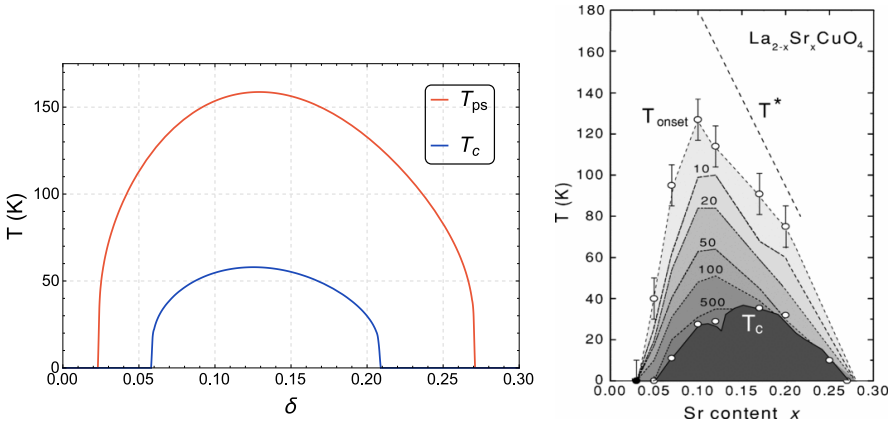

Figure 5.5: Left panel: theoretical prediction for the phase diagram: T_{ps} (red line) corresponds to the onset of the Nernst signal, while the blue line marks the superconductive transition. Right panel: critical temperature and onset of the Nernst signal as experimentally measured in $La_{2-x}Sr_xCu_2O_4$, taken from Ref. [208].

A more detailed analysis of the dynamics of the gauged XY model will be given in the next Section when discussing the superfluid density; here we briefly comment on the mechanism: $|\Delta_0^s|$ will acquire a non-zero value at T_{ps}, corresponding to an infinite effective temperature for the gauge XY model. Decreasing the temperature the spinon order parameter $|\Delta_0^s|$ grows and the effective temperature lowers; critically the effective temperature is a monotonically increasing function of the physical temperature. Finally one reaches the low-temperature phase for the XY model, marking the superconducting transition and the critical temperature T_c. The critical temperature is plotted in Fig. 5.5 as a function of the doping, shown good agreement with experimental data.

In conclusion we note that the pictorial representation of holon pairing, as a process mediated by the attraction of spin vortices on different Nèel sublattices can be extended to describe the full superconducting transition. A finite density of incoherent spinon pair appears provided that τ is sufficiently big, i.e. the spinon attractive potential is mediated by the holons. Moreover coherence is achieved through the action of the h/s gauge field A_μ, which is introduced when splitting the holon into the product of a holon and a spinon

and, finally, plays a key role in reconstructing the hole. Denoting the gauge field by a wavy line the pairing mechanism can be depicted as in Fig. 5.4.

5.3 A gauge approach to superfluid density

The superfluid density can be defined, following for instance Ref. [209], as the coefficient governing the Gaussian fluctuations of the phase Φ in an effective action for superconductivity[12]:

$$S_{\text{eff}} = \frac{\rho_s}{2} \int \mathrm{d}V \, (\nabla\Phi)^2 + (\text{other terms}) \ , \tag{5.100}$$

which by gauge invariance is equivalent to

$$S_{\text{eff}} = \int \mathrm{d}V \left[\frac{\rho_s}{2} \mathbf{A}^2_{\text{em}} (\tau, \mathbf{r}) + (\text{other terms}) \right] \ . \tag{5.101}$$

i.e. the mass of the electromagnetic field[13] A^{em}_μ below T_c due to the Anderson-Higgs mechanism, and as a consequence of that it also is related to the London penetration depth λ of a magnetic field in a superconductor [36]:

$$\lambda = \sqrt{\frac{m}{\mu_0 \rho_s e^2}} \ , \tag{5.102}$$

e and m being the charge and the mass, respectively, of each charge carrier, μ_0 being the vacuum permeability. Experimental measurements of superfluid density are generally obtained indirectly through the measurement of the London penetration depth; Refs. [210, 211] provide an extensive review of experimental techniques and of ways of measuring superfluid density.

The London penetration depth is the distance the perpendicular component of an external magnetic field can travel inside a superconductor before being reduced by a factor $1/e$ as a result of the Meissner effect, in formulas:

$$B_\perp(x) = B_0 \exp\left(-\frac{x}{\lambda}\right) \ , \tag{5.103}$$

B_0 being the modulus of the magnetic field at the edge of the superconductor, x being a coordinate normal to the surface. Usually the penetration depth is microscopical, e.g. hundreds of nanometer in the case of cuprates, so that commonly the Meissner effect is described as a bulk superconductor effectively expelling a magnetic field.

[12] Some ambiguity in literature arises by calling superfluid density both the superfluid (mass) density defined above and the superfluid (number) density $n_s = 2m\rho_s$; here we will always refer to the former quantity, unless otherwise specified.

[13] The "em" superscript is needed to distinguish the electromagnetic field from the A_μ, generated by the h/s symmetry.

Coming to cuprates, the superfluid density is easily experimentally accessible and has been the object of a great number of experimental investigations; the superfluid density profile is characterized by a dichotomy appearing in many other experimental features of cuprates. The linear T-dependence at low temperatures is consistent with BCS-like dynamics for the holes and with the well-defined gapped Fermi-arcs observed through ARPES spectroscopy [212], while, on the other hand, the non-mean-field critical exponent for the superfluid density $^2/_3$ is at odds with a BCS-like description, and would suggest that cuprates should lie in the $3DXY$ universality class [213–215]. Fig. 5.6 sketches the different behaviors of the superfluid density in cuprates (solid line) as compared to the usual BCS-like superfluid density (dashed line). Finally the Uemura [216] relation, i.e. that empirical observation that

$$\rho_s(T=0) \propto T_c \tag{5.104}$$

for moderate underdopings is, again, in contrast with a BCS-like description of the dynamics of cuprates.

The gauge approach to cuprates used in the present work provides a natural solution to this puzzle [7]: as shown previously the hole is decomposed into a charge-only fermionic excitation (holon) and a spin-only bosonic excitation (spinon). We are going to show that they give separate contributions (ρ_s^h and ρ_s^s) to the superfluid density, and that these contributions sum according to a Ioffe-Larkin-like composition rule: in the vicinity of the critical temperature the spinon contribution dominates, giving the correct critical exponent, while at low temperature the holon contribution is fundamental in reproducing the correct slope. An interplay of the holonic d-wave BCS contribution and the spinonic 3DXY contribution naturally accounts for all the experimentally-observed features in the whole range of temperatures $0 < T < T_c$ and reproduces the superfluid density profile in the underdoping regime within very good accuracy [7]. We stress that the 3D nature of the XY model is *not* a consequence of inter-layer coupling. Finally we derive analytically an approximate Uemura relation.

5.3.1 Composition rule for superfluid density

We recall the definition of superfluid density in Eq. (5.100), i.e. the coefficient governing the Gaussian phase fluctuations in an effective action for superconductivity; the relevant Lagrangian in this case can be read from Eq. (5.94), to which we must also couple to electromagnetic field A_μ^{em}. The h/s gauge invariance allows one to do so in many equivalent ways, in fact it can be shown that any choice of ϵ in the following coupling to the electromagnetic field

$$S_s(A + \epsilon A_{em}) + S_h(A - (1-\epsilon)A_{em}) \tag{5.105}$$

is indeed equivalent [217] to any other choice of ϵ by h/s invariance. In the present work we choose to couple the electromagnetic field to the holons, i.e.

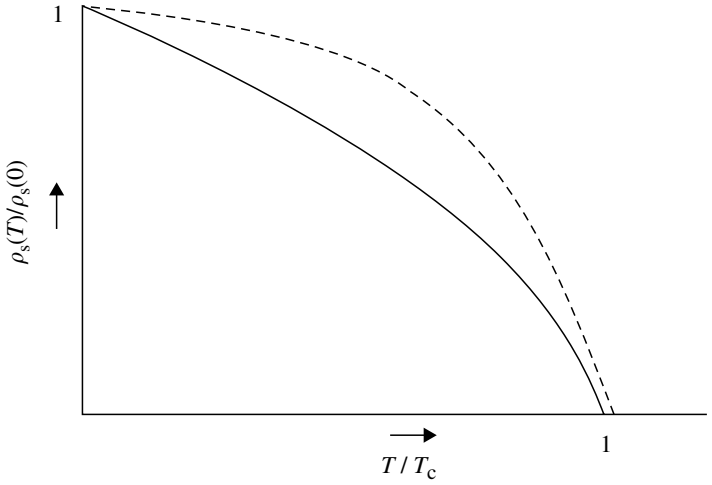

Figure 5.6: A sketch of the superfluid density in a BCS superconductor (dashed line) and in cuprates (solid line). The zero-temperature value of the superfluid density is normalized to 1, as well as the critical temperature. The different low-temperature behavior and the different critical exponent are evident. From [13].

$\epsilon = 0$; starting from the Lagrangian in Eq. (5.94) and using the Eqs. (5.85) we get

$$\mathscr{L}^{\rm em} = \frac{1}{6\pi M}\Big\{ f_{\mu\nu}^2 + |\Delta_0^s|^2\, \eta^{\mu\nu}(A_\mu - \partial_\mu \frac{\phi^s}{2})(A_\nu - \partial_\nu \frac{\phi^s}{2})\Big\} + \\ + (a_\mu - A_\mu^{\rm em})\Pi_h^{\mu\nu}(a_\nu - A_\nu^{\rm em}) \quad (5.106)$$

having straightforwardly introduced the field strength $f_{\mu\nu} = \partial_{[\mu} a_{\nu]}$ and the pseudo-metric $\eta^{\mu\nu} = \mathrm{diag}(2, 2, 1)$. The last term in the r.h.s. in Eq. (5.106) accounts for the holonic contribution to the phase-gauge Langragian, $\Pi_h^{\mu\nu}$ being the vacuum polarization of the holons in the low energy limit. We neglected this term when deriving the spinon gap equation; it will turn out to be quite important as far as the superfluid density is concerned.

When writing down the partition function as

$$\mathcal{Z} \sim \int \mathcal{D}A_\mu \mathcal{D}\phi_s \mathcal{D}\phi_h e^{-\int \mathrm{d}^3 x \mathscr{L}^{\rm em}[A_\mu, \phi_s, \phi_s]} \quad (5.107)$$

it must be noted that the integration using the measure $\mathcal{D}A_\mu \mathcal{D}\phi_s \mathcal{D}\phi_h$ wrongly integrates over configurations belonging to the same gauge orbit, so that a gauge fixing is needed [5]. In this case it is particularly convenient to introduce a new variable $\phi_> = \frac{\phi^h + \phi^s}{2}$, performing a change of variables in

the definition of the partition function[14]:

$$\mathcal{Z} \sim \int \mathcal{D}a_\mu \mathcal{D}\phi \mathcal{D}\phi_> e^{-\int \mathrm{d}^3 x \mathscr{L}^{\mathrm{em}}[a_\mu, \phi]} \tag{5.108}$$

which is now expressed in terms of $\phi_>$ and the physical electron phase $\phi = \frac{\phi^h - \phi^s}{2}$. The gauge is then fully fixed by choosing the function $F = \phi_> - \omega(x)$ as the gauge condition, using the usual Faddeev-Popov procedure [218]; as the Lagrangian, critically, does not depend on $\phi_>$ when expressed in terms of the new integration variables, it maintains the same form after the gauge fixing, and the integration over $\mathcal{D}\phi_>$ factors out along with the divergency.

It is then straightforward to integrate out the ϕ and a_μ fields, in this order, obtaining an effective Lagrangian for superconductivity up to subleading $\mathcal{O}\big(|\Delta_s^0|^4\big)$ terms:

$$\mathscr{L}_{\mathrm{em,eff}} = \frac{1}{4} A_\mu^{\mathrm{em}} \left[\frac{K^{\mu\alpha} \Pi_h^{\beta\nu}}{K^{\alpha\beta} + \Pi_h^{\alpha\beta}} \right] A_\nu^{\mathrm{em}} \,, \tag{5.109}$$

and $K_{\mu\nu} = (3\pi M)^{-1}(\partial^\mu \partial^\nu - \partial^2 g^{\mu\nu} + m^{\mu\nu})$ appears as $A_\mu K^{\mu\nu} A_\nu$ in the spinon part of the effective Lagrangian and can be obtained from Eq. (5.106) integrating by parts.

By noting that $K^{\mu\nu}$ ($\Pi_h^{\mu\nu}$) is a gauge invariant quantity on its own, and that it corresponds to the total superfluid density of the system when the holonic (spinonic) sector is neglected, the static limit of $K^{\mu\nu}$ and $\Pi_h^{\mu\nu}$ can be readily identified as the spinonic and holonic, respectively, contributions to the total superfluid density. They sum in the following peculiar way[15]:

$$\rho_s = \frac{\rho_s^s \rho_s^h}{\rho_s^s + \rho_s^h} \tag{5.110}$$

where obviously ρ_s^h denotes the superfluid density from the holon subsector and ρ_s^s the superfluid density from the spinon subsector. The most evident consequence of the equation above is that the zero of the superfluid density is determined by the smallest among ρ_s^s and ρ_s^h. It is also remarkable that the formula in Eq. (5.110) has the same structure of the Ioffe-Larkin composition rule [219] meaning that in an spin-charge separated approach superfluid densities sum in the same way as conductivities do [173].

5.3.2 Superfluid density from spinons

As clear from the effective action in Eq. (5.94) the dynamics of the spinon phase are described by a gauged anisotropic 3D XY model. We preliminarily

[14] We omit the Jacobian factor which is an overall multiplicative constant in the partition function.

[15] We also used the isotropy in the (true) spatial directions so that the coefficient to $A_i^{\mathrm{em}} A_{\mathrm{em}}^i$ is be the same for $i = 1, 2$.

note, see for instance [220], that for a bosonic system the superfluid density can be defined in terms of the phase stiffness $\mathcal{Y}$, i.e. the leading order free energy increase when the phase of the system is infinitesimally twisted:

$$F\left(\phi \to \phi + Q_\mu x^\mu\right) \approx F(\phi) + \frac{1}{2}\mathcal{Y}\left|Q\right|^2 + \mathcal{O}\left(|Q|^4\right) \tag{5.111}$$

and the superfluid density is related to the phase stiffness [220] by:

$$\rho_s = \frac{1}{b}\frac{m^2}{\hbar^2}\mathcal{Y} \tag{5.112}$$

b being the layer spacing along the c axis. Preliminarly we need to show that the gauge field in Eq. (5.94) does not yield relevant contributions to the free energy and, consequently, to the superfluid density, which will then be the one of a an anisotropic three-dimensional XY model. In order to do so it is convenient to choose a different gauge fixing, decoupling the gauge and phase parts of the Lagrangian; after performing the usual Faddeev-Popov procedure, using as gauge-fixing function:

$$F = \frac{1}{\xi}m^{\mu\nu}\left(\partial_\mu A_\nu\right)\phi^s - \frac{\xi}{2}\phi^s - \omega\left(x\right) \tag{5.113}$$

where ξ is a real parameter, the partition function reads:

$$\mathcal{Z} = \int \mathcal{D}A_\mu \mathcal{D}\phi^s e^{-S[A_\mu]} e^{-S[\phi^s]} \tag{5.114}$$

with

$$S[A_\mu] = \int \mathrm{d}^3x A_\mu \frac{-\partial^2 g^{\mu\nu} + \partial^\mu\partial^\nu + m^{\mu\nu} - \frac{1}{\xi^2}m^{\mu\mu'}m^{\nu\nu'}\partial_{\mu'}\partial_{\nu'}}{3\pi M} A_\nu \tag{5.115}$$

and

$$S[\phi^s] = \frac{1}{12\pi M}\int \mathrm{d}^3x \phi^s \left(-\frac{\left|\Delta_0^s\right|^2}{2}\eta^{\mu\nu}\partial_\mu\partial_\nu + \frac{\xi^2}{2}\right)\phi^s \ . \tag{5.116}$$

The A_μ and ϕ^s fields are now decoupled, so that the partition function factors as $\mathcal{Z} = \mathcal{Z}_{A_\mu}\mathcal{Z}_{\phi^s}$. Taking the $\xi \to 0$ limit (Landau gauge) the mass term in the phase part disappears, at the expense of introducing an arbitrarily large $\xi^{-2}m^{\mu\mu'}m^{\nu\nu'}\partial_{\mu'}\partial_{\nu'}$ term in the gauge part. It can shown by direct calculation [170] that the contribution to the superfluid density from the gauge part is proportional to $\left|\Delta_0^s\right|^4$ and bounded from above for every value of the gauge parameter ξ; on the other hand the leading term contribution to superfluid density from the phase part is proportional to $\left|\Delta_0^s\right|^2$, its order of magnitude being fixed by the XY coupling constant, allowing us to retain only the phase part $S[\phi^s]$, up to a good approximation[16], also confirmed by numerics [170].

[16]For typical values of $\left|\Delta_s^0\right|^2$ the subleading contribution is at least two orders of magnitude smaller than the leading term.

In other words the superfluid density for the system is essentially determined by a three-dimensional XY model, defined by the following (Euclidean) Lagrangian:

$$\mathscr{L}_{\mathrm{XY}} = \frac{|\Delta_0^s|^2}{6\pi M}\eta^{\mu\nu}\partial_\mu\frac{\phi_s}{2}\partial_\nu\frac{\phi_s}{2} \tag{5.117}$$

It is important noting that the imaginary time component now plays the same role as the two spatial components, and that the effective inverse temperature

$$\Theta^{-1} = \frac{|\Delta_0^s|^2}{3\pi M} \tag{5.118}$$

plays the role of the physical inverse temperature β. The behavior of the model is not altered from a qualitative point of view, because Θ^{-1} is a monotonically decreasing function of the temperature as is β: the low-temperature and high-temperature phases of the 3DXY model are not mixed or switched, however the transition between the two is now determined by $|\Delta_0^s|^2$ as a function of temperature. We can give an estimate for the critical value $|\Delta_0^s|_c^2$ as follows, by writing down the condition for which the system is at the critical point:

$$\Theta\left(T\right) = T_c^{3DXY} \tag{5.119}$$

with $T_c^{3DXY} \approx 2.20$, as given in Ref. [221], the solution being:

$$|\Delta_0^s|_c^2 = m_s^2\left[1 - \frac{m_s}{24\pi T_c^{3DXY}}\right] \tag{5.120}$$

neglecting higher order corrections at least two orders of magnitude smaller than the leading term. It is clear that the properties of the spinon contribution to superfluid density are mediated by the effective temperature: Θ goes to zero as T goes to zero, as a consequence of the structure of the spinon gap equation in Eq. (5.97); also $\Theta\left(T\right)$ is differentiable and non-singular at T_c so that the critical exponent of the three-dimensional XY model is preserved, i.e.:

$$\rho_s^s \sim \left|\frac{T - T_c}{T_c}\right|^{\frac{2}{3}} \tag{5.121}$$

as $T \longrightarrow T_c$. From the theory of the XY model [222] we also know that at low temperatures the following relationship holds:

$$\mathcal{Y} = J - \frac{1}{4\beta} + O\left(\frac{1}{\beta^2 J}\right) \xrightarrow{T\to 0} J \tag{5.122}$$

βJ being the XY coupling constant, so that combining it with Eq. (5.112) we get the following formula for the zero-temperature superfluid density:

$$\rho_s^s(0) \approx \xi\left[\frac{\mathrm{d}\Theta}{\mathrm{d}T}(0)\right]^{-1} \tag{5.123}$$

with a scale renormalization ξ accounting for short-distance effects. The finite-temperature behaviour is then obtained from the theory of the 3DXY model [223], i.e.

$$\rho_s^s(T) = \rho_s^s(0)\rho_{XY}\left(\frac{\Theta(T)}{\Theta(T_c)}\right) , \tag{5.124}$$

where ρ_{XY} is the spin stiffness of an anisotropic 3D XY model, which has been obtained through a Monte Carlo simulation, using the cluster update algorithm proposed in Ref. [224] to speed up the thermalization, particularly near the critical point.

5.3.3 Superfluid density from holons

The holon dynamics below T_c is essentially that of a d-wave condensate of fermions; an expression for the superfluid density can be derived in BCS approximation [225, 226], considering the two Fermi surfaces for holons in the present context it reads

$$\rho_s^h(T) = \frac{2\epsilon_F}{\pi}\left(1 - \frac{\log(2)}{2\Delta_h}T\right) \tag{5.125}$$

ϵ_F being the Fermi energy for holons and Δ_h being the modulus of the order parameter. We note that being $T_{ph} \gg T_c$ the holon contribution can be deemed, in first approximation, as constant in the pseudogap region. However the temperature dependence of the holon order parameter turns out to be very important when T_{ph} gets closer to T_c, i.e. in the strange metal region. The temperature dependence is also needed in order to correctly determine T_{ps}.

5.3.4 Comparison with experimental data

Finally we can sum the spinonic and holonic contributions to superfluid density in Eq. (5.124) and in Eq. (5.125) according to the Ioffe-Larkin-like composition rule in Eq. (5.110), obtaining a result we can compare with experimental data. We preliminary observe that the spinonic contribution to the superfluid density goes to zero at T_c, while the holon contribution is zero at $T_{ph} \gtrsim T_c$; consequently the total superfluid density will go to zero at T_c, as a consequence of the composition rule and, as already mentioned, the critical exponent and the properties near the transition will be that of the spinonic part of the theory, i.e. in the proximity of T_c the total superfluid density will be

$$\rho_s \sim \left|\frac{T - T_c}{T_c}\right|^{\frac{2}{3}} . \tag{5.126}$$

The equation above is in agreement with the experimental observation that the critical transition in cuprates is in the 3D XY universality class [213–

215]. Moreover it turns out that the majority of the temperature profile is dominated by the contribution from spinons, except for the a small region a low temperature, where the holonic contribution is important, for instance, in determining the first derivative in zero.

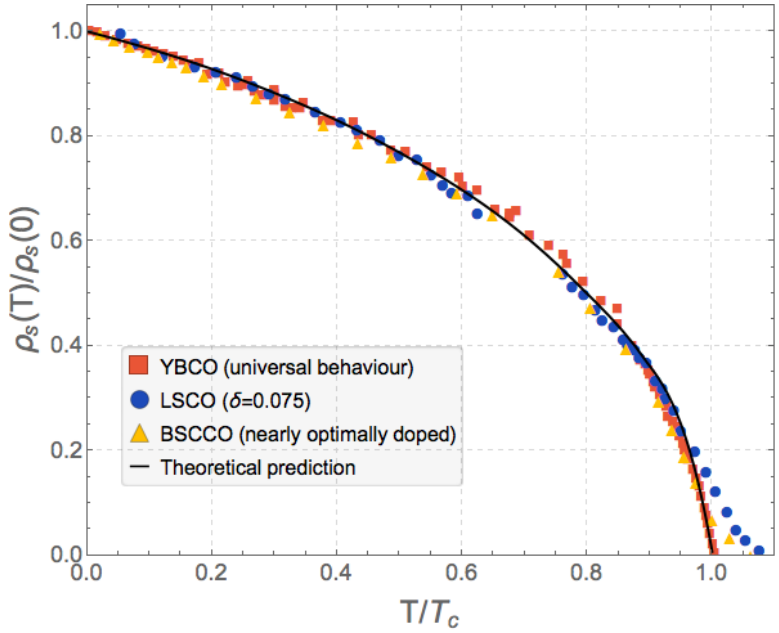

Figure 5.7: Normalized superfluid density, as a function of the normalized temperature, compared with experimental data from Refs. [227–230]

.

In Fig. 5.7 we report our results [7] for the normalized superfluid density

$$\frac{\rho_s(\frac{T}{T_c})}{\rho_s(T=0)} \ . \tag{5.127}$$

Our theoretical prediction is compared with the following experimental measurements:

- YBCO, a-axis (red squares), over a wide range of dopings [211, 227, 228, 231].
- Nearly optimally doped BSSCO (yellow triangles), as reported in Ref. [229].
- Underdoped LSCO ($\delta = 0.075$, blue circles), as reported in Ref. in [230].

showing good agreement in the whole temperature range up to the critical temperature.

We note data Hg-1201 data from Ref. [230], is also fitted reasonably well in the underdoped regime. On the other hand data from b-axis YBCO [228], not shown, is correctly fitted only up to slight underdopings; at optimal doping and beyond we conjecture that the effect of the chains, and the consequent YBCO $a-b$ anisotropy, ruins the agreement.

The authors in Ref. [230] comment that the superfluid density results in the vicinity of the critical point may be affected by doping inhomogeneities fluctuations; in fact LSCO and BSSCO data deviate from the usual critical exponent behavior near the transition; in order to account for this effect we identified an inflection point in the superfluid density profile in experimental data and we fitted the data only up to that point. The procedure allows for a very good agreement between experimental data and theory.

We stress that, besides the δ, T-independent scale renormalization ξ, our theory has no other free parameter, all other quantities being fixed for the pseudogap region by a comparison with the phase diagram, as in [5].

To conclude, it has been observed [228] in YBCO samples that the normalized superfluid density should be nearly-universal as the doping is modified. This feature is reproduced by the present model in a in a wide range of dopings, in Fig. 5.8 we analyzed this experimental feature for $\delta = 0.08$, $\delta = 0.12$ and $\delta = 0.16$.

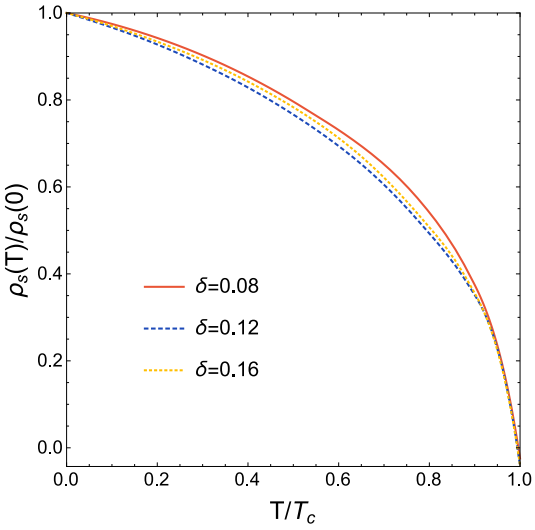

Figure 5.8: Doping near-universality: the normalized superfluid density as a function of the normalized temperature shows near-universal behavior in the underdoped regime.

5.3.5 The Uemura relation

In the present Subsection we demonstrate that the present formalism allows for the derivation of an approximate Uemura relation valid in the underdoped regime. As Δ_s is the solution of the gap equation in Eq. (5.97), its temperature dependence is naturally written in term of T/T_{ps}, furthermore it is convenient writing

$$\Delta_s^2 = m_s^2 F(T/T_{ps}) \tag{5.128}$$

for an opportune function F. Numerics prove that the function F has some important features:

- $F(0) \approx 1$; this is equivalent as requiring $\Delta_s(T=0) \approx m_s$ and is indeed a consequence of the structure of the spinon gap equation.
- The dependence of F upon the doping is very feeble so that it can be considered δ-universal in first approximation.
- $F(1) = 0$, a trivial consequence of the parameterization chosen for the temperature and of the definition of T_{ps}.

All these properties can be verified "visually" in the panel in the lower right in Fig. 5.9, showing F for three different doping choices. The properties in fact hold over a very wide doping range, except for the limit doping values where the superconductive dome meets the x axis and T_c tends to zero.

The effective temperature Θ, as defined in Eq. (5.118), can now be rewritten in terms of F as

$$\Theta(T) = \frac{3\pi}{m_s} \frac{1 - F(T/T_{ps})}{F(T/T_{ps})} \tag{5.129}$$

and consequently one can rewrite the spinon contribution to the superfluid density as in (5.123), which happens to be the dominating contribution, as:

$$\rho_s^s(0) \approx \frac{\xi m_s T_{ps} F(0)^2}{3\pi |F'(0)|}. \tag{5.130}$$

The criticality condition can be found by setting the effective temperature equal to the critical temperature of the three-dimensional XY model $\Theta(T_c) \equiv T_c^{XY} \approx 2.20$ [221]. A linear expansion of F yields:

$$T_c \approx \frac{T_{ps}}{|F'(0)|} \frac{F(0) - 1 + F(0) m_s T_c^{XY}/(3\pi)}{1 + m_s T_c^{XY}/(3\pi)} \tag{5.131}$$

allowing one to easily calculate the critical temperature as a function of the doping, which turns out to be parabolic as observed on phenomenological grounds [13, 177], see also Eq. (5.1), see the main panel of Fig. 5.9.

Using the property $F(0) \approx 1$, using Eq. (5.124) and the Ioffe-Larkin composition rule we obtain:

$$T_c \approx \frac{T_c^{XY}}{\xi}\rho_s(0)\frac{1}{(1-\rho_s(0)/\rho_s^h(0))(1+m_s T_c^{XY}/(3\pi))} \tag{5.132}$$

which is an approximate form of the Uemura relation, once we remind that the terms in the denominator are subleading, because $m_s T_c^{XY}/(3\pi) \ll 1$ and the holon contribution is subleading, meaning that[17] $\rho_s^h(0) \gg \rho_s^s(0)$.

The Uemura relation for the present formalism can also be verified graphically, as in Fig.5.9, main panel. where the dashed line corresponds to our theoretical estimate for T_c, while the solid line corresponds to the zero-temperature superfluid density.

Finally we note that $\Theta(T)$ is approximately proportional to T over the entire temperature range up to the T_c. Assuming, again, a subleading contribution from holons, the superfluid density which is proportional to $\rho_{XY}(\Theta(T)/\Theta(T_c))$ is also approximately proportional to $\rho_{XY}(T/T_c)$. When combined with the Uemura relation in Eq. (5.132), this implies that

$$\rho_s(0) \approx cT_c \,, \tag{5.133}$$

c being a doping-independent constant. For low temperatures one can expand $\rho_s(T)/\rho_s(0)$ at the first order in T/T_c, obtaining

$$\rho_s(T) - \rho_s(0) \approx c\left(\frac{\mathrm{d}\rho_{XY}(0)}{\mathrm{d}(T/T_c)}\right)T \,, \tag{5.134}$$

meaning the the slope of $\rho_s(T)$ is almost doping independent, as can be seen in the upper right panel of Fig. 5.9. This feature has been discussed on experimental grounds in Ref. [232].

[17] The Ioffe-Larkin-like composition rule counterintuitively implies that the leading contribution should be the *smaller* one.

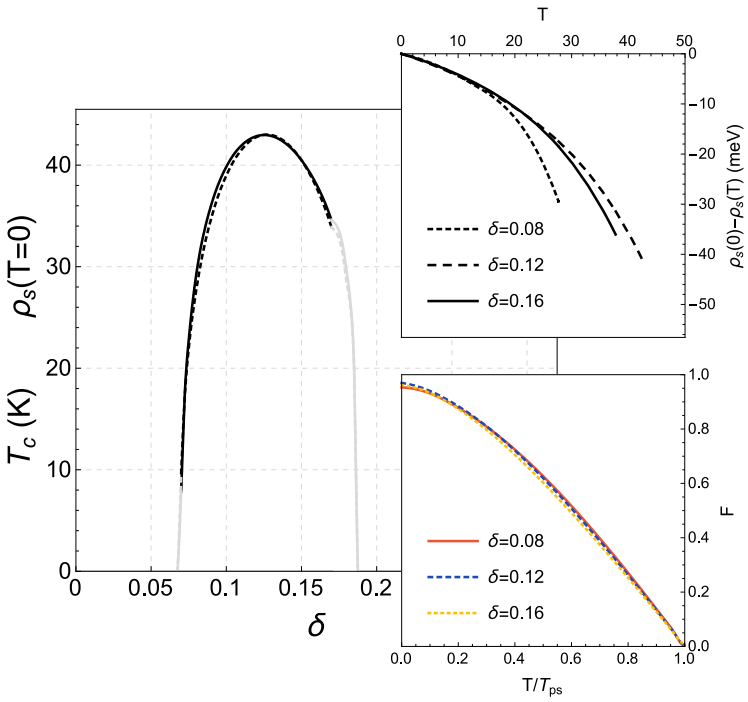

Figure 5.9: Main panel: theoretically calculated $T = 0$ superfluid density (solid line, arbitrary units) and critical temperature (dashed line) vs. δ exhibiting an approximate Uemura relation over the broad doping range considered here. Insets, from top to bottom: approximate δ-universality of the slope of ρ_s near $T = 0$ (upper inset) and of F (lower inset).

5.4 Three universality classes for ρ_s

Fig. 5.7 shows that in the moderate underdoping to optimal doping region the normalized superfluid density profile has a universal behavior; in this Section we extend the analysis beyond the optimal doping to the overdoped region. In order to do so in Fig. 5.10 we report the normalized superfluid density for the following cuprates samples:

1. YBCO, a-axis, over a wide range of dopings [211, 227, 228, 231].
2. Nearly optimally doped BSSCO, as reported in Ref. [229].
3. Underdoped LSCO ($\delta = 0.075$), as reported in Ref. in [230].
4. Bi-2212, $T_c = 93\,\mathrm{K}$, from Ref. [233].
5. Hg1223, optimally doped, $T_c = 134\,\mathrm{K}$, from Ref. [234]
6. $HgBa_2CuO_{4+x}$, $x = 0.154$, from Ref. [230]

7. $HgBa_2CuO_{4+x}$, $x = 0.37$, corresponding to $\delta = 0.22$, from Ref. [230].
8. Overdoped $TlBa_2CuO_{6+\delta}$ from Broun et al., in Ref. [211]
9. Strongly overdoped LSCO, $\delta = 0.24$, from Ref. [230].

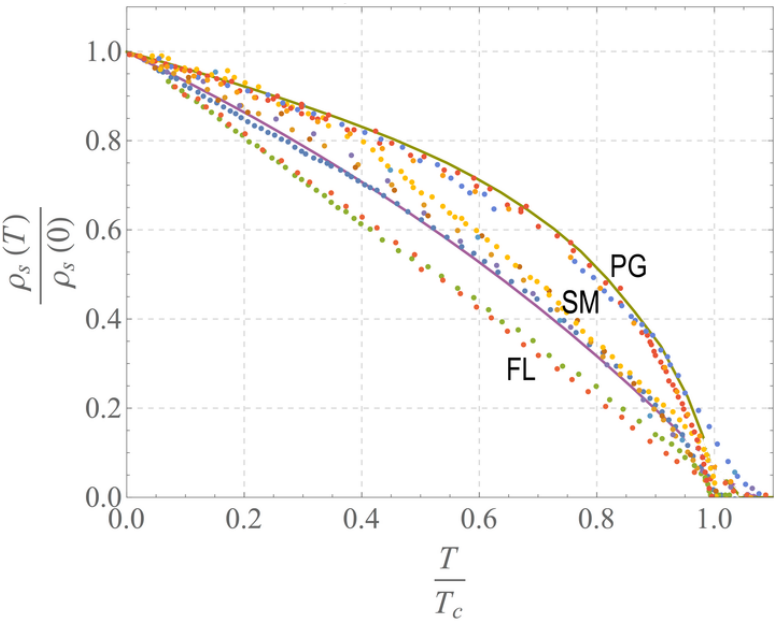

Figure 5.10: Three "universality classes" in normalized superfluid density as a function of the normalized temperature. See the main text for details about the samples analyzed.

It is possible recognizing, particularly in the vicinity of the superconducting transition, three different "universality classes", from top to bottom in Fig. 5.10:

- We identify the pseudogap (PG) universality class whose behavior we have already analyzed, and compared with the present model, green solid line. Samples: 1, 2, 3.
- We identify the strange metal (SM) universality class which seems approximately in agreement with the standard BCS d-wave behavior of superfluid density, shown with a solid violet line [235]. Samples: 4, 5, 6, 7.
- Finally, we identify a third universality class, which we name Fermi liquid (FL), for samples showing a strictly linear behaviour as far as ρ_s is concerned, up to the critical point. Samples: 8 and 9.

Albeit we do not give a complete explanation of this observation in terms of the present model, we do note that it could be explained quite naturally by considering the three classes as three different coherence states of the holon+spinon system

- The PG universality corresponds to the situation we already analyzed in commenting Fig. 5.8.
- In the SM universality class the Ioffe-Larkin-like composition rule for superfluid density still holds, but the holon contribution becomes more and more relevant. The "transition" from the pseudogap to the strange metal regime is interpreted in our formalism as the disappearance of the π-flux per plaquette; as a consequence the small Fermi surface, with enclosed area $\sim \delta$ become a large one with enclosed area $\sim 1-\delta$ and similarly the Fermi energy $\epsilon_F \sim 2t\delta$ in pseudogap becomes $\epsilon_F \sim 2t(1+\delta)$ in strange metal [206]. The different behavior of holons also indirectly influences, through the τ^2 term, the dynamics of spinons, and ongoing work is being carried out in order to establish whether this picture is compatible with the SM universality class we observe. We stress that in the vicinity of T_c the critical exponent still seems to be $2/3$, confirming, within the present formalism, the Ioffe-Larkin rule. In fact a d-wave behavior for the superfluid density profile except for the critical region where a different critical exponent appears strongly supports a composite approach like the present one.
- Finally the strictly linear temperature profile of the superfluid density in the FL class could be interpreted as a breakdown of the composition rule, as here holon and spinon are expected to be strongly bound, behaving like an elementary excitation. Unfortunately the data does not allow for a precise determination of the critical exponent in the FL samples, which seems compatible both with the 3DXY one and with a mean-field exponent.

6

Conclusions and future perspectives

In Chapter 2 we discussed the BCS-BEC crossover from a historical perpsective, along with a brief review of its experimental realization in ultracold Fermi gases. In Chapter 3 the mean-field theory for the crossover has been introduced, whereas in Chapter 4 the order parameter fluctuations have been discussed, on top of the mean-field approximation. While presenting the general formalism a number of topics related to the BCS-BEC crossover has been considered.

Specifically in Section 3.5 the condensate fraction for a spin-unbalanced Fermi gas has been investigated both in the uniform and trapped case, by modeling a harmonic trapped in local density approximation. The results reproduce the phase separation observed in experiments, more quantitatively a comparison with experimental data shows a good agreement for low polarization values, with an overestimation of the critical polarization. We conclude that the main source to disagreement is to be found in an incorrect determination of the phase boundary, due to the approximations made in modeling the normal phase.

In Section 4.2 we have extended the standard result of Landau's hydrodynamic theory of a superfluid, which leads to a purely linear spectrum implying a collinear Beliaev decay. By including a gradient term in the Hamiltonian, we have recovered the Bogoliubov-like spectrum for bosonic excitations in a superfluid, producing a larger phase-space for the Beliaev decay. We have shown that even slight variations from linearity of the spectrum can give important modifications to the decay rate of the process we consider. We have applied our result to an interacting Fermi gas in the BCS-BEC crossover: we have shown that the Beliaev decay is not allowed at zero temperature in the deep BCS regime, due to kinematics constraints,

as the spectrum grows less than linearly. As the strength of the attractive interaction is increased, the collective mode spectrum increases linearly or faster as $y = (k_F a_s)^{-1} \gtrsim -0.14$, thus allowing the decay of one collective excitation into lower energy excitations. This mechanism becomes more and more relevant as the coupling gets stronger. We observe that in the BCS regime in the low-temperature limit a collective excitation can decay only by breaking down into two fermions at the threshold energy $E_{\rm th}$; on the other hand at unitarity and in the BEC regime a collective excitation can also decay in two collective excitations by means of the Beliaev decay.

In Section 4.3 we have shown that the Berezinskii-Kosterlitz-Thouless critical temperature of the superfluid-normal phase transition can be extracted from a description of the superfluid density, which takes into account Gaussian fluctuations in the finite-temperature equation of state. The agreement with very recent experimental data for both the critical temperature [148] and the sound velocity [236] is remarkably good and crucially depends on the inclusion of Gaussian fluctuations.

In Section 4.4 starting from a theory of attractive fermions, performing cutoff regularization plus renormalization of Gaussian fluctuations we have obtained a remarkable relationship between the scattering length a_b of composite bosons and the scattering length a_s of fermions. Our formula $a_b = (2/3)\, a_s$ is fully consistent with previous semi-analytical and numerical calculations [111, 117, 165–167]. We stress that our approach, limited to the quartic term in the low-momentum expansion of bosonic collective excitations, is fully reliable in the BEC regime but it cannot describe the entire 3D BCS-BEC crossover. In fact in the BCS region, where the chemical potential μ is positive, the sign of the coefficient λ of the collective spectrum is negative (pair instability) and further terms must be included in the momentum expansion.

Chapter 5 deals with high-T_c superconductivity in cuprates. After a review of the main experimental features, a theoretical framework is introduced, based on a gauge approach to the $t-J$ model and on spin-charge separation: the hole is decomposed as the product of spin-only excitation, a spinon, and a charge-only excitation, a holon. The holon and the spinon are then bound to statistical fluxes, allowing one to modify their statistics. A semionic choice for the statistics and an opportune mean-field treatment lead to an effective representation of the $t-J$ model in terms of holons and spinons. The model is characterized by three different temperature scales, corresponding, respectively, to the appearance of a finite density of incoherent holon pairs, to the appearance of a finite density of incoherent spinon pairs and, finally, to the phase coherence leading to the onset of superconductivity. We have shown that this theoretical framework is able to correctly reproduce the superfluid density profile observed in underdoped and optimally-doped cuprates. Using a single scale parameter ξ accounting phenomenologically for small scale physics, our model fits rather well normalized superfluid density data from YBCO (a-axis), BSCCO, Hg-1201 and LSCO in the aforementioned doping

range. The universal critical exponent 2/3 and the near-universality of 3D XY typee of the normalized superfluid density are also reproduced independently of ξ, as well as the approximate Uemura relation which is analytically derived.

Finally we mention some future perspective and some possible extensions of the work presented in this Thesis:

- The contribution of Gaussian fluctuations to the equation of state has a relevance reaching far beyond the BCS-BEC crossover: an extension of the results found for in the present Thesis for the two-dimensional case could allow for a better understanding of the strong-coupling limit of other two-dimensional systems undergoing BCS-like pairing, e.g. bilayers of fermionic polar molecules [163, 237] or exciton-polariton condensates [238].

- Throughout this Thesis the interaction in the BCS-BEC crossover has been always modeled as a contact potential, adequate for many ultracold gases in the dilute limit. Modeling the interatomic interaction with a realistic potential would allow for the study of long-range interactions which are relevant, e.g. in the description of ultracold polar atoms and molecules.

- Another direction, motivated by very recent experimental observations [239], would be the investigation of non-equilibrium properties of ultracold Fermi gases the BCS-BEC crossover, in particular soliton dynamics.

- The estimate we give for the Berezinskii-Kosterlitz-Thouless critical temperature for a two-dimensional Fermi gas does not account for the renormalization of superfluid density due to vortices. This point is the subject of ongoing work, preliminary results show that vortices do not substantially modify T_{BKT}, however the agreement with experimental data could be slightly improved.

- In Section 4.4 an analytical regularization scheme has been introduced in the deep-BEC limit, on the other hand in Section 4.3 a numerical investigation of the beyond-mean-field equation of state for the two-dimensional BCS-BEC crossover has been pursued by using numerical techniques. Is it possible to obtain analytical results across the whole crossover?

- Finally, as far as high-T_c superconductivity in cuprates is concerned, ongoing work is being carried out in order to extend our investigation of superfluid density to the whole phase diagram, investigating the strange metal region, for slightly overdoped cuprates, and to the Fermi liquid region, for strongly overdoped samples. Preliminary results show that

the approach used in this Thesis should be indeed capable of adequately modeling the superfluid density in the strange metal phase.

7 Acknowledgements

I gratefully thank my supervisor Prof. Luca Salasnich who patiently followed my work, encouraging, mentoring and guiding me through the world of ultracold atoms.

My collaboration with Prof. Pieralberto Marchetti started when writing my Master's thesis and fruitfully continued during my Ph.D., I thank him for his patience and for the stimulating, enlightening discussions.

Moreover during the last year I had the pleasure of collaborating with Prof. Flavio Toigo, whom I thank for the sharing with me many suggestions and brilliant intuitions.

Part of the present Thesis is based on a paper I coauthored with Giovanni Mazzarella and Luca Dell'Anna, whom I thank along with all the great condensed matter theorists in Padua. Giovanni Lombardi in Antwerp provided many useful suggestions and help, particularly regarding Belgian beers and Matsubara sums.

During most of my Ph.D. studies I shared my office with Kirill and Jagjit, while Denise was in the *neighboring* office. Thank you for the good times!

A warm, heartfelt thank you goes to my parents for their constant support, to my sister Claudia and to all my family, in particular my uncle Luigi who encouraged and followed my doctoral studies.

My friends deserve a special acknowledgement for their closeness even when my studies left me very little spare time or made me travel; among them a special mention goes to Soncio and Gabbo.

A

Infinite series through contour integration

In this Appendix we introduce a technique for the evaluation of infinite series by rewriting them as a countour integration in the complex plane [36, 240]. We start from a series of the form

$$s = \frac{1}{\beta} \sum_n f(i\,\omega_n) \tag{A.1}$$

where β is a parameter and $\omega_n = (2n+1)\pi/\beta$ are fermionic Matsubara frequencies. The main idea is creating a holomorphic function defined on the complex plane having an infinite number of poles evenly spaced on the imaginary axis. The function is to be defined such that the residue at each pole is equal to a term in the infinite series above, so that a contour integral over an infinite circuit enclosing the imaginary axis is equivalent to the sum of the infinite series s. In fact the following equality holds

$$s = \frac{1}{\beta} \sum_n f(i\,\omega_n) = \frac{1}{\beta} \oint_C dz\, f(z) \frac{\beta}{2} \tanh\left(\frac{\beta z}{2}\right) \tag{A.2}$$

provided that C is a contour enclosing counterclockwise the entire imaginary axis, avoiding any other pole that the integrand may have. Since

$$\mathrm{Res}\left[\frac{\beta}{2} \tanh\left(\frac{\beta z}{2}\right)\right](i\,\omega_n) = 1 \tag{A.3}$$

the value of each residue is exactly the value of a term in the infinite series, as wanted. The integration along the contour C is equivalent to the integration of the contour C' shown in the left panel of Fig. A.1 where the radius R of each semicircle is taken to be $R \to \infty$. The integrand needs to go to zero

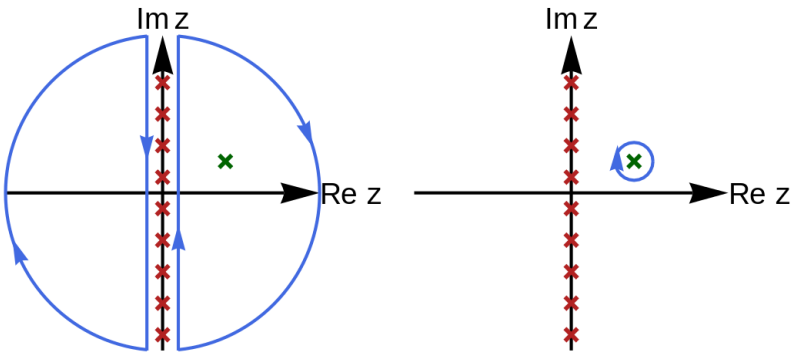

Figure A.1: Scheme of the contour integration employed for computing the sum over the fermionic Matsubara frequencies, modified from Wikimedia Commons.

faster than z^{-1} as $|z| \to \infty$ for the Jordan's lemma to hold [240], allowing one to close the contour at infinity adding the semicircles without modifying the value of the integral.

Finally the contour C' can be continuosly deformed into the contour C'', as shown in the right panel of Fig. A.1, including only the poles of the function $f(z)$. By using the properties of holomorphic functions in the complex plane we transformed a sum over an infinite number of terms in a sum over a finite number of terms, in fact our summation reduces to

$$s = -\frac{1}{\beta} \sum_i \mathrm{Res} \left[f(z) \frac{\beta}{2} \tanh\left(\frac{\beta z}{2}\right) \right] (z_i) \tag{A.4}$$

where z_i are the poles of $f(z)$. The minus sign is due to the fact that the deformed contour encloses the poles in the clockwise direction.

We can now then evaluate the sum in Eq. (3.64), i.e.:

$$-\frac{1}{\beta} \sum_n \frac{1}{(\mathrm{i}\omega_n)^2 - x^2} \,. \tag{A.5}$$

Referring to Eq. (A.1) and Eq. (A.2) in this case $f(z) = -(z^2 - x^2)^{-1}$. Clearly the poles of $f(z)$ are for $z = \pm x$ and a direct calculation shows that the residue is the same at both poles, namely

$$\mathrm{Res} \left[\frac{-1}{z^2 - x^2} \frac{\beta}{2} \tanh\left(\frac{\beta z}{2}\right) \right] (z = \pm x) = \frac{-\beta \tanh(\beta x/2)}{4x} \,. \tag{A.6}$$

Applying Eq. (A.4) one readily finds

$$-\frac{1}{\beta} \sum_n \frac{1}{(\mathrm{i}\omega_n)^2 - x^2} = \frac{\tanh(\beta x/2)}{2x} \,. \tag{A.7}$$

as anticipated in Eq. (3.64). An analogous result can be obtained for sums over *bosonic* frequencies, by modifying the weighting factor introduced in Eq. (A.2) [36, 240].

B

Matrix element for the Beliaev decay

In this Appendix we calculate the matrix element $H_{if}^{(3)}$ of the Hamiltonian in Eq (4.25), i.e.:

$$\hat{H}^{(3)} = \int \mathrm{d}^3 r \Big[(\nabla\hat{\phi}) \frac{\hat{\rho}'}{2} (\nabla\hat{\phi}) + \frac{1}{6} \left(\frac{\mathrm{d}}{\mathrm{d}\rho} \frac{u^2}{\rho} \right) \hat{\rho}'^3 - \lambda \frac{\hbar^2}{8m^2} (\nabla\hat{\rho}')^2 \frac{\hat{\rho}'}{\rho^2} \Big] \,. \quad \text{(B.1)}$$

between the following initial and final states:

$$|i\rangle = \hat{b}^\dagger_{\mathbf{p}} |\Omega\rangle \quad \text{(B.2)}$$

$$|f\rangle = \hat{b}^\dagger_{\mathbf{q}_1} \hat{b}^\dagger_{\mathbf{q}_2} |\Omega\rangle \,, \quad \text{(B.3)}$$

using the same notation as in Section 4.2. In order to make the subsequent calculations simpler, we define the following functional[1]:

$$\hat{V}[f] = \frac{1}{\sqrt{2V}} \sum_{|\mathbf{k}|\neq 0} f(\mathbf{k}) \left(\hat{b}_{\mathbf{k}} e^{\mathbf{i}\mathbf{k}\cdot\mathbf{r}} + \hat{b}^\dagger_{\mathbf{k}} e^{-\mathbf{i}\mathbf{k}\cdot\mathbf{r}} \right) \quad \text{(B.4)}$$

which can clearly reproduce all the operators appearing in the Hamiltonian in Eq. (4.19) , i.e. $\hat{\rho}$ and $\nabla\hat{\phi}$, for an adequate choice of f; note that it cannot reproduce $\hat{\phi}$. Every term appearing in the Hamiltonian in Eq. (4.19) is the product of three operators, let us see how we can rewrite such a term. In general a term composed by three operators is to be rewritten as:

$$\hat{V}[f]\ \hat{V}[g]\ \hat{V}[h] = (2V)^{-\frac{3}{2}} \sum_{|\mathbf{k}_i|\neq 0, i=1,2,3} f(\mathbf{k}_1) g(\mathbf{k}_2) h(\mathbf{k}_3) X_{\mathbf{r}}(\mathbf{K}) \,. \quad \text{(B.5)}$$

[1] Actually it is an operator-valued functional, hence the hat.

With a slightly abuse of notation, to avoid being too verbose, we define $\mathbf{K} \equiv \{\mathbf{k}_1, \mathbf{k}_2, \mathbf{k}_3\}$, and:

$$X_{\mathbf{r}}(\mathbf{K}) \approx \hat{b}_{\mathbf{k}_1}\hat{b}_{\mathbf{k}_2}\hat{b}^\dagger_{\mathbf{k}_3} e^{\mathrm{i}(\mathbf{k}_1+\mathbf{k}_2-\mathbf{k}_3)} + \hat{b}_{\mathbf{k}_1}\hat{b}^\dagger_{\mathbf{k}_2}\hat{b}_{\mathbf{k}_3} e^{\mathrm{i}(\mathbf{k}_1-\mathbf{k}_2+\mathbf{k}_3)} + \hat{b}^\dagger_{\mathbf{k}_1}\hat{b}_{\mathbf{k}_2}\hat{b}_{\mathbf{k}_3} e^{\mathrm{i}(-\mathbf{k}_1+\mathbf{k}_2+\mathbf{k}_3)} \,. \tag{B.6}$$

Why the approximate equality sign $\approx$ instead of a true equality? Many other terms should appear in the expression above, however we retained only the terms with two annihilation operators and one creation operator; the other terms are going to zero when calculating the matrix element between $|i\rangle$ and $|f\rangle$, and can then be ignored for the sake of the present calculation.

We can now rewrite the Hamiltonian as:

$$\hat{H}^{(3)} = \int \mathrm{d}^3 r \left(C_1 \hat{V}[l]\ \hat{V}[m]\ \hat{V}[l] + C_2 \hat{V}[m]\ \hat{V}[m]\ \hat{V}[m] \right) \tag{B.7}$$

with $C_1 = 1/2$, $C_2 = 1/6 \frac{\mathrm{d}}{\mathrm{d}\bar{\rho}} \frac{c^2}{\bar{\rho}}$, $l(\mathbf{k}) = (\mathrm{i}\hbar)(\mathrm{i}\mathbf{k})A^{-1}_{\mathbf{k}} = -\hbar\mathbf{k}A^{-1}_{\mathbf{k}}$, $m(\mathbf{k}) = A_{\mathbf{k}}$; it is easily verified that this Hamiltonian corresponds to Eq. (4.19). Using the expression found above for the product of three $\hat{V}$ functionals we get:

$$H^{(3)}_{if} = (2V)^{-\frac{3}{2}} \sum_{|\mathbf{k}_i|\neq 0, i=1,2,3} \left(C_1 l(\mathbf{k}_1) m(\mathbf{k}_2) l(\mathbf{k}_3) + C_2 m(\mathbf{k}_1) m(\mathbf{k}_2) m(\mathbf{k}_3) \right) X_{if} \tag{B.8}$$

having defined:

$$X_{if} = \langle i | \int \mathrm{d}^3 r X_{\mathbf{r}}(\mathbf{K}) | f \rangle \tag{B.9}$$

and the $\mathrm{d}^3 r$ integration has been taken inside the matrix element, as the only $\mathbf{r}$-dependent term is $X_{\mathbf{r}}(\mathbf{K})$.

B.1 Wick's theorem comes in handy

Preliminarly we want calculate the following matrix element (here we also anticipate the result):

$$\langle i | \hat{b}_{\mathbf{k}_1}\hat{b}_{\mathbf{k}_2}\hat{b}^\dagger_{\mathbf{k}_3} | f \rangle = \langle \Omega | \hat{b}_{\mathbf{p}}\hat{b}_{\mathbf{k}_1}\hat{b}_{\mathbf{k}_2}\hat{b}^\dagger_{\mathbf{k}_3}\hat{b}^\dagger_{\mathbf{q}_1}\hat{b}^\dagger_{\mathbf{q}_2} | \Omega \rangle = \sum_L \delta_{\mathbf{p},\mathbf{l}_1}\delta_{\mathbf{k}_1,\mathbf{l}_2}\delta_{\mathbf{k}_2,\mathbf{l}_3} \tag{B.10}$$

The last sum being over $\mathbf{l}_i$, which are all the permutations of the final-state momenta $\{\mathbf{k}_3, \mathbf{q}_1, \mathbf{q}_2\}$. Explicitely:

$$L = \{\{\mathbf{l}_1 = \mathbf{k}_3, \mathbf{l}_2 = \mathbf{q}_1, \mathbf{l}_3 = \mathbf{q}_2\}, \{\mathbf{l}_1 = \mathbf{k}_3, \mathbf{l}_2 = \mathbf{q}_2, \mathbf{l}_3 = \mathbf{q}_1\}, \cdots\} \tag{B.11}$$

Also we note that the δ functions appearing in Eq. (B.10) are Kronecker δ's: this is consistent with the fact that the momenta are defined by discrete summations, which will eventually be converted to integrals.

The calculations leading to Eq. (B.10) using a direct approach would be quite cumbersome, but the result can be straightforwardly derived by

using Wick's theorem [241], which allows one to rewrite the product of many annihilation/creation operators as the sum of its normal-ordering and its contractions:

$$\hat{A}\hat{B}\cdots\hat{Z} =: \hat{A}\hat{B}\cdots\hat{Z} : + \sum_{\text{singles}} : \hat{A}\hat{B}\cdots\hat{Z} : + \\ + \sum_{\text{doubles}} : \hat{A}\hat{B}\cdots\hat{Z} : + \sum_{\text{triples}} : \hat{A}\hat{B}\cdots\hat{Z} : + \cdots \quad \text{(B.12)}$$

where the first sum is over all the possible terms created by applying one contraction to the initial product, subsequently applying the normal ordering. Similarly the second summation is over all the possible normal-ordered 2-contractions, and so on.

We apply the theorem to the following product:

$$\hat{b}_{\mathbf{p}}\hat{b}_{\mathbf{k}_1}\hat{b}_{\mathbf{k}_2}\hat{b}^{\dagger}_{\mathbf{k}_3}\hat{b}^{\dagger}_{\mathbf{q}_1}\hat{b}^{\dagger}_{\mathbf{q}_2} \quad \text{(B.13)}$$

Being interested in the product of six operators we can stop evaluating the summations in Eq. (B.12) after the term with three contractions, which actually will be our only contribution. In fact the 0-contraction term, being normal ordered, will evaluate to zero because

$$\langle\Omega| \text{ something normal ordered } |\Omega\rangle = 0 \,. \quad \text{(B.14)}$$

Analogously the 1-contraction and 2-contraction terms will have a non-contracted part which, being a normal ordered product of operators, will evaluate to zero when touching $|\ \Omega\rangle$ on the right. So we are left with the following equality:

$$\langle\Omega|\hat{b}_{\mathbf{p}}\hat{b}_{\mathbf{k}_1}\hat{b}_{\mathbf{k}_2}\hat{b}^{\dagger}_{\mathbf{k}_3}\hat{b}^{\dagger}_{\mathbf{q}_1}\hat{b}^{\dagger}_{\mathbf{q}_2}|\Omega\rangle = \langle\Omega| \sum_{\text{triples}} : \hat{b}_{\mathbf{p}}\hat{b}_{\mathbf{k}_1}\hat{b}_{\mathbf{k}_2}\hat{b}^{\dagger}_{\mathbf{k}_3}\hat{b}^{\dagger}_{\mathbf{q}_1}\hat{b}^{\dagger}_{\mathbf{q}_2} :|\Omega\rangle \quad \text{(B.15)}$$

By noting that the only non-zero contraction is between a creation and an annihilation operator, remembering the canonical commutation relationship $[b_{\mathbf{k}}, b^{\dagger}_{\mathbf{q}}] = \delta_{\mathbf{k},\mathbf{q}}$, we explicitly list all the contractions:

$$\begin{cases} \overbrace{b_{\mathbf{k}}b_{\mathbf{q}}} = b_{\mathbf{k}}b_{\mathbf{q}} - : b_{\mathbf{k}}b_{\mathbf{q}} := 0 \\ \overbrace{b^{\dagger}_{\mathbf{k}}b^{\dagger}_{\mathbf{q}}} = b^{\dagger}_{\mathbf{k}}b^{\dagger}_{\mathbf{q}} - : b^{\dagger}_{\mathbf{k}}b^{\dagger}_{\mathbf{q}} := 0 \\ \overbrace{b_{\mathbf{k}}b^{\dagger}_{\mathbf{q}}} = b_{\mathbf{k}}b^{\dagger}_{\mathbf{q}} - : b_{\mathbf{k}}b^{\dagger}_{\mathbf{q}} := b_{\mathbf{k}}b^{\dagger}_{\mathbf{q}} - b^{\dagger}_{\mathbf{q}}b_{\mathbf{k}} = \delta_{\mathbf{k},\mathbf{q}} \end{cases} \quad \text{(B.16)}$$

It is now easy to see that all the possible 3-contractions in Eq. (B.15) correspond to what anticipated above in Eq. (B.10).

Going back to Eq. (B.10), there are $3! = 6$ different permutations; however only two of them, i.e. the permutations explicitly listed in Eq. (B.11), have physical meaning. The other four permutations, along with the momentum conservation constraint $\mathbf{p} = \mathbf{q}_1 + \mathbf{q}_2$, impose one of the following constraints:

- $\mathbf{p} = \mathbf{q}_1$, $\mathbf{q_2} = 0$: the initial state $\mathbf{p}$ "continues" to $\mathbf{q}_1$, a 0-momentum excitation is created, i.e. there is no decay.
- $\mathbf{p} = \mathbf{q}_2$, $\mathbf{q_1} = 0$: the initial state $\mathbf{p}$ "continues" to $\mathbf{q}_2$, a 0-momentum excitation is created, i.e. there is no decay.

Neither of those contributions is relevant for the present treatment, so that we are left with:

$$\langle\Omega|\hat{b}_{\mathbf{p}}\hat{b}_{\mathbf{k}_1}\hat{b}_{\mathbf{k}_2}\hat{b}^\dagger_{\mathbf{k}_3}\hat{b}^\dagger_{\mathbf{q}_1}\hat{b}^\dagger_{\mathbf{q}_2}|\Omega\rangle \approx \delta_{\mathbf{p},\mathbf{k}_3}\delta_{\mathbf{k}_1,\mathbf{q}_1}\delta_{\mathbf{k}_2,\mathbf{q}_2} + (\mathbf{k}_1 \leftrightarrow \mathbf{k}_2) \equiv X_0 \,. \tag{B.17}$$

We can now use this result to easily calculate X_{if}:

$$\begin{aligned} X_{if} = \langle i|\int \mathrm{d}^3 r e^{\mathbf{i}\mathbf{r}\cdot(\mathbf{k}_1+\mathbf{k}_2-\mathbf{k}_3)} b_{\mathbf{k}_1} b_{\mathbf{k}_2} b^\dagger_{\mathbf{k}_3}|f\rangle + \langle i|\int \mathrm{d}^3 r e^{\mathbf{i}\mathbf{r}\cdot(\mathbf{k}_1-\mathbf{k}_2+\mathbf{k}_3)} b_{\mathbf{k}_1} b^\dagger_{\mathbf{k}_2} b_{\mathbf{k}_3}|f\rangle + \\ + \langle i|\int \mathrm{d}^3 r e^{\mathbf{i}\mathbf{r}\cdot(-\mathbf{k}_1+\mathbf{k}_2+\mathbf{k}_3)} b^\dagger_{\mathbf{k}_1} b_{\mathbf{k}_2} b_{\mathbf{k}_3}|f\rangle \end{aligned} \tag{B.18}$$

Recalling that $\int \mathrm{d}^3 r e^{\mathbf{i}\mathbf{r}\cdot\mathbf{k}} = (2\pi\hbar)^3\,\delta^{(3)}(\mathbf{k})$ we can rewrite X_{if} as:

$$\begin{aligned} X_{if} = (2\pi\hbar)^3 \Big[& \delta^{(3)}\left(\mathbf{k}_1 + \mathbf{k}_2 - \mathbf{k}_3\right) \langle i|b_{\mathbf{k}_1} b_{\mathbf{k}_2} b^\dagger_{\mathbf{k}_3}|f\rangle + \\ & + \delta^{(3)}\left(\mathbf{k}_1 - \mathbf{k}_2 + \mathbf{k}_3\right) \langle i|b_{\mathbf{k}_1} b^\dagger_{\mathbf{k}_2} b_{\mathbf{k}_3}|f\rangle + \\ & + \delta^{(3)}\left(-\mathbf{k}_1 + \mathbf{k}_2 + \mathbf{k}_3\right) \langle i|b^\dagger_{\mathbf{k}_1} b_{\mathbf{k}_2} b_{\mathbf{k}_3}|f\rangle \Big] = \end{aligned} \tag{B.19}$$

remembering that the operators commute, having different arguments, and using Eq. (B.17) one finally gets:

$$\begin{aligned} X_{if} = (2\pi\hbar)^3 \Big[& \delta^{(3)}\left(\mathbf{k}_1 + \mathbf{k}_2 - \mathbf{k}_3\right) X_0 + \delta^{(3)}\left(\mathbf{k}_1 - \mathbf{k}_2 + \mathbf{k}_3\right) X_0\left(\mathbf{k}_2 \leftrightarrow \mathbf{k}_3\right) + \\ & + \delta^{(3)}\left(-\mathbf{k}_1 + \mathbf{k}_2 + \mathbf{k}_3\right) X_0\left(\mathbf{k}_1 \leftrightarrow \mathbf{k}_3\right) \Big] \end{aligned} \tag{B.20}$$

Plugging in the explicit expression for X_0 from the second member of Eq. (B.17) we see that each term in the previous formula is the product of 4 Dirac (or Kronecker) δ functions, and there are 6 terms in total. By repeatedly applying the formula $f(x)\delta(x-a) = f(a)\delta(x-a)$ (respectively $f_a\delta_{a,b} = f_b\delta_{a,b}$) we see that finally X_{if} can be rewritten[2] as:

$$X_{if} = (2\pi\hbar)^3\,\delta^{(3)}(\mathbf{p} - \mathbf{q}_1 - \mathbf{q}_2) \sum_L \delta_{\mathbf{k}_1,\mathbf{l}_1}\delta_{\mathbf{k}_2,\mathbf{l}_2}\delta_{\mathbf{k}_3,\mathbf{l}_3} \tag{B.21}$$

and the sum over the permutations L is just like the sum in Eq. (B.10). The Dirac δ function just imposes momentum conservation, from now on we will just write, for the sake of simplicity:

$$\delta^{(3)}(\mathbf{p} - \mathbf{q}_1 - \mathbf{q}_2) = \delta^{(3)}(\text{momentum}) \tag{B.22}$$

[2]The full calculation is very lengthy but straightforward.

Replacing the Kronecker δ with a Dirac δ function in the continuum limit[3]

$$\delta_{\mathbf{k},\mathbf{q}} \longrightarrow \frac{(2\pi)^3}{V}\delta^{(3)}\left(\mathbf{k}-\mathbf{q}\right) \tag{B.23}$$

we can rewrite X_{if} as follows:

$$X_{if} = (2\pi\hbar)^3\,\delta^{(3)}(\text{momentum})\frac{(2\pi)^9}{V^3}\sum_L \delta^{(3)}\left(\mathbf{k}_1-\mathbf{l}_1\right)\delta^{(3)}\left(\mathbf{k}_2-\mathbf{l}_2\right)\delta^{(3)}\left(\mathbf{k}_3-\mathbf{l}_3\right) \tag{B.24}$$

B.2 Putting everything back together

Having found a simple expression for X_{if} we can go back to Eq. (B.8). As seen before:

$$H_{if}^{(3)} = (2V)^{-\frac{3}{2}} \sum_{|\mathbf{k}_i|\neq 0, i=1,2,3} \left(C_1 l(\mathbf{k}_1)m(\mathbf{k}_2)l(\mathbf{k}_3) + C_2 m(\mathbf{k}_1)m(\mathbf{k}_2)m(\mathbf{k}_3)\right) X_{if} \tag{B.25}$$

Moreover we take the continuum limit:

$$\sum_{\mathbf{k}} \to \frac{V}{(2\pi)^3}\int \mathrm{d}^3k \tag{B.26}$$

$$\sum_{\mathbf{k_i}\neq 0, i=1,2,3} \to \frac{V^3}{(2\pi)^9}\int \mathrm{d}^3k_1\mathrm{d}^3k_2\mathrm{d}^3k_3\ , \tag{B.27}$$

obtaining:

$$\begin{aligned} H_{if}^{(3)} = (2V)^{-\frac{3}{2}} \int \prod_{i=1}^{3} \mathrm{d}^3k_i \left(C_1 l(\mathbf{k}_1)m(\mathbf{k}_2)l(\mathbf{k}_3) + C_2 m(\mathbf{k}_1)m(\mathbf{k}_2)m(\mathbf{k}_3)\right) \times \\ \times (2\pi\hbar)^3\,\delta^{(3)}(\text{momentum})\sum_L \delta^{(3)}\left(\mathbf{k}_1-\mathbf{l}_1\right)\delta^{(3)}\left(\mathbf{k}_2-\mathbf{l}_2\right)\delta^{(3)}\left(\mathbf{k}_3-\mathbf{l}_3\right) \end{aligned} \tag{B.28}$$

Performing the three d^3k_i integrations using the Dirac δ functions we get:

$$H_{if}^{(3)} = (2V)^{-\frac{3}{2}}\,(2\pi\hbar)^3\,\delta^{(3)}(\text{momentum})\left(2C_1\left(M_1+M_2+M_3\right)+6C_2M_4\right) \tag{B.29}$$

Now, for simplicity's sake, we modify the notation a little:

$$\delta^{(3)}(\text{momentum})f(\mathbf{p},\mathbf{q}_1,\mathbf{q}_2) = \delta^{(3)}(\mathbf{p}-\mathbf{q}_1-\mathbf{q}_2)f(\mathbf{p},\mathbf{q}_1,\mathbf{p}-\mathbf{q}_1)\ . \tag{B.30}$$

[3]It can be justified by noting that: $\sum_{\mathbf{k}}\delta_{\mathbf{k},\mathbf{q}} = 1 \to \frac{V}{(2\pi)^3}\int \mathrm{d}^3k\frac{(2\pi)^3}{V}\delta^{(3)}\left(\mathbf{k}-\mathbf{q}\right) = 1$.

So $\mathbf{q}_2$ is replaced by $\mathbf{p}-\mathbf{q}$, because of momentum conservation, and we can drop the subscript in $\mathbf{q}_1$, redefining $\mathbf{q}_1 \to \mathbf{q}$. Writing Eq. (B.29) we introduced the quantities M_i, we now write them explicitely:

$$\begin{cases} M_1 = m(\mathbf{p})l(\mathbf{q})l(\mathbf{p}-\mathbf{q}) = \hbar(\mathbf{p}\cdot\mathbf{q}-q^2)\left(\frac{\hbar\bar{\rho}}{c}\right)^{-\frac{1}{2}}\sqrt{\frac{|\mathbf{p}|}{|\mathbf{q}||\mathbf{p}-\mathbf{q}|}} \\ M_2 = m(\mathbf{q})l(\mathbf{p}-\mathbf{q})l(\mathbf{p}) = \hbar(p^2-\mathbf{p}\cdot\mathbf{q})\left(\frac{\hbar\bar{\rho}}{c}\right)^{-\frac{1}{2}}\sqrt{\frac{|\mathbf{q}|}{|\mathbf{p}||\mathbf{p}-\mathbf{q}|}} \\ M_3 = m(\mathbf{p}-\mathbf{q})l(\mathbf{p})l(\mathbf{q}) = \hbar(\mathbf{p}\cdot\mathbf{q})\left(\frac{\hbar\bar{\rho}}{c}\right)^{-\frac{1}{2}}\sqrt{\frac{|\mathbf{p}-\mathbf{q}|}{|\mathbf{p}||\mathbf{q}|}} \\ M_4 = m(\mathbf{p})m(\mathbf{q})m(\mathbf{p}-\mathbf{q}) = \left(\frac{\hbar\bar{\rho}}{c}\right)^{\frac{3}{2}}\sqrt{pq\,|\mathbf{p}-\mathbf{q}|} \end{cases} \tag{B.31}$$

At first we calculate them as Landau does, i.e. in a low transferred momentum approximation, assuming that the product particle momenta are collinear one to each other, and also with respect to the initial-state momentum. Subsequently we calculate the exact values.

B.2.1 Approximate Landau's result

In this Subsection we calculate the approximate matrix element. As far as this Subsection is concerned we are going to use a linear Bogoliubov spectrum:

$$\hbar\omega_{\mathbf{p}} \approx u|\mathbf{p}| \tag{B.32}$$

where u is the sound velocity. The energy and momentum conservation relations for the process are:

$$\begin{cases} 0 = E_f - E_i = u\left(|\mathbf{p}| - |\mathbf{q}_1| - |\mathbf{q}_2|\right) \\ 0 = \mathbf{p} - \mathbf{q}_1 - \mathbf{q}_2 \end{cases} \tag{B.33}$$

The two relations together imply that $|\mathbf{q}_1 - \mathbf{q}_2| = |\mathbf{q}_1| - |\mathbf{q}_2|$, which can be satisfied only if the angle between $\mathbf{q}_1$ and $\mathbf{q}_2$ is zero; it is easily seen that this implies that also the angle between $\mathbf{q}_i$ and $\mathbf{p}$ is zero: a linear spectrum for the excitations implies a collinear decay.

We thus note that in the collinear limit ($\mathbf{p}/\!/\mathbf{q}$) the following identities hold:

$$\mathbf{p}\cdot\mathbf{q} = pq\cos(\theta) = pq \tag{B.34}$$

and

$$|\mathbf{p}-\mathbf{q}| = \sqrt{p^2+q^2-2pq\cos(\theta)} = \sqrt{p^2+q^2-2pq} = \sqrt{(p-q)^2} = |p-q| \tag{B.35}$$

where $\theta \approx 0$ is the angle between $\mathbf{p}$ and $\mathbf{q}$. Consequently:

$$M_1^{\text{Landau}} = \hbar\left(\frac{\hbar\bar{\rho}}{c}\right)^{-\frac{1}{2}}(pq-q^2)\sqrt{\frac{p}{q\,|p-q|}} = \hbar\left(\frac{\hbar\bar{\rho}}{c}\right)^{-\frac{1}{2}}\operatorname{sgn}(p-q)\sqrt{pq\,|p-q|} \tag{B.36}$$

The conservation of energy also implies $|\mathbf{p}| \geq \mathbf{q}_i$, so that we can take $\mathrm{sgn}(p-q) = 1$. Going on with the calculation of the other quantities one finds:

$$M_2^{\text{Landau}} = M_3^{\text{Landau}} = \hbar \left(\frac{\hbar\bar{\rho}}{c}\right)^{-\frac{1}{2}} \sqrt{pq\,|p-q|} = M_1^{\text{Landau}} \tag{B.37}$$

$$M_4^{\text{Landau}} = \hbar \left(\frac{\hbar\bar{\rho}}{c}\right)^{\frac{3}{2}} \sqrt{pq|p-q|}\,. \tag{B.38}$$

Finally inserting the results into Eq. (B.29) and simplifying a bit we obtain:

$$H_{if}^{(3)} = \frac{(2\pi\hbar)^3}{(2V)^{\frac{3}{2}}} \cdot \delta^{(3)}(\text{momentum}) \cdot 3 \left(\frac{\hbar\bar{\rho}}{c}\right)^{-\frac{1}{2}} \sqrt{pq|p-q|} \left(1 + \frac{1}{3}\frac{\hbar^2\bar{\rho}^2}{c^2}\frac{\mathrm{d}}{\mathrm{d}\bar{\rho}}\frac{u^2}{\bar{\rho}}\right) \tag{B.39}$$

in agreement with Refs. [120, 126, 127].

B.2.2 Exact result

Not making any assumption on the form of the spectrum or on the collinearity of decay products we have:

$$M_1 = \hbar \left(\frac{\hbar\bar{\rho}}{c}\right)^{-\frac{1}{2}} \frac{p\cos\theta - q}{|\mathbf{p}-\mathbf{q}|} \sqrt{pq\,|\mathbf{p}-\mathbf{q}|}\,, \tag{B.40}$$

$$M_2 = \hbar \left(\frac{\hbar\bar{\rho}}{c}\right)^{-\frac{1}{2}} \frac{p - q\cos\theta}{|\mathbf{p}-\mathbf{q}|} \sqrt{pq\,|\mathbf{p}-\mathbf{q}|}\,, \tag{B.41}$$

$$M_3 = \hbar \left(\frac{\hbar\bar{\rho}}{c}\right)^{-\frac{1}{2}} \cos\theta \sqrt{pq\,|\mathbf{p}-\mathbf{q}|}\,. \tag{B.42}$$

Their sum reads

$$M_1 + M_2 + M_3 = \hbar \left(\frac{\hbar\bar{\rho}}{c}\right)^{-\frac{1}{2}} \left(\frac{(p-q)(\cos\theta+1)}{q|\mathbf{p}-\mathbf{q}|} + \cos\theta\right) \sqrt{pq\,|\mathbf{p}-\mathbf{q}|}\,. \tag{B.43}$$

Finally

$$M_4 = 3\hbar \left(\frac{\hbar\bar{\rho}}{c}\right)^{\frac{3}{2}} \sqrt{pq|\mathbf{p}-\mathbf{q}|}\,. \tag{B.44}$$

Inserting into Eq. (B.29) at last one finds the matrix element for the Beliaev decay:

$$H_{if}^{(3)} = \frac{(2\pi\hbar)^3}{(2V)^{\frac{3}{2}}} \cdot \delta^{(3)}(\text{momenta}) \cdot 3 \left(\frac{\hbar\bar{\rho}}{c}\right)^{-\frac{1}{2}} \sqrt{pq\,|\mathbf{p}-\mathbf{q}|} \left(1 + \chi\frac{\hbar^2\bar{\rho}^2}{c^2}\frac{\mathrm{d}}{\mathrm{d}\bar{\rho}}\frac{u^2}{\bar{\rho}}\right) \tag{B.45}$$

with

$$\chi^{-1} = \frac{p-q}{|\mathbf{p}-\mathbf{q}|}(1+\cos(\theta)) + \cos(\theta) \tag{B.46}$$

and of course to recover the approximate treatment of the previous Subsection we just need to set $\cos\theta = 0$, which in turn implies $\chi = \frac{1}{3}$.

Bibliography

[1] G. Bighin, G. Mazzarella, L. Dell'Anna, and L. Salasnich, "Pair condensation of polarized fermions in the BCS–BEC crossover", Journal of Physics B: Atomic, Molecular and Optical Physics **47**, 195302 (2014).

[2] G. Bighin, L. Salasnich, P. A. Marchetti, and F. Toigo, "Beliaev damping of the Goldstone mode in atomic Fermi superfluids", Physical Review A **92**, 023638 (2015).

[3] G. Bighin and L. Salasnich, "Finite-temperature quantum fluctuations in two-dimensional Fermi superfluids ", Physical Review B **93**, 014519 (2016).

[4] L. Salasnich and G. Bighin, "Scattering length of composite bosons in the three-dimensional BCS-BEC crossover", Physical Review A **91**, 033610 (2015).

[5] P. A. Marchetti, F. Ye, Z. B. Su, and L. Yu, "Hole pairing from attraction of opposite-chirality spin vortices: Non-BCS superconductivity in underdoped cuprates", Physical Review B **84**, 214525 (2011).

[6] J. Fröhlich and P. A. Marchetti, "Slave fermions, slave bosons, and semions from bosonization of the two-dimensional $t-J$ model", Physical Review B **46**, 6535 (1992).

[7] P. A. Marchetti and G. Bighin, "Gauge approach to superfluid density in underdoped cuprates", EPL (Europhysics Letters) **110**, 37001 (2015).

[8] M. Randeria, W. Zwerger, and M. Zwierlein, "The BCS–BEC Crossover and the Unitary Fermi Gas", in *The BCS-BEC Crossover and the Unitary Fermi Gas* (Springer Berlin Heidelberg, Berlin, Heidelberg, 2012), pp. 1–32.

[9] A. J. Leggett and S. Zhang, "The BEC–BCS Crossover: Some History and Some General Observations", in *The BCS-BEC Crossover and the Unitary Fermi Gas* (Springer Berlin Heidelberg, Berlin, Heidelberg, 2012), pp. 33–47.

[10] W. Ketterle and M. W. Zwierlein, "Making, probing and understanding ultracold Fermi gases", in *Ultra-cold Fermi gases, Proceedings of the International School of Physics "Enrico Fermi"*, edited by M. Inguscio, W. Ketterle, and C. Salomon (IOS Press, 2007), pp. 351–383.

[11] M. Randeria and E. Taylor, "Crossover from Bardeen-Cooper-Schrieffer to Bose-Einstein Condensation and the Unitary Fermi Gas", Annual Review of Condensed Matter Physics **5**, 209 (2014).

[12] M. Randeria, "Crossover from BCS Theory to Bose-Einstein condensation", in *Bose-Einstein Condensation*, edited by A. Griffin, D. W. Snoke, and S. Stringari (Cambridge University Press, 1995), pp. 355–392.

[13] A. J. Leggett, *Quantum Liquids: Bose Condensation and Cooper Pairing in Condensed-Matter Systems*, Oxford Graduate Texts (Oxford University Press, Oxford, 2006).

[14] J. Bardeen, L. N. Cooper, and J. R. Schrieffer, "Microscopic theory of superconductivity", Physical Review **106**, 162 (1957).

[15] H. K. Onnes, *Through Measurement to Knowledge: The Selected Papers of Heike Kamerlingh Onnes 1853-1926*, edited by K. Gavroglu and Y. Goudaroulis, Boston Studies in the Philosophy of Science (Springer, 1991).

[16] D. Goodstein and J. Goodstein, "Richard Feynman and the History of Superconductivity", Physics in Perspective **2**, 30 (2000).

[17] M. Born and R. Oppenheimer, "Zur Quantentheorie der Molekeln", Annalen der Physik **389**, 457 (1927).

[18] M. Brack, "The physics of simple metal clusters: self-consistent jellium model and semiclassical approaches", Rev. Mod. Phys. **65**, 677 (1993).

[19] P. Townsend and J. Sutton, "Investigation by Electron Tunneling of the Superconducting Energy Gaps in Nb, Ta, Sn, and Pb", Physical Review **128**, 591 (1962).

[20] L. N. Cooper, "Bound electron pairs in a degenerate Fermi gas", Physical Review **104**, 1189 (1956).

[21] S. Bose, "Plancks Gesetz und Lichtquantenhypothese", Zeitschrift für Physik **26**, 178 (1924).

[22] A. Einstein, "Quantentheorie des einatomigen idealen Gases", Sitzungsberichte der Preußischen Akademie der Wissenschaften, Physikalisch-mathematische Klasse, 261 (1924).

[23] P. Kapitza, "Viscosity of Liquid Helium below the λ-Point", Nature **141**, 3558 (1938).

[24] J. F. Allen and A. D. Misener, "Flow of liquid helium II", Nature **141**, 75 (1938).

[25] M. H. Anderson, J. R. Ensher, M. R. Matthews, C. E. Wieman, and E. A. Cornell, "Observation of Bose-Einstein condensation in a dilute atomic vapor", Science **269**, 198 (1995).

[26] K. B. Davis, M. O. Mewes, M. R. Andrews, N. J. van Druten, D. S. Durfee, D. M. Kurn, and W. Ketterle, "Bose-Einstein condensation in a gas of sodium atoms", Physical Review Letters **75**, 3969 (1995).

[27] S. Jochim, M. Bartenstein, A. Altmeyer, G. Hendl, S. Riedl, C. Chin, J. H. Denschlag, and R. Grimm, "Bose-Einstein Condensation of Molecules", Science **302**, 2101 (2003).

[28] M. W. Zwierlein, C. A. Stan, C. H. Schunck, S. M. F. Raupach, S. Gupta, Z. Hadzibabic, and W. Ketterle, "Observation of Bose-Einstein Condensation of Molecules", Physical Review Letters **91**, 250401 (2003).

[29] J. M. Blatt, K. W. Böer, and W. Brandt, "Bose-Einstein condensation of excitons", Physical Review **126**, 1691 (1962).

[30] J. P. Eisenstein and A. H. MacDonald, "Bose–Einstein condensation of excitons in bilayer electron systems", Nature **432**, 691 (2004).

[31] J. Klaers, J. Schmitt, F. Vewinger, and M. Weitz, "Bose–Einstein condensation of photons in an optical microcavity", Nature **468**, 545 (2010).

[32] O. Penrose and L. Onsager, "Bose-Einstein Condensation and Liquid Helium", Physical Review **104**, 576 (1956).

[33] C. N. Yang, "Concept of off-diagonal long-range order and the quantum phases of liquid He and of superconductors", Reviews of Modern Physics **34**, 694 (1962).

[34] V. I. Yukalov, "Bose-Einstein condensation and gauge symmetry breaking", Laser Physics Letters **4**, 632 (2013).

[35] S. Weinberg, "Superconductivity for Particular Theorists", Prog. Theor. Phys. Suppl. **86**, 43 (1986).

[36] A. Altland and B. Simons, *Condensed Matter Field Theory* (Cambridge University Press, 2006).

[37] H. Ibach and H. Lüth, *Solid-State Physics: An Introduction to Principles of Materials Science*, Advanced texts in physics (Springer, Berlin, 2003).

[38] L. Salasnich, N. Manini, and A. Parola, "Condensate fraction of a Fermi gas in the BCS-BEC crossover", Physical Review A **72**, 023621 (2005).

[39] L. V. Keldysh and A. N. Kozlov, "Collective properties of excitons in semiconductors", Soviet Physics JETP **27**, 521 (1968).

[40] V. N. Popov, "Theory of a Bose gas produced by bound states of Fermi particles", Soviet Physics JETP **50**, 1034 (1966).

[41] D. M. Eagles, "Possible Pairing without Superconductivity at Low Carrier Concentrations in Bulk and Thin-Film Superconducting Semiconductors", Physical Review **186**, 456 (1969).

[42] A. J. Leggett, "Diatomic molecules and Cooper pairs", in *Modern Trends in the Theory of Condensed Matter* (Springer Berlin Heidelberg, Berlin, Heidelberg, 1980), pp. 13–27.

[43] C. A. Sà De Melo, M. Randeria, and J. R. Engelbrecht, "Crossover from BCS to Bose superconductivity: Transition temperature and time-dependent Ginzburg-Landau theory", Physical Review Letters **71**, 3202 (1993).

[44] P. Nozières and S. Schmitt-Rink, "Bose condensation in an attractive fermion gas: From weak to strong coupling superconductivity", J. Low. Temp. Phys. **59**, 195 (1985).

[45] M. Randeria, J.-M. Duan, and L.-Y. Shieh, "Superconductivity in a two-dimensional Fermi gas: Evolution from Cooper pairing to Bose condensation", Physical Review B **41**, 327 (1990).

[46] A. Perali, P. Pieri, and G. C. Strinati, "Quantitative Comparison between Theoretical Predictions and Experimental Results for the BCS-BEC Crossover", Physical Review Letters **93**, 100404 (2004).

[47] J. G. Bednorz and K. A. Müller, "Possible high-T_c superconductivity in the Ba-La-Cu-O system", Zeitschrift für Physik B Condensed Matter **64**, 189 (1986).

[48] C. Pethick and H. Smith, *Bose-Einstein Condensation in Dilute Gases* (Cambridge University Press, Cambridge, 2002).

[49] E. A. Cornell and C. E. Wieman, "Nobel Lecture: Bose-Einstein condensation in a dilute gas, the first 70 years and some recent experiments", Rev. Mod. Phys. **74**, 875 (2002).

[50] F. M. Marchetti, "Course in three lectures on Superfluidity in Ultracold Fermi Gases", lecture notes available on the author's website.

[51] S. Chu, "Nobel Lecture: The manipulation of neutral particles", Rev. Mod. Phys. **70**, 685 (1998).

[52] C. N. Cohen-Tannoudji, "Nobel Lecture: Manipulating atoms with photons", Rev. Mod. Phys. **70**, 707 (1998).

[53] W. D. Phillips, "Nobel Lecture: Laser cooling and trapping of neutral atoms", Rev. Mod. Phys. **70**, 721 (1998).

[54] P. Bouyer, V. Boyer, S. G. Murdoch, G. Delannoy, Y. Le Coq, A. Aspect, and M. Lécrivain, "RF-Induced Evaporative Cooling And BEC In A High Magnetic Field", in *Bose-Einstein Condensates and Atom Lasers* (Springer US, Boston, MA, 2002), pp. 165–186.

[55] R. Grimm, M. Weidemüller, and Y. N. Ovchinnikov, "Optical dipole traps for neutral atoms", Adv. At. Mol. Opt. Phys. **42**, 170 (2000).

[56] I. Bloch, "Ultracold quantum gases in optical lattices", Nature Physics **1**, 23 (2005).

[57] Y. Ohashi and A. Griffin, "BCS-BEC Crossover in a Gas of Fermi Atoms with a Feshbach Resonance", Physical Review Letters **89**, 130402 (2002).

[58] C. Chin, R. Grimm, P. Julienne, and E. Tiesinga, "Feshbach resonances in ultracold gases", Rev. Mod. Phys. **82**, 1225 (2010).

[59] M. Holland and J. Wachter, "Two-channel models of the BCS/BEC crossover", in *Ultra-cold Fermi gases, Proceedings of the International School of Physics "Enrico Fermi"*, edited by M. Inguscio, W. Ketterle, and C. Salomon (IOS Press, 2007), pp. 351–383.

[60] L. Salasnich, "From narrow to broad Feshbach resonances: Condensate fraction of Cooper pairs and preformed molecules", Physical Review A **86**, 055602 (2012).

[61] M. W. Zwierlein, A. Schirotzek, C. H. Schunck, and W. Ketterle, "Fermionic Superfluidity with Imbalanced Spin Populations", Science **311**, 492 (2006).

[62] T. Langen, R. Geiger, and J. Schmiedmayer, "Ultracold Atoms Out of Equilibrium", Annual Review of Condensed Matter Physics **6**, 201 (2015).

[63] K. K. Ni, S. Ospelkaus, D. Wang, G. Quéméner, B. Neyenhuis, M. H. G. de Miranda, J. L. Bohn, J. Ye, and D. S. Jin, "Dipolar collisions of polar molecules in the quantum regime", Nature **464**, 1324 (2010).

[64] M. W. Zwierlein, J. R. Abo-Shaeer, A. Schirotzek, C. H. Schunck, and W. Ketterle, "Vortices and superfluidity in a strongly interacting Fermi gas", Nature **435**, 1047 (2005).

[65] T. Carsten, "Theory of Superconductivity", lecture notes available on the author's website.

[66] J. Tempere, "Path integral description of the superfluid properties at the BEC/BCS crossover", in *Ultra-cold Fermi gases, Proceedings of the International School of Physics "Enrico Fermi"*, edited by M. Inguscio, W. Ketterle, and C. Salomon (IOS Press, 2007), pp. 639–655.

[67] J. Tempere and J. P. A. Devreese, "Path-Integral Description of Cooper Pairing", in *Superconductors - Materials, Properties and Applications* (InTech, 2012), pp. 1–32.

[68] L. Salasnich, "Condensate fraction of a two-dimensional attractive Fermi gas", Physical Review A **76**, 015601 (2007).

[69] S. Giorgini, L. P. Pitaevskii, and S. Stringari, "Theory of ultracold atomic Fermi gases", Rev. Mod. Phys. **80**, 1215 (2008).

[70] G. Garberoglio, S. Taioli, and S. Simonucci, "The BEC-BCS crossover in ultracold Fermi gases beyond the contact-potential approximation", The European Physical Journal D **67**, 129 (2013).

[71] H. T. C. Stoof, K. B. Gubbels, and D. B. M. Dickerscheid, *Ultracold Quantum Fields* (Springer, Dordrecht, 2009).

[72] Y. Nambu, "Quasiparticles and Gauge Invariance in the Theory of Superconductivity", Physical Review **117**, 648 (1960).

[73] Q. Chen, J. Stajic, S. Tan, and K. Levin, "BCS–BEC crossover: From high temperature superconductors to ultracold superfluids", Physics Reports **412**, 1 (2005).

[74] C. E. Campbell, in *Condensed Matter Theories, vol. 12*, edited by J. W. Clark and P. V. Panat (Nova Science, 1997), pp. 131–132.

[75] H. Vivas, "Path Integral Treatment of Fluctuations in the BCS-BEC Crossover in Superfluid Fermi Gases", (2005), arXiv:`cond-mat/0504600v2 [cond-mat.str-el]`.

[76] N. Nagaosa, *Quantum Field Theory in Condensed Matter Physics* (Springer, Berlin, 1999).

[77] H. Kleinert, "Hubbard-Stratonovich Transformation: Successes, Failure, and Cure", Electronic Journal of Theoretical Physics **25**, 57 (2015).

[78] A. Altland, "Lecture notes in Advanced Quantum Mechanics", lecture notes available on the author's website.

[79] B. A. Lippmann and J. Schwinger, "Variational principles for scattering processes. I", Physical Review **79**, 469 (1950).

[80] W. H. Dickhoff and D. Van Neck, *Many-body Theory Exposed!: Propagator Description Of Quantum Mechanics In Many-body Systems* (World Scientific, Singapore, 2005).

[81] M. Marini, F. Pistolesi, and G. C. Strinati, "Evolution from BCS superconductivity to Bose condensation: analytic results for the crossover in three dimensions", Eur. Phys. J. B **1**, 151 (1998).

[82] P. F. Bedaque, H. Caldas, and G. Rupak, "Phase Separation in Asymmetrical Fermion Superfluids", Physical Review Letters **91**, 247002 (2003).

[83] J. Carlson and S. Reddy, "Asymmetric Two-Component Fermion Systems in Strong Coupling", Physical Review Letters **95**, 060401 (2005).

[84] C. H. Pao, S.-T. Wu, and S. K. Yip, "Superfluid stability in the BEC-BCS crossover", Physical Review B **73**, 132506 (2006).

[85] D. T. Son and M. A. Stephanov, "Phase diagram of a cold polarized Fermi gas", Physical Review A **74**, 013614 (2006).

[86] T. Mizushima, K. Machida, and M. Ichioka, "Direct Imaging of Spatially Modulated Superfluid Phases in Atomic Fermion Systems", Physical Review Letters **94**, 060404 (2005).

[87] D. E. Sheehy and L. Radzihovsky, "BEC-BCS Crossover in "Magnetized" Feshbach-Resonantly Paired Superfluids", Physical Review Letters **96**, 060401 (2006).

[88] M. Mannarelli, G. Nardulli, and M. Ruggieri, "Evaluating the phase diagram of superconductors with asymmetric spin populations", Physical Review A **74**, 033606 (2006).

[89] P. Pieri and G. C. Strinati, "Trapped Fermions with Density Imbalance in the Bose-Einstein Condensate Limit", Physical Review Letters **96**, 150404 (2006).

[90] X.-J. Liu and H. Hu, "BCS-BEC crossover in an asymmetric two-component Fermi gas", EPL (Europhysics Letters) **75**, 364 (2007).

[91] H. Hu and X.-J. Liu, "Mean-field phase diagrams of imbalanced Fermi gases near a Feshbach resonance", Physical Review A **73**, 051603 (2006).

[92] C.-C. Chien, Q. Chen, Y. He, and K. Levin, "Intermediate-Temperature Superfluidity in an Atomic Fermi Gas with Population Imbalance", Physical Review Letters **97**, 090402 (2006).

[93] Z.-C. Gu, G. Warner, and F. Zhou, "Fermion pairing with population imbalance: energy landscape and phase separation in a constrained Hilbert subspace", (2006), arXiv:`cond-mat/0603091 [cond-mat.other]`.

[94] J.-P. Martikainen, "Ultracold polarized Fermi gas at intermediate temperatures", Physical Review A **74**, 013602 (2006).

[95] M. Iskin and C. A. R. Sá de Melo, "Two-Species Fermion Mixtures with Population Imbalance", Physical Review Letters **97**, 100404 (2006).

[96] T. N. De Silva and E. J. Mueller, "Profiles of near-resonant population-imbalanced trapped Fermi gases", Physical Review A **73**, 051602 (2006).

[97] M. Haque and H. T. C. Stoof, "Pairing of a trapped resonantly interacting fermion mixture with unequal spin populations", Physical Review A **74**, 011602 (2006).

[98] W. Yi and L. M. Duan, "Trapped fermions across a Feshbach resonance with population imbalance", Physical Review A **73**, 031604 (2006).

[99] J. Kinnunen, L. M. Jensen, and P. Törmä, "Strongly Interacting Fermi Gases with Density Imbalance", Physical Review Letters **96**, 110403 (2006).

[100] M. M. Parish, F. M. Marchetti, A. Lamacraft, and B. D. Simons, "Finite-temperature phase diagram of a polarized Fermi condensate", Nature Physics **3**, 124 (2007).

[101] D. E. Sheehy and L. Radzihovsky, "BEC–BCS crossover, phase transitions and phase separation in polarized resonantly-paired superfluids", Annals of Physics **322**, 1790 (2007).

[102] G. B. Partridge, W. Li, R. I. Kamar, Y. Liao, and R. G. Hulet, "Pairing and phase separation in a polarized Fermi gas", Science **311**, 503 (2006).

[103] C. H. Schunck, Y. Shin, A. Schirotzek, M. W. Zwierlein, and W. Ketterle, "Pairing Without Superfluidity: The Ground State of an Imbalanced Fermi Mixture", Science **316**, 867 (2007).

[104] P. Fulde and R. A. Ferrell, "Superconductivity in a strong spin-exchange field", Physical Review **135**, A550 (1964).

[105] A. Recati, C. Lobo, and S. Stringari, "Role of interactions in spin-polarized atomic Fermi gases at unitarity", Physical Review A **78**, 023633 (2008).

[106] Y.-i. Shin, C. H. Schunck, A. Schirotzek, and W. Ketterle, "Phase diagram of a two-component Fermi gas with resonant interactions", Nature **451**, 689 (2008).

[107] A. Lamacraft, "Cold atoms for condensed matter theorists", Graduate lectures delivered in Hilary Term 2006 at Oxford, lecture notes available online.

[108] M. W. Zwierlein, C. A. Stan, C. H. Schunck, S. M. F. Raupach, A. J. Kerman, and W. Ketterle, "Condensation of Pairs of Fermionic Atoms near a Feshbach Resonance", Physical Review Letters **92**, 120403 (2004).

[109] Y. Inada, M. Horikoshi, S. Nakajima, M. Kuwata-Gonokami, M. Ueda, and T. Mukaiyama, "Critical Temperature and Condensate Fraction of a Fermion Pair Condensate", Physical Review Letters **101**, 180406 (2008).

[110] G. Ortiz and J. Dukelsky, "BCS-to-BEC crossover from the exact BCS solution", Physical Review A **72**, 043611 (2005).

[111] G. E. Astrakharchik, J. Boronat, J. Casulleras, and S. Giorgini, "Equation of State of a Fermi Gas in the BEC-BCS Crossover: A Quantum Monte Carlo Study", Physical Review Letters **93**, 200404 (2004).

[112] L. He and X.-G. Huang, "BCS-BEC crossover in three-dimensional Fermi gases with spherical spin-orbit coupling", Physical Review B **86**, 014511 (2012).

[113] J. Tempere, M. Wouters, and J. T. Devreese, "Imbalanced Fermi superfluid in a one-dimensional optical potential", Physical Review B **75**, 184526 (2007).

[114] A. M. Clogston, "Upper Limit for the Critical Field in Hard Superconductors", Physical Review Letters **9**, 266 (1962).

[115] C. Lobo, A. Recati, S. Giorgini, and S. Stringari, "Normal State of a Polarized Fermi Gas at Unitarity", Physical Review Letters **97**, 200403 (2006).

[116] Z. Hadzibabic and M. Kohl, "Low-Dimensional Atomic Bose Gases", in *Ultracold Bosonic and Fermionic Gases*, Vol. 5, edited by A. L. F. Kathryn Levin and D. M. Stamper-Kurn, Contemporary Concepts of Condensed Matter Science (Elsevier, 2012), pp. 95–120.

[117] R. B. Diener, R. Sensarma, and M. Randeria, "Quantum fluctuations in the superfluid state of the BCS-BEC crossover", Physical Review A **77**, 023626 (2008).

[118] S. N. Klimin, J. Tempere, and J. T. Devreese, "Pseudogap and preformed pairs in the imbalanced Fermi gas in two dimensions", New Journal of Physics **14**, 103044 (2012).

[119] J. Keeling, P. R. Eastham, M. H. Szymańska, and P. B. Littlewood, "BCS-BEC crossover in a system of microcavity polaritons", Physical Review B **72**, 115320 (2005).

[120] L. Landau and E. Lifshitz, *Course of Theoretical Physics: Statistical Physics, part II* (Pergamon Press, Oxford, 1969).

[121] H. J. Maris, "Phonon-phonon interactions in liquid helium", Rev. Mod. Phys. **49**, 341 (1977).

[122] N. G. Mills, R. A. Sherlock, and A. Wyatt, "Evidence for Upward Phonon Dispersion in Liquid ^{4}He from the Angular Spreading of Phonon Beams", Physical Review Letters **32**, 978 (1974).

[123] E. Hodby, O. M. Maragò, G. Hechenblaikner, and C. J. Foot, "Experimental Observation of Beliaev Coupling in a Bose-Einstein Condensate", Physical Review Letters **86**, 2196 (2001).

[124] N. Katz, J. Steinhauer, R. Ozeri, and N. Davidson, "Beliaev Damping of Quasiparticles in a Bose-Einstein Condensate", Physical Review Letters **89**, 220401 (2002).

[125] Z. Ristivojevic and K. A. Matveev, "Decay of Bogoliubov quasiparticles in a nonideal one-dimensional Bose gas", Physical Review B **89**, 180507 (2014).

[126] S. T. Beliaev, "Energy-spectrum of a non-ideal Bose gas", Soviet Physics JETP **2**, 299 (1958).

[127] L. Pitaevskii and S. Stringari, *Bose-Einstein Condensation*, International Series of Monographs on Physics (Clarendon Press, Oxford, 2003).

[128] L. Salasnich and F. Toigo, "Extended Thomas-Fermi density functional for the unitary Fermi gas", Physical Review A **78**, 053626 (2008).

[129] J. Goldstone, "Field theories with «Superconductor» solutions", Il Nuovo Cimento **19**, 154 (1961).

[130] G. Strinati, "Pairing Fluctuations Approach to the BCS–BEC Crossover ", in *The BCS-BEC Crossover and the Unitary Fermi Gas*, edited by W. Zwerger (Springer-Verlag, Berlin Heidelberg, 2012), pp. 99–126.

[131] V. N. Popov, *Functional Integrals in Quantum Field Theory and Statistical Physics* (Springer Netherlands, 1983).

[132] E. P. Gross, "Structure of a quantized vortex in boson systems", Il Nuovo Cimento (1955-1965) **20**, 454 (1961).

[133] L. P. Pitaevskii, "Vortex lines in an imperfect Bose gas", Soviet Physics JETP **40**, 646 (1961).

[134] E. Taylor, A. Griffin, N. Fukushima, and Y. Ohashi, "Pairing fluctuations and the superfluid density through the BCS-BEC crossover", Physical Review A **74**, 063626 (2006).

[135] E. Gubankova, M. Mannarelli, and R. Sharma, "Collective modes in asymmetric ultracold Fermi systems", Annals of Physics **325**, 1987 (2010).

[136] J. R. Engelbrecht, M. Randeria, and C. A. R. Sà de Melo, "BCS to Bose crossover: Broken-symmetry state", Physical Review B **55**, 15153 (1997).

[137] R. Combescot, M. Y. Kagan, and S. Stringari, "Collective mode of homogeneous superfluid Fermi gases in the BEC-BCS crossover", Physical Review A **74**, 042717 (2006).

[138] M. Marini, "Risultati analitici sul problema dell'evoluzione dalla superconduttività BCS alla condensazione di Bose-Einstein", MSc Thesis (University of Camerino, 1998).

[139] N. Manini and L. Salasnich, "Bulk and collective properties of a dilute Fermi gas in the BCS-BEC crossover", Physical Review A **71**, 033625 (2005).

[140] N. Andrenacci, P. Pieri, and G. C. Strinati, "Evolution from BCS superconductivity to Bose-Einstein condensation: Current correlation function in the broken-symmetry phase", Physical Review B **68**, 144507 (2003).

[141] N. D. Mermin and H. Wagner, "Absence of ferromagnetism or antiferromagnetism in one-or two-dimensional isotropic Heisenberg models", Physical Review Letters **17**, 1133 (1966).

[142] P. C. Hohenberg, "Existence of Long-Range Order in One and Two Dimensions", Physical Review **158**, 383 (1967).

[143] S. R. Coleman, "There are no Goldstone bosons in two-dimensions", Commun. Math. Phys. **31**, 259 (1973).

[144] V. L. Berenzinskii, "Destruction of long-range order in one-dimensional and two-dimensional systems possessing a continuous symmetry group. II. Quantum systems", Soviet Physics JETP **34** (1972).

[145] J. M. Kosterlitz and D. J. Thouless, "Ordering, metastability and phase transitions in two-dimensional systems", Journal of Physics C: Solid State Physics **6**, 1181 (1973).

[146] Z. Hadzibabic, P. Krüger, M. Cheneau, B. Battelier, and J. Dalibard, "Berezinskii–Kosterlitz–Thouless crossover in a trapped atomic gas", Nature **441**, 1118 (2006).

[147] W. H. Nitsche, N. Y. Kim, G. Roumpos, C. Schneider, M. Kamp, S. Höfling, A. Forchel, and Y. Yamamoto, "Algebraic order and the Berezinskii-Kosterlitz-Thouless transition in an exciton-polariton gas", Physical Review B **90**, 205430 (2014).

[148] P. A. Murthy, I. Boettcher, L. Bayha, M. Holzmann, D. Kedar, M. Neidig, M. G. Ries, A. N. Wenz, G. Zürn, and S. Jochim, "Observation of the Berezinskii-Kosterlitz-Thouless Phase Transition in an Ultracold Fermi Gas", Physical Review Letters **115**, 010401 (2015).

[149] D. R. Nelson and J. M. Kosterlitz, "Universal Jump in the Superfluid Density of Two-Dimensional Superfluids", Physical Review Letters **39**, 1201 (1977).

[150] D. J. Bishop and J. D. Reppy, "Study of the Superfluid Transition in Two-Dimensional ^{4}He Films", Physical Review Letters **40**, 1727 (1978).

[151] G. Bertaina and S. Giorgini, "BCS-BEC Crossover in a Two-Dimensional Fermi Gas", Physical Review Letters **106**, 110403 (2011).

[152] L. He, H. Lü, G. Cao, H. Hu, and X.-J. Liu, "Quantum fluctuations in the BCS-BEC crossover of two-dimensional Fermi gases", Physical Review A **92**, 023620 (2015).

[153] L. Salasnich and F. Toigo, "Composite bosons in the two-dimensional BCS-BEC crossover from Gaussian fluctuations", Physical Review A **91**, 011604 (2015).

[154] M. Randeria, J. M. Duan, and L. Y. Shieh, "Bound states, Cooper pairing, and Bose condensation in two dimensions", Physical Review Letters **62**, 981 (1989).

[155] E. Lipparini, *Modern Many-Particle Physics*, 2nd ed. (World Scientific, Singapore, 2008).

[156] L. Salasnich, "Low-temperature thermodynamics of the unitary Fermi gas: Superfluid fraction, first sound, and second sound", Physical Review A **82**, 063619 (2010).

[157] L. Landau, "Theory of the Superfluidity of Helium II", Physical Review **60**, 356 (1941).

[158] I. M. Khalatnikov, *An Introduction to the Theory of Superfluidity*, Advanced Books Classics Series (Advanced Book Program, Perseus Pub., 2000).

[159] T. Ozawa and S. Stringari, "Discontinuities in the First and Second Sound Velocities at the Berezinskii-Kosterlitz-Thouless Transition", Physical Review Letters **112**, 025302 (2014).

[160] X.-J. Liu and H. Hu, "First and second sound in a two-dimensional harmonically trapped Bose gas across the Berezinskii–Kosterlitz–Thouless transition", Annals of Physics **351**, 531 (2014).

[161] A. L. Fetter and J. D. Walecka, *Quantum Theory of Many-Particle Systems (Dover Books on Physics)* (Dover Publications, June 1971).

[162] L. Salasnich, P. A. Marchetti, and F. Toigo, "Superfluidity, sound velocity, and quasicondensation in the two-dimensional BCS-BEC crossover", Physical Review A **88**, 053612 (2013).

[163] N. T. Zinner, B. Wunsch, D. Pekker, and D. W. Wang, "BCS-BEC crossover in bilayers of cold fermionic polar molecules", Physical Review A **85**, 013603 (2012).

[164] V. Makhalov, K. Martiyanov, and A. Turlapov, "Ground-State Pressure of Quasi-2D Fermi and Bose Gases", Physical Review Letters **112**, 045301 (2014).

[165] D. S. Petrov, C. Salomon, and G. V. Shlyapnikov, "Weakly Bound Dimers of Fermionic Atoms", Physical Review Letters **93**, 090404 (2004).

[166] H. Hu, X. J. Liu, and P. D. Drummond, "Equation of state of a superfluid Fermi gas in the BCS-BEC crossover", EPL (Europhysics Letters) **74**, 574 (2007).

[167] P. Pieri and G. C. Strinati, "Strong-coupling limit in the evolution from BCS superconductivity to Bose-Einstein condensation", Physical Review **B61**, 15370 (2000).

[168] A. M. J. Schakel, *Boulevard of Broken Symmetries: Effective Field Theories of Condensed Matter* (World Scientific Publishing Company, Singapore, 2008).

[169] J. C. Collins, *Renormalization: an introduction to renormalization, the renormalization group, and the operator-product expansion*, Cambridge monographs on mathematical physics (Cambridge University Press, Cambridge, 1984).

[170] G. Bighin, "A gauge approach to the superfluid density in high-T_c cuprates", MSc Thesis (University of Padova, 2012).

[171] M. Buchanan, "Mind the pseudogap", Nature **409**, 8 (2001).

[172] A. Schilling, M. Cantoni, J. D. Guo, and H. R. Ott, "Superconductivity above 130 K in the Hg-Ba-Ca-Cu-O system", Nature **363**, 56 (1993).

[173] P. A. Lee, N. Nagaosa, and X.-G. Wen, "Doping a Mott insulator: Physics of high-temperature superconductivity", Rev. Mod. Phys. **78**, 17 (2006).

[174] E. G. Maksimov and O. V. Dolgov, "A note on the possible mechanisms of high-temperature superconductivity", Physics-Uspekhi **50**, 933 (2007).

[175] D. J. Scalapino, "The case for $d_{x^2-y^2}$ pairing in the cuprate superconductors", Physics Reports **250**, 329 (1995).

[176] C. C. Tsuei and J. R. Kirtley, "Pairing symmetry in cuprate superconductors", Reviews of Modern Physics **72**, 969 (2000).

[177] M. R. Presland, J. L. Tallon, R. G. Buckley, and R. S. Liu, "General trends in oxygen stoichiometry effects on T_c in Bi and Tl superconductors", Physica C **176**, 95 (1991).

[178] C. Varma, "High-temperature superconductivity: Mind the pseudogap", Nature **468**, 184 (2010).

[179] P. A. Marchetti, G. Orso, Z. B. Su, and L. Yu, "Transport properties in the strange-metal phase of high-T_c cuprates: Spin-charge gauge theory versus experiments", Physical Review B **71**, 134510 (2005).

[180] F. Zhang and T. Rice, "Effective Hamiltonian for the superconducting Cu oxides", Physical Review B **37**, 3759 (1988).

[181] N. B. Brookes, G. Ghiringhelli, O. Tjernberg, L. H. Tjeng, T. Mizokawa, T. W. Li, and A. A. Menovsky, "Detection of Zhang-Rice Singlets Using Spin-Polarized Photoemission", Physical Review Letters **87**, 237003 (2001).

[182] S. M. Hayden, G. Aeppli, R. Osborn, and A. D. Taylor, "High-energy spin waves in La_2CuO_4", Physical Review Letters **67**, 3622 (1991).

[183] A. Damascelli, Z. Hussain, and Z. X. Shen, "Angle-resolved photoemission studies of the cuprate superconductors", Rev. Mod. Phys. **75**, 473 (2003).

[184] P. A. Marchetti and M. Gambaccini, "Gauge approach to the 'pseudogap' phenomenology of the spectral weight in high T_c cuprates", Journal of Physics: Condensed Matter **24**, 475601 (2012).

[185] P. A. Marchetti, "Interplay of Superconductivity and Magnetism in a $t-t'-J$ Approach to High-T_c Cuprates", Journal of Superconductivity and Novel Magnetism **28**, 735 (2014).

[186] E. Pavarini, I. Dasgupta, T. Saha-Dasgupta, O. Jepsen, and O. K. Andersen, "Band-Structure Trend in Hole-Doped Cuprates and Correlation with $T_{c,\max}$", Physical Review Letters **87**, 047003 (2001).

[187] A. LeClair, "Thermodynamics of the Two-Dimensional Hubbard Model Based on the Exact Two-Body S-Matrix", Brazilian Journal of Physics **42**, 28 (2012).

[188] P. A. Marchetti, Z. B. Su, and L. Yu, "Dimensional reduction of $U(1) \times SU(2)$ Chern-Simons bosonization: Application to the $t-J$ model", Nuclear Physics B **482**, 731 (1996).

[189] J. Hubbard, "Calculation of partition functions", Physical Review Letters **3**, 77 (1959).

[190] R. L. Stratonovich, "On a method of calculating quantum distribution functions", Sov. Phys. Doklady **2**, 416 (1958).

[191] P. W. Anderson, "The Resonating valence bond state in La_2CuO_4 and superconductivity", Science **235**, 1196 (1987).

[192] P. W. Anderson, in *Frontiers and borderlines in many-particle physics*, edited by R. A. Broglia et al. (North-Holland, 1988).

[193] B. J. Kim, H. Koh, E. Rotenberg, S. J. Oh, H. Eisaki, N. Motoyama, S. Uchida, T. Tohyama, S. Maekawa, Z. X. Shen, and C. Kim, "Distinct spinon and holon dispersions in photoemission spectral functions from one-dimensional $SrCuO_2$", Nature Physics **2**, 397 (2006).

[194] W. O. Putikka, R. L. Glenister, R. Singh, and H. Tsunetsugu, "Indications of spin-charge separation in the two-dimensional $t-J$ model", Physical Review Letters **73**, 170 (1994).

[195] J. M. Leinaas and J. Myrheim, "On the theory of identical particles", Il Nuovo Cimento B **37**, 1 (1977).

[196] R. B. Laughlin, "The Relationship Between High-Temperature Superconductivity and the Fractional Quantum Hall Effect", Science **242**, 525 (1988).

[197] R. B. Laughlin, "Current status of semionic pairing theory of high-T_c superconductors", Int. J. Mod. Phys. **B5**, 1507 (1991).

[198] P. Jordan and E. P. Wigner, "Über das Paulische Äquivalenzverbot", Z. Phys. **47**, 631 (1928).

[199] H. Frahm and V. E. Korepin, "Critical exponents for the one-dimensional Hubbard model", Physical Review B **42**, 10553 (1990).

[200] P. A. Marchetti, Z. B. Su, and L. Yu, "$U(1) \times SU(2)$ Chern-Simons gauge theory of underdoped cuprate superconductors", Physical Review B **58**, 5808 (1998).

[201] G. Orso, "Spin-charge gauge approach to HTS cuprates: Theory versus Experiments", Ph.D. Thesis (SISSA, Trieste, 2003).

[202] I. Affleck and J. B. Marston, "Large-n limit of the Heisenberg-Hubbard model: Implications for high-T_c superconductors", Physical Review B **37**, 3774 (1988).

[203] E. Fradkin, *Field Theories of Condensed Matter Systems* (Addison-Wesley, New York, 1991).

[204] J. Fröhlich, "Classical and quantum statistical mechanics in one and two dimensions: Two-component Yukawa — and Coulomb systems", Commun. Math. Phys. **47**, 233 (1976).

[205] P. A. Marchetti, F. Ye, Z. B. Su, and L. Yu, "A non-BCS mechanism for superconductivity in underdoped cuprates via attraction between spin vortices", EPL (Europhysics Letters) **93**, 57008 (2011).

[206] M. Gambaccini, "Pairing and superconductivity in a spin-charge gauge approach to HTS cuprates", Ph.D. Thesis (University of Padova, 2011).

[207] S. S. Botelho and C. A. R. Sá de Melo, "Vortex-Antivortex Lattice in Ultracold Fermionic Gases", Physical Review Letters **96**, 040404 (2006).

[208] Y. Wang, L. Li, and N. P. Ong, "Nernst effect in high-T_c superconductors", Physical Review B **73**, 024510 (2006).

[209] N. V. Prokof'ev and B. V. Svistunov, "Two definitions of superfluid density", Physical Review B **61**, 11282 (2000).

[210] J. R. Schrieffer, ed., *Handbook of High-Temperature Superconductivity*, Theory and Experiment (Springer-Verlag, New York, 2007).

[211] W. N. Hardy, S. Kamal, and D. A. Bonn, "Magnetic penetration depths in cuprates: a short review of measurement techniques and results", in *The Gap Symmetry and Fluctuations in High-T_c Superconductors*, Vol. 371, edited by J. Bok, G. Deutscher, D. Pavuna, and S. A. Wolf, NATO Science Series: B (Plenum Press, 1998), pp. 373–402.

[212] W. S. Lee, I. M. Vishik, K. Tanaka, D. H. Lu, T. Sasagawa, N. Nagaosa, T. P. Devereaux, Z. Hussain, and Z. X. Shen, "Abrupt onset of a second energy gap at the superconducting transition of underdoped Bi2212", Nature **450**, 81 (2007).

[213] T. Schneider, "Magnetic field induced 3D-1D crossover in type-II superconductors", Journal of Physics: Condensed Matter **20**, 423201 (2008).

[214] T. Schneider, "Evidence for three-dimensional XY critical properties in underdoped $YBa_2Cu_3O_{7-\delta}$", Physical Review B **75**, 174517 (2007).

[215] P. W. Anderson, "Personal history of my engagement with cuprate superconductivity, 1986-2010", International Journal of Modern Physics B **25**, 1 (2011).

[216] Y. J. Uemura, G. M. Luke, B. J. Sternlieb, and J. H. Brewer, "Universal Correlations between T_c and n_s/m^* (Carrier Density over Effective Mass) in High-T_c Cuprate Superconductors", Physical Review **62**, 2317 (1989).

[217] L. Yu, "Gauge field theory and metal-insulator crossover in cuprate superconductors", Lecture notes for the Workshop on Emergent Materials and Highly-correlated Electrons.

[218] M. E. Peskin and D. V. Schroeder, *An Introduction to Quantum Field Theory* (Westview Press, Boulder, 1995).

[219] L. B. Ioffe and A. I. Larkin, "Gapless fermions and gauge fields in dielectrics", Physical Review B **39**, 8988 (1989).

[220] M. E. Fisher, M. N. Barber, and D. Jasnow, "Helicity Modulus, Superfluidity, and Scaling in Isotropic Systems", Physical Review A **8**, 1111 (1973).

[221] A. P. Gottlob, M. Hasenbusch, and S. Meyer, "Critical behaviour of the 3D XY-model: a Monte Carlo study", Physica A **201**, 593 (1993).

[222] T. Ohta and D. Jasnow, "XY model and the superfluid density in two dimensions", Physical Review B **20**, 139 (1979).

[223] H. Kleinert, *Gauge Fields in Condensed Matter* (World Scientific, 1989).

[224] U. Wolff, "Collective Monte Carlo Updating for Spin Systems", Physical Review Letters **62**, 361 (1989).

[225] S. G. Sharapov and H. Beck, "Effective action approach and Carlson-Goldman mode in d-wave superconductors", Physical Review B **65**, 134516 (2002).

[226] A. Paramekanti and M. Randeria, "Fermi-liquid interactions and the superfluid density in d-wave superconductors", Physical Review B **66**, 214517 (2002).

[227] K. Zhang, D. A. Bonn, S. Kamal, R. Liang, D. J. Baar, W. N. Hardy, D. Basov, and T. Timusk, "Measurement of the ab Plane Anisotropy of Microwave Surface Impedance of Untwinned $YBa_2Cu_3O_{6.95}$ Single Crystals", Physical Review Letters **73**, 2484 (1994).

[228] W. N. Hardy et al., in *Proceedings of the 10th anniversary HTS workshop*, edited by B. Batlogg (World Scientific, 1996).

[229] T. Jacobs, S. Sridhar, Q. Li, G. D. Gu, and N. Koshizuka, "In-Plane and $\hat{c}$-Axis Microwave Penetration Depth of $Bi_2Sr_2Ca_1Cu_2O_{8+\delta}$ Crystals", Physical Review Letters **75**, 4516 (1995).

[230] C. Panagopoulos, B. D. Rainford, J. R. Cooper, and W. Lo, "Effects of carrier concentration on the superfluid density of high-T_c cuprates", Physical Review B **60**, 14617 (1999).

[231] D. A. Bonn, K. Zhang, R. Liang, D. J. Baar, D. C. Morgan, and W. N. Hardy, "Oxygen vacancies, zinc impurities, and the intrinsic microwave loss of $YBa_2Cu_3O_{7-\delta}$", Journal of Superconductivity **6**, 219 (1993).

[232] J. Stajic, A. Iyengar, K. Levin, B. R. Boyce, and T. R. Lemberger, "Cuprate pseudogap: Competing order parameters or precursor superconductivity", Physical Review B **68**, 024520 (2003).

[233] S.-F. Lee, D. C. Morgan, R. J. Ormeno, D. M. Broun, R. A. Doyle, J. R. Waldram, and K. Kadowaki, "$a-b$ Plane Microwave Surface Impedance of a High-Quality $Bi_2Sr_2CaCu_2O_8$ Single Crystal ", Physical Review Letters **77**, 735 (1996).

[234] C. Panagopoulos, J. R. Cooper, G. B. Peacock, and I. Gameson, "Anisotropic magnetic penetration depth of grain-aligned $HgBa_2Ca_2Cu_3O_{8+\delta}$", Physical Review B **53**, R2999 (1996).

[235] R. Prozorov and R. W. Giannetta, "Magnetic penetration depth in unconventional superconductors", Superconductor Science and Technology **19**, R41 (2006).

[236] N. Luick, "Local probing of the Berezinskii-Kosterlitz-Thouless transition in a two-dimensional Bose gas", MSc Thesis (University of Hamburg, 2014).

[237] M. A. Baranov, A. Micheli, S. Ronen, and P. Zoller, "Bilayer superfluidity of fermionic polar molecules: Many-body effects", Physical Review A **83**, 043602 (2011).

[238] T. Byrnes, N. Y. Kim, and Y. Yamamoto, "Exciton–polariton condensates", Nature Physics **10**, 803 (2014).

[239] T. Yefsah, A. T. Sommer, M. J. H. Ku, L. W. Cheuk, W. Ji, W. S. Bakr, and M. W. Zwierlein, "Heavy solitons in a fermionic superfluid", Nature **499**, 426 (2013).

[240] W. Appel, *Mathematics for Physics and Physicists*, 1st ed. (Princeton University Press, 2007).

[241] G. C. Wick, "The Evaluation of the Collision Matrix", Physical Review **80**, 268 (1950).